To the Graduate Council:

I am submitting herewith a dissertation written by Richard A. Campbell entitled "Crystallization of Isotactic Polypropylene at Atmospheric Pressure and Elevated Pressure." I have examined the final copy of this dissertation for form and content and recommend that it be accepted in partial fulfillment of the requirements for the degree of Doctor of Philosophy, with a major in Polymer Engineering.

Paul J. Phillips, Major Professor

We have read this dissertation
and recommend its acceptance:

Roberto S. Benson

Edward S. Clark

Joe E. Spruiell

Alexander Van Hook

Accepted for the Council:

Vice Provost
and Dean of The Graduate School

Crystallization of Isotactic Polypropylene at Atmospheric Pressure and Elevated Pressure

A Dissertation

Presented for the

Doctor of Philosophy

Degree

The University of Tennessee, Knoxville

Richard A. Campbell

August 1991

Acknowledgements

The author would like to express his most sincere thanks to his advisor, Professor Paul J. Phillips, for his support and guidance.

Sincere thanks are extended to the author's committee, professors Joe E. Spruiell, Roberto S. Benson, Edward S. Clark, and Alexander Van Hook, for their efforts in making this work possible.

The author appreciates the discussions with his fellow students, the work performed by the undergraduate technicians, and the support provided by the Materials Science office personnel and the electronics and machine shops.

The deepest appreciation is extended to my wife Sandra for her unfailing support, patience, and encouragement. Truly, this work would not have been accomplished without her help.

Abstract

The crystallization of iPP was studied at atmospheric and elevated pressures. The objective was to study the effect of pressure on the regime transitions in order to gain further insight into the crystallization mechanism. However, the elevated pressure kinetics exhibited behavior that has not been previously observed in polymers. At pressures between atmospheric and 200 MPa, where two crystal forms, α and γ, are known to exist, the product of the fold and lateral surface free energies $\sigma\sigma_e$ increased to a value nearly three times that at atmospheric pressure. But, on further increasing the pressure to 200 MPa, where essentially all the material is in the γ form, the kinetics exhibited behavior similar to that at atmospheric and the value of $\sigma\sigma_e$ was comparable to atmospheric values. With increasing in pressure, the regime behavior changes from Regime II-Regime III at atmospheric to Regime I-Regime II at intermediate pressures (35 MPa < P_c <150 MPa), and back to Regime II-Regime III behavior at higher pressures. Crystallization behavior of competing crystal forms has not been previously reported. This behavior could only be interpreted on the basis of the proposed orthorhombic unit cell for the γ form, and in the difference in the arrangement of chain stems between the α and the γ forms A 'poisoning' mechanism is proposed where a stem deposited on the growth face of a given

form could poison the face if deposited in a manner consistent with the alternative form. This poisoning would mostly affect the rate of surface nucleation i since a chain deposited essentially in a crystallographic manner could rapidly complete the substrate, but a chain deposited noncrystallographically would require, either, removal from the growth face, or, a significant time for realignment during which time the growth face is essentially inactive, or 'poisoned'.

The morphology and thermal behavior of the elevated pressure crystallized materials were consistent with the proposed orthorhomobic crystal structure. The lamellar thickness decreased with increasing pressure (or increasing γ content) and this decrease is expected from the differences in arrangement of chain stems in the lamellae for the α and γ forms. The elevated temperature WAXD and SAXS supported the orthorhombic crystal structure also. WAXD indicated a conversion from the γ to α form on increasing the sample temperature to a value below the atmospheric pressure DSC peak melting temperature. The γ material would convert to α at a temperature where only a small amount of the material was shown to melt. The elevated temperature SAXS indicated that the lamellar thickness of the elevated pressure crystallized material increased with increasing temperature. The observed increase in lamellar thickness for the pressure

crystallized material was larger than that for the atmospheric pressure crystallized material. At a SAXS scan temperature of 145°C, the lamellar thickness of the γ form approached that of the α form.

Table of Contents

Section		Page
1	Introduction	1
2	Review of Theoretical Background and Literature	3
	2.1 Polymer Crystallization and Morphology	3
	2.2 Polymer Fold Surface	20
	2.3 Crystallization Theory	26
	2.4 Melting of Polymer Crystals	50
	2.5 The Effects of Pressure	55
	2.6 Molecular Weight Effects	60
	2.7 Polymerization	63
	2.8 Polymer Molecular Weights	64
	2.9 Tacticity Analysis	66
	2.10 Small Angle X-ray Scattering	72
3.	Experimental and Analytical Techniques	88
	3.1 Materials	88
	3.2 Crystallization	88
	3.3 Morphology	95
	3.4 Thermal Analysis	96
	3.5 Small Angle X-ray Scattering	97
4.	Results	103
	4.1 Wide Angle X-ray Diffraction	103
	4.2 Small Angle X-ray Scattering	121
	4.3 Thermal Analysis	152
	4.4 Infrared Spectroscopy of Polypropylene	161
	4.5 Optical and Electron Microscopy	177
	4.6 Crystallization - Atmospheric Pressure	195
	4.7 Crystallization - Elevated Pressure	203
5.	Discussion	212
	5.1 Crystallinity	212
	5.2 Small Angle X-ray Scattering	214
	5.3 T_{mo}, σ_e	247
	5.4 Kinetics Analysis	264
6.	Conclusions	314
	6.1 Morphology	315
	6.2 Thermal Behavior	316
	6.3 Crystallization Behavior	316
	6.4 Growth Front 'Poisoning'	317
7.	Recommendations for Further Work	319
	7.1 T_m^o of γ Polypropylene	319
	7.2 Stem Length Determination in α and γ PP	320
	7.3 Copolymer Studies	320
	7.4 Additional Elevated Pressure Studies	320

List of References 322

VITA 331

List of Tables

Table		Page
2.1	Keith-Padden Classification of Polypropylene Spherulites.	14
2.2	Polymers Exhibiting Regime Transitions	46
2.3	Surface Free Energies and Work of Chain Folding for -C-C- Polymers.	47
2.4	Kinetics Analysis of Isotactic Polypropylene from Literature.	49
2.5	Kinetics Results for Elevated Pressure Crystallization.	51
2.6	Infrared Band Assignments for Isotactic Polypropylene.	71
3.1	Isotactic Polypropylene Material Parameters.	89
4.1	X-ray Relative Intensities for Isotactic Polypropylene Isothermally Crystallized at Atmospheric Pressure...	106
4.2	WAXD Apparent Crystal Size (110).	107
4.3	FTIR Relative Intensities for Isotactic Polypropylene Crystallized at Atmospheric Pressure and Elevated Pressure; Reference Frequency = 1380 cm^{-1}.	174
4.4	FTIR Relative Intensities for Isotactic Polypropylene Crystallized at Atmospheric Pressure and Elevated Pressure; Reference Frequency = 2866 cm^{-1}.	179
5.1	SAXS Data for Isotactic Polypropylene Homopolymer Mw = 151,000 isothermally crystallized at atmospheric pressure.	216
5.2	SAXS Data for Isotactic Polypropylene Copolymer M_w = 151,000 isothermally crystallized at atmospheric pressure.	217
5.3	SAXS Data for Isotactic Polypropylene Homopolymer M_w = 151,000 isothermally crystallized at various elevated pressures, $\Delta T = 50°C$.	226
5.4	Comparison of Long Periods Determined from SAXS Observed Intensity and Electron Density Correlation Function.	232

5.5 Equilibrium melting temperature and thickening factor for atmospheric pressure crystallization. 251

5.6 Values of fold surface free energy for isotactic polypropylene. 256

5.7 Values of the Equilibrium melting temperature, T_m^o, and the Thickening factor, γ, for isotactic polypropylene crystallized at elevated pressure. 260

5.8 Isotactic Polypropylene Input Parameters for Atmospheric Pressure Kinetics Analysis. 267

5.9 Kinetics Analysis of Isotactic Polypropylene Crystallized at Atmospheric Pressure. 271

5.10 Kinetics Analysis with Variation of U* for Isotactic Polypropylene, Mw = 83,000 Crystallized at Atmospheric Pressure. 276

5.11 Kinetics Analysis for Isotactic Polypropylene 83,000 M_w Homopolymer - $f(T_m^o, T_g)$. 278

5.12 Isotactic Polypropylene Input Parameters for Kinetics Analysis at Various Elevated Pressures. 282

5.13 Kinetics Analysis of Isotactic Polypropylene Crystallized at Elevated Pressure. 290

5.14 Kinetics Analysis with Variation of T_m^o for Isotactic Polypropylene Crystallized at Elevated Pressure..... 291

5.15 Comparison of Kinetics Analysis from Linear Growth Data, Half-Time Data, and Nucleation Corrected Half-Time Data for Atmospheric Pressure Crystallization.. 303

5.16 Comparison of Kinetics Analysis from Linear Growth Data, Half-Time Data, and Nucleation Corrected Half-Time Data for Elevated Pressure Crystallization..... 304

List of Figures

Figure		Page
2.1	Schematic of a polyethylene single crystal.	5
2.2	Schematic of chain stem arrangements in unit cell of A. γ polypropylene, and B. α polypropylene.	8
2.3	Schematic of a polymer spherulite.	10
2.4	Possible polymer growth paths.	11
2.5	Schematic of branching and 'cross-hatching' in isotactic polypropylene	16
2.6	Epitaxial packing schematic for branching of α tangential branch on α radial branch.	18
2.7	Representation of chain configurations in isotactic polypropylene.	19
2.8	Polymer chain folding models: A. adjacent re-entry, B. switchboard.	21
2.9	Fringed micelle model.	22
2.10	Lauritzen-Hoffman crystallization regimes schematic.	28
2.11	Free energy of formation of chain folded surface nucleus.	30
2.12	Polymer lamellar crystal idealized schematic.	38
2.13	Infrared spectra of stereoregular forms of polypropylene: A. atactic, B. syndiotactic, C. isotactic.	68
2.14	Vibrational modes of the CH_3 group in isotactic polypropylene. Axial C-C bonds are shown in heavy lines.	69
2.15	Vibrational modes of the CH_2 group and the CH group in isotactic polypropylene.	70
2.16	Schematic of various electron density distributions and the associated correlation functions.	75

2.17 SAXS apparent long period Lapp versus H. 80

2.18 Schematic of coordinate system for branching and curving lamellae. 83

2.19 Appearance of a two-dimensional correlation function to account for lamellar branching and curving . . 85

3.1 Molecular weight distribution curves for isotactic polypropylene homopolymer samples as received. ... 90

3.2 Elevated pressure system schematic and photograph. .. 92

3.3 Elevated pressure cell schematic and photograph. 93

3.4 Elevated pressure system heat exchanger schematic. .. 94

3.5 Schematic of the NCSASR 10 meter SAXS spectrometer at ORNL. 99

3.6 In situ SAXS experimental equipment for measurement of SAXS at elevated temperatures. 102

4.1 WAXD as a function of crystallization temperature for isotactic polypropylene 151,000 M_w homopolymer crystallized at atmospheric pressure 104

4.2 Flat plate WAXD of atmospheric pressure and elevated pressure isothermally crystallized isotactic polypropylene, ΔT = 50°C; A. Atmospheric pressure, B. 100 MPa, and C. 200 MPa. 109

4.3 WAXD as a function of crystallization pressure for isotactic polypropylene 151,000 M_w homopolymer, ΔT = 50°C. 110

4.4 Composition from WAXD of isotactic polypropylene crystallized at elevated pressure. 111

4.5 WAXD at elevated temperature of isotactic polypropylene isothermally crystallized at atmospheric pressure, T_c = 129°C. Scan temperatures indicated on figure. ... 115

4.6 Length of the a axis and the b axis of isotactic polypropylene monoclinic unit cell as a function of scan temperature from WAXD. 116

4.7 WAXD at elevated temperature of isotactic polypropylene isothermally crystallized at elevated pressure, ΔT = 50°C, P_c = 100 MPa. Scan temperatures indicated on figure. 119

4.8 SAXS two-dimensionally averaged contour plot for isotactic polypropylene 151,000 M_w isothermally crystallized at T_c = 138°C 123

4.9 SAXS radially averaged intensity I versus scattering vector q for isotactic polypropylene 151,000 M_w homopolymer isothermally crystallized at atmospheric pressure and several crystallization temperatures. . 124

4.10 SAXS Lorentz corrected data for the data of Figure 4.9. 125

4.11 Comparison of the Lorentz corrected SAXS behavior for the isotactic polypropylene 151,000 M_w homopolymer and copolymer at two isothermal crystallization temperatures, 129°C and 146°C. 127

4.12 SAXS radially averaged intensity I versus scattering vector q for isotactic polypropylene 151,000 M_w copolymer (0.5% ethylene) isothermally crystallized at atmospheric pressure and several crystallization temperatures. 128

4.13 SAXS Lorentz corrected data for the data of Figure 4.12 129

4.14 SAXS radially averaged intensity versus scattering vector as a function of crystallization time at T_c = 129°C for isotactic polypropylene 151,000 M_w homopolymer. 132

4.15 SAXS Lorentz corrected data for the data of Figure 4.14. 134

4.16 SAXS radially averaged intensity versus scattering vector as a function of crystallization time at T_c = 146°C for isotactic polypropylene 151,000 homopolymer. 135

4.17 SAXS Lorentz corrected data for the data of Figure 4.16. 137

4.18 SAXS radially averaged intensity versus scattering vector as a function of crystallization pressure. . 138

4.19 SAXS Lorentz corrected data for the data of Figure 4.18. 140

4.20 SAXS one-dimensional radially averaged intensity as a function of crystallization temperature at a crystallization pressure of 100 MPa. 141

4.21 SAXS Lorentz corrected data for the data of Figure 4.20. 143

4.22 SAXS one-dimensional radially averaged intensity as a function of crystallization temperature at a crystallization pressure of 200 MPa. 144

4.23 SAXS radially averaged intensity I vs scattering vector q for isotactic polypropylene isothermally crystallized at T_c = 129°C, atmospheric pressure; SAXS intensity profiles recorded at temperatures indicated. 146

4.24 SAXS long period from Lorentz corrected data versus in situ scan temperature for isotactic polypropylene isothermally crystallized at T_c = 129°C; atmospheric pressure. 148

4.25 SAXS observed intensity profile for the 100 MPa crystallized data as a function of scan temperature. 149

4.26 SAXS long period from Lorentz corrected data versus in situ scan temperature for isotactic polypropylene isothermally crystallized at ΔT = 50°C; various pressures. 151

4.27 DSC melting behavior for isotactic polypropylene 83,000 M_w as a function of isothermal crystallization temperature; heating rate = 10°C/min. 153

4.28 Comparison of DSC melting behavior for isotactic polypropylenes isothermally crystallized at atmospheric pressure, T_c = 129°C; heating rate = 10° C/min. 154

4.29 Atmospheric pressure DSC melting behavior for isotactic polypropylene isothermally crystallized at ΔT = 50°C, atmospheric and elevated pressure; heating rate = 10°C/min. 156

4.30 Typical depolarized light intensity melting curves as a function of isothermal crystallization temperature for isotactic polypropylene crystallized at atmospheric pressure; heating rate = 10°C/min. 158

4.31 Typical depolarized light intensity melting curves as a function of isothermal crystallization temperature for isotactic polypropylene crystallized at various pressures; heating rate = 3°C/min. 160

4.32 Typical depolarized light intensity melting curves as a function of isothermal crystallization temperature for isotactic polypropylene crystallized at 50 MPa; heating rate = 3°C/min. 162

4.33 Infrared absorbance spectra for isotactic polypropylene 151,000 M_w homopolymer isothermally crystallized at the indicated temperatures. 164

4.34 Infrared absorbance spectra of Figure 4.33 for the frequency range 1500 $cm^{-1} < \nu < 500\ cm^{-1}$. 165

4.35 Relative intensities of various frequencies (reference frequency = 1380 cm^{-1}) as a function of isothermal crystallization temperature for isotactic polypropylene 151,000 M_w homopolymer. 166

4.36 Infrared absorbance spectra for isotactic polypropylene 151,000 M_w copolymer isothermally crystallized at the indicated temperatures. 168

4.37 Infrared absorbance spectra of Figure 4.36 for the frequency range 1500 $cm^{-1} < \nu < 500\ cm^{-1}$. 169

4.38 Relative intensities of various frequencies (reference frequency = 1380 cm^{-1}) as a function of isothermal crystallization temperature for isotactic polypropylene 151,000 M_w copolymer. 170

4.39 Comparison of Infrared absorbance for isotactic polypropylene 151,000 M_w homopolymer and copolymer $4000 < \nu < 400\ cm^{-1}$. 171

4.40 Comparison of Infrared absorbance for isotactic polypropylene 151,000 M_w homopolymer and copolymer, $1500\ cm^{-1} < \nu < 500\ cm^{-1}$. 172

4.41 Infrared absorbance spectra for isotactic polypropylene 151,000 M_w homopolymer isothermally crystallized at elevated pressure. 175

4.42 Infrared absorbance spectra of Figure 4.41 for the frequency range 1500 $cm^{-1} < \nu < 500\ cm^{-1}$. 176

4.43 Relative intensities of various frequencies (reference frequency = 1380 cm^{-1}) as a function of crystallization pressure for isotactic polypropylene 151,000 M_w homopolymer. 178

4.44 TEM micrographs of isotactic polypropylene 151,000 M_w copolymer (0.5% ethylene) isothermally crystallized at atmospheric pressure; A. T_c = 135°C, and B. T_c = 145°C. 181

4.45 TEM micrographs of isotactic polypropylene 151,000 M_w homopolymer isothermally crystallized at atmospheric pressure; A. T_c = 145°C, B. T_c = 145°C, enlargement of tangential branching. 182

4.46 TEM micrographs of isotactic polypropylene 151,000 M_w homopolymer isothermally crystallized at atmospheric pressure; A. T_c = 135°C, B. T_c = 145°C, ... 183

4.47 Reflection optical micrographs of permanganic etched surfaces of elevated pressure crystallized isotactic polypropylene, 151,000 M_w; A. 25 MPa, B. 50 MPa. .. 185

4.48 Reflection optical micrographs of permanganic etched surfaces of isotactic polypropylene homopolymer, ΔT = 50°C; A. 75 MPa, and B. 100 MPa. 186

4.49 Reflection optical micrographs of permanganic etched surfaces of elevated pressure crystallized isotactic polypropylene 151,000 M_w (ΔT = 50°C); A. 125 MPa, and B. 200 MPa. 187

4.50 TEM micrographs of elevated pressure crystallized isotactic polypropylene 151,000 M_w homopolymer; A. 25 MPa, B. 50 MPa. 189

4.51 TEM micrographs of elevated pressure crystallized isotactic polypropylene 151,000 M_w homopolymer; A. 50 MPa, B. 75 MPa. 190

4.52 TEM micrograph of elevated pressure crystallized isotactic polypropylene 151,000 M_w homopolymer (ΔT = 50°C); P_c = 100 MPa. 191

4.53 Schematic of branching in isotactic polypropylene . 193

4.54 Schematic of γ lamellae 194

4.55 Linear growth rate determination from radius versus time at several crystallization temperatures for isotactic polypropylene homopolymer, M_w = 83,000 (atmospheric pressure). 196

4.56 Linear growth rates as a function of crystallization temperature for isotactic polypropylene isothermally crystallized at atmospheric pressure. 198

4.57 Induction times determined from depolarized light intensity (DLI) as a function of supercooling for isotactic polypropylene isothermally crystallized at atmospheric pressure. 200

4.58 Nucleation density N versus crystallization temperature T_c for isotactic polypropylene crystallized at atmospheric pressure. 202

4.59 Linear growth rate determination from radius versus time at several crystallization temperatures for isotactic polypropylene 151,000 M_w homopolymer (P_c = 75 MPa). 204

4.60 Linear growth rates as a function of crystallization temperature for isotactic polypropylene isothermally crystallized at atmospheric and elevated pressure. . 205

4.61 Induction times determined from DLI as a function of supercooling for isotactic polypropylene isothermally crystallized at elevated pressure. 207

4.62 Induction times determined from DLI as a function of supercooling for isotactic polypropylene isothermally crystallized at atmospheric and elevated pressure. . 209

4.63 Nucleation density N versus crystallization temperature T_c for isotactic polypropylene crystallized at atmospheric and elevated pressure. 210

5.1 Crystallization temperature Tc versus % crystallinity from WAXD for isotactic polypropylene 151,000 M_w isothermally crystallized at atmospheric pressure. .. 213

5.2 Crystallization temperature Tc versus lamellar thickness from SAXS q-I data for isotactic polypropylene 151,000 M_w homopolymer and copolymer isothermally crystallized at atmospheric pressure. 218

5.3 Definition of SAXS characteristic parameters D and H.220

5.4 Crystallization temperature Tc versus SAXS H for isotactic polypropylene 151,000 M_w homopolymer and copolymer isothermally crystallized at atmospheric pressure. 221

5.5 SAXS long period from q-I data versus SAXS H for isotactic polypropylene 151,000 M_w homopolymer and copolymer isothermally crystallized at atmospheric pressure. 223

5.6 Crystallization temperature Tc versus SAXS D for isotactic polypropylene 151,000 M_w homopolymer and copolymer isothermally crystallized at atmospheric pressure 224

5.7 Theoretical Electron density distribution for spheres, rods, and disks. 231

5.8 Electron density distribution for isotactic polypropylene isothermally crystallized (ΔT = 47°C, atmospheric pressure). SAXS intensity profile recorded at 25°C. 233

5.9 Electron density distribution correlation function for isotactic polypropylene isothermally crystallized (ΔT = 47°C, atmospheric pressure). SAXS intensity profile recorded at 25°C. 235

5.10 SAXS long period from observe intensity profile versus long period from SAXS electron density correlatin function. 236

5.11 Electron density distribution for isotactic polypropylene isothermally crystallized (ΔT = 58°C, atmospheric pressure). SAXS intensity profiles recorded at temperatures indicated (°C). 238

5.12 Electron density distribution correlation function for isotactic polypropylene isothermally crystallized (ΔT = 58°C, atmospheric pressure). SAXS intensity profiles 239

5.13 Electron density distribution for isotactic polypropylene isothermally crystallized (ΔT = 50°C, P_c = 100 MPa). SAXS intensity profiles recorded at temperatures indicated (°C). 241

5.14 Theoretical SAXS intensity profiles from varaible stack model with Gaussian thickness distribution (σ_x = 0.1) and Gaussian crystallinity distribution (σ_c as indicated). 245

5.15 Theoretical SAXS intensity profiles from varaible stack model with Gaussian crystallinity distribution (σ_c = 0.1) and Gaussian thickness distribution (σ_x as indicated). 246

5.16 Melting temperature (DLI) vs isothermally crystallized temperature for isotactic polypropylene crystallized at atmospheric pressure. 249

5.17 Reciprocal lamellar thickness from SAXS Lorentz corrected data vs melting temperature from DSC retur-to-baseline for isotactic polypropylene 151,000 M_w homopolymer and copolymer isothermally crystallized at atmospheric pressure. 252

5.18 Reciprocal supercooling versus lamellar thickness from SAXS Lorentz corrected data for isotactic polypropylene 151,000 Mw homopolymer and copolymer isothermally crystallized at atmospheric pressure. 254

5.19 Crystallization temperature versus initial lamellar thickness l_g^* calculated from SAXS Lorentz corrected data and DSC thickening factor γ. Curves are theoretical predictions with indicated fold surface free energy σ_e. 258

5.20 Melting temperature (DLI) vs isothermally crystallized temperature for isotactic polypropylene crystallized at atmospheric pressure and elevated pressure. 259

5.21 Equilibrium melting temperature T_m^o vs crystallization pressure for isotactic polypropylene. Line represents theoretical calculation from Clapeyron equation for α polypropylene. 262

5.22 Reciprocal lamellar thickness from SAXS Lorentz corrected data versus melting temperature from DLI for isotactic polypropylene isothermally crystallized at 100 MPa and 200 MPa. 263

5.23 Kinetics analysis for isotactic polypropylene crystallized at atmospheric pressure. (U^* = 1500 cal/mole, T_m^o = 187°C, T_g = -12°C). 269

5.24 Kinetics analysis of atmospheric pressure crystallized isotactic polypropylene with variation of U^*. 274

5.25 Kinetics analysis for isotactic polypropylene crystallized at atmospheric pressure and 25 MPa. .. 284

5.26 Kinetics analysis for isotactic polypropylene crystallized at 35, 50, and 75 MPa. 285

5.27 Kinetics analysis for isotactic polypropylene crystallized at 100, 150, and 200 MPa. 286

5.28 Supercooling of regime transitions versus crystallization pressure. 287

5.29 Crystallization Pressure Pc (MPa) versus regime transition temperature TII/III for isotactic polypropylene. 289

5.30 Nucleation constant K_g versus crystallization pressure P_c. 292

5.31 Calculated linear growth rates with experimental data superposed on the curve (isotactic polypropylene 151,000 M_w homopolymer, atmospheric pressure). 294

5.32 Nucleation and diffusion components of linear growth rate for isotactic polypropylene 151,000 M_w homopolymer. 296

5.33 Crystallization temperature vs log of the linear growth rate for Regimes I, II, and III calculated from kinetics analysis for isotactic polypropylene 151,000 M_w homopolymer crystallized at atmospheric pressure. ... 297

5.34 Kinetics analysis comparison for linear growth data, half-time data, and nucleation corrected half-time data302

5.35 Comparison of experimentally observed bulk crystallization behavior and that theoretically calculated from linear growth rate for isotactic polypropylene homopolymer T_c = 140°C. 307

5.36 Schematic of growth front poisoning for isotactic polypropylene; A. α growth front, B. γ growth front.312

Chapter 1

Introduction

Since the discovery of stereospecific polymerization in 1954, polypropylene has become one of the most important commodity plastics and further improvements are still expected. The demand for polypropylene continues to grow, due to polypropylene's relatively low cost and the availability of a wide range of resins. Injection molded products presently use about a third of the annual consumption. Since the injection molding process, as well as other fabrication processes, involves the application of pressure to the polymer during crystallization, an understanding of the relation between pressure and polymer crystallization is of considerable importance.

The effect of pressure on polymer crystallization has not been extensively studied. Crystallization at elevated pressure can be significantly different from that at atmospheric pressure. For some polymers, crystal structure and morphology change dramatically. During the past twenty-five years, the research on the effects of pressure on polymers has mainly concentrated on morphology and bulk crystallization. Some recent elevated pressure research has evaluated linear growth. The work of Phillips and Edwards [59] was the first extensive source of crystallization

kinetics data at elevated pressure. Phillips and Edwards studied the linear growth of cis-polyisoprene for pressures up to 400 MPa. More recently, Phillips and Dalal [94] and Phillips and Tseng [56] have applied secondary nucleation theory to elevated pressure kinetics data for cis-polyisoprene, poly(ethyleneterephthalate) and polyethylene. The effect of pressure on the regime transition temperature can give information on the nature of the transition. A diffusion controlled mechanisms would exhibit a regime transition shift with pressure that follows the glass transition shift with pressure. A nucleation controlled mechanism would exhibit a regime transition shift with pressure that follows the equilibrium melting temperature shift with pressure.

The objective of this dissertation is to obtain the linear growth data for isotactic polypropylene as a function of crystallization pressure. Linear growth rates were obtained by direct optical measurement in a custom high pressure hot stage apparatus. The morphology of elevated pressure crystallized samples was studied with optical microscopy, electron microscopy, wide angle X-ray diffraction, and small angle X-ray scattering.

Chapter 2

Review of Theoretical Background and Literature

2.1 Polymer Crystallization and Morphology

When polymer molecules can crystallize, the extent of crystallization is affected by such factors as structural regularity, chain substituents, and branching. Crystalline polymers are distinguished from other crystalline materials in that they are only semicrystalline. The density of a crystalline polymer is found to be between that of fully crystalline polymer and that of fully amorphous polymer. The x-ray diffraction pattern, while indicating the existence of long-range order, is usually in the form of rings superimposed on a diffuse background.

Polymers capable of crystallizing can form ordered structures from the melt or from dilute solution. These ordered structures contain the polymer molecules folded back and forth on themselves to some degree. The crystallization process involves the transformation of the disordered amorphous state to the ordered crystalline state. These crystals form in platelets or ribbons, usually referred to as lamellae.

2.1.1 Single Crystals

Single crystals of a polymer can be formed by cooling a dilute polymer solution, Keller [1] having grown polyethylene single crystals by this method. These crystals are lamellar in habit and are approximately 100 angstroms thick (Figure 1). Electron diffraction indicates that the polymer molecules are normal to the relatively large upper and lower surfaces of the crystal. Keller thus concluded that the polymer molecules are folded back and forth on themselves within the crystals. Similar observations by Fischer [2] and Till [3] supported this conclusion. Thus the upper and lower crystal surfaces must consist of molecular folds of one form or other (Figure 2.1). Factors controlling the size and shape of single crystals include solvent, concentration, and temperature. The thickness of lamellae is affected by the crystallization temperature and by any further annealing treatments.

From a nucleus, the lamella grows along its lateral edges, with the molecules folding back and forth along these edges. Sectors of growth are distinguished by the plane of folding, thus the single crystal can by subdivided into sectors of growth. Single crystals usually form a nonflat hollow pyramid-like morphology, the different sectors forming the pyramid's panels (Figure 2.1). The pyramids often

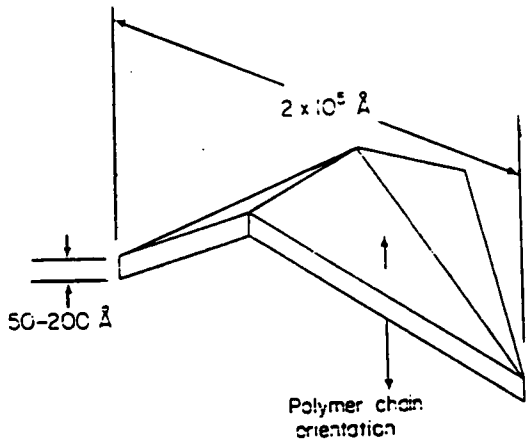


Figure 2.1 Schematic of a polyethylene single crystal.

collapse and flatten during normal sample collection resulting in crystals with corrugations.

2.1.2 Crystalline Structure in IPP

The crystalline structure of isotactic polypropylene can be addressed on three distinctly different morphological levels. On the level of the spherulite, isotactic polypropylene exhibits a variety of spherulite types classified typically on the basis of the sign and magnitude of the birefringence. At the crystal lattice level, isotactic polypropylene exhibits a range of polymorphs, distinguished by the arrangement of the chains of otherwise identical conformation (3_1 helices). At the lamellar level, isotactic polypropylene can produce lamellae differing in nature as well as arrangement (radial-tangential). There has been shown to be an interrelation between the structural multiplicity on the three distinct levels.

The predominant crystal structure of isotactic polypropylene is the monclinic α structure, first determined by Natta and Corradini [4]. The hexagonal β structure [5] occurs sporadically at low isothermal crystallization temperature ($T_c < 130°C$) or in crystallization in a temperature gradient. This polymorph generally is only a minor component in the bulk sample, with the remaining material crystallizing as the a structure. A third polymorph γ was observed by Turner-Jones et al. [6]. The γ form was

originally assigned a triclinic unit cell with the unit cell being similar to that of the α form, with a slip along the c-axis direction. The γ form has been observed from crystallization of low molecular weight fractions (M_w = 15,000) and stereoblock copolymers, and from crystallization at elevated pressure. Recently, Brückner and Meille [7] have proposed a face-centered orthorhombic unit cell for the γ form with the unique arrangement of non-parallel chain stems in the unit cell. Figure 2.2 represents the arrangement of chain stems in the α monoclinic and the γ orthorhombic unit cell. While this non-parallel arrangement of chain stems is unique among polymers, the driving force for such packing could be the favorable registration of helices.

The monoclinic unit cell has dimensions a = 6.65 Å, b = 20.96 Å, and c = 6.50 Å, with $\alpha = \gamma = 90°$, and $\beta = 99.3°$. The space group has been assigned C2/c for the statistically ordered arrangement of up and down stems in the unit cell or alternately the $P2_1/c$ space group for the random arrangement of up and down stems in the unit cell. The γ form has dimensions for the orthorhombic unit cell of a = 8.54 Å, b = 9.93 Å, and c = 42.41 Å with space group Fddd or Fdd2. The previously reported triclinic unit cell [8] has dimensions of a = 6.54 Å, b = 21.40 Å, c = 6.50 Å, $\alpha = 89°$, $\beta = 99.6°$, and $\gamma = 99°$. In the orthorhombic unit cell, the chains lie parallel to both the diagonals in the a-b plane (which

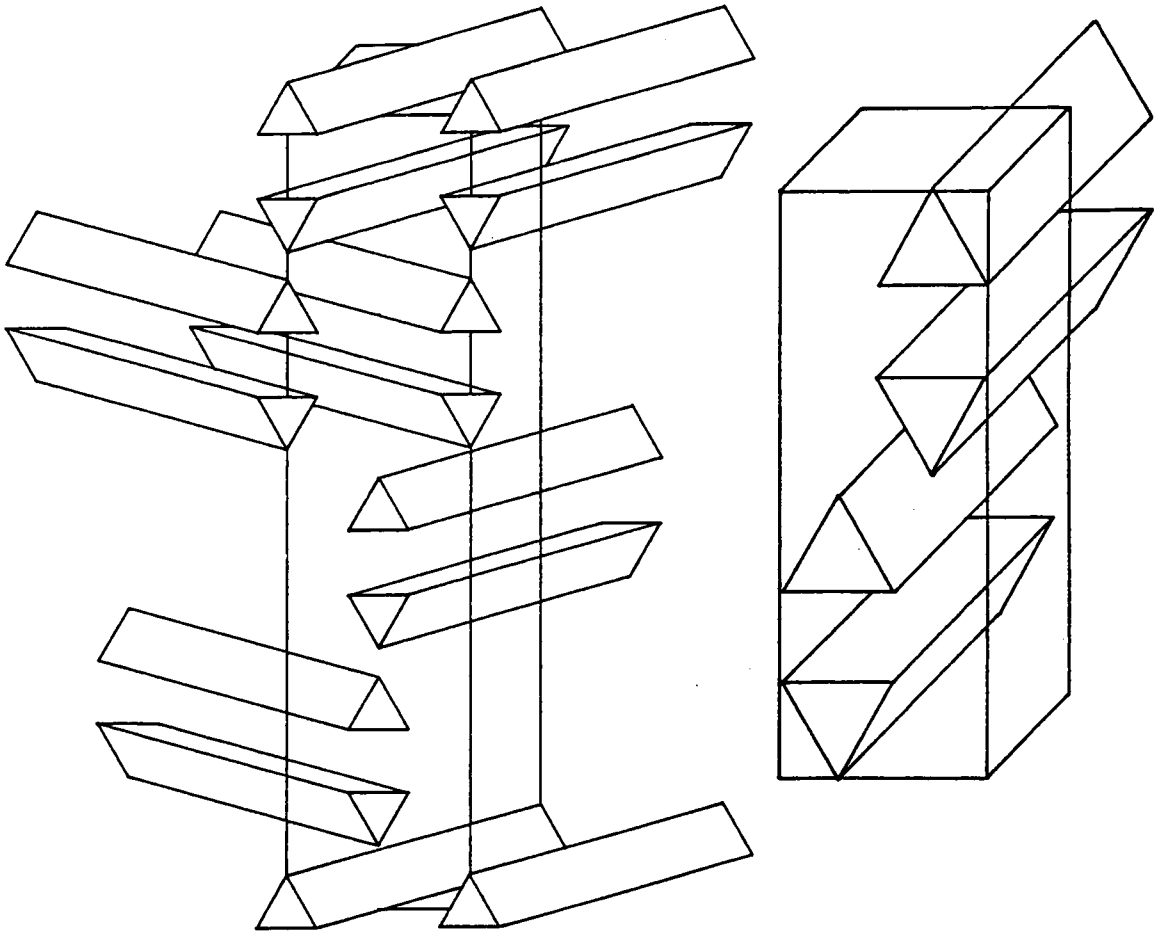


Figure 2.2 Schematic of chain stem arrangements in unit cell of A. γ polypropylene, and B. α polypropylene.

measure 13.08 Å or twice the isotactic polypropylene helical periodicity) and form an angle of 81.2°. This angle is approximately that formed by the chain axes in branched a polypropylene crystals.

2.1.3 Spherulites

Spherulitic aggregates of a crystallizable polymer can be formed by cooling a quiescent polymer melt. Spherulites consist of chain folded lamellae radiating outward from a central nucleus (Figure 2.3). The radial dimension of the spherulite increases linearly with time until the spherulite impinges on other growing spherulites. The fibrillar lamellae that compose the spherulite are on the order of 100 A thick and may be several hundred or even thousands of angstroms in width. Although exact details of its composition are unknown, the nucleus is considered to be a single crystal or fibril, a stack of single crystals or fibrils, or an inhomogeneity such as a dust particle. The spherulite develops from the nucleus through the growth path shown in Figure 2.4. In primary crystallization, the growing entity evolves from the nucleus through sheaf-like structures into the growing spherulite. Growth continues until the spherulite impinges with other growing spherulites, becoming a polyhedron. Secondary crystallization occurs within the spherulite, transforming a portion of the interlamellar

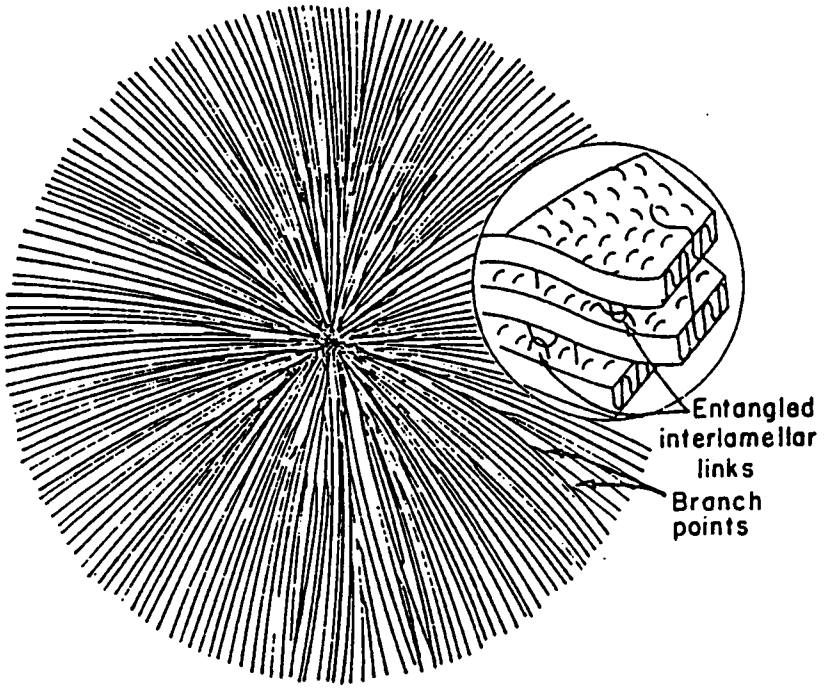


Figure 2.3 Schematic of a polymer spherulite.

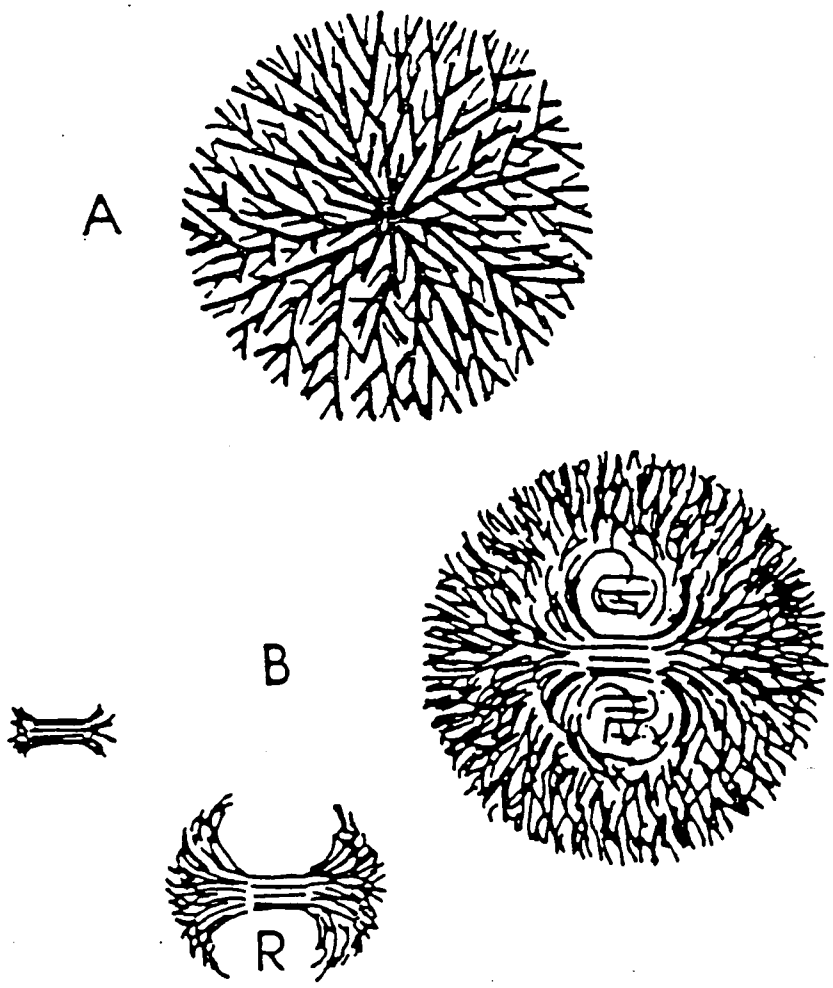


Figure 2.4 Possible polymer growth paths.

material into crystalline material. The fine structure of the spherulite will depend on the nature of branching of the growing radial lamellae and on the form of the crystals between branches. Spherulites have generally been described as radially growing lamellae branching at small angles.

Isotactic polypropylene (iPP) can exhibit at least four distinct crystal structures: the α-form, which is monoclinic and generally predominant; the β-form which is hexagonal; the γ-form which is triclinic; and a "smectic" form believed to be associated with the amorphous phase. The morphology observed in melt crystallized isotactic polypropylene spherulites was first reported by Padden and Keith [9] who classified the spherulites depending on crystallization temperature, T_c, and the observed birefringence and growth rates. For T_c less than 132°C, isotactic polypropylene spherulites are of α_I form and exhibit a positive birefringence. For T_c greater than approximately 138°C, the spherulites are of α_{II}-form and exhibit a negative birefringence. However, for T_c less than 140°C, the largest number of observed spherulites are 'mixed' in that they possess no distinct Maltese cross and are revealed as radiating arrays of intermingled areas of positive and negative birefringence. The birefringence change of α-form spherulites has been related to a variation of the relative amounts of radial and tangential lamellae inside the spherulites [10]. Thus the low T_c spherulites

have high tangential lamella content. At high T_c (145°C) lamellae are nearly all radial and straight for long distances, sometimes the length of a radius. However cross-hatching has been observed as high as 155°C. Radial lamellae are thicker than tangential lamellae.[11] If positive α-form spherulites are taken near T_m, they turn negative, suggesting that the tangential lamellae melt leaving only the radial lamellae. These phenomena tend to indicate that tangential lamellae crystallize subsequently, possibly due to a segregation effect due to molecular weight or tacticity. The β-form spherulites occur infrequently below T_c = 132°C. The β-form nucleates at a much lower rate than α-form, but grows faster by between 20 percent and 70 percent [5]. Table 2.1 lists spherulite types according to Keith and Padden's classification. It has been shown that certain nucleating agents favor β-form crystallization. Quenching of the melt also produces large amounts of β-form [12]. The β-form consists of broad, locally parallel stacked lamellae just as in spherulites of other polymers. The lamellae are extended sheet structures in all dimensions rather than lath-like entities of the α-form spherulites. The γ-form appears in samples crystallized from fractions or crystallized at pressure [13]. The temperature ranges of the spherulite types should not be regarded as rigid values but rather representing trends. The ranges of formation and specific

Table 2.1. Keith-Padden Classification of Polypropylene Spherulites

Spherulite Type	I	Mixed	II	III	IV
Crystal Structure	α	α	α	β	β
Sign of Birefringence	$+\nu_e$	$+\nu_e$	$-\nu_e$	$-\nu_e$	$-\nu_e$
Magnitude of Birefringence	≈0.003	≈0.002	≈0.002	0.007	0.007
Crystallization Temperature	<134°C	134-138°C	>138°C	<122°C	126-132°C

details are influenced by several factors, including molecular weight, molecular weight distribution, and stereoregularity.

2.1.4 Axialites

Axialitic crystals can be formed from a polymer melt under certain conditions. High crystallization temperatures favor formation of axialites in certain polymers. Axialites are crystal lamellae grouped so that they resemble two slightly open books placed back to back. Axialites then can exhibit the optical properties of spherulites or single crystals depending on the viewing angle. Tie molecules or crystalline areas between lamellae have been suggested as limiting the splaying of the lamellae [14], but the phenomenon is not really understood.

2.1.5 Lamellae

The complex arrangement of lamellae that can be observed in isotactic polypropylene is also unique to polymers. Isotactic polypropylene has been shown to produce under certain conditions a three-dimensional array of nearly orthogonal 'cross-hatched' lamellae. Figure 2.5 shows schematically the lamellar arrangement observed in isotactic polypropylene. The radial-tangential lamellar arrangement does not exist for the β form. The β form rather exists as smooth stacks and sheets similar to the morphology of other

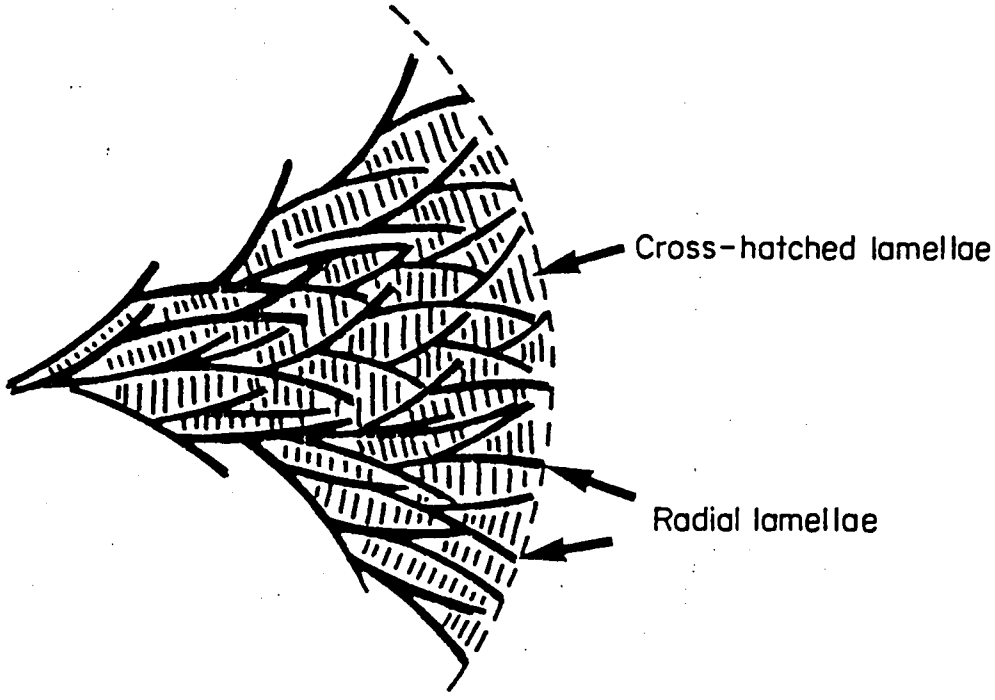


Figure 2.5 Schematic of branching and 'cross-hatching' in isotactic polypropylene (from Norton and Keller [11]).

polymers. There have been several proposed mechanisms for the radial-tangetial branching observed in isotactic polypropylene [15,16] but probably the most accepted currently is that of Lotz and Wittmann. Lotz and Wittmann propose that the arrangement of radial-tangential lamellae in isotactic polypropylene is a result of crystallographic and sturcutral interactions between the lattices of radial and tangential lamellae, with the interactions being of epitaxial character. Figure 2.6 represents the helical interactions for branching in isotactic polypropylene. This epitaxial branching mechanism led to the proposed orthorhombic unit. cell.

Chain Conformations of Isotactic Polypropylene

Isotactic polypropylene can exhibit four distinct conformations. These conformations are shown in Figure 2.7. The asymmetrically substituted carbon atom yields two stereoisomeric configuratons of the $CH(CH_3)$ group. The *d* and *l* configurations are distinguished by viewing along the chain axis. If the methyl group appears on the upper right hand side, the configuration is designated *d*. If rather the methyl group appears on the upper left had side, the configuration is designated *l*. A 100% isotactic chain can be represented by an all *d* or all *l* configuration, which are equivalent for isotactic polypropylene.

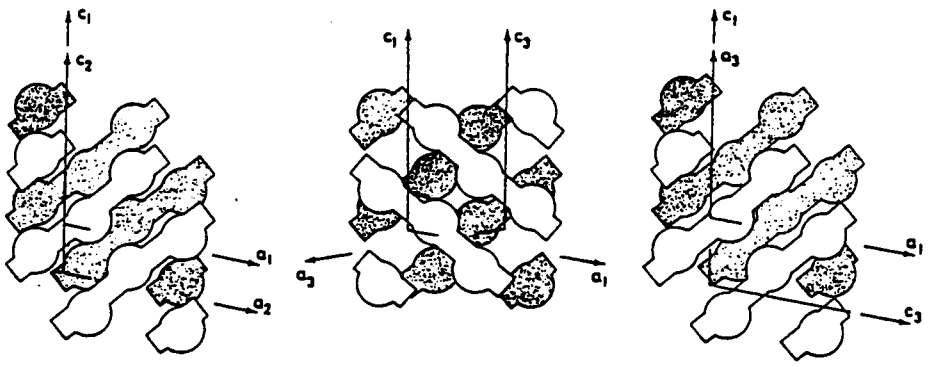


Figure 2.6 Epitaxial packing schematic for branching of α tangential branch on α radial branch (from [15]).

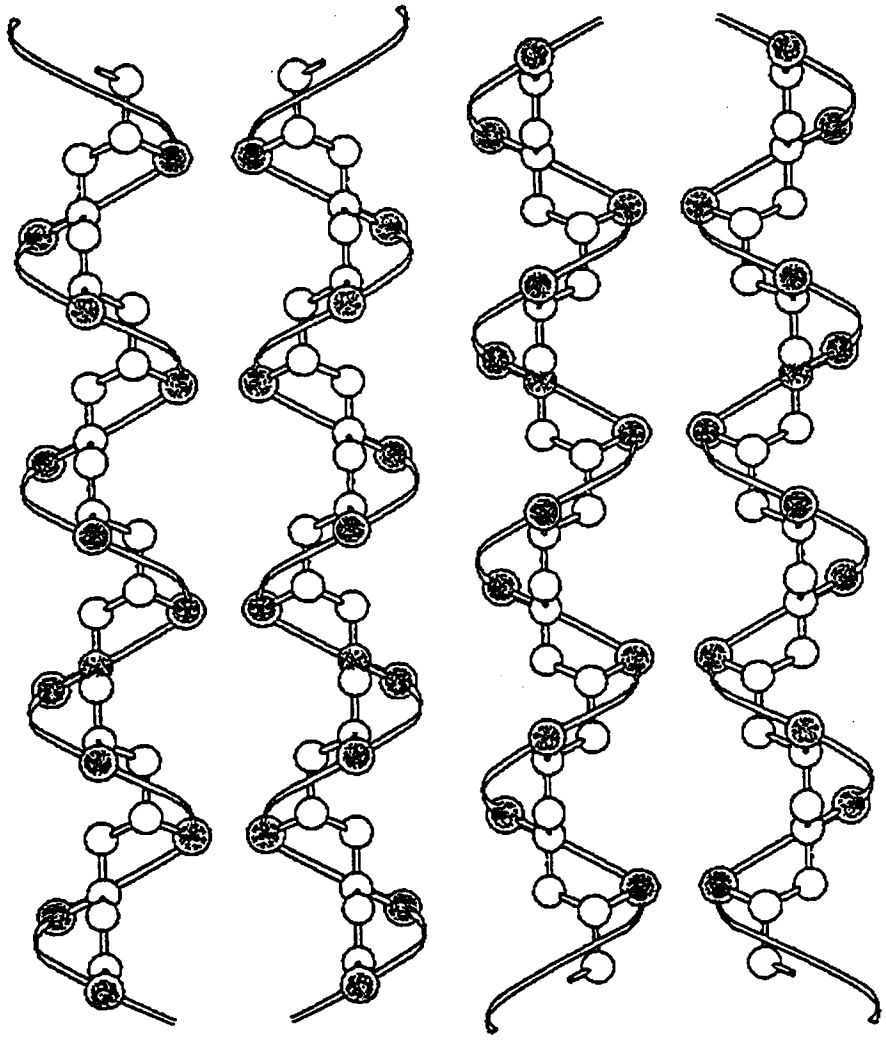


Figure 2.7 Representation of chain configurations in isotactic polypropylene.

2.2 Polymer Fold Surface

2.2.1 Fold Surface Nature

The nature of the fold surface of chain-folded polymer crystals is much debated. Various models describing the possible structure of the fold surface have been proposed . The adjacent re-entry model (AR) and the switchboard model (SB) are limiting extremes, represented schematically in Figure 2.8a and 2.8b. The AR model, proposed by Keller [1] , involves regular folding with short, uniform folds. The SB model, proposed by Flory [17] has irregular re-entry of the folded chains resulting in random, loose folds.

The fringed-micelle model proposed by Hermann et al.[18] was the first to address polymer crystallization. This model consists of long molecules traversing regions of order (crystalline) and disorder (amorphous). Figure 2.9 is a schematic of the fringed-micelle model. The limited information from x-ray line broadening suggested a small crystal size. The necessity of polymer chains folding on crystallization was identified by Keller [1], Till [3] , and Fisher [19]. The experimental evidence from electron microscopy and x-ray diffraction on polyethylene single crystals indicated that the polyethylene molecules lay in the crystals with the chain direction normal to the crystal surface.

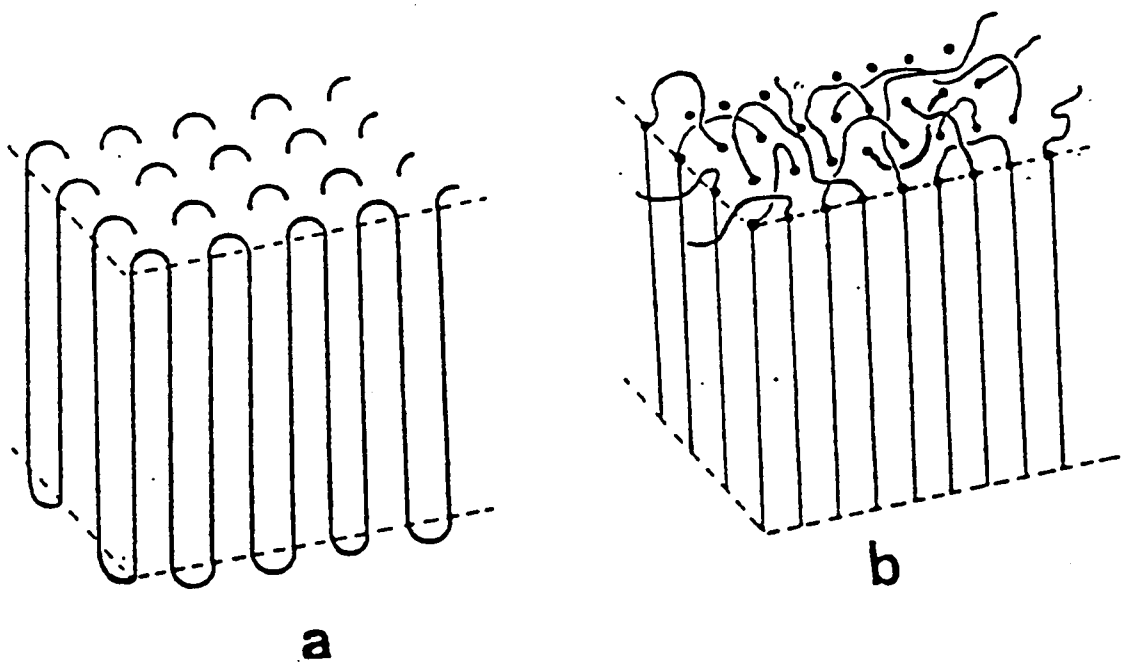


Figure 2.8 Polymer chain folding models: A. adjacent re-entry, B. switchboard.

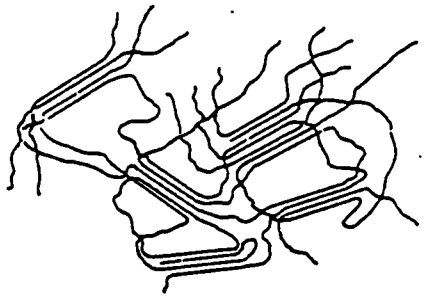


Figure 2.9 Fringed micelle model.

In the adjacent re-entry model, the nature of the folds results in a regularly folded surface. The only possible defects are the ends of the molecules which could either form as short length flexible rods above the surface (cilia) or else fold back into the crystal so that a "hole" is created within the crystal. A detailed analysis of infrared spectra of mixtures of deuterated and nondeuterated polyethylenes led Bank and Krimm [20] to conclude that the predominant type of folding involves adjacent re-entry. However the known existence of intercrystalline and interlamellar links show that non-adjacent re-entry must occur to some extent. The probability of adjacent re-entry being less than unity is accepted by most researchers that support the adjacent re-entry model. The probability of adjacent re-entry (P_{ar}) = 0.6 to 0.8 is typically claimed, and Hoffman [21] suggested P_{ar} = 0.3 to 0.5 is possible under conditions of high molecular weight and large supercoolings.

Various modifications of the adjacent re-entry model exist which include $P_{ar} < 1$. A model based on the "Gambler's Ruin" problem of mathematical statistics [22] predicts the minimum fraction of stems tightly folded in a semicrystalline polymer to be 2/3 for a simple cubic lattice with the stems normal to the surface. Hoffman [23] introduced a "variable cluster model" for crystallization at moderately large supercoolings.

The switchboard model is postulated primarily on the basis of space limitations at the crystal-liquid interface and the density defect nature of single crystals. In this model, while folding of the molecules exists, the molecules re-enter the crystal predominantly in a non-adjacent manner. The resulting fold surface is somewhat irregular with loops of various lengths due to random re-entry, entanglements, etc. Fischer [24] and Mandelkern [25] have proposed similar models. Mandelkern's interzonal model layers an interzonal region between the outermost amouphous region and the innermost crystalline region.

Different crystallizaton conditions lead to somewhat different macroscopic morphologies, observed directly using optical or electron microscopy. It is reasonable to assume that polymer molecules could have different fold structures dependent on the crystallization conditions. It is then difficult to apply either extreme model to describe the crystal structure as a function of various crystallization conditions. However, in order to obtain a reasonably simple treatment, the assumption of AR is used in most kinetic theories of polymer crystal growth. The various kinetic theories assuming adjacent re-entry or predominant adjacent re-entry have achieved some success in explaining several experimental observations. The theories adequately predict

growth rate and lamellar thickness for crystallization both from the melt at low supercoolings and from dilute solution.

2.2.2 Summary Arguments on Fold Surface Structure

Results from density and neutron scattering experiments and arguments based on the mobility of the crystallizing melt question the validity of the models of the polymer fold surface. The arguments against adjacent re-entry folding based on these observations follow.

Density: The densities measured for polymer single crystals are less than the densities determined from the unit cell dimensions of the polymer. The SB model and the AR model account for the discrepency in densities with the fold surfaces. The non-adjacent re-entry of the SB model creates a largely amorphous fold surface. The adjacent re-entry folds in the AR model also create a fold surface with a density lower than the crystal's interior, reducing the overall density of the crystal.

Neutron Scattering: Small angle neutron scattering can be used to determine dimensions and trajectories of isotopically labeled molecules in a host matrix. At very small angles, the radius of gyration of the labeled molecules can be determined in the host. Results on melt grown crystals show that the radius of gyration of the labeled molecules is only slightly smaller after crystallization than it was in the melt. Flory and Yoon [26] claim this small

reduction in radius of gyration supports the SB model, arguing that adjacent re-entry would have a larger effect on the radius of gyration. Hoffman [21] states that tie molecules and multiple nucleations on the same molecule result in the observed liquid-like radius of gyration. Hoffman [27] suggests that the radius of gyration is the limiting interlamellar spacing.

Mobility: Yoon and Flory [29] suggest that the rates of molecular disentanglements are sufficiently low to preclude AR folding. DiMarzio et al.[28] contend that reptation of the polymer molecule increases the expected rate of rearrangement such that sequences of AR folds are possible.

2.3 Crystallizaton Theory

Kinetic theories for polymer crystallization are based mostly on a modification of surface nucleation theory [29,30,31] but other theories exist that are not nucleation controlled [32]. The theory of Hoffman et al. will be reviewed extensively.

2.3.1 Background

Secondary nucleation theory predicts the growth rate and fold period of single crystals from solution and lamellae from the melt as a function of supercooling ΔT. The extent of supercooling determines the kinetic crystallization procedure of the polymer. Lauritzen and Hoffman [33] have

developed a kinetic theory for low and moderate supercooling. Regime I (single nucleation) kinetics describe crystallization at low supercoolings while Regime II (multiple nucleation) kinetics describe crystallization at moderate supercoolings. For large supercoolings, a more recent complementary kinetic theory [21,34] added another possible kinetic procedure. Regime III predicts narrowly spaced niches on the growth front.

2.3.2 Model

The idealized schematic model, shown in Figure 2.10, describes polymer lamellar crystal growth. The width, thickness, and height of the surface nucleus are represented by a, b, and l, respectively. The surface nucleus grows in the g direction, but the measured growth is in the G direction. The surface nucleus is considered to be started by a polymer segment or segments from the supercooled melt attaching to the lamellar surface. The first stem is formed at a cost of $2bl\sigma$. The molecule then folds back on itself in a position adjacent to the first stem. The adjacent positionis the most probable position for re-entry after folding since attachment on a nonadjacent position would cost $2ab\sigma_e$ $2bl\sigma$ rather than $2ab\sigma_e$. The surface nucleus, through repeated folding, will approach stability as it grows in the g direction. When ν stems and $\nu_f = \nu - 1$ folds have been

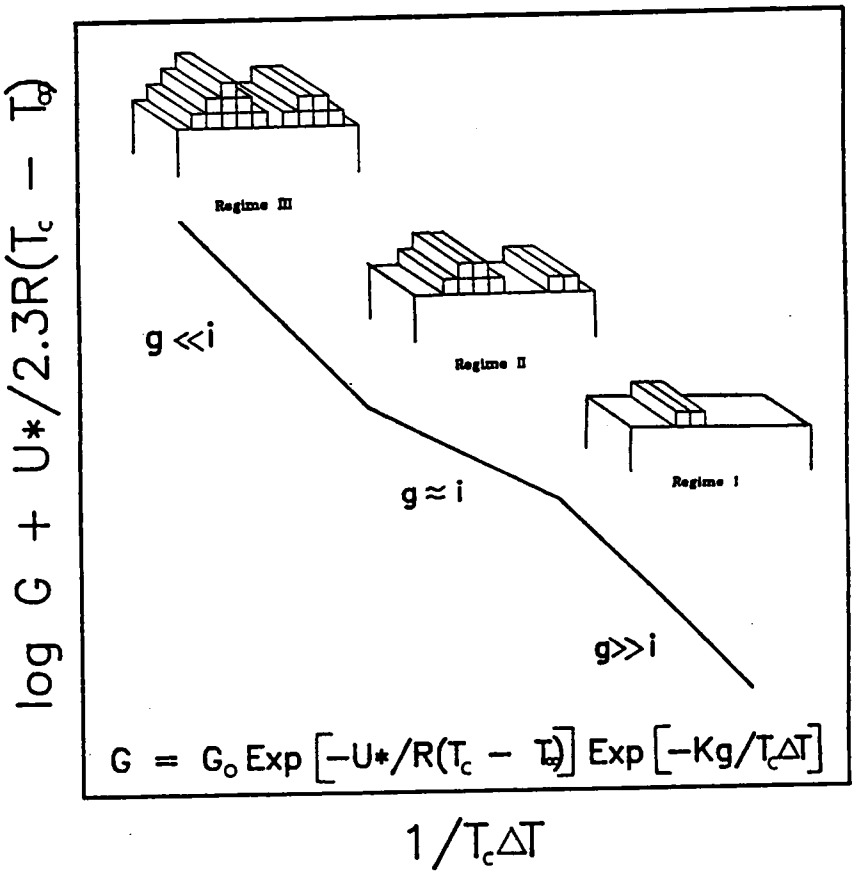


Figure 2.10 Lauritzen-Hoffman crystallization regimes schematic.

formed, the free energy of formation is (ignoring negligible chain end effects):

$$\varphi_v = 2bl\sigma + 2\nu_f ab\sigma_e - \nu abl\Delta f \qquad (2.1)$$

For large ν, the equation becomes:

$$\varphi_v = 2bl\sigma + \nu ab(2\sigma_e - l\Delta f) \qquad (2.2)$$

The free energy of formation of the surface nucleus goes through a maximum at or near the first stem (ν = 1) and approaches stability as the surface nucleus increases in size (Figure 2.11). A set of connected rate processes for the forward and backward reactions corresponds in general to a nucleation controlled process. In the nucleation controlled process, a large barrier resulting from the creation of new surfaces must be overcome to initiate the nucleus.

2.3.3 Total Flux

The flux S represents the net flow of polymer from sites in the liquid to the first stem of polymer in the nucleus. The first step in the surface nucleation problem is to find the general steady-state expression for S in terms of the rate constants for the forward and reverse reactions and the

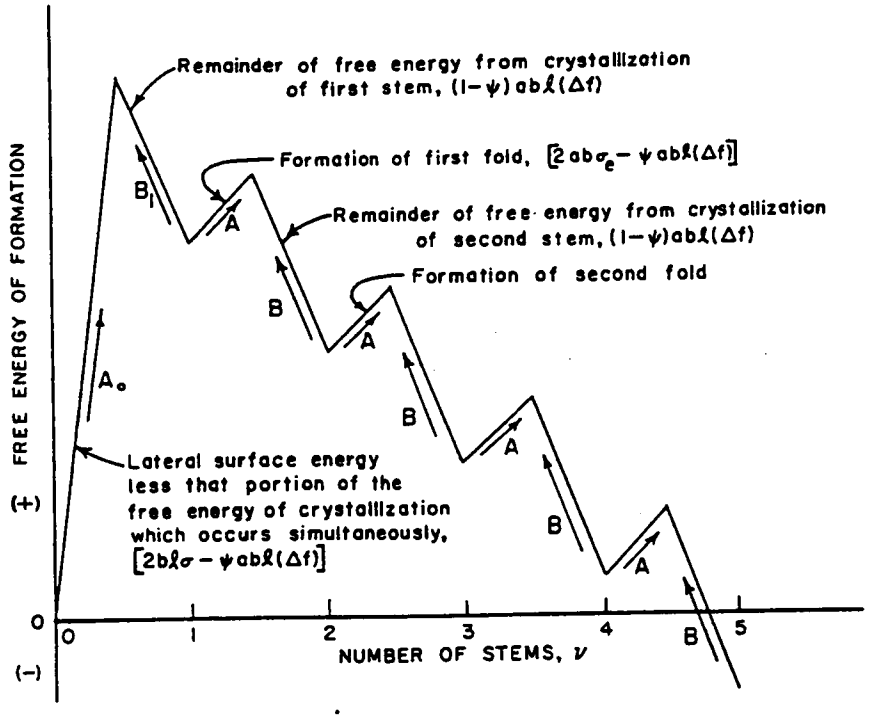


Figure 2.11 Free energy of formation of chain folded surface nucleus (from Hoffman et al. [21]).

occupation numbers. In terms of these rate constants and occupation numbers we have

$$S = N_o A_o - N_1 B_1 \tag{2.3}$$

where A_o and B_1 are the rate constants for the forward and reverse reactions and N_o and N_1 are the occupation numbers for the states $\nu=0$ and $\nu=1$.

The rate constants can be expressed as

$$A_o = ß\exp\{-(2bl\sigma/kT_c) + [\varphi abl(\Delta f)/kT_c] \tag{2.4}$$

$$B_1 = ß\exp[-(1-\varphi)abl(\Delta f)/kT_c] \tag{2.5}$$

where ß is a factor which accounts for retardations to molecular motion for the transport of polymer molecules or segments to the site of crystallization; φ is the fraction of the free energy of fusion to the activation energy of the forward reaction. This apportioning of the free energy attempts to account for the complex intermediate steps by which a segment attaches to the substrate. The value of φ may be related to whether or not the segment is physically adsorbed on the substrate surface prior to actual crystallographic attachment. The net rate of formation of nuclei of length l is given by

$$S(l) = bN_o\exp\{[-2bl\sigma + \varphi abl(\Delta f)/kT]\} \tag{2.6}$$

$$x \quad [1-\exp\{[-abl(\Delta f)-2ab\sigma_e]/kT\}]$$

The total flux, S_T, is found by integrating equation (2.6) over all possible values of l, the lower limit of l being set by $2\sigma_e/\Delta f$ and the upper limit infinity.

$$S_T = \frac{1}{l_n} \int_{\frac{2\sigma e}{\Delta f}}^{\infty} S(l)\, dl \qquad (2.7)$$

$$= N_o(\beta/l_n)P\exp(2ab\sigma_e\varphi/kT)\exp[-4b\sigma\sigma_e/(\Delta f)kT]$$

where

$$P = \frac{kT}{2b\sigma - ab\Delta f} - \frac{kT}{2b\sigma + (1-\psi)ab\Delta f} \qquad (2.8)$$

At low supercoolings the factor $\exp[-4b\sigma\sigma_e/(\Delta f)kT]$ controls S_T. Thus the overall growth rate G will be proportional to this factor at low supercoolings for growth processes that are proportional to the first power of the nucleation rate.

2.3.4 Initial Lamellar Thickness

The initial lamellar thickness l_g^* of a chain-folded lamella, which is kinetically determined, is of the form

$$l_g^* = (2\sigma_e/\Delta f) + \gamma l \qquad (2.9)$$

The average value of the lamellar thickness, $\langle l \rangle_{av}$, which can be identified with l_g^*, is calculated from the flux by

$$l_g^* = (1/l_n) \int_{2\sigma_e/\Delta f}^{\infty} lS(l)dl \Big/ (1/l_n) \int_{2\sigma_e/\Delta f}^{\infty} S(l)dl \qquad (2.10)$$

and this can be expressed as

$$l_g^* = \frac{2\sigma_e}{\Delta f} + \frac{kT}{2b\sigma} \times \frac{[2 + (1-2\psi)a\Delta f]/2\sigma}{(1-a\Delta f\psi/2\sigma)[1+a\Delta f(1-\psi)/2\sigma]} \qquad (2.11)$$

The last term is the γl of Equation (2.9), and is a strong function of φ.

The behavior of γl at various values of φ is interesting. By setting $\varphi = 1$,

$$\delta l = \frac{kT}{2b\sigma} \times \frac{(4\sigma/a) - \Delta f}{(2\sigma/a) - \Delta f} \qquad (2.12)$$

It can be shown that δl becomes infinite at the critical supercooling ΔT_c given by

$$\Delta T_c = 2\sigma T_m^{\circ}/(\Delta h_f)a \qquad (2.13)$$

This is the "δl catastrophe." However, no sharp upswing in l_g^* corresponding to the δl catastrophe is found experimentally.

At $\varphi = 0$,

$$\delta l = \frac{kT}{2b\sigma} \times \frac{(4\sigma/a) + \Delta f}{(2\sigma/a) - \Delta f} \qquad (2.14)$$

Here there is no "δl catastrophe" and l_g^* decreases continuously with decreasing temperature.

As φ is decreased, the value of T_c corresponding to the "δl catastrophe" is lowered. The term $(2\sigma_e/\Delta f)$ is the main contribution to l_g^* near the melting point. As the supercooling is increased, the contribution from $(2\sigma_e/\Delta f)$ decreases and that from δl increases.

In some systems the lamellae can undergo isothermal thickening. This slow and spontaneous increase occurs naturally when the molecular mobility exists in the chain-folded crystal, because a thick crystal is more stable from a thermodynamic viewpoint. The crystal increases its stability by decreasing the area of its high-energy surface by reducing the number of chain folds. This thickening is more rapid near the melting point. At sufficiently low crystallization temperatures, the lamellae do not thicken appreciably and the expressions for l_g^* may by applied.

2.3.5 Retardation Factor, ß

Since the overall growth rate G is a function of the total flux S_T for all regimes and S_T according to equation (2.7) contains the retardation factor, it is necessary to comment on the nature of ß. Polymers at high supercoolings become extremely viscous so that the retardations represented by ß are the controlling feature of the flux. Thus it is

necessary to establish the functional form for ß in order to understand growth rate experiments.

For bulk polymeric systems at high supercoolings, the jump rate for local motions can be used for ß. This is expressed as

$$ß = (kT/h)J_1 \exp[-U^*/R(T_c-T_\infty)] \qquad (2.15)$$

The factor $\exp[-U^*/R(T_c-T_\infty)]$ represents the temperature dependence of the segmental jump rate in polymers. The factors U^* and T_∞ are derived from bulk viscosity experiments. The activation energy U^* for the transport of segments to the site of crystallization is generally within 10 - 15% of 4100 cal/mole [35]. The temperature T_∞ is a hypothetical temperature where all motion associated with viscous flow ceases and is related to the glass transition temperature T_g of the polymer. The temperature T_∞ is usually within about 5 - 10 K of being 50 K below T_g. At moderate to high molecular weights where T_g does not vary significantly, neither U^* nor T_g is a strong function of molecular weight. The values of U^* and T_∞ that apply to the crystallization process need not be exactly the same as those that apply to bulk fluidity, because crystallizaton may occur from an adsorbed layer rather than directly from the bulk amorphous melt ($\varphi < 1$). A procedure that assumes an initial set of

values of U^* and T_∞ and then linearly fits ln G + $U^*/R(T_c-T_\infty)$ to $1/T(\Delta T)$ has resulted in a better linear fit for the kinetics data of some polymers. The values U^* and T_∞ are varied separately to maximize the linear fit. This method is similar to that suggested by Suzuki and Kovacs [36] in which the transport parameters are analyzed on the basis of the Williams-Landel-Ferry (WLF) equation.

The J_1 term allows for any barriers not accounted for by the exponential term. Compared to the temperature dependence of the exponential term, that of J_1 is small, so J_1 generally will act as a pre-exponential factor that reduces ß.

2.3.6 Free Energy of Fusion

The bulk free energy of fusion, Δf, is the driving force for crystallization in the expression for total flux. The free energy of fusion can be approximated near the melting point by assuming that Δh_f is independent of temperature so that

$$\Delta f = \Delta h_f - T\Delta S_f = \frac{\Delta h_f - T(\Delta h_f)}{Tm^\circ} \qquad (2.16)$$

where Δh_f is the heat of fusion per unit volume of crystal at the equilibrium melting temperature T_m° and ΔT is the supercooling $T_m^\circ - T_c$. Hoffman and Weeks [37] introduced a correction factor f to compensate for any error in the

assumption of the temperature independence of Δf. This factor is of the form

$$f = 2T_c/(T_m^\circ + T_c) \qquad (2.17)$$

This modifies the Δf Equation (2.16) to give

$$\Delta f = f(\Delta h_f \Delta T/T_m^\circ) \qquad (2.18)$$

The factor is approximately unity at low supercoolings but decreases Δf considerably at high supercoolings to account for the decrease in Δh_f at high supercoolings.

2.3.7 Growth Rates: Regimes I, II, and III

In the three growth regimes the overall growth rate G is a function of the product of the layer thickness and the net nucleation rate $i = S_T/aN_a$ where N_a is Avogadro's number. The difference in the surface nucleation process at different ranges of supercoolings gives rise to the three different regimes of crystal growth, Regime I, II, and III. The model for each regime is shown schematically in Figure 2.12.

2.3.7.1 Regime I Growth

In the idealized case for Regime I growth, a nucleus is formed on the growing lamellar surface followed by lateral growth on the surface, forming a new layer of thickness b.

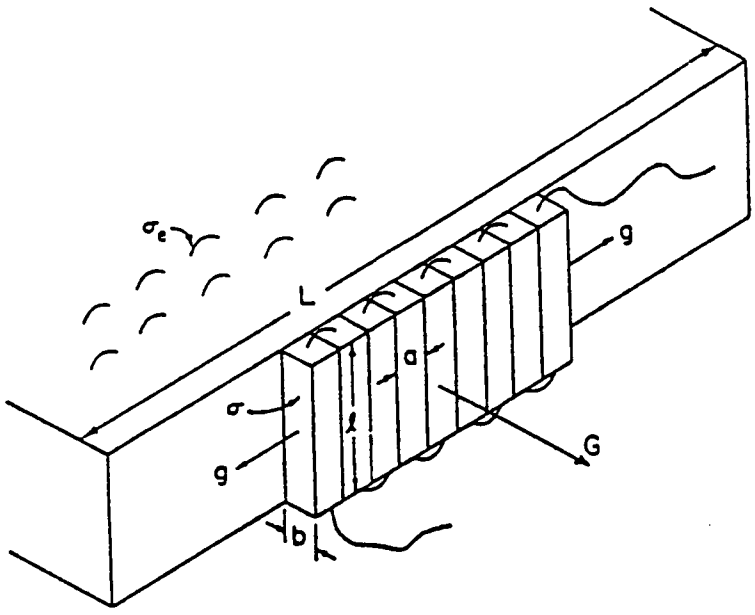


Figure 2.12 Polymer lamellar crystal idealized schematic (from Hoffman et al. [21]).

Thus each surface nucleation act results in the addition of a new surface layer before a second nucleation occurs. In this regime the rate of lateral growth g is much greater than the rate of surface nucleation and the overall growth rate is nucleation controlled. The overall growth rate is given by [38]:

$$G_I = biL = bLS_T/aN_a \qquad (2.19)$$

Inserting the net flux, equation (2.6) into equation (2.19) gives

$$G_I = G_{o,I}\exp[-U^*/R(T_c - T_\infty)]\exp[-4b\sigma\sigma_e/(\Delta f)kT] \qquad (2.20)$$

where $G_{o,I}$ includes factors not strongly dependent on temperature gathered into pre-exponential form. Then $G_{o,I}$ is given by

$$G_{o,I} = b(kT/h)n_s J_1 \exp(2ab\sigma_e\varphi/kT) \qquad (2.21)$$

where n_s is the number of sites or steps corresponding to the length of the surface, i.e. L/a.

2.3.7.2 Regime II Growth

In Regime II growth, many new surface nuclei form before the previous layer is complete. Sanchez and Dimarzio [39]

indicated that the overall growth rate is proportional to the square root of the surface nucleation rate. The overall growth rate is then

$$G_{II} = b(ig)^{1/2} = b(S_T g/aN_a)^{1/2} \qquad (2.22)$$

Inserting the net flux into equation (2.22) gives

$$G_{II} + G_{o,II}\exp[-U^*/R(T_c - T_\infty)]\exp[-2b\sigma\sigma_e/(\Delta f)kT] \qquad (2.23)$$

where

$$G_{o,II} = b(kT/h)J_1\exp[ab\sigma_e(2\varphi - 1)/kT] \qquad (2.24)$$

The ratio of the G_o values for Regimes I and II is

$$G_{o,I}/G_{o,II} = n_s\exp(ab\sigma_e/kT) \qquad (2.25)$$

It is clear that $G_{o,I} >> G_{o,II}$ for a given polymer. Regime II crystallization leads to a rough growth front on a molecular scale.

2.3.7.3 Regime III Growth

In Regime III, the rate of surface nucleation is much greater than the rate of substrate completion and nuclei form on partially grown strips. The effective substrate length is restricted by the abundance of niches so that the crystallization is accomplished by nucleation of stems on the

surface [3] as is Regime I. The overall growth rate is then expected to be proportional to the nucleation rate and is given by

$$G_{III} = biL' = bin_s'a = bLS_T/aN_a \qquad (2.26)$$

where $L' = n_s'a$ is an "effective" substrate length; n_s' is the mean number of stems laid down in the niche adjacent to the newly nucleated stem. The quantity n_s' is generally taken to be between 2 and 4 and independent of the overall substrate length L. Substituting the flux into Equation (2.25) gives

$$G_{III} = G_{o,III}\exp[-U^*/R(T_c - T_\infty)]\exp[-4b\sigma\sigma_e/(\Delta f)kT] \qquad (2.27)$$

where

$$G_{o,III} = b(kT/h)n_s'J_1\exp(2ab\sigma_e\varphi/kT) \qquad (2.28)$$

The Regime I and Regime III overall growth rate equations differ only in their pre-exponential factors such that

$$G_{o,I}/G_{o,III} = n_s/n_s' \approx n_s/3 \qquad (2.29)$$

2.3.8 Regime Test

A general form for the growth rate equation for the three regimes is given by

$$G = G_o \exp[-U^*/R(T_c - T_\infty)] \exp[-K_g/T\Delta Tf] \qquad (2.30)$$

where for Regimes I and III

$$K_{g(I)},\ K_{g(III)} = 4b\sigma\sigma_e T_m^o/(\Delta h_f)k \qquad (2.31)$$

A plot of log $G + U^*/R(T_c - T_\infty)$ versus $1/T(\Delta T)f$ will have the same slopes for Regimes I and III, which is twice that of Regime II (see Figure 2.12).

Lauritzen [38] introduced the dimensionless parameter Z to estimate whether crystallization in a given polymer is in Regime I or Regime II. Z is given by

$$Z = iL^2/4g \qquad (2.32)$$

If $Z < 0.01$, strict adherence to Regime I behavior is expected and $K_g = 4b\sigma\sigma_e T_m^o/(\Delta h_f)k$. If $Z = 0.1$, Regime I behavior is approximated. When $Z > 1$, Regime II behavior is expected and $K_g = 2b\sigma\sigma_e T_m^o/(\Delta h_f)k$. Overall growth rate data is used to evaluate K_g. Using the measured value of K_g, a range of values for L that are consistent with Regime I or Regime II behavior is estimated. The estimated values for L frequently are reasonable for one regime but completely unrealistic for the other. The value of L must be in accord with morphological information. A model for the physical

origin of the substrate length L is proposed by Hoffman [40]. L is treated as the persistence length between defects which have a capacity to inhibit surface completion.

2.3.9 Limitations of Secondary Nucleation Theory

2.3.9.1 Adjacent Re-entry

Surface nucleation theories assume chain folding with adjacent re-entry in order to make the model tractable. The probability of adjacent re-entry is normally expected to be less than one, and a modified, predominantly adjacent re-entry model has been used by many authors. The probability of non-adjacent re-entry of Gaussian chains can reach a maximum of 1/3 as shown by Guttman et al.[41] using the mathematical "Gambler's Ruin" method. In addition, Lauritzen-Hoffman secondary nucleation theory assumes nucleation from a chain end only.

Since secondary nucleation theory assumes regular adjacent re-entry and a large number of folds (at least five), polymer crystallization with fully extended chains or very few folds cannot be well explained. Point and Kovacs [42] claimed that secondary nucleation theory breaks down for the case of extended chain crystals of low molecular weight poly(ethylene oxide) because it results in σ values that are chain length dependent.

2.3.9.2 Constant Fold Period

In secondary nucleation theory, a fold plane once nucleated will grow with a constant fold period. The length of the first stem, which is a function of ΔT and φ, determines this fold period. Direct observations of the lamellar thickness of polyethylene by electron microscopy have shown that constant lamellar thickness is questionable. Several authors have addressed this problem [34,43]. The theory of Lauritzen and Passaglia accounts for all possible fold periods but fails to eliminate the "δl catastrophe". The δl catastrophe in Lauritzen-Hoffman secondary nucleation theory is a direct result of the imposed integration limits. Recent work suggests that the fold period is constant prior to thickening in several polymers.

2.3.10 Applications of Secondary Nucleation Theory

2.3.10.1 Atmospheric Pressure - General

Secondary nucleation theory has been applied to several polymer systems. Of these systems, a Regime I-Regime II transition has been observed in polyethylene, poly(3,3-dimethyl thietane), polydioxolane, and poly(L-lactic acid) crystallized from the melt. The Regime II-Regime III transition has been observed in polyethylene, polyoxymethylene, polypropylene, cis-poly(isoprene), poly(p-phenyl sulfide), poly(3,3-dimethyl thietane),

poly(pivalolactone), and poly(3-hydroxybutyrate). Of the polymer systems exhibiting regime transitions, relatively few exhibit both a Regime I-Regime II and a Regime II-Regime III transtion within a given sample. Table 2.2 highlights some of the polymers exhibiting regime transitions. Generally the systems that show both I-II and II-III behavior in the same sample have been of relatively low molecular weight. Relatively few systems been studied over an extensive molecular weight range. At present, these are polyethylene [44], cis-poly(isoprene) [45], poly(ethylene oxide) [46] poly(3,3-dimethythietane) [47], and isotactic polypropylene [48]

It is interesting to observe the behavior of the surface free energy σ_e and the work of chain folding q determined from the application of secondary nucleation theory. Table 2.3 summarizes some results for -C-C- backbone polymers. The work of chain folding increases with increasing chain stiffness as measured by the equilibrium melting temperature T_m^o. The lateral surface free energy σ , which should decrease with increasing chain stiffness due to the decreased entropy change, does not correlate well with the T_m^o. The fold surface free energy σ_e also does not correlate well with chain stiffness. The primary contribution to σ_e is the work of chain folding q. This is a measure of the work required to bend the polymer chain back upon itself so that is can re-

Table 2.2 Polymers Exhibiting Regime Transitions

Polymer	ΔT_{I-II}	ΔT_{II-III}
Polyethylene	16	23 (predicted)
Polyoxymethylene	23	40
Poly(ethylene oxide)	24	-
Polypropylene	37	48
cis-polyisoprene	54	66
Poly(p-phenylene sulphide)	-	107
Poly(3,3-dimethyl thietane)	15	23
Polydioxolane	33	-

Table 2.3 Surface Free Energies and Work of Chain Folding for -C-C- Polymers.

Polymer	T_m^o (°C)	Regime	σ (erg/cm^2)	σ_e (erg^2/cm^4)	q (kcal)	Ref.
PB	128	II	7.2	30.8	4.9	a
PE	145	I,II,III	11.1-14.1	93.8	5.3-5.7	b
sPP	161	II	-	49.9	5.8	c
iPP	185	II,III	11.5	65-70	6.4-6.8	c
iPS	242	II	7.6	35	7.1	d

enter the crystal in a manner consistent with the lattice structure. However, other factors contribute to the fold surface free energy and these factors can vary, depending on the crystallization mechanims and the manner of chain folding. Additional factors contributing to σ_e are the existence of cilia and chain ends, the extent of adjacent re-entry, the strain imposed by the fold, and the interzonal region. While the maximum amount of nonadjacent re-entry is considered fixed at 1/3, the nonadjacent re-entry amount can change from Regime I through Regime III which should result in a change in σ_e. The maximum amount of nonadjacent re-entry expressed above is for a cubic unit cell.

2.3.10.2 Atmospheric Pressure - Polypropylene

Several investigators have studied the crystallization of isotactic polypropylene over a sufficient temperature range to successfully apply secondary nucleation theory. The literature results for isotactic polypropylene are summarized in Table 2.4. It is seen that over a wide molecular weight range, the σ_e varies nearly 35%, with the highest value 74.2 erg/cm^2 and the lowest 54.9 erg/cm^2. However, for a given set of data, secondary nucleation theory fits the data well and in all cases, a Regime II-Regime III transition was observed at an approximate supercooling $\Delta T = 48°$. The lowest molecular weight data, that of Cheng and Janimak, exhibited a T_m^o of ≈170°C, about 17°C lower than that for the other

Table 2.4 Kinetics Analysis of Isotactic Polypropylene from Literature.

Source	M_w x 10^{-3} / M_n X 10^{-3}	K_g x 10^{-5}, K^2	log G_o, cm/s	σ_e, erg/cm^2	q, Kcal/ mole	III/II
			Regime I			
Janimak	29/17	2.66	4.86	56.6	5.5	2.2
			Regime II			
Binsbergen	350(h)	1.516	-0.52	62.3	6.2	2.4
Falkai	152(h)	1.599	-0.45	65.7	6.4	2.0
Goldfarb	435/60	1.637	-0.06	67.2	6.4	2.0
Janimak	29/17	1.23	0.66	52.3	5.1	2.1
			Regime III			
Binsbergen		3.613	3.99	74.2	7.3	
Falkai		3.183	3.02	65.4	6.5	
Goldfarb		3.260	3.55	66.9	6.6	
Janimak		2.59	3.86	54.9	5.4	

samples. However, the supercooling of the transition remained constant. The value of the supercooling for the low molecular weight would be 65° if T_m^o = 187°C

2.3.10.3 Elevated Pressure

Few studies have applied secondary nucleation theory to the kinetics of elevated pressure crystallization of polymers. The polymers that have been sufficiently studied are polyethylene [49], poly(ethylene terephthalate) [56], and cis-poly(isoprene) [50]. Table 2.5 summarizes the kinetics reuslts for elevated pressure crystallization. It is seen that for polyethylene the $\sigma\sigma_e$ product is relatively unaffected by pressure up to 2.0 kbar (200 MPa), while the PET shows a continuing increase in $\sigma\sigma_e$ with increasing pressure and cis-IP shows a discontinous increase near 50 MPa, but little change above 50 MPa to 200 MPa.

2.4 Melting of Polymer Crystals

The melting temperature of a lamellar polymer crystal is controlled by several factors, including the lamellar thickness, the surface free energies, lattice imperfections, internal stress field, etc. Lamellar thickness and surface free energies are dominant factors while lattice imperfections and internal stress fields are often neglected for simplicity. It is important to derive an expression for

Table 2.5 Kinetics Results for Elevated Pressure Crystallization.

Pressure (kbar)	K_g ($\times 10^{-5}$) (K^2)	$\sigma\sigma_e$ erg^2/cm^4	σ_e erg/cm^2	Regime
LPE				
atm	1.10	1240	87.9	
0.5	1.25	1335	94.6	
1.0	1.22	1266	89.8	
1.5	1.25	1214	86.1	
2.0	1.35	1342	95.2	
PET				
atm	0.6	658	56.7	
0.5	1.48	1619	139.5	
1.0	2.18	2389	205.8	
1.5	2.70	2961	255.2	
2.0	3.66	4014	345.9	
cisIP				
atm	2.56	290	21	
0.5	2.96	330	24	
1.0	5.89	590	42	
1.5	5.68	550	39	
2.0	5.72	570	41	

melting point in terms of lamellar thickness and surface free energies.

2.4.1 Thermodynamic Considerations

The free energy of formation of a single lamellar polymer crystal as shown in Figure 6 may be written as [51]

$$\Delta\phi = 2(a+b)l\sigma + 2ab\sigma_e - abl\Delta f \qquad (2.33)$$

where a and b are the lateral dimensions, l the thickness, σ and σ_e are the lateral and fold surface free energies respectively, and Δf is the bulk free energy of fusion. Since a>>l and b>>l, the first term in Equation (2.33) is much smaller than the second and third terms and may be neglected. At the crystal's melting temperature T_m, $\Delta\phi = 0$. Substituting $\Delta\phi = 0$ and $\Delta f = \Delta h_f \Delta T/T_m^{\circ}$ into Equation (2.33), one obtains

$$T_m = T_m^{\circ}(1 - 2\sigma_e/\Delta h_f l) \qquad (2.34)$$

where Δh_f is the heat of fusion per unit volume of crystal. Thus the observed melting point for a thin crystal is depressed below that of an infinite crystal (T_m°) by the amount $2\sigma_e/\Delta h_f l$. A plot of T_m versus 1/l must be linear with intercept T_m° and σ_e determined from the slope.

2.4.2 Kinetic Considerations

Secondary nucleation theory predicts the initial lamellar thickness l_g^* according to Equation (2.11). Due to isothermal thickening, the measured l is larger than l_g^*. The average lamellar thickness at the end of crystallization can be expressed as [39]

$$l = \gamma l_g^* \tag{2.35}$$

where γ, the thickening factor, has a value greater than one. Combining this with Equation (2.9) and substituting for Δf from Equation 2.18 leads to

$$l = \frac{2\sigma_e T_m^o \gamma}{\Delta h_f \Delta T} + \gamma \delta l \tag{2.36}$$

Equation 2.36 relates l to the supercooling, thus relating l to T_c. Substituting Equation 2.36 into Equation 2.34 gives

$$T_m = T_m^o - (\Delta T/\gamma)(1 + K\Delta T)^{-1} \tag{2.37}$$

where $K = \Delta h_f \gamma l / 2\sigma_e T_m^o$. Hoffman et al. [51] assumed $2\sigma_e/\Delta f >> \gamma l$, thus $K\Delta T \approx 0$ and then

$$T_m = T_m^o - \Delta T/\gamma \tag{2.38}$$

This is a fairly good approximation for crystals formed at low supercoolings. Equation (2.38) may be written in terms of T_m and T_c to give

$$T_m' = T_m^o(1 - 1/\gamma) - T_c/\gamma \tag{2.39}$$

where T_m' is the melting temperature subject to the assumption $K\Delta T \approx 0$. Equation (2.39) suggests that the melting temperature of a polymer that has thickened by a factor γ during crystallization at T_c is a linear function of T_c.

However, $K\Delta T \approx 0$ is not always a good approximation, leading to curvature in a plot of the actual melting temperature T_m versus T_c. In some cases there is an upward curvature in T_m versus T_c data due to an increase in γ at higher temperatures. Since typically $K\Delta T << 1$, a binomial series expansion of Equation (2.37) gives

$$T_m = T_m^o - (\Delta T/\gamma)[1 - (K\Delta T) + (K\Delta T)^2] \tag{2.40}$$

Rearranging Equation (2.40) and combining with Equation 2.39 leads to

$$T_m' = T_m - (\Delta T/\gamma)[(K\Delta T) - (K\Delta T)^2] \tag{2.41}$$

The initial values of γ and T_m^o are estimated from a T_m versus T_c plot and by an iterative method relatively accurate final values for γ and T_m^o are obtained and thus values of T_m, obtained.

2.5 The Effects of Pressure

Hydrostatic pressure is known to affect the crystallization and physical properties of polymers. The glass transition temperature T_g and the melting temperature T_m are two important parameters for kinetics analysis at high pressures as well as at atmospheric pressure. Some experimental observations and theoretical treatments for morphology, crystallization, glass transition temperature, and melting temperature are briefly discussed in this section.

2.5.1 Morphology

The effects of pressure on the morphology of several polymers have been studied. For polyethylene at sufficiently high pressures, extended chain lamellae of increasing thickness become dominant. Geil at al.[52] reported the morphology of polyethylene samples which were melt crystallized under pressure. These samples showed little or no folding. Wunderlich and Arakawa [53] reported that two different types of crystals form in high density

polyethylene, depending on temperature and pressure. A new hexagonal liquid crystalline high pressure phase for polyethylene was reported by Bassett and Turner [54]. At high pressures polyethylene passes through a hexagonal intermediate phase [55] and this phase is responsible for chain extension occuring. Tseng and Phillips [56] reported banded spherulites for LPE below 350 MPa hydrostatic pressure and extended chain crystals above 350 MPa.

For cis-polyisoprene at pressures up to 300 MPa, three morphologies existed. These were single crystals, spherulites, and oblate spheroids [57]. Chain-extended lamellae have not been observed in cis-polyisoprene.

The γ-form of isotactic polypropylene has been observed in samples isothermally crystallized and slow cooled from the melt at pressures above 32.4 MPa [58]. As the pressure is increased, a larger proportion of the sample crystallizes in the γ-form until at 506.6 MPa only the γ-form is present.

2.5.2 Crystallization Kinetics

There have been relatively few studies of the effect of pressure on the crystallization kinetics of polymer systems. Phillips and Edwards [59] obtained linear growth rate data for cis-polyisoprene for pressures ranging from atmospheric to 400 MPa. The bell-shaped growth rate curves shift to higher temperatures with the application of pressure. An increase in the maximum growth rate is observed over the

first 140 MPa of applied pressure. A large and sudden increase in fold surface free energy (σ_e) with increased pressure is attributed to a pressure-induced change in fold conformation.

Trans-polyisoprene exhibited a decrease in the maximum growth rate with an increase in pressure [60]. The decrease in maximum growth rate is attributed to a decrease with pressure of the temperature range (T_m - T_∞) available for crystallization.

Tseng and Phillips investigated the pressure effects on the growth rate kinetics of linear polyethylene(LPE) and polyethylene terphthalate(PET). For PET, analysis of the growth rate data in terms of secondary nucleation theory yielded a possible Regime II-III transition. Fold surface free energy was found to increase dramatically with pressure. This is possibly due to the increase of non-adjacent re-entry and significant amount of loose folds. For LPE, the σ_e was independent of pressure up to 200 MPa, implying that the structure of the fold surface does not change. The pressure dependence of the Regime I-II transition in LPE paralleled the pressure dependence of T_m^o, indicating that the transition is thermodynamic.

2.5.3 Melting Response

As the pressure increases, the melting temperature usually increases. The Clausius-Clapeyron equation gives a

quantitative expression for (dT/dP) from thermodynamic considerations as the following:

$$(dT/dP)_{eq} = \Delta H/T\Delta V \qquad (2.42)$$

where ΔH and ΔV are the changes in enthalpy and volume respectively. The Clausius-Clapeyron equation can be written as

$$(dT_m/dP) = T_m\Delta V/\Delta H \qquad (2.43)$$

Baer and Kardos [61] have studied the effect of pressure on the melting response for various polymers. They noted that the melting temperature and range of melting increased with increasing pressure for all polymers studied. The effect of pressure on the melting temperature of several polyamides [62] and trans-polyisoprene [63] have been reported. A linear increase in melting temperature with applied pressure is observed which is 16°C per 100 MPa for nylon-6 and 15°C per 100 MPa for trans-polyisoprene.

The Clausius-Clapeyron equation can be written to express the equilibrium melting temperature at pressure as a function of the equilibrium melting temperature at atmospheric pressure. This is given by

$$(T_m^o)_p = (T_m^o)_{1\ atm} \exp[\Delta V/\Delta hf(P - 1)] \qquad (2.44)$$

where $\Delta V = V_a - V_c$; V_a and V_c are the specific volumes of amorphous and crystalline material and P is the pressure in atmospheres. According to Equation 2.44, T_m^o is a steep function of pressure. Dalal [50] obtained equilibrium melting temperatures at pressures up to 260 MPa for cis-polyisoprene. Melting temperature data at pressure was obtained with an optical turbidimetric technique. The plots of crystallization temperature versus melting temperature were linear and shifted to higher temperatures with increasing pressure.

2.5.4 Glass Transition Temperature

The glass transition temperature increases approximately linearly with pressure. Since Fox and Flory [64] proposed that the free volume remains constant in the glassy state, free volume theories predict the change of the glass transition temperature with pressure (dT_g/dP) to be given by

$$dT_g/dP = ß_f/\alpha_f \approx \Delta ß/\Delta\alpha \qquad (2.45)$$

where $ß_f$ and α_f are the free volume compressibility and expansion coefficient, respectively, and $\Delta ß$ and $\Delta\alpha$ are the differences between the liquid and glass compressibilities and expansion coefficients, respectively.

The glass transtion is assumed to be a true second-order transition with equilibrium properties by thermodynamic theories [65]. Then the variation of a second-order transition is given by the Ehrenfest relation

$$dT_2/dP = \Delta\beta/\Delta\alpha = (TV\Delta\alpha)/\Delta C_p \qquad (2.46)$$

where ΔC_p is the difference in heat capacities between the glass and the liquid at the transition.

O'Reilly [66] has tabulated the emperical values of dT_g/dP for several polymers, with most of the values around 20° - 24° per 100 MPa of pressure. Mizoguchi and Ishikawa [67] have derived an expression for dT_g/dP based on Eyring's modified hole theory. The calculated results from this theory are in better agreement with experimental data than those obtained from free volume theory $\Delta\beta/\Delta\alpha$. Relatively few polymer T_g's have been measured as a function of pressure.

2.6 Molecular Weight Effects

Molecular weight and molecular weight distribution affect the rate of polymer crystallization, degree of crystallinity, and the observed melting temperature. The effect of molecular weight on a number of polymer systems has been studied. Poly(phenyl-p-silphenylene)siloxane (TMPS) [68] growth kinetics were studied at different crystallization temperatures as a function of molecular

weight. Linear growth rate increased with decreasing molecular weight. However, the crystallization temperature of the maximum in the growth rate curves did not change for the different molecular weight fractions. Magill reported that the pre-exponential term G_o increased with decreasing molecular weight in the molecular weight range 8,000 - 430,000.

Mandelkern et al.[69] analyzed polyethylene fractions data and determined that the interfacial free energy σ_e increased with increasing molecular weight. They suggested the change in σ_e with molecular weight indicated a change in the interfacial structure. Fatou and Mandelkern [70] reported an asymptotic value of 138.5°C for the melting temperature in a study of the effect of molecular weight on melting for polyethylene fractions. Ergoz et al.[71] found that for polyethylene the crystallization rate at fixed supercooling goes through a maximum as a function of molecular weight. They also showed that the maximum degree of crystallinity decreased as molecular weight increased. Hoffman et al.[72] observed two morphologies in polyethylene fractions. For fractions with molecular weight higher than 115,000, only spherulitic morphology was observed. For low molecular weight fractions (3,600 to 18,000) only axialitic growth was observed. For intermediate molecular weight fractions (18,000 to 115,000) spherulites were found at large

supercooling ($\Delta T > 18°$) but at low supercoolings, axialites were found. The transition occured around 127°C ($\Delta T = 18°$). The change in morphology is attributed to a change in growth mechanism, with the high supercoolings associated with Regime II and the low supercooling associated with Regime I. The Regime I-II transition temperature was found to be molecular weight dependent. The transition temperature increased as the molecular weight increased in the range 18,000 to 115,000.

Allen [73] observed a noticeable molecular weight effect on linear growth rate in isotactic polypropylene in the molecular weight range 52,000 to 520,000. Unlike polyethylene, a maximum in the growth rate as a function of molecular weight occurs at fairly high supercoolings. At high supercoolings, the growth rates are relatively invariant with molecular weight.

The reptation concept proposed by de Gennes [74] suggests that under appropriate conditions, the overall friction coefficient of a linear polymer chain in the liquid state is proportional to its length. Recently Hoffman [30] has tested the reptation concept for the case of crystallization of polyethylene from the melt. The inclusion of the reptation concept in the kinetic nucleation theory allows the molecular weight dependence of the growth rate to be obtained.

2.7 Polymerization

Isotactic polypropylene (scattering) was first made by Natta [75] in Italy using modified Ziegler-type initiators. This initiator system, referred to as Ziegler-Natta or coordination initiators, consists of an organometallic compound of a Group I-III metal with a halide or other derivative of a Group IV-VIII transition metal. The polymerizations are carried out in hydrocarbon solvents. A typical conventional coordination initiator system for the polymerizaton of propene to isotactic polypropylene is titanium trichloride ($TiCl_3$), the transition metal component, and diethylaluminum chloride [$(C_2H_5)2AlCl$], the Group I-III metal component. The initiator system performs two functions. First, the system supplies the species which initiates the polymerization. Second, the initiator complex coordinates the propagating chain end and the incoming monomer so as to orient the monomer with respect to the growing chain end to induce stereospecific addition. Recently process improvements and initiator system improvements have greatly improved the isotactic polypropylene produced. The new processes have broadened the applicability of isotactic polypropylene. The polymerizaton of isotactic polypropylene can be controlled to improve the properties for specific applications. The coordination

initiator systems now yield as much as forty times the amount of polymer per unit of initiator than commercial systems of the early 1980's. The initiator systems are also more selective. The isotactic polypropylene has higher stereoregularity compared to the isotactic polypropylene produced by conventional systems. This improves the properties and eliminates a post-reactor step normally required to remove the atactic polypropylene.

2.8 Polymer Molecular Weights

Polymers are mixtures of various components. Linear polymers are mixtures of various chain lengths or molecular weights. Stereoregular polymers, such as polypropylene, are mixtures of lengths and numbers of d and l units as well as chain lengths. Branched polymers are polydisperse with respect to chain length and chain structure. Different experimental techniques to determine polymer molecular weights measure different kinds of average molecular weights. The most important kinds of molecular weight averages in polymers are the number average, the weight average, the z and the (z + 1) average, and the viscosity average.

The number average molecular weight, Mn, is usually measured with membrane osmometry or vapor-phase osmometry and is expressed by the following:

$$M_i = \frac{\sum_i n_i (M_i)_n}{\sum_i n_i} \tag{2.48}$$

where N_i is the number of molecules with weight M_i.

The weight average molecular weight, M_w, is measured with quasielastic light scattering and is expressed by the following:

$$M_w = \frac{\sum_i m_i (M_i)_w}{\sum_i m_i} \tag{2.49}$$

The z average average molecular weight is

$$M_z = \frac{\sum_i z_i (M_i)_z}{\sum_i z_i} \tag{2.50}$$

The z and (z + 1) averages as well as the number and weight averages can be determined with a calibrated size exclusion chromatography system.

The viscosity average molecular weight, M_η, is

$$M_\eta = \left(\sum_i w_i M_i{}^{a_\eta}\right)^{1/a_\eta} \tag{2.51}$$

where a is the exponent of the molecular weight in the Mark-Houwink-Sakurad intrinsic viscosity $[\eta]$ versus molecular weight relation

$$[\eta] = KM^a \tag{2.52}$$

The weight average molecular weight is always greater than or equal to the number average molecular weight while the viscosity average molecular weight is between the number average and the weight average. The ratio M_w/M_n is often used as as measure of the polydispersity of a polymer sample. If a polymer is monodisperse, this ratio is unity. As the ratio increases, the polydispersity increases. At a fixed value of Mw/Mn there are an infinite number of different molecular weight distributions possible.

2.9 Tacticity Analysis

For polypropylene, the stereoregularity is dependent on the catalyst system that is used to synthesize the polymer. While changes in the catalyst systems have significantly increased the stereoregularity of isotactic polypropylene, the polymer still contains some syndiotactic placements. It is desirable to describe the monomer sequences or sequence distributions for each chain length. Average polymer structural information can be determined using either infrared (IR), ultraviolet (UV), or nuclear magnetic resonance (NMR) techniques. However, presently only NMR is capable of determining average sequence distributions and number-average sequence lengths.

2.9.1 Tacticity from IR Spectroscopy

The IR spectra of isotactic polypropylene of different tacticities have been investigated by several authors . The conformational ordering has a strong influence on the mIR spectra as shown in Figure 2.13 . Polarized IR studies of uniaxially drawn polypropylene have been essential to the analysis. Wave number assignments for the absorption maxima for isotactic polypropylene and sPP have been obtained by calculation and comparison with the spectra of deuterated polypropylene samples. This information allows characterization of average polymer structure but not sequence distributions and sequence length, which require NMR. Figures 2.14 and 2.15 show the vibrational modes of the CH_3 group and the CH_2 and CH groups, respectively, for isotactic polypropylene. Table 2.5 gives some of the infrared band assignments for the observed vibrational modes of isotactic polypropylene.

2.9.2 Tacticity from NMR Spectroscopy

Both proton (^1H) and carbon 13 (^{13}C) NMR have been successfully used for tacticity analysis of polymers. An NMR spectrum represents directly the average polymer molecule. The characterization of tacticity from NMR involves three quantitiative measurements [76]:

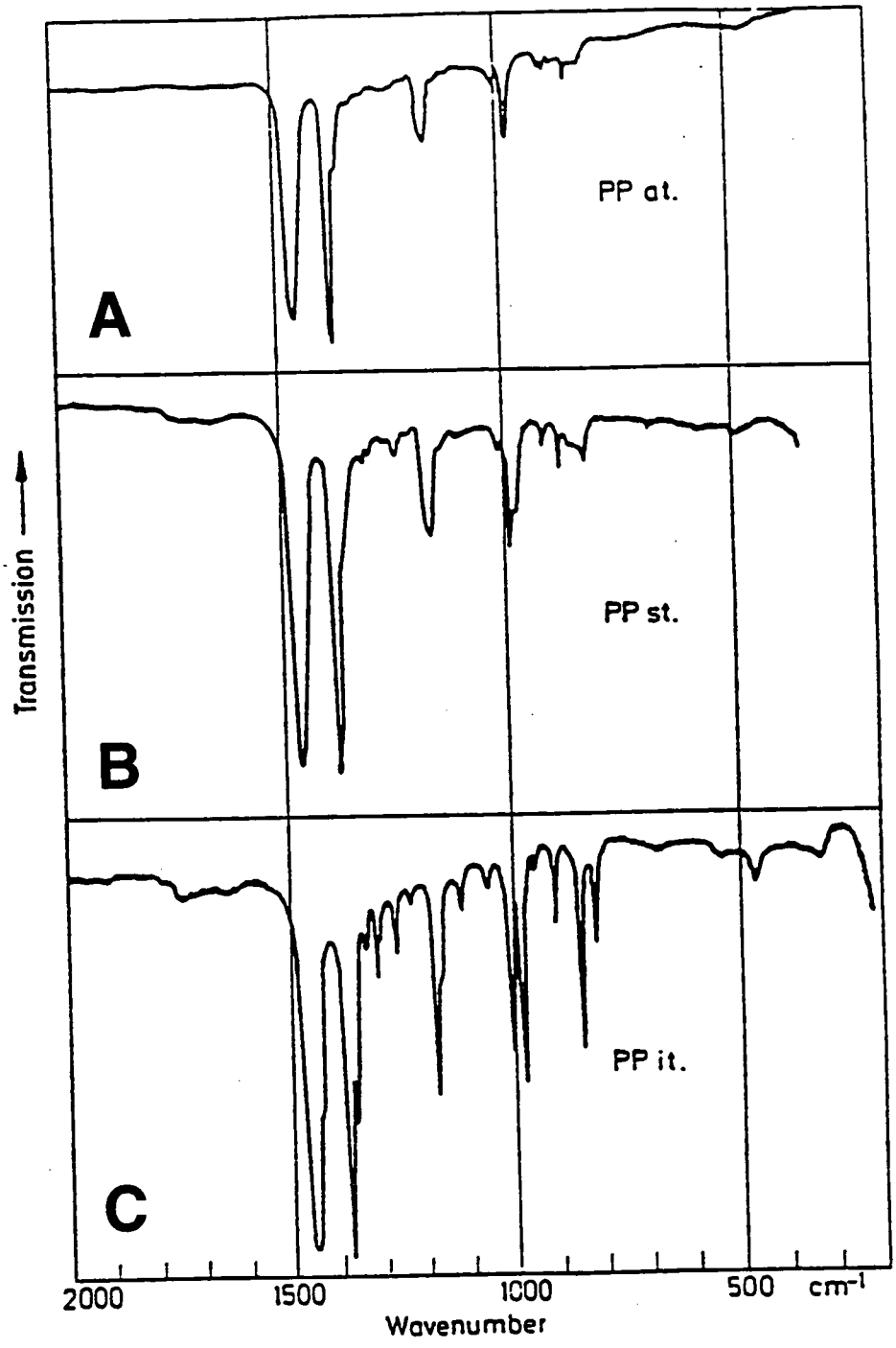


Figure 2.13 Infrared spectra of stereoregular forms of polypropylene: A. atactic, B. syndiotactic, C. isotactic.

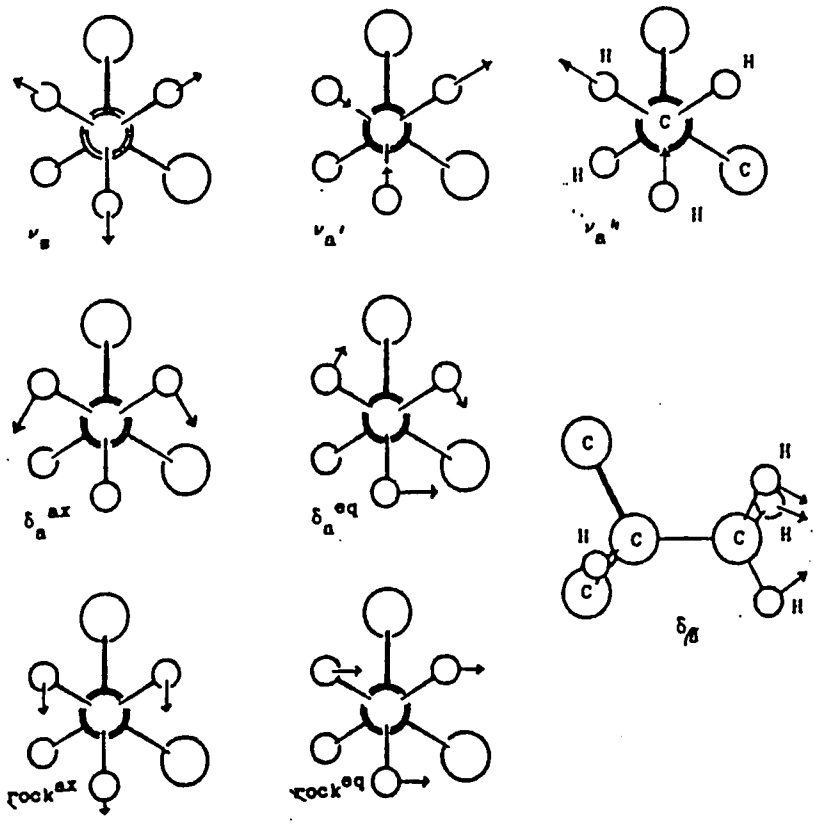
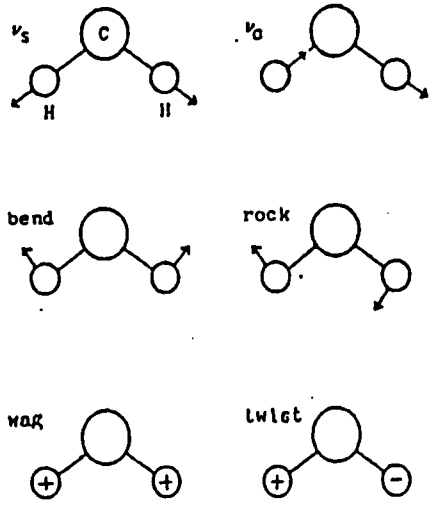


Figure 2.14 Vibrational modes of the CH_3 group in isotactic polypropylene. Axial C-C bonds are shown in heavy lines (from [Ketley]).



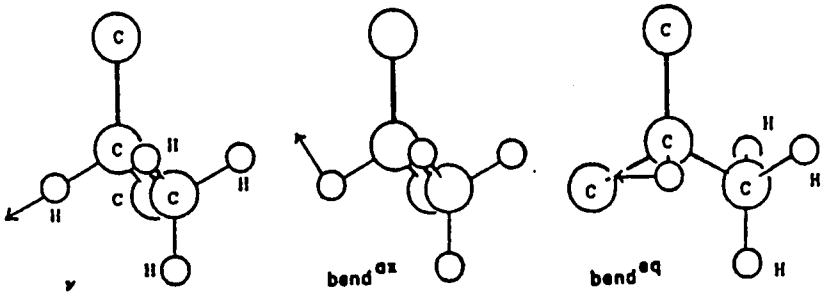


Figure 2.15 Vibrational modes of the CH_2 group and the CH group in isotactic polypropylene (from [Ketley])..

Table 2.6 Infrared Band Assignments for Isotactic Polypropylene.

Peak (cm^{-1})	Assignment
1365	CH_2 wag, CH bend^{ax}
1360	CH bend, CH_2 twist
1326	CH bend
1304	CH_2 wag, CH_2 twist
1254	CH_2 twist, CH bend
1168	r_{cc}^{ax}, CH_3 rock^{ax}
1045	r_{cm}, r_{cc}^{eq}
998	CH_3 rock^{eq}, r_{cm}, CH bend
973	CH_3 rock^{ax}, r_{cc}^{ax}, r_{cc}^{eq}
899	CH_3 rock^{eq}, CH_2 rock
842	CH_2 rock
809	CH_2 rock, r_{cm}, r_{cc}^{eq}

a) distributions of configurations of successive units such as dyads, triads, tetrads, etc.

b) number-average sequence length of like configurations.

c) number-average sequence lengths of meso and racemic dyads

where meso applies to adjacent monomer pairs with the same configuration while the opposite configuration is called racemic.

2.10 Small Angle X-ray Scattering

Small Angle X-ray scattering (SAXS) is an appropriate technique to study the morphology of semicrystalline polymers. Alternating crystalline and amorphous regions result in fluctuations in electron density over distances typically in the range of 30 Å to 1000 Å. This inhomogeneity generates X-ray scattering at very small angles, typically less than 2° with Cu K_α wavelength radiation. While the results from SAXS are sometimes in apparent disagreement with direct techniques, such as SEM and TEM [77], this discrepancy may be attributed partly to SAXS biasing larger, more perfect stacks of lamellae [78] as well as the direct techniques showing very localized features.

The scattering intensity function for an isotropic system with particles separated by a distance r can be expressed as:

$$I(s) = V\int 4\pi r^2 \gamma(r) \exp(-isr)\, dr \qquad (2.53)$$

where the scattering vector $s = (4\pi/\lambda)\sin(\Theta/2)$ and the correlation function $\gamma(r)$ describes the spatial correlations of the electron density distributions and is defined by:

$$\gamma(r) = \langle[\rho(x_o) - \langle\rho\rangle][\rho(x_o + x) - \langle\rho\rangle]\rangle \qquad (2.54)$$

where r(x) is the electron density distribution normal to a lamellae and <r> is the mean electron density. The intensity function can then be written as:

$$I(s) = V\int 4\pi r^2 \gamma(r) \frac{\sin(sr)}{sr} dr \qquad (2.55)$$

SAXS Distance Distribution and Correlation Function

The SAXS intensity of the two-phase model can be related to the spatial correlation of the electron density fluctuations throught the one-dimensional correlation function, $\gamma(r)$, originally developed by Debye [79]. The normalized electron-density correlation function is defined as:

$$\gamma(r) = \frac{\langle [\rho(r_o) - \langle\rho\rangle][\rho(r_o + r) - \langle\rho\rangle]\rangle}{\langle\rho^2\rangle} \qquad (2.56)$$

where $\rho(r_o)$ is the electron density distribution normal to the lamellae at a given r_o, $\rho(r_o + r)$ is the distribution at a displacement r, and $\langle r\rangle$ is the mean electron density. The angle brackets indicate averaging over all r_o. The $\gamma(r)$ can be expressed as:

$$\gamma(r) = \frac{\int_0^\infty q^2 I(q) \cos^2 \pi q r dq}{\int_0^\infty q^2 I(q) dq} \qquad (2.57)$$

The model of the electron density distribution determines the corresponding shape of the correlation function. Figure 2.16 shows several models for the electron density distribution $\rho(r)$ and the corresponding correlation function $\gamma(r)$. In the figure, A represents a two-phase model with constant lamellar thickness and constant long period, B incorporates long period variations, C includes long period variations and lamellar thickness variations, and D includes a diffuse boundary between amorphous and crystalline regions. The invariant **Q** can be evaluated using the expression:

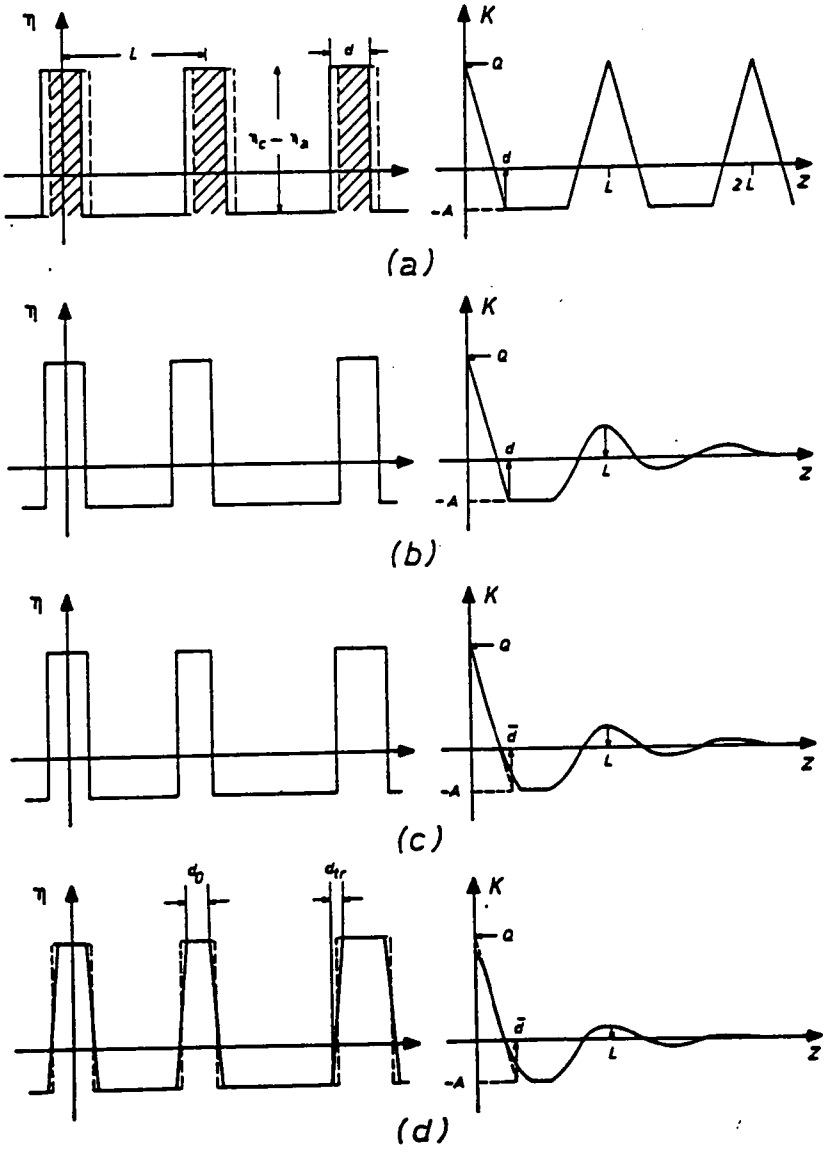


Figure 2.16 Schematic of various electron density distributions and the associated correlation functions (from [112]).

$$Q = \int_0^{\infty} q^2 I(q)\, dq \qquad (2.58)$$

The distance distribution function $\rho(r)$ [80,81]can be defined in terms of the electron density correlation function as:

$$\rho(r) = \gamma(r) r^2 \qquad (2.59)$$

The distance distribution function can also be expressed as the Fourier transformation of the scattering intensity function as:

$$\rho(r) = \frac{1}{2\pi} \int_0^{\pi} I(q)\,(qr)\sin(qr)\, dq \qquad (2.60)$$

The distance distribution function can be used to classify the shape and structure of the scattering particles [82]. A complication in the analysis of the $\rho(r)$ and $\gamma(r)$ functions is due to the nature of the Fourier transformation. Since the experimental data are collected over a finite range of q and the transformation requires integration from q = 0, the data will exhibit an artificial oscillation.

2.10.1 Interpretation of SAXS from Polypropylene

SAXS of semicrystalline polymers have been generally interpreted in terms of theories that were previously reviewed. In most studies, the long period was evaluated from observed scattering vector (or scattering angle) and then correlated with crystallization conditions, such as the isothermal crystallization temperature. Other studies have evaluated material parameters such as χ_c, l_c, etc. from the scattering data on the basis of the theories. a relatively few number of studies have attempted a comparison o the experimental data with theoretical predictions. SAXS data for semicrystalline polymers such as polyethylene and polypropylene typically exhibit near zero-angle diffuse scattering and one or more broad Bragg peaks. The Bragg peak is interpreted as a result of a regular alternation of crystalline and amorphous regions with an average periodicity between ≈ 30 Å and 500 Å. The application of Bragg theory to the first order maximum gives a measure of the average periodic repeat distance of the alternating regions.

For polypropylene, most of the SAXS literature correlates l_c with T_m to determine T_m^o and σ_e by application of the Thomson-Gibbs equation 2.34. Mucha [83] evaluated L from SAXS using the Bragg equation and T_m from DSC. The crystallinity used to determine l_c was also evaluated from SAXS [84]. The peak melting temperatures of the low

temperature melting peak and the high temperature melting peak were interpreted as resulting from melting of β-polypropylene and α-polypropylene, respectively. Linear regression of the melting temperature versus the reciprocal of lamellar thickness data resulted in T_m^o = 212°C, σ_e = 188 erg/cm^2 for α-polypropylene and T_m^o = 172°C, σ_e = 24 erg/cm^2 for β-polypropylene. More recently, Janimak [48], using a more sensitive instrument, evaluated l_c from SAXS for polypropylene of two M_w's as a function of T_c. The SAXS data were interpreted using the electron density correlation function [85]. The onset melting temperature was sued. The resulting linear regression of T_m versus $1/l_c$ gave T_m^o = 185°C and σ_e = 70 erg/cm^2. These are representative of polypropylene SAXS literature and show the wide variation in the analysis of SAXS data.

Little work has been done on the SAXS modeling of polypropylene. However, recently Lee [86] performed an extensive study comparing SAXS experimental data with theoretical modeling for polyethylene. It was shown that a variable stack model with crystallinity distribution and thickness distribution could fit the SAXS curves from highly disperse lamellar systems such as low density polyethylene (LDPE), cross-linked polyethylene (XLPE), and linear low density polyethylene (LLDPE). The modeling showed that the near zero-angle intensity increased with increasing

crystallinity distribution with a fixed thickness distribution. Lorentz correction was found necessary for a more reasonable prediction of the 'true' long period. The observed SAXS intensity curves contain information on the nature of the crystallinity distribution and the thickness distribution that may be of use in correcting the apparent long period for these effects. Figure 2.17 shows the apparent long period versus the height ratio H that resulted from Lee's SAXS modeling. In the model, the 'true' long period would be 1.0 with no crystallinity distribution or thickness distribution.

2.10.2 Complications in SAXS Analysis

Solution grown polymer crystals can give rise to up to four orders of diffraction in SAXS. This is due to the narrow thickness distribution of the alternating crystalline and amorphous regions. However, bulk crystallized polymers rarely give more than two orders of diffraction and many only give one broad first-order peak. This is partly due to the more dispersed nature of lamellae for melt crystallized samples. One result of the dispersity is that the Bragg long period can be significantly different from other measured average periods of the structure. While the techniques that measure the periodic structure of polymer systems, such as SAXS,TEM, and Raman LAM, may give different values for the

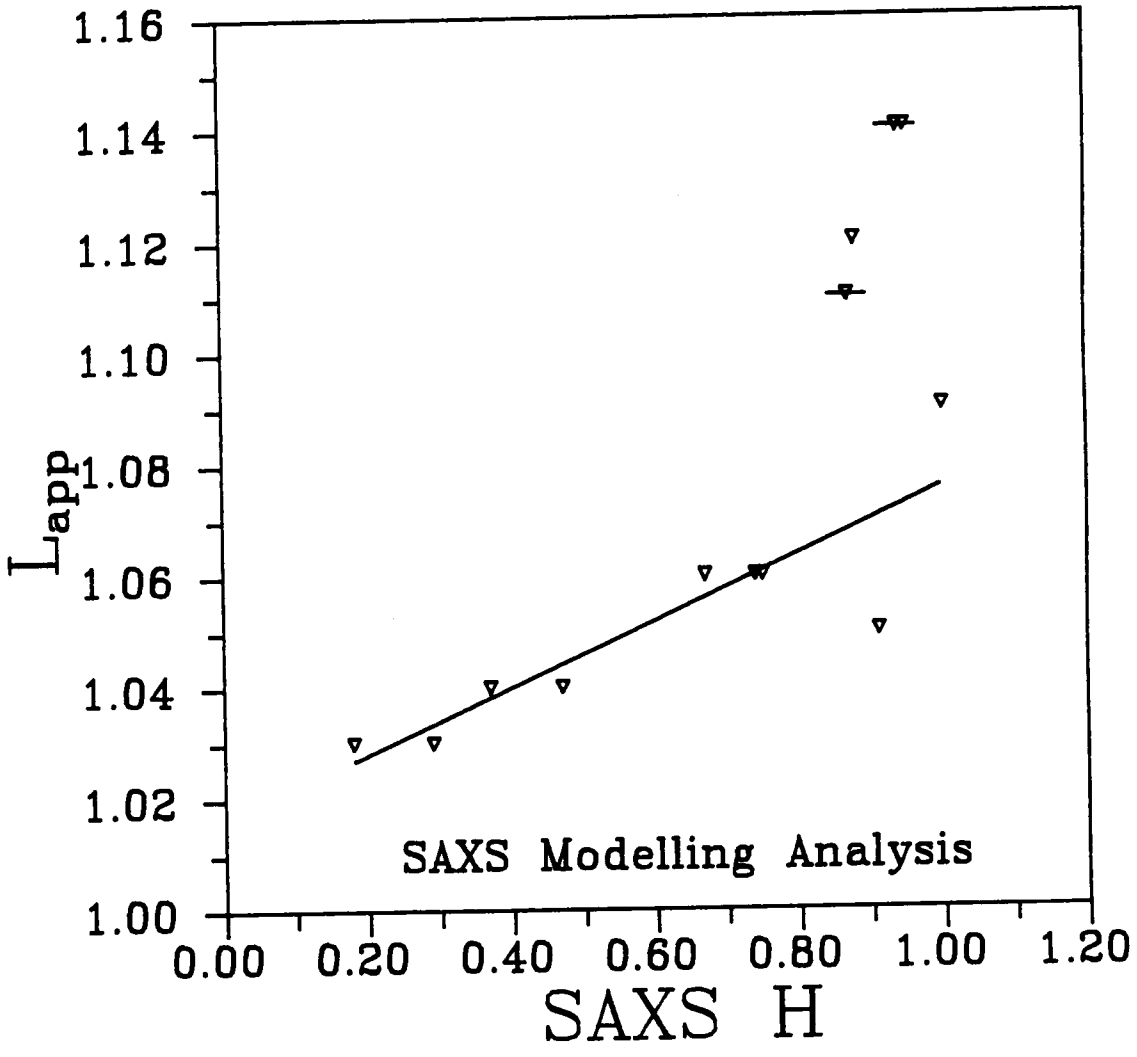


Figure 2.17 SAXS apparent long period L_{app} versus H.

average period of the structure, this does not necessarily imply that the results from a given technique are contradictory, but rather that the techniques are complimentary [78] Some studies have shown that materials with broad molecular weight distributions can crystallize with bimodal thickness distributions due to a molecular weight segregation effect. This bimodal distribution can be detected by SAXS and Raman LAM. However, narrow fractions of polyethylene have also exhibited bimodal lamellar thickness distributions in TEM that were not detected in SAXS. Thus the thin lamellae were not representative features. SAXS will tend to bias larger, more perfect crystals in a thickness distribution. This can result in a sharp SAXS peak and a broad Raman LAM peak. This is because the existence of discrete diffraction maxima depends on the interference effect due to the lamellar periodicity while Raman LAM is apparently unaffected by stacking regularity. A structure with a sharp bimodal distribution of lamellar thickness but with poor lamellar stacking regularity can give rise to a sharp Raman LAM peak and a broad SAXS peak [87]. The simplest model for interpreting SAXS is the infinite stack model with densely packed, isotropically distributed stacks of parallel lamellae. The dimensions of the stacks parallel and normal to the malellar surfaces are assumed to be large compared to the interlammar distance. However, this is not

necessarily a true model of a melt crystallized polymer. Electron micrographs reveal lamellae that are curved, branched, and inclined to one another. One must address the applicability of the SAXS model. The situation of branched lamellae is extremely pertinent to polypropylene, in which the tangential brancing component can be significant. Correlation function analysis can be modified to account for this lamellar structure. The one-dimensional electron density distribution correlation function for the linear system is defined as the average:

$$K(z) = \langle [\eta(z') - \langle\eta\rangle][\eta(z' + z) - \langle\eta\rangle] \rangle \qquad (2.61)$$

A more realistic model of the lamellar structure may be as shown schematically in figure 2.18. A local coordinate system must be established with one axis ez oriented perpendicular to the nearest surface and the other er oriented parallel to it. On the basis of these locally oriented coordinate systems, a two-dimensional correlation function K_2 can be defined:

$$K_2(z,\rho) = \langle [\eta(x) - \langle\eta\rangle][\eta\{x + ze_z(x) + \rho e_\rho(x)\} - \langle\eta\rangle] \rangle \qquad (2.62)$$

As in the one-dimensional correlation function, the angular

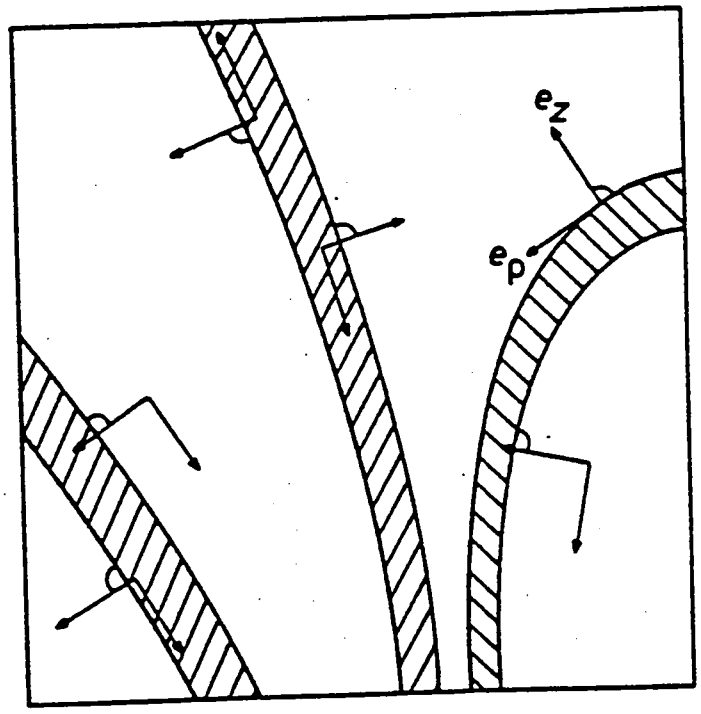


Figure 2.18 Schematic of coordinate system for branching and curving lamellae (from []).

brackets indicate averaging over all sample points x. Figure 2.19 gives the appearance of the two-dimensional correlation function $K_2(z,0)$ which gives the lamellar thickness as does the one-dimensional correlation function $K(z)$ and the appearance of $K_2(0,\rho)$ which indicates the lamellar curvature and tilting. The two-dimensional correlation function must be related to $K(r)$ since this is the only information that can be obtained experimentally. It can be calculated by replacing the cylindrical coordinates z,r by spherical coordinates r,Q and integrating over Q:

$$K(r) = \frac{1}{2\pi r^2}\int_0^{\pi/2} K_2(z = r\sin\Theta, \rho = r\cos\Theta)\, 2\pi r^2 \cos\Theta d\Theta \qquad (2.63)$$

By applying the Fourier transformation in the form appropriate for the linear model, one obtains $d[rK(r)]/dr$ which can be related to $K_2(z,\rho)$:

$$\frac{d}{dr}[r,K(r)] = \frac{d}{dr}\int_0^r K[z\ \rho = (r^2 - z^2)^{1/2}]dz$$

$$= K(z, r = 0) + \int_0^r \frac{\partial K}{\partial r}[z\ \rho = (r^2 - z^2)^{1/2}\frac{\partial \rho}{\partial r}]dz \qquad (2.64)$$

For the case of all plane, parallel lamellae, $(\partial K/\partial r) = 0$, and one has the same resule as the one-dimensional

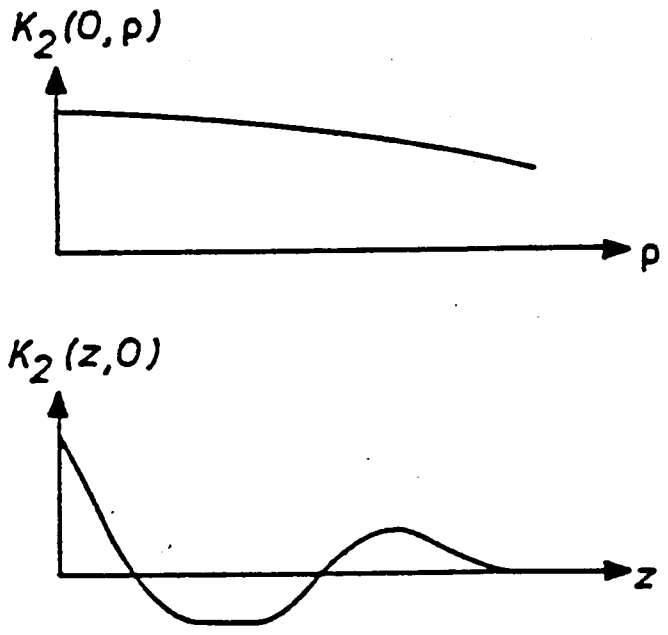


Figure 2.19 Appearance of a two-dimensional correlation function to account for lamellar branching and curving (from [112]).

correlation function. The second term contributes when lamellae are curved or tilted. This allows a qualitative measure of the effect of curvature or tilting of lamellae.

With the shortcomings of SAXS, it might appear that the better tichnique would be electron microscopy. Since the electron microscope looks at lamellae in real space, the accuracy is not limited by the lamellar size. However, the accuracy is never high for several reasons:

1) Sample preparation for EM may produce artifacts of distortions in the structure;

2) The very small sample volumes typically observed may not be representative of the entire structure;

3) Difficulty in accurate calibration of the microscope.

2.10.3 Interpretation of Zero-Angle Intensity

While the interpretation of the diffuse scattering at near zero-angle is not without dispute, some researchers have attempted to use the intensity at near zero-angle. Difficulties in interpreting this intensity arise in part to the difficulties in measuring the zero-angle intensity experimentally. Interparticle interference, which may be present in solid polymers, will contribute to the diffuse scattering. *In situ* experiments on high density polyethylene (HDPE) cooled from the melt in the SAXS exhibited a decrease in the near zero-angle intensity with the development of the

Bragg peak [88]. This behavior has been attributed to a change from a single particle scattering system to an interference system. Song et al. [89] suggested that the change in near zero-angle intensity reflected a structural change from a disordered lamellar structure, with broad lamellar thickness distribution, to a well-defined lamellar stack structure.

Chapter 3

Experimental and Analytical Techniques

3.1 Materials

Isotactic polypropylene was used in the experiments. Bulk isotactic polypropylenes having different molecular weights but similar molecular weight distributions and stereoregularities were studied. Table 3.1 lists the data for the as-received polypropylenes. Figure 3.1 shows the molecular weight distributions of the two isotactic polypropylene homopolymers as received.

3.2 Crystallization

The crystallization of isotactic polypropylene was followed using optical microscopy. Experiments were performed at atmospheric pressure and elevated pressure.

The spherulitic growth rate at temperatures corresponding to supercoolings between approximately 30° and 60°C was measured at atmospheric and elevated pressures using optical microscopy. At atmospheric pressure, the polypropylene was melted on a Mettler hot stage and then rapidly cooled to the desired crystallization temperature. The growth of crystallizing entities was followed as a function of time with the optical microscope and recorded with a camera attached to the microscope. The linear growth rate was determined from the slope of the plot of spherulitic

Table 3.1. Characteristics of Polypropylene Materials

Sample	Resin Type	Melt Index	M_n	M_w	M_z	M_w/M_n	Tacticity(%)
PP1	Homopolymer	35	58	150	287	2.58	>99
PP4	Homopolymer	1400	27	82	159	3.00	>99
PP5	Copolymer (0.5% ethylene)	34	58	148	266	2.55	

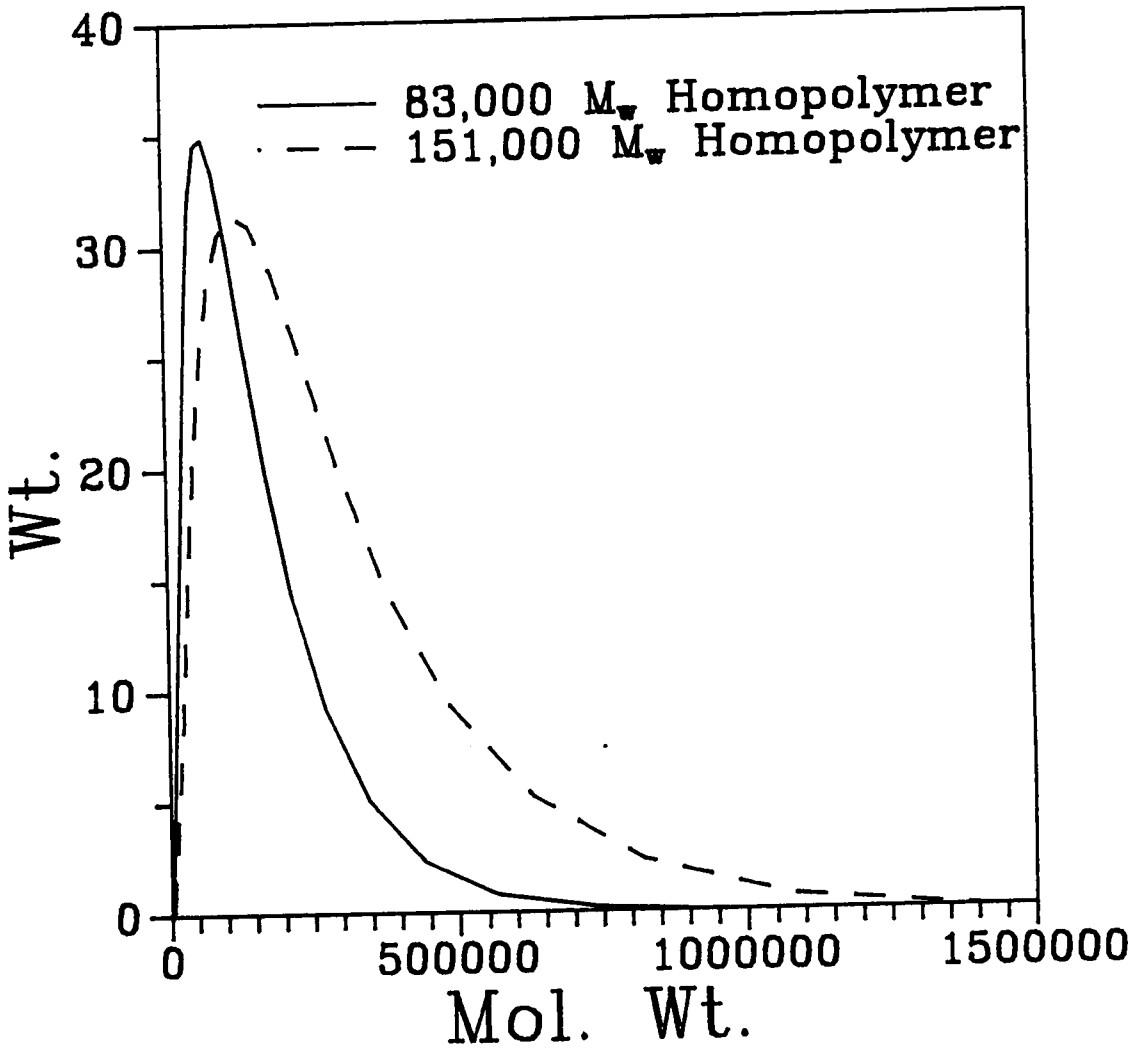
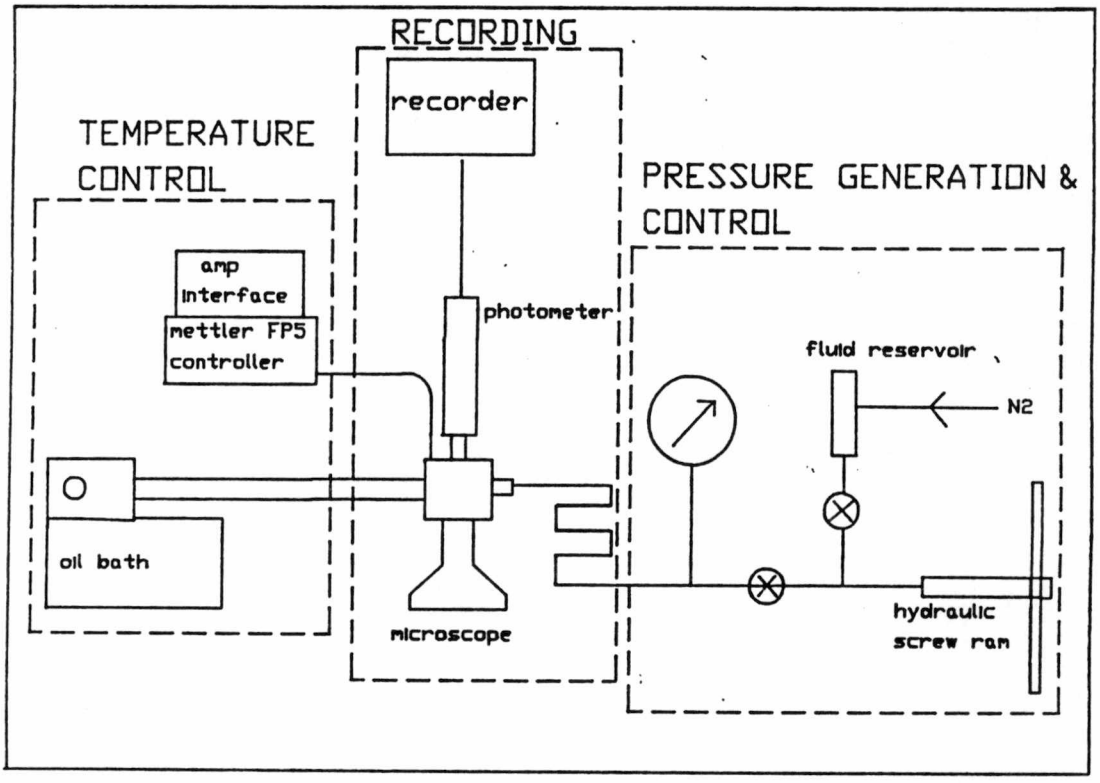


Figure 3.1 Molecular weight distribution curves for isotactic polypropylene homopolymer samples as received.

radius versus time. The nucleation density was determined as a function of time at a given crystallization temperature from the optical micrographs. The linear growth rates and nucleation data were then compared to literature data for polypropylene.

The linear growth rates at elevated pressure were determined in a similar fashion to those at atmospheric pressure. The necessary equipment, however, was different. The elevated pressure experiments required a system that is capable of producing and maintaining pressure as well as controlling temperature. Figure 3.2 represents a schematic of the elevated pressure system. Pressure was developed using a screw type hydraulic ram. Temperature was controlled through a Mettler temperature control unit, which was connected to the pressure cell's cartridge heaters through an interfacing amplifier, and an auxiliary circulating oil bath. The designs of the elevated pressure sample cell and the heat exchanger are shown in Figure 3.3 and 3.4.

The linear growth rate data was analyzed using secondary nucleation theory. Certain parameters for the application of secondary nucleation theory to the experimental data were either experimentally evaluated where feasible or taken from the literature. The parameters that could be experimentally evaluated included the equilibrium melting temperature and the glass transition temperature. Literature values were



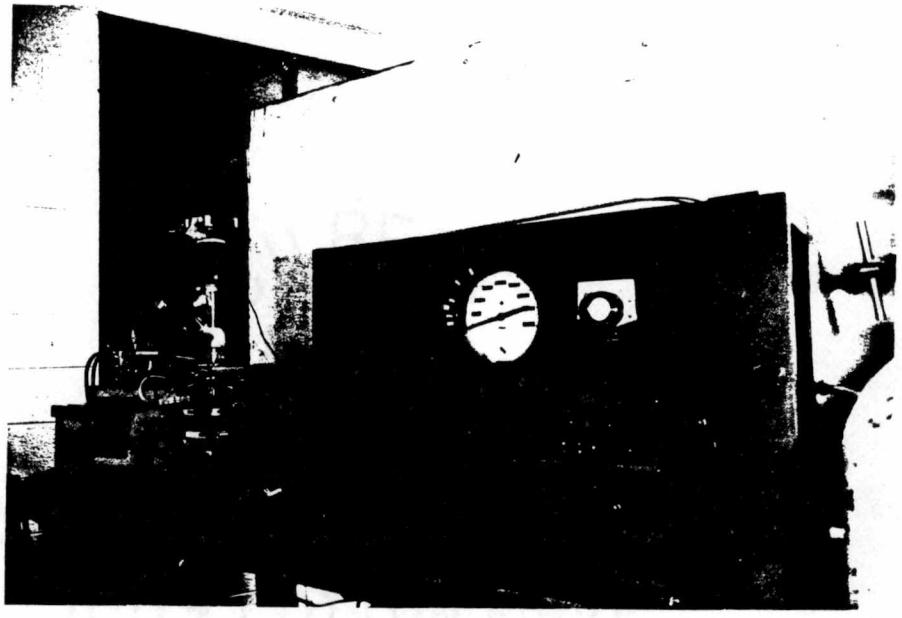


Figure 3.2 Elevated pressure system schematic and photograph.

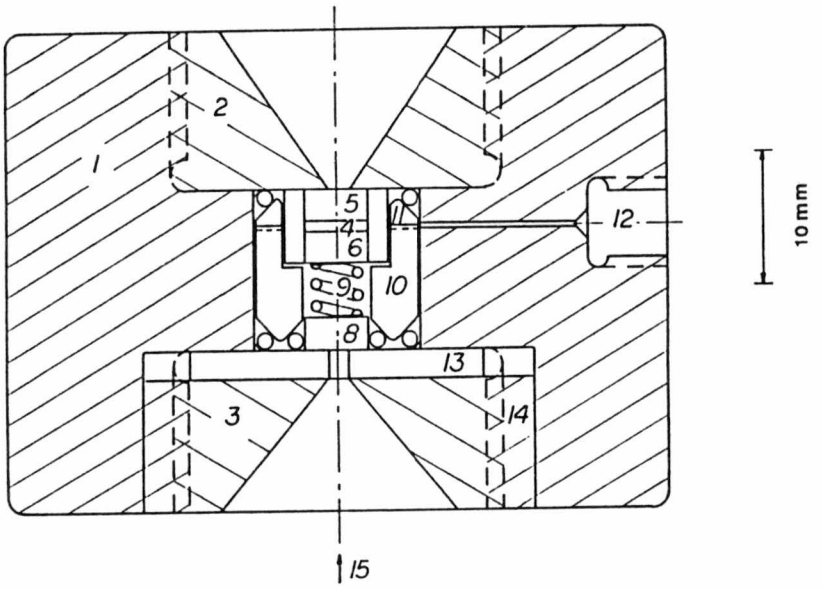


Figure 3.3 Elevated pressure cell schematic and photograph.

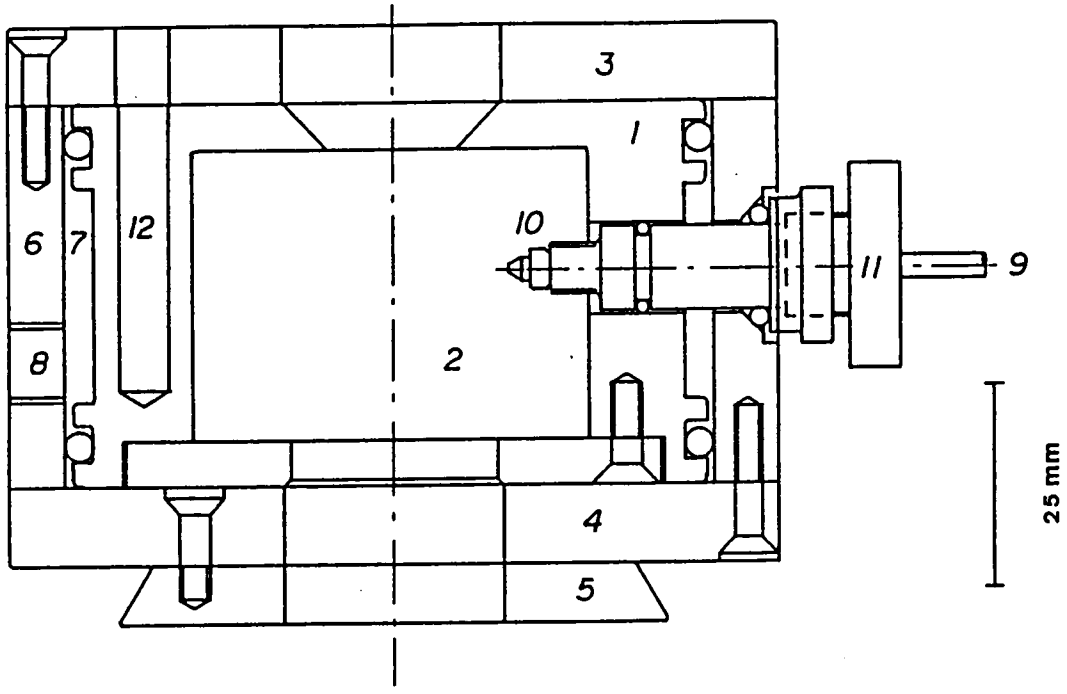


Figure 3.4 Elevated pressure system heat exchanger schematic.

used for U^*. The results of the atmospheric pressure kinetics data for the homopolymers were compared to literature data in order to determine the effect of molecular weight on regime transitions and on the fold surface energy. The copolymer data was compared to the homopolymer data to determine the effect of the comonomer on crystallization kinetics. The results of the elevated pressure kinetics data were compared to the atmospheric kinetics data in order to determine the effect of pressure on regime transitions and on the fold surface free energy. The experimental data were also compared to the available literature pressure kinetics data of other polymers in order to compare the effects of pressure as a result of polymer structure.

3.3 Morphology

The nature of the morphology of isotactic polypropylene is complex. By applying several available tools for studying morphology at various structural levels, the effect on morphology of the experimental processing variables temperature and pressure and the molecular variables weight and structure can be correlated at the different levels. Three distinct levels of morphological structure of the isothermally crystallized samples were studied using optical and electron microscopy, small angle X-ray scattering (SAXS), and wide angle X-ray diffraction (WAXD). The optical microscope was used to distinguish the various spherulite

types by the sign and magnitude of the birefringence. The qualitative texture of the spherulites as a function of the crystallization temperature and pressure was evaluated. WAXD was used to study the effect of crystallization pressure and copolymer composition on the crystal lattice. Polypropylene is known to exist in several forms and WAXD can easily distinguish the forms. SAXS and EM was used to study the lamellar level of structual development. Both scanning electrom microscopy (SEM) and transmission electron microscopy (TEM) were used to observe the effect of crystallization temperature and pressure on the lamellar structure, particularly the development of radial and tangential components. SAXS was used to evaluate average long period as a function of crystallization temperature and pressure. Lamellar thickness, l, was determined assuming a two-phase model from measured long periods from SAXS and estimated crystallinities from WAXD. The relationsip between l and melting temperature allows an independent determination of the equilibrium melting temperature T_m^o and the fold surface free energy σ_e.

3.4 Thermal Analysis

The value of the equilibrium melting temperature T_m^o is required to carry out secondary nucleation analysis of the experimental kinetics data. Differential scanning calorimetry (DSC) and depolarized light intensity (DLI) were

used to evaluate the thermal behavior of isothermally crystallized samples. For atmospheric pressure crystallized samples, the melting behavior measured with DLI was correlated to that observed with DSC. The DLI technique to measure melting temperatue employed the same equipment as the DLI crystallization experiments. The procedure involved heating the isothermally crystallized sample at a constant rate and recording the light intensity as a function of temperature. The thermal lag of the Mettler hot stage and the high pressure cell was calibrated. From the DLI trace, the melting temperature was determined with a modified return-to-baseline technique. This correlation was then employed with DLI melting measurements of elevated pressure crystallized samples. Hoffman-Weeks plots of T_m versus T_c were constructed to evaluate the equlibrium melting temperature and the thickening factor γ. Experimental equilibrium melting temperatures as a function of pressure were compared to calculated values from the Clausius-Clapyron equation.

3.5 Small Angle X-ray Scattering

The small angle X-ray scattering experiments were conducted at the National Center for Small Angle Scattering Research at the Oak Ridge National Laboratory in Oak Ridge, TN. All measurements were performed with a sample to detector distance of 5 m. The NCSASR SAXS system consists of

a rotating anode X-ray source, crystal monochromator, pin-hole collimation, and a two-dimensional position-sensitive proportional counter. The SAXS system schematic is shown in Figure 3.5.

The Rigaku-Denki rotating anode X-ray source with tungsten filament is operated at 40 KV and 100 mA. The source to sample distance is 162 cm with monochromatization achieved using a pyrolytic graphite crystal to select Cu Ka and collimation is achieved using two 1-mm diameter pin-holes separated by 154 cm. The entire source-to-sample-to-detector flight path is operated under a vacuum of > 50 μm Hg.

The material parameters required to collect the SAXS pattern are the sample thickness, measured with a micrometer, and the sample transmission coefficient. The transmission coefficient (the ratio of the intensity transmitted through the sample to that of the incident X-ray beam) is given as:

$$T_o = \frac{I_{gc+s} - 0.7I_s}{I_{gc} - 0.7I_{DC}}$$

where Igc+s is the intensity of the X-ray beam with glassy carbon and sample in the X-ray path, Is is the intensity of the X-ray beam with only the sample in the X-ray path, Igc is the intensity with only the glassy carbon in the path, and IDC is the intensity without anything in the X-ray path. The

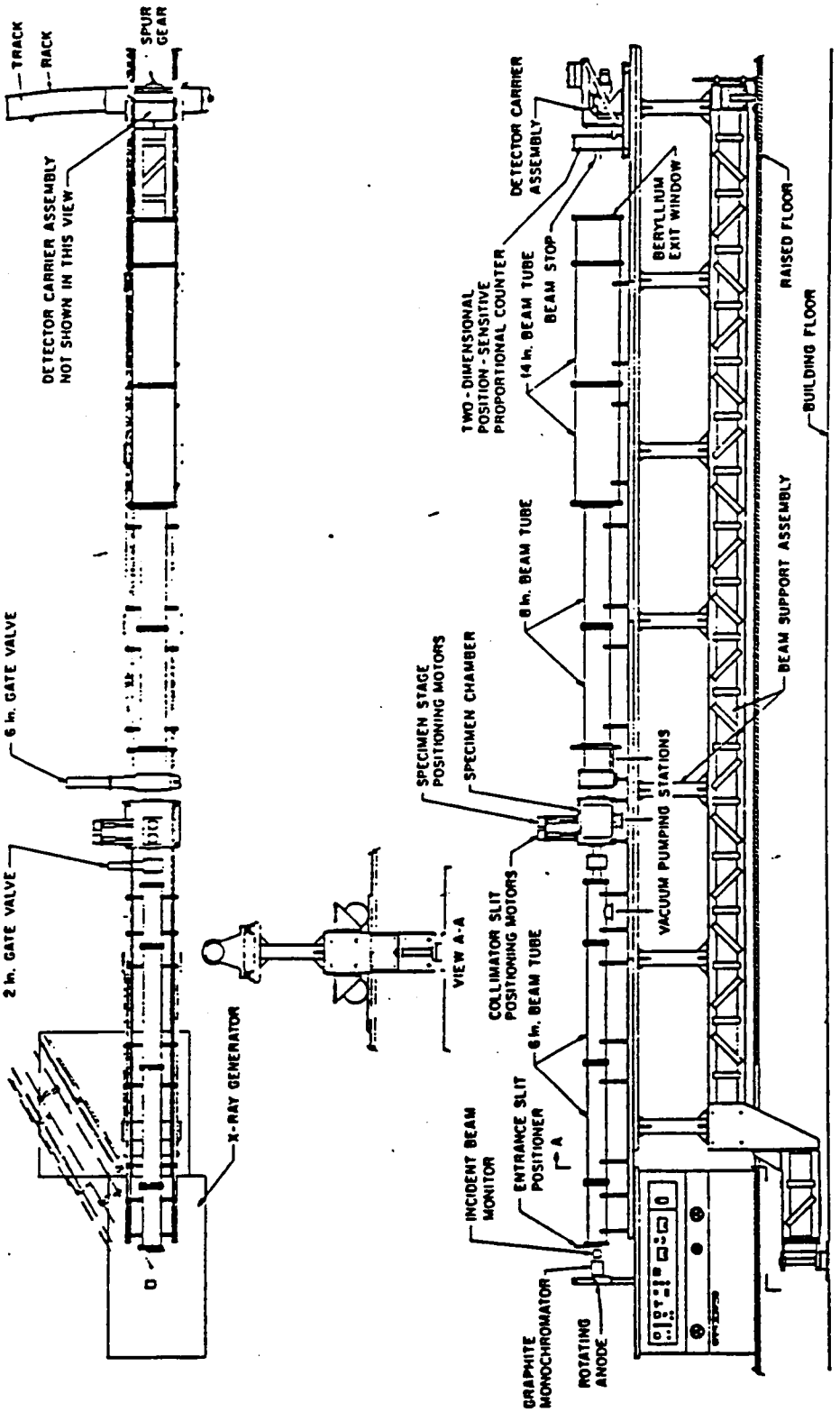


Figure 3.5 Schematic of the NCSASR 10 meter SAXS spectrometer at ORNL.

coefficient 0.7 is the transmission coefficient of glassy carbon.

Samples were prepared for SAXS analysis using one procedure for atmospheric pressure samples and another for elevated pressure samples. The procedure for atmospheric samples is as follows. Samples with dimensions approximately 1cm x 3cm x 3mm were cut from a sheet of isotactic polypropylene that had been prepared by melting at 190°C, then air cooling. The samples were wrapped in aluminum foil, submerged into silicone heating fluid maintained at the desired melt temperature with a Haake temperature bath, and maintained at the melt temperature for approximately 20 minutes. The sample was then rapidly transferred into another Haake bath with silicone heating fluid maintained at the desired isothermal crystallization temperature. The sample was removed from the isothermal crystallization bath after sufficient time to ensure complete primary crystallization, which was determined from depolarized light intensity bulk crystallization experiments.

The procedure for elevated pressure samples is as follows. Samples with dimensions approximately 3mm thick and 2.5cm in diameter were cut from a sheet of isotactic polypropylene. The samples were placed into the elevated pressure crystallization cell (described previously in section 3.3), melted at atmospheric pressure at 190°C for 20

minutes. Pressure was then rapidly increased to the desired crystallization pressure and the temperature adjusted to the desired crystallization temperature. After sufficient time to ensure complete crystallization, the temperature was reduced to room temperature, followed by the release of pressure.

In situ SAXS

A series of elevated temperature SAXS were carried out by in situ experiments. The standard sample holder was replaced by a specially designed sample holder that consisted of a small aluminum block sample holder fitted into a copper heat exchanger. A Lauda circulating temperature bath with ethylene glycol as a heat transfer medium was connected to the heat exchanger through special ports in a modified vacuum sample chamber by insulated Fluran tubing. A thermocouple attached to the sample measured the sample temperature. The isothermal temperature experiment was controlled to ± 0.5°C. Figure 3.6 shows the in situ SAXS experimental equipment schematic.

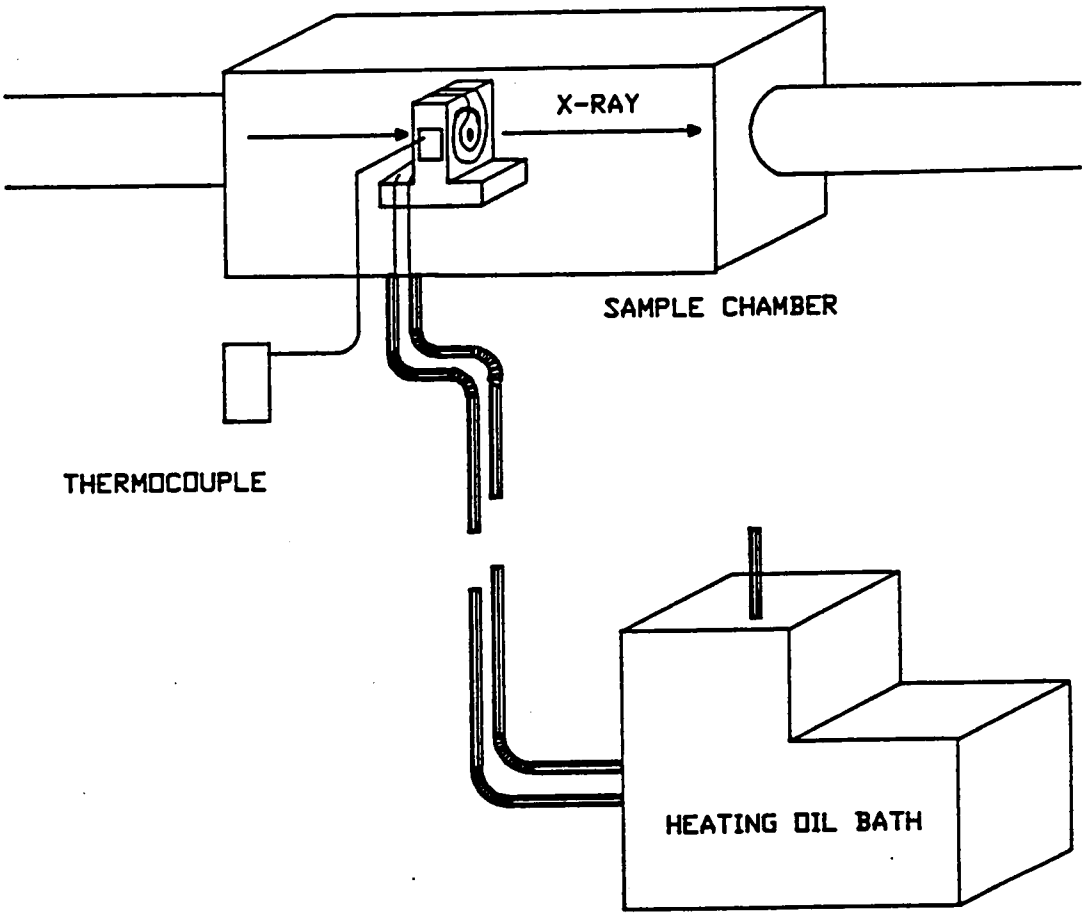


Figure 3.6 In situ SAXS experimental equipment for measurement of SAXS at elevated temperatures.

Chapter 4

Results

4.1 Wide Angle X-ray Diffraction

4.1.1 Atmospheric Pressure - f(Tc)

The wide angle X-ray diffraction behavior at various isothermal crystallization temperatures at atmospheric pressure for isotactic polypropylene were obtained using a Rigaku Denki diffractometer as well as recording the WAXD image with a flat plate camera. The diffraction scans were recorded from $2\Theta = 5°$ to $2\Theta = 50°$. All scans showed the characteristic scattering of the monoclinic form of isotactic polypropylene. Figure 4.1 shows representative WAXD scans for isotactic polypropylene M_w = 151,000 homopolymer for various crystallization temperatures. The diffraction scans of samples crystallized at certain temperatures showed evidence of a peak around $2\Theta = 19°$, which corresponds to the d = 4.42 Å diffraction planes of the γ-form of isotactic polypropylene. The most intense scattering occurred for the (110) diffraction planes. The height ratio of the (040) and (130) peaks relative to the (110) peaks ranged from 0.36 to 0.75 for the (040) and from 0.35 to 0.58 for the (130). For certain crystallization temperatures the height of the (130) peak was greater than that for the (040) peak. This is particularly true for crystallization temperatures greater

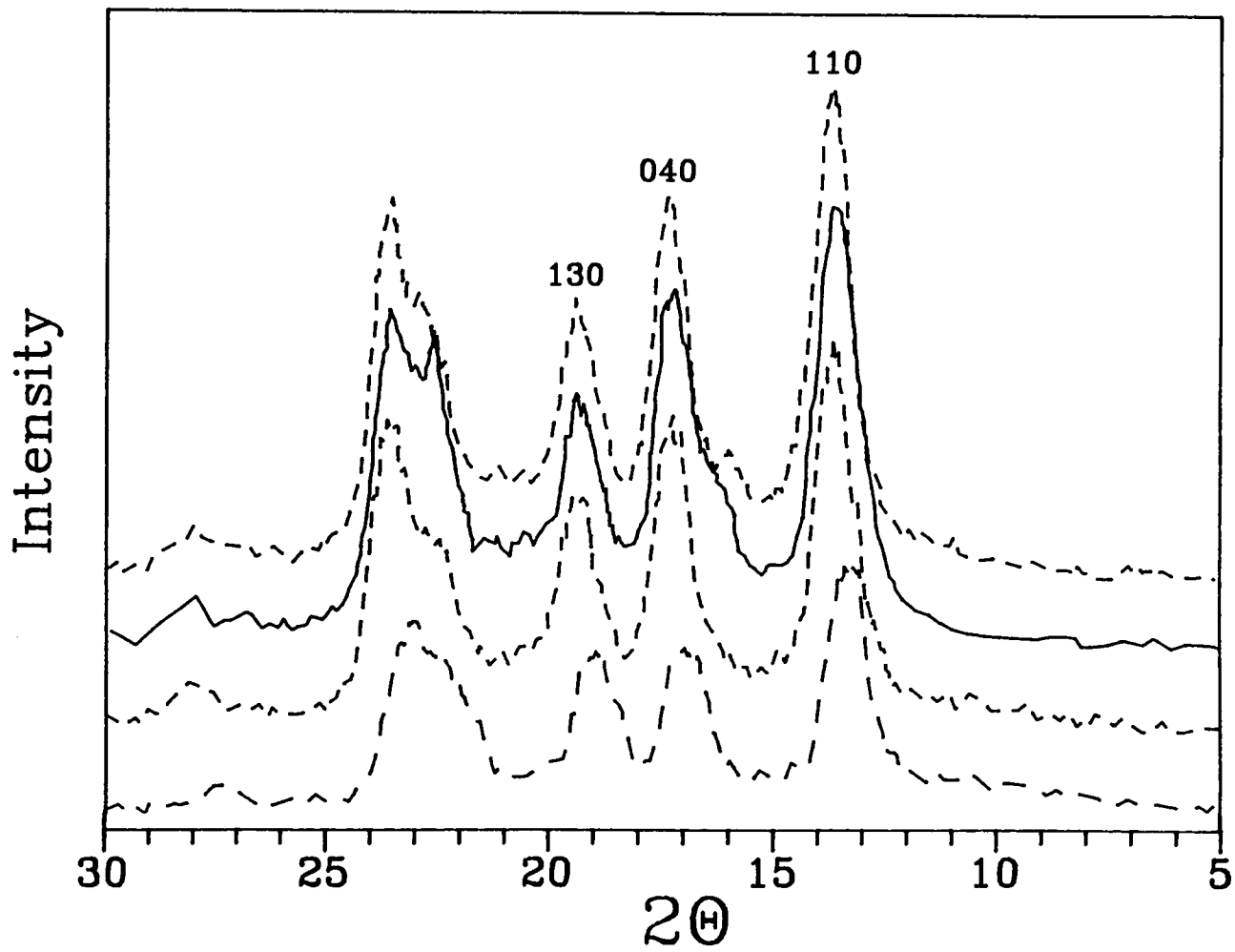


Figure 4.1 WAXD as a function of crystallization temperature for isotactic polypropylene 151,000 M_w homopolymer crystallized at atmospheric pressure.

than 140°C. Certain scans showed somewhat indistinct splitting of the (041), (131), and (111) peaks. Most of the scans that showed this behavior also showed some evidence of the peak associated with the γ-form of isotactic polypropylene. The splitting varied from a single peak with a slight shoulder to distinct sharp double peaks. In all scans with distinct splitting, the intensity of the (041) - (131) peak was greater than that for the (111) peak. Table 4.1 summarizes WAXD intensity ratios for several peaks of the homopolymer and the copolymer.

It is seen that the homopolymer and copolymer show qualitatively similar WAXD behavior as a function of crystallization temperature. However, the relative intensities of the (040) and (130) to the (110) are lower for the copolymer at most temperatures. Apparent crystal sizes normal to the (110), (040), and (130) planes have been calculated using Scherrer's equation: $L_{hkl} = A/\delta S$ where A is geometry dependent and (δS) is the peak breadth at half-height expressed in units of S, $Å^{-1}$ [90]. Table 4.2 gives the apparent crystal sizes for the homopolymer and copolymer as a function of crystallization temperature, based on the (110) plane.

4.1.2 Elevated Press.- f(P_c)

The WAXD behavior of isotactic polypropylene M_w = 151,000 homopolymer as a function of crystallization pressure

Table 4.1 X-ray Relative Intensities for Isotactic Polypropylene Isothermally Crystallized at Atmospheric Pressure.

Tc, °C	Relative Intensities I_{040}/I_{110}		I_{130}/I_{110}	
	Homopolymer	Copolymer	Homopolymer	Copolymer
127	75	28	43	28
129	68	24	39	21
134	68	34	43	27
135	43	43	39	35
136	36	46	39	41
137	40	44	35	40
138	68	30	47	42
139	58	40	47	42
140	72	31	49	35
141	47	44	54	44
142	46	37	50	35
143	54	36	49	40
144	42	45	48	43
145	42	44	47	54

Table 4.2 WAXD Apparent Crystal Size (110).

T_c (°C)	151,000 M_w Homopolymer χ_c	l_{WAXD}[a] (Å)	151,000 M_w Copolymer χ_c	l_{WAXD}[a] (Å)
127	52.8	98	64.9	177
129	52.6	104	63.5	196
134	57.4	126	67.8	221
135	59.8	177	60.8	136
136	63.1	196	64.2	136
137	65.4	161	59.6	131
138	57.5	118	72.5	236
139	60.8	98	66.6	168
140	61.1	126	65.9	272
141	62.6	196	65.8	114
142	66.1	196	64.7	98
143	65.4	93	67.7	147
144	71.7	177	63.9	93
145	57.9	147	67.7	196
146	55.1	118	77.2	321

Notes:
a Apparent crystal size on (110) using Scherrer's equation

at $\Delta T = 50°C$ was recorded at atmospheric pressure with a Rigaku Denki diffractometer and a flat plat camera. The diffraction scans were recorded for 2Θ between 5° and 50°. Figure 4.2A, B, and C are flat plate images of samples crystallized at atmospheric pressure, 100 MPa, and 200 MPa, respectively. The flat plate images clearly show the change in crystal structure with no preferred orientation observed within the samples. Figure 4.3 shows the diffraction scans for samples crystallized at atmospheric pressure, 25 MPa, 50 MPa, 100 MPa, and 200 MPa. The atmospheric pressure scan exhibits behavior consistent with the monoclinic crystal structure while the 200 MPa exhibits behavior consistent with the orthorhombic crystal structure published by Brückner et al. [7]. The diffraction patterns of polypropylene crystallized at pressures between atmospheric pressure and 200 MPa exhibit peaks characteristic of the monoclinic and the orthorhombic crystal structures, indicating a mixture of the crystal structures within the samples. The elevated pressure crystallized samples' diffraction behavior is consistent with that of other bulk polypropylenes that have been pressure crystallized [91]. The ratio of the areas of the 2Θ peak between 18° and 19° for the α form and the 2Θ peak between 19° and 21° for the γ form has been used as a measure of the composition as a function of crystallization pressure. Figure 4.4 shows the γ polypropylene content as a

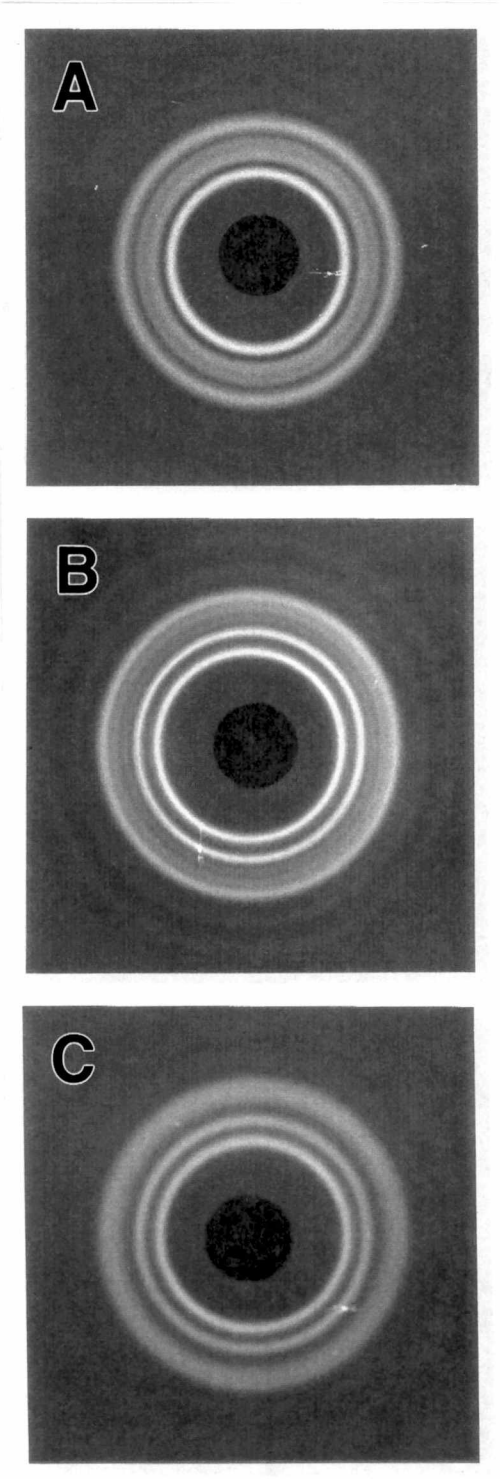


Figure 4.2 Flat plate WAXD of atmospheric pressure and elevated pressure isothermally crystallized isotactic polypropylene, $\Delta T = 50^{\circ}C$; A. Atmospheric pressure, B. 100 MPa, and C. 200 MPa.

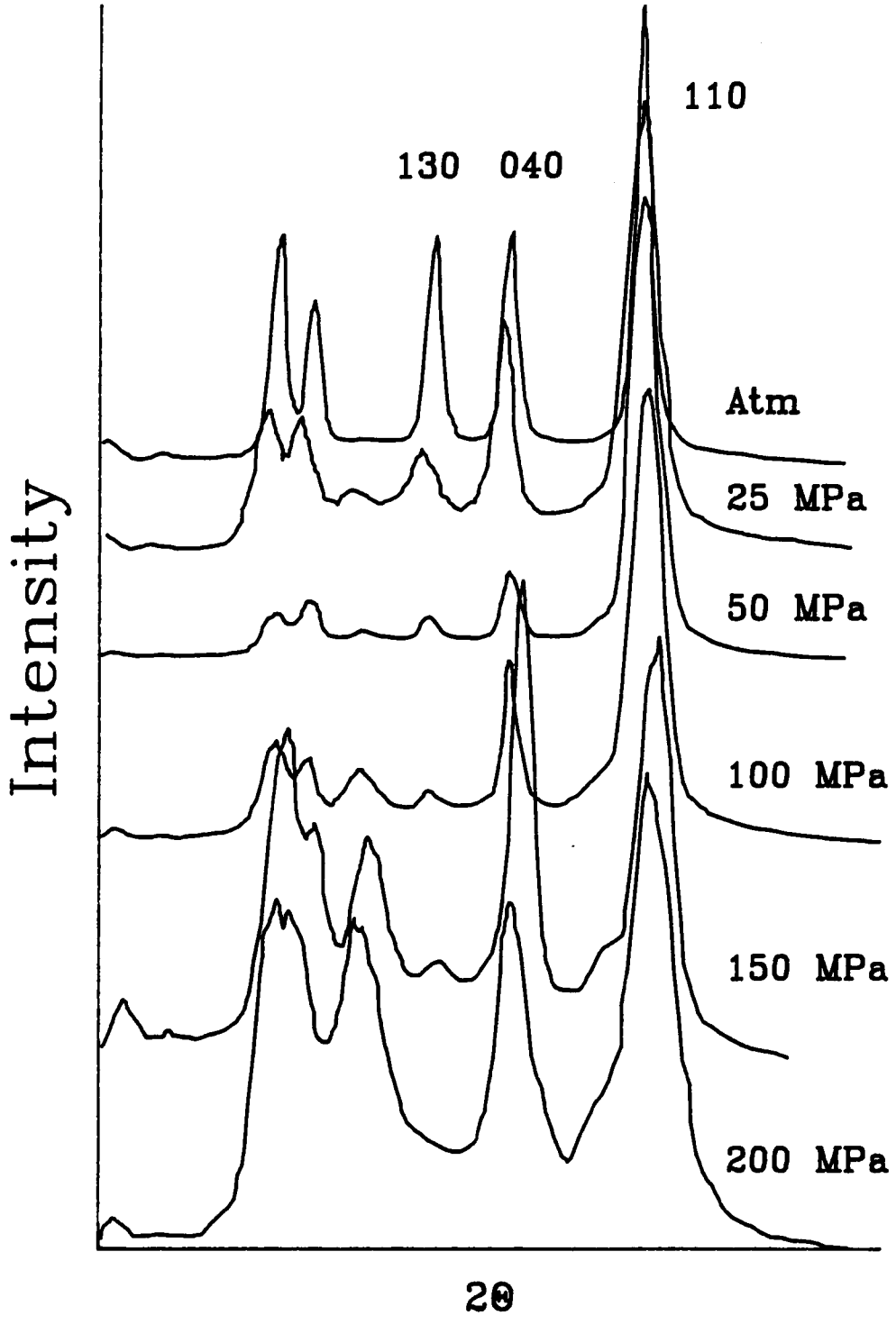


Figure 4.3 WAXD as a function of crystallization pressure for isotactic polypropylene 151,000 M_w homopolymer, ΔT = 50°C.

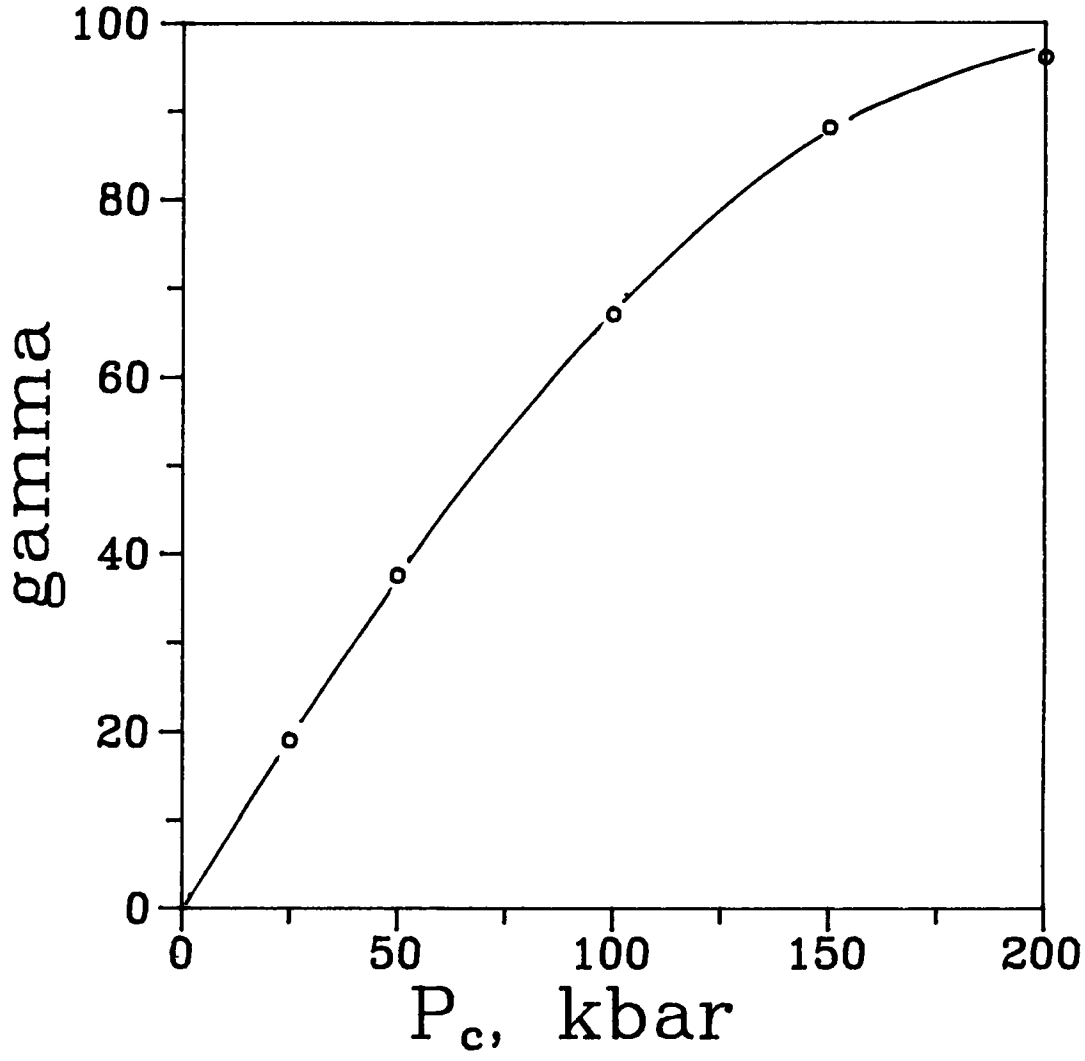


Figure 4.4 Composition from WAXD of isotactic polypropylene crystallized at elevated pressure.

function of crystallization pressure. While the WAXD scans of the pressure crystallized polypropylene samples show a change in crystal structure as exhibited by the near complete loss of the peak at $2\Theta = 19°$ and the appearance of the peak at $2\Theta = 20.5°$ at 200 MPa, it is observed that the diffraction scan of the pressure crystallized polypropylene, especially the 200 MPa sample, is different from the diffraction scan of low molecular weight polypropylene that has been crystallized in the γ-form [92]. This difference in the diffraction scans would be expected on the basis of the molecular weight difference of the two samples (M_w = 151,000 for the elevated pressure crystallized, M_w = 6,300 for the atmospheric pressure crystallized). For the proposed orthorhombic crystal structure, the integrated intensity is largest for the peak at $2\Theta = 13.8°$ (111) with the next two integrated intensities being the peaks at $2\Theta = 16°$. (008) and $2\Theta = 20°$ (117). While this is in fair agreement with the experimental 200 MPa sample, the peaks are significantly broader for the pressure crystallized material. The diffraction scans reported for pressure crystallized polypropylene are in good agreement with the experimental scans, even for samples that were crystallized at much higher pressures. It is apparent that some of the observed differences can be accounted for by differences between samples that have been used to generate the γ-form. Only incomplete information is available for the

samples in the literature. Morrow reported a molecular weight of $M_n < 3800$, Pae a molecular weight of 325,000 (M_η), and Brückner a molecular weight of 6,300 (M_n). No MWD information is reported for Morrow or Pae's samples. While none of the elevated pressure literature references reported stereoregularity information, it is known that the stereoregularity of commercial samples two decades ago (or even one decade ago) was lower than most currently available commercial materials. Janimak [55] has shown that polypropylene WAXD behavior is strongly dependent on the stereoregularity. In general, the intensities of the diffraction peaks decrease and the half-widths increase with decreasing isotacticity. The 2Θ positions of the diffraction peaks also shift to lower values with decreasing isotacticity. The shifting of the peak positions is a result of the packing of chains with tacticity variation. Significant differences existed for polypropylenes with isotacticities of 0.988 and 0.953.

4.1.3 Elevated Pressure - $f(T_c)$

The WAXD behavior of isotactic polypropylene that had been isothermally crystallized at several fixed supercoolings at 100 MPa and 200 MPa was studied. This allowed for observations in changes in crystallinity and γ content as a function of supercooling. At a fixed supercooling, it allowed for observations in changes in crystallinity and γ

content as a function of crystallization time. It was observed that, at times shorter than t_∞ at a fixed supercooling and 100 MPa, the γ content was somewhat lower than that of a completely crystallized sample. However, at 200 MPa, for the experimental crystallization temperature range, it was observed that the γ content changed only slightly with short crystallization times.

4.1.4 Elevated Temperature

The WAXD of samples that had been isothermally crystallized at atmospheric pressure and elevated pressure at ΔT = 50°C were recorded as a function of temperature using a Rigaku Denki diffractometer with high temperature stage. The high temperature stage was calibrated using standard methods and the temperature of the sample could be controlled within 0.2 K within the temperature range studied.

The atmospheric pressure crystallized sample M_w = 151,000 was studied from 25° to 161°C. The resulting diffraction scans, shown in Figure 4.5, exhibit little change in the amorphous region from 25° to 130°C, which is expected since the sample was crystallized at T_c = 135°C and the DSC shows no melting below 135°C. The peak positions shift only slightly and the shift is in agreement with the known thermal expansion coefficients for isotactic polypropylene (monoclinic form) [93]. Figure 4.6 shows the plot of the

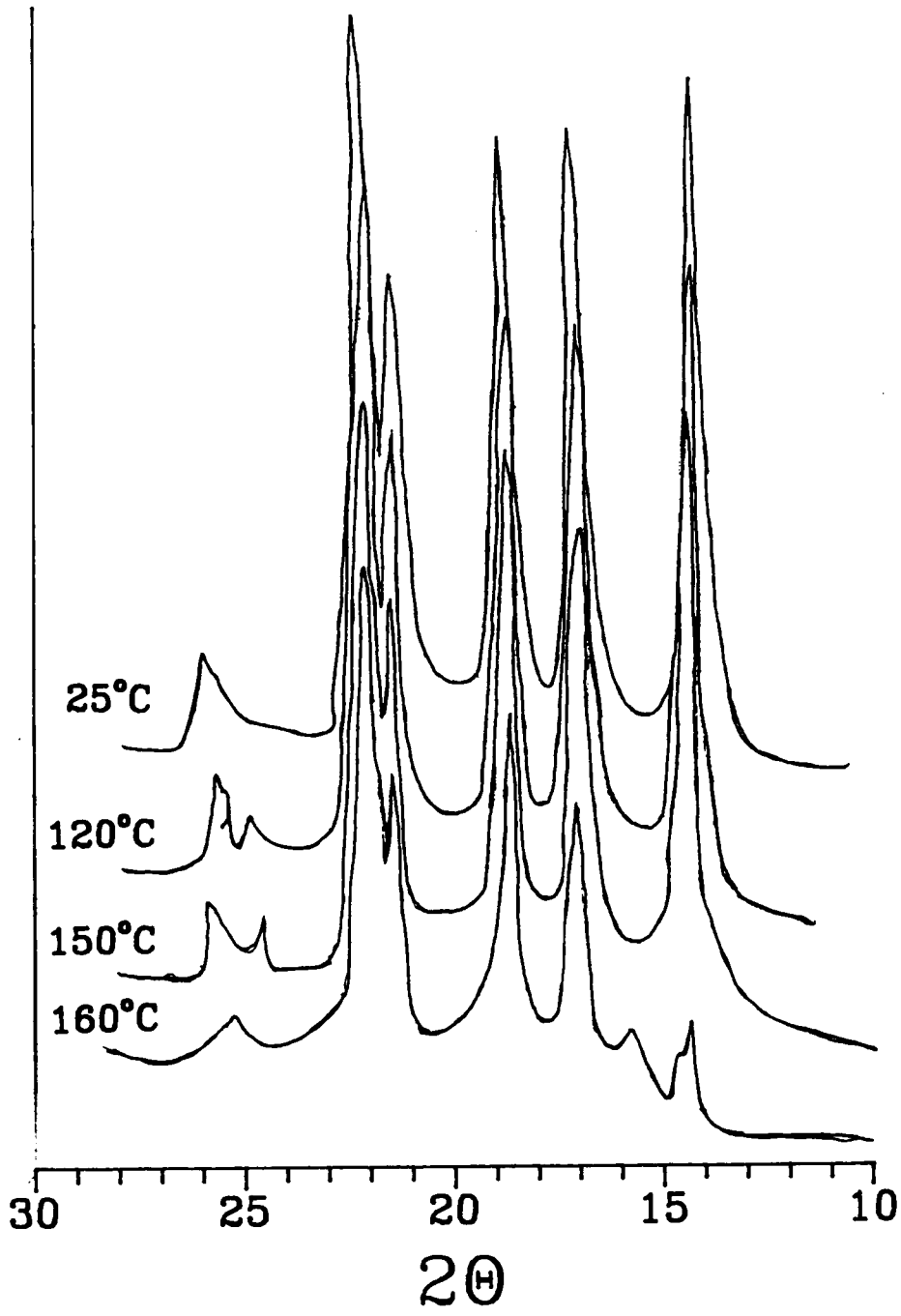


Figure 4.5 WAXD at elevated temperature of isotactic polypropylene isothermally crystallized at atmospheric pressure, T_c = 129°C. Scan temperatures indicated on figure.

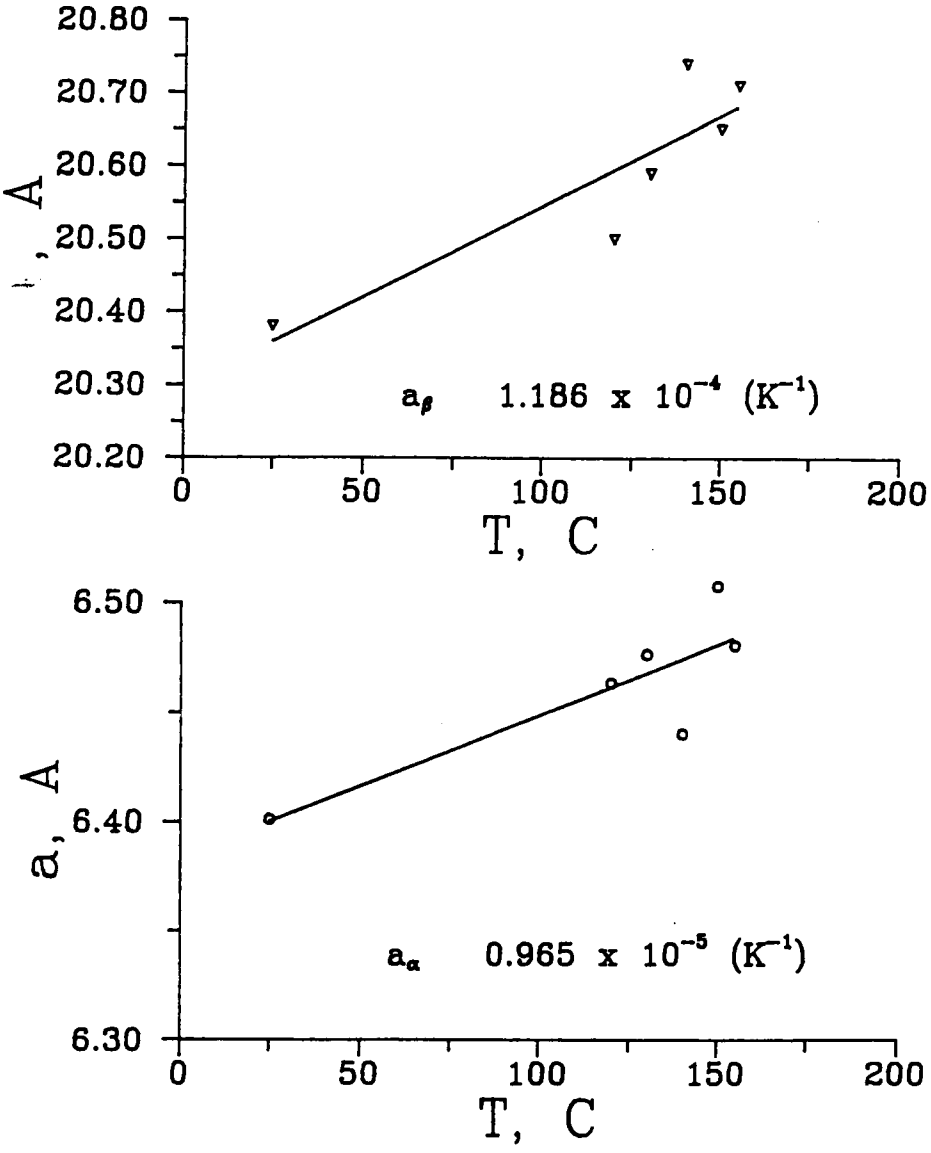


Figure 4.6 Length of the a axis and the b axis of isotactic polypropylene monoclinic unit cell as a function of scan temperature from WAXD.

lengths of the a axis and the b axis as a function of temperature. The b axis length was determined from the (040) plane spacing and the a axis length was determined from the (110) and (130) plane spacings. The thermal expansion coefficients were then determined from the data. The thermal expansion coeffient α_a of the a axis was determined to be $0.965 \times 10^{-4}\ K^{-1}$ and the thermal expansion coeficient α_b of the b axis was determined to be $1.186 \times 10^{-4}\ K^{-1}$. The reported values for the thermal expansion coefficients range from $\approx 1.1 \times 10^{-4}$ to $0.6 \times 10^{-4}\ K^{-1}$ for the a axis and from $\approx 2.3 \times 10^{-4}$ to $1.5 \times 10^{-4}\ K^{-1}$ for the b axis . The range of values has been reported to be due to the different limiting structures in isotactic polypropylene with the lower α values associated with the order limiting structure α_1 (C2/c) and the higher values associated with the disorder limiting structure α_2 ($P2_1/c$). The 150°C scan shows an increase in the intensity of the amorphous background and a decrease in the intensities of several of the crystalline peaks. For scans above 150°C the amorphous background intensity increases while the intensities of the crystalline peaks decreases. The (110) peak shows the largest decrease in intensity while the peaks associated with the (111) and (131),(041) planes show the least change in intensity. As for the lower temperatures, the peak positions shift in agreement with thermal expansion.

The WAXD of elevated pressure crystallized samples was measured at 25°, 140°, and 155°C. Figure 4.7 shows typical results for the 100 MPa sample. The temperatures were chosen so that a comparison with literature results could be made [94,95,100]. In general, the elevated pressure crystallized samples showed more change in WAXD behavior with temperature than that of the atmospheric pressure sample. At 25 MPa, where approximately 18% of the material is γ (see Figure 4.3), the α (130) peak shows little change from 25 to 140°C. However, there is an increase in the α peak at 2Θ = 19° (130) from 140° to 155°C. There is also a decrease in the γ peak at 2Θ = 20.5°. The changes in the amorphous background at 140°C and 155°C were similar to the changes observed for the atmospheric pressure crystallized sample. The 50 MPa sample WAXD showed changes with temperature that were similar to those observed for the 25 MPa sample. The intensity of the alpha peak at 2Θ = 19 increases slightly with increasing temperature while the intensity of the γ peak at 2Θ = 20.5° decreases. The behavior in the 2Θ range from 21° to 23° changes from a broad single peak with shoulder at 25° and 140°C to two distinct peaks at 155°C. While the separation of this 2Θ region is consistent with α polypropylene or low molecular weight γ polypropylene, in general the splitting for pressure crystallized polypropylene experimentally as well as in the literature is less distinct

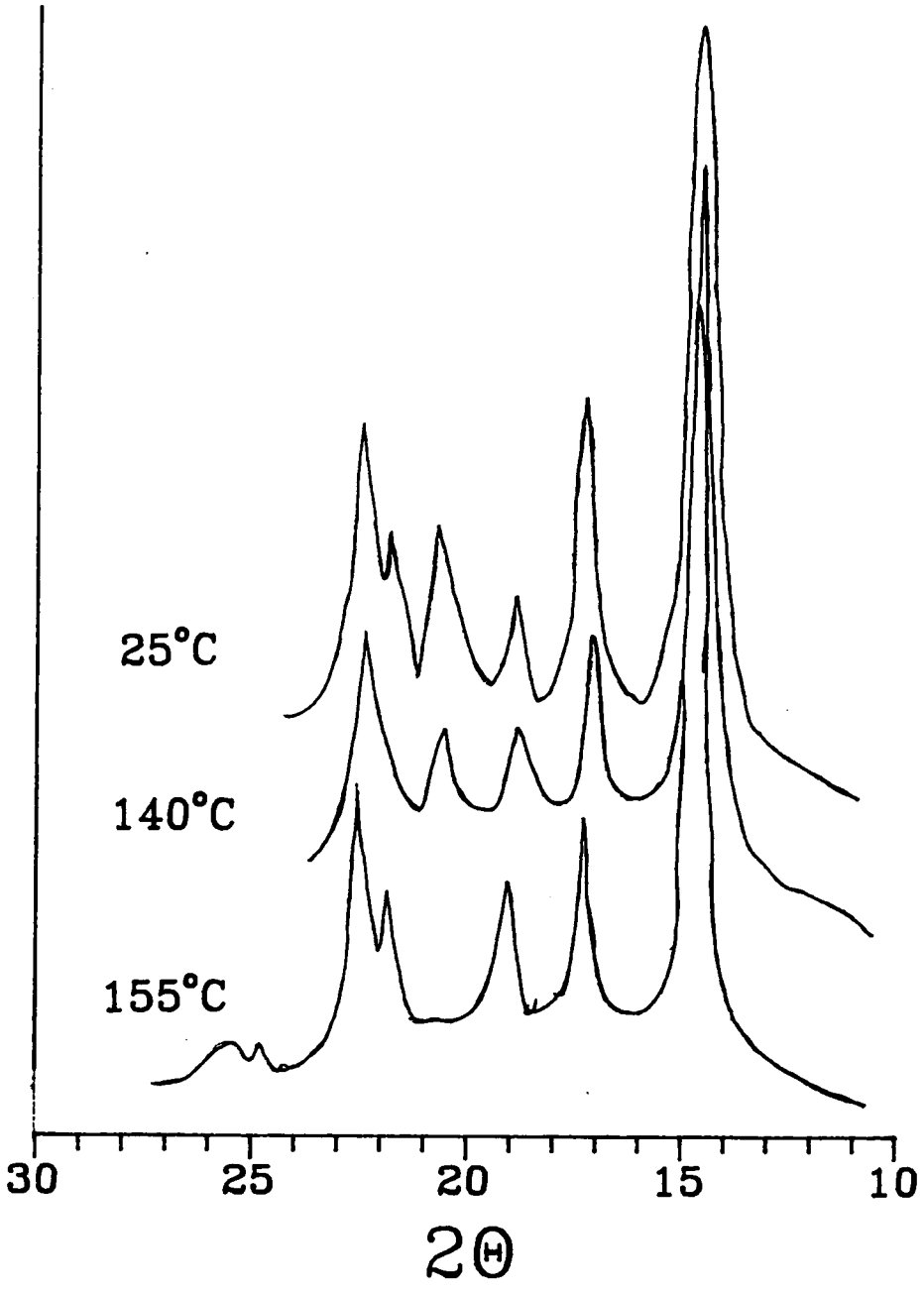


Figure 4.7 WAXD at elevated temperature of isotactic polypropylene isothermally crystallized at elevated pressure, ΔT = 50°C, P_c = 100 MPa. Scan temperatures indicated on figure.

than for α polypropylene. The 75 MPa sample's behavior was much like that of the 50 MPa sample. Again, the peak at 2Θ = 19° increases with increasing temperature. For 100 MPa, after 30 min. at 140°C, the γ peak has decreased significantly while the α peak is relatively unchanged. However after 30 min. at 155°C, both the α and γ peaks have changed significantly. Essentially all of the γ peak is gone. The WAXD scan after 30 min. at 155°C for the 100 MPa sample was not the same as that for the atmospheric sample after 30 min. at 155°C. While there is clearly a change in the α - γ composition of 100 MPa sample at 155°C, the material retains some pressure crystallization history. For crystallization pressures above 100 MPa, the amorphous background increases significantly more than for samples crystallized at pressures below 100 MPa. The 125 MPa sample exhibits a moderate decrease in the gamma peak as well as an increase in the amorphous background at 140°C. At 155°C, the γ peak no longer exists, even at short times. The α peak has increased as well as the amorphous background. The peak at 2Θ = 14.0° (α (110),γ (111)) shows little change with temperature while this peak on the atmospheric pressure crystallized sample decreased significantly at 155°C. For the 175 MPa and 200 MPa samples, the γ peak decreases at 140°C and disappears at 155°C. The peak at 2Θ = 14.0° does not change significantly, but the peak at 2Θ = 16.9° (α (040), γ (008)) decreases with

increasing temperature. Pae [94] reported the temperature dependence of isotactic polypropylene that had been crystallized at an elevated pressure of 4.14 kbar (414 MPa). For temperatures of 156°C and 150°C, approximately 74% and 37%, respectively, of the γ-form material had converted to α-form within 10 minutes. This initially rapid conversion was then followed by a linear rate of conversion of 12%/hr for 156°C and 11%/hr for 150°C. At 139°C, approximately 5% of the γ-form converted within 80 minutes, followed by a linear rate of conversion of 0.21%/hr. Morrow [95] reported the conversion of γ-polypropylene to α-polypropylene at 150°C for pressure crystallized polypropylene. While the conversion rate is somewhat different than that of Pae, the results indicate essentially 100% conversion within six hours. In both references, the starting material was reported as 100% γ-form polypropylene.

4.2 Small Angle X-ray Scattering

4.2.1 Atmospheric Pressure T_c Series

Small angle X-ray scattering data were collected for the M_w = 151,000 homopolymer and copolymer as a function of isothermal crystallization temperature. The samples were crystallized isothermally for sufficient time (t_∞) to ensure complete primary crystallization. This time was determined *a priori* by bulk crystallization experiments.

The SAXS data were initially collected as two-dimensionally averaged scattering intensities. All the atmospheric pressure crystallized samples exhibited circularly shaped two-dimensional plots, indicating no preferred orientation within the sample. Figure 4.8 shows a SAXS contour plot for the M_w = 151,000 homopolymer isothermally crystallized at T_c = 138 C. The two-dimensional SAXS data was then radially averaged to obtain one-dimensional SAXS intensity data. Figure 4.9 shows the radially averaged SAXS intensity versus scattering vector q for the M_w = 151,000 homopolymer as a function of isothermal crystallization temperature increases, the shape of the scattering curve changes. The peak shifts to lower q values (higher long period) and the breadth of the peak decreases, indicating a change in lamellar thickness and crystallinity distributions. The intensity curves in general show relatively well defined Bragg maxima, which can be related to the stacking of two entities with different electron densities - the amorphous and crystalline layers. The SAXS one-dimensional intensity data corrected by the Lorentz geometric factor are presented in Figure 4.10 for the data of Figure 4.9. The data typically showed a relatively sharp primary peak with occasionally a secondary peak of much lower intensity at higher scattering factor values.

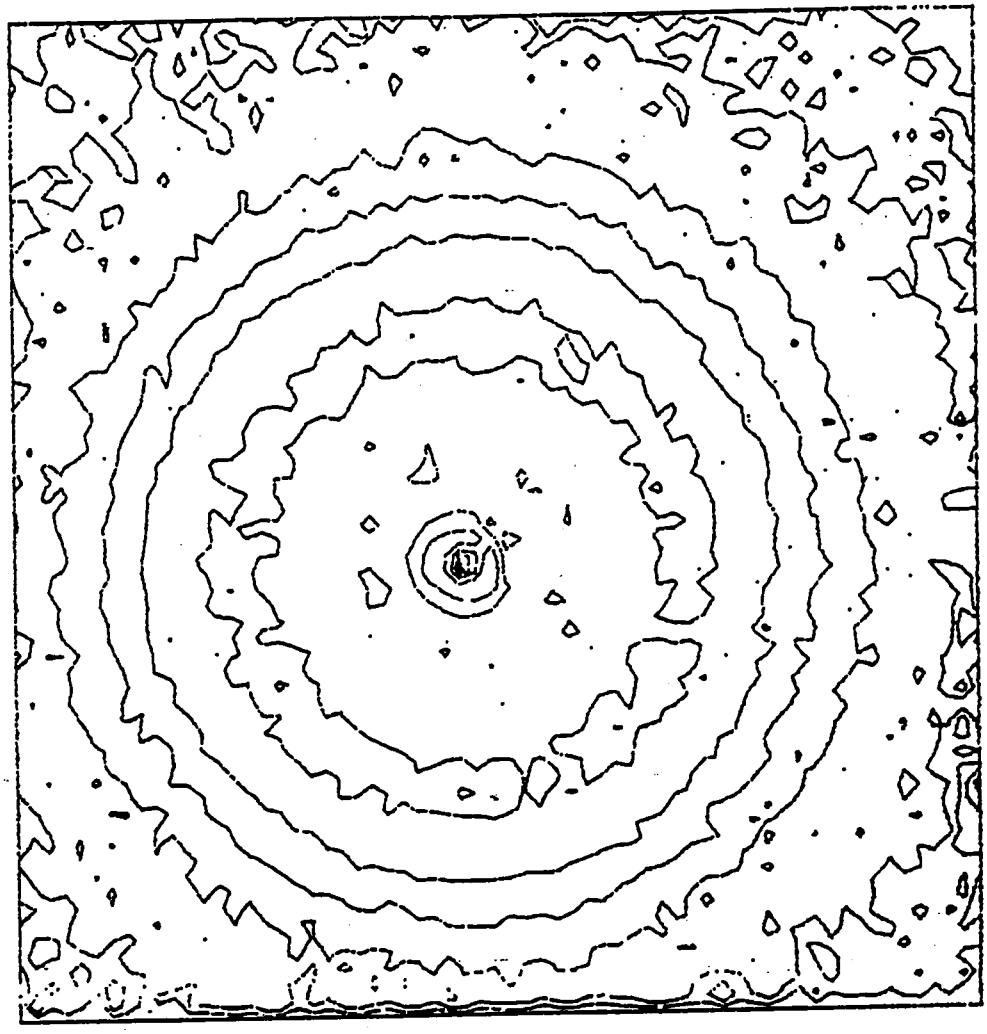


Figure 4.8 SAXS two-dimensionally averaged contour plot for isotactic polypropylene 151,000 M_w isothermally crystallized at T_c = 138°C

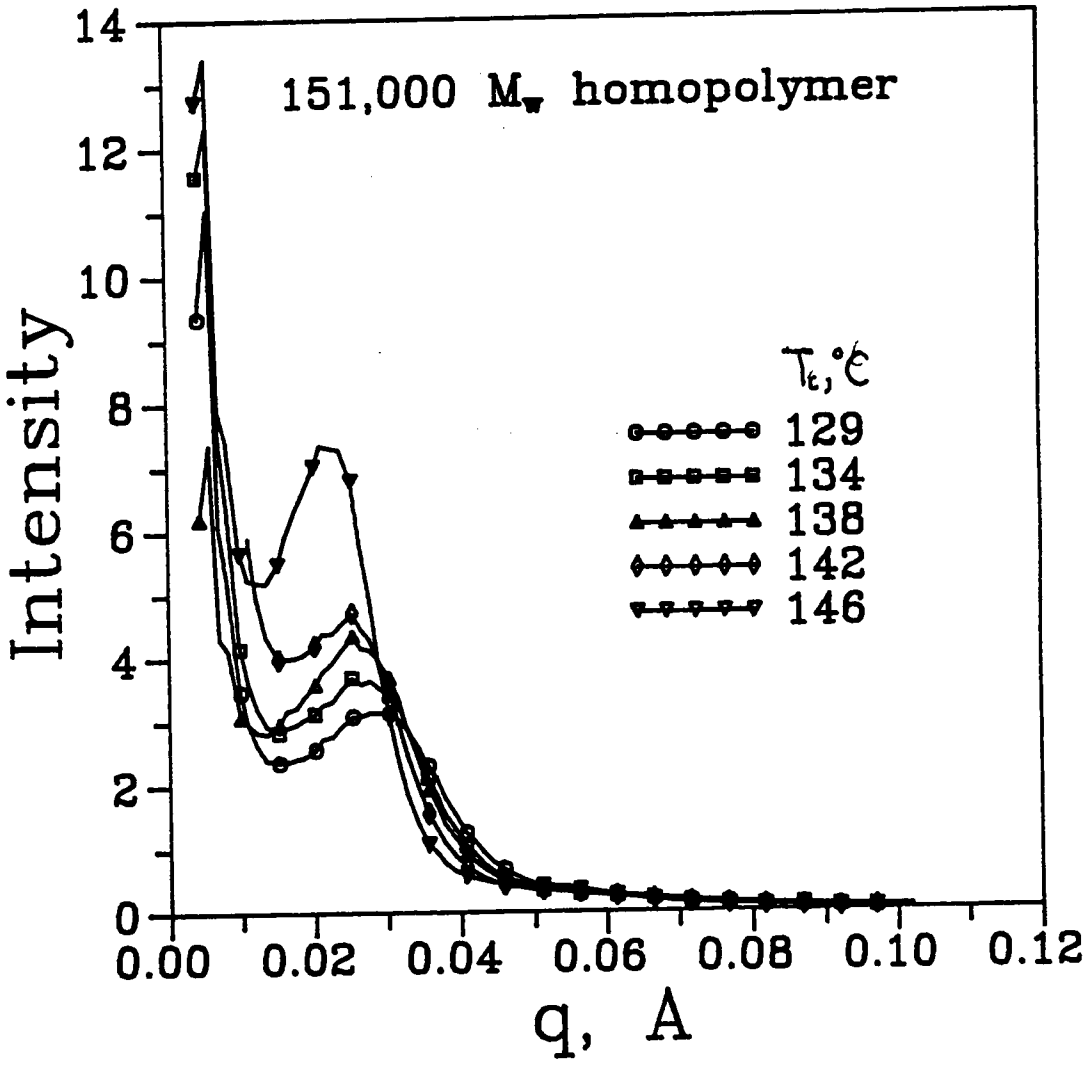


Figure 4.9 SAXS radially averaged intensity I versus scattering vector q for isotactic polypropylene 151,000 M_w homopolymer isothermally crystallized at atmospheric pressure and several crystallization temperatures.

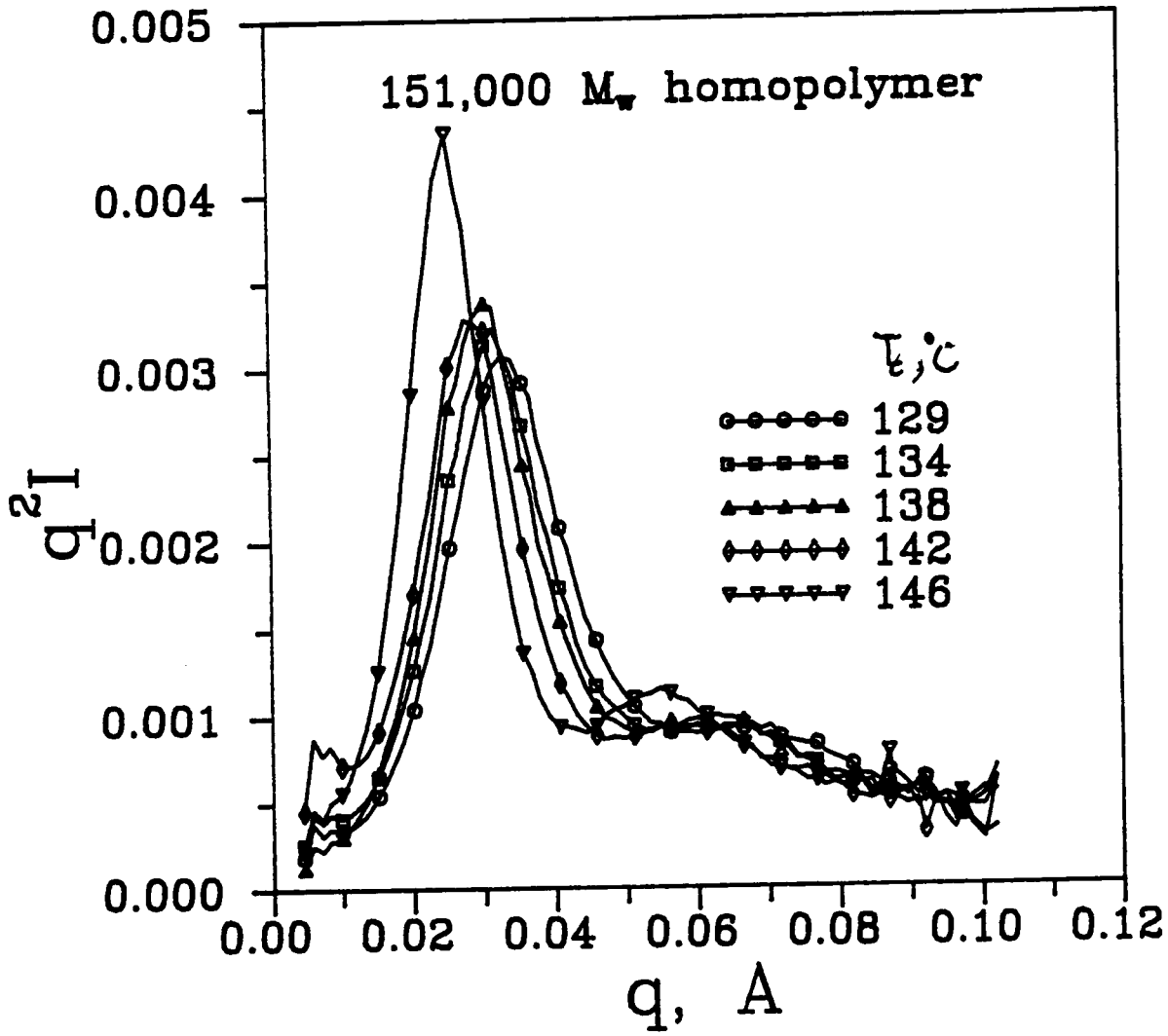


Figure 4.10 SAXS Lorentz corrected data for the data of Figure 4.9.

The SAXS data for the isotactic polypropylene M_w = 151,000 copolymer as a function of crystallization temperature were similar to those of the homopolymer. Figure 4.11 shows a comparison of the SAXS one-dimensional radially averaged data for the homopolymer and copolymer at T_c = 129°C and T_c = 146°C. At both crystallization temperatures, the scattering curves are very similar for the homopolymer and the copolymer. This is interesting because the bulk crystallization behavior and the linear growth rates for the two samples are so significantly different that one might expect a difference in the lamellar morphology. One might expect a change in lamellar thickness distribution or crystallinity distribution, either of which should result in changes in the SAXS behavior. The one-dimensional SAXS behavior for the copolymer as a function of T_c is shown in Figure 4.12. As with the homopolymer, with increasing T_c, the scattering curve changes shape. The peak becomes less broad with increasing crystallization temperature. Figure 4.13 shows the copolymer SAXS one-dimensional intensity data corrected by the Lorentz factor. The data show relatively sharp peaks with a secondary peak of much lower intensity at higher scattering factors for T_c > 135°C.

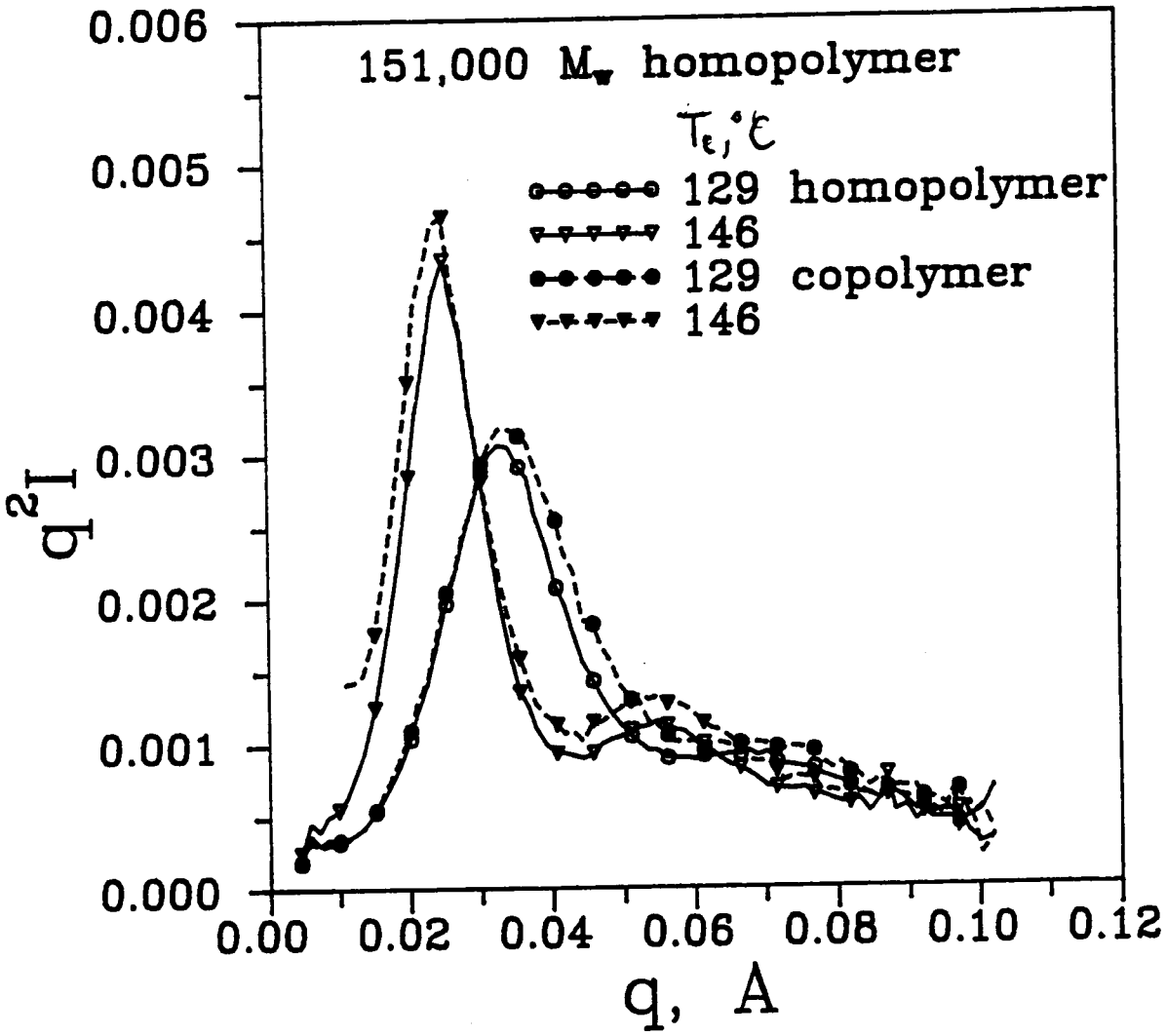


Figure 4.11 Comparison of the Lorentz corrected SAXS behavior for the isotactic polypropylene 151,000 M_w homopolymer and copolymer at two isothermal crystallization temperatures, 129°C and 146°C.

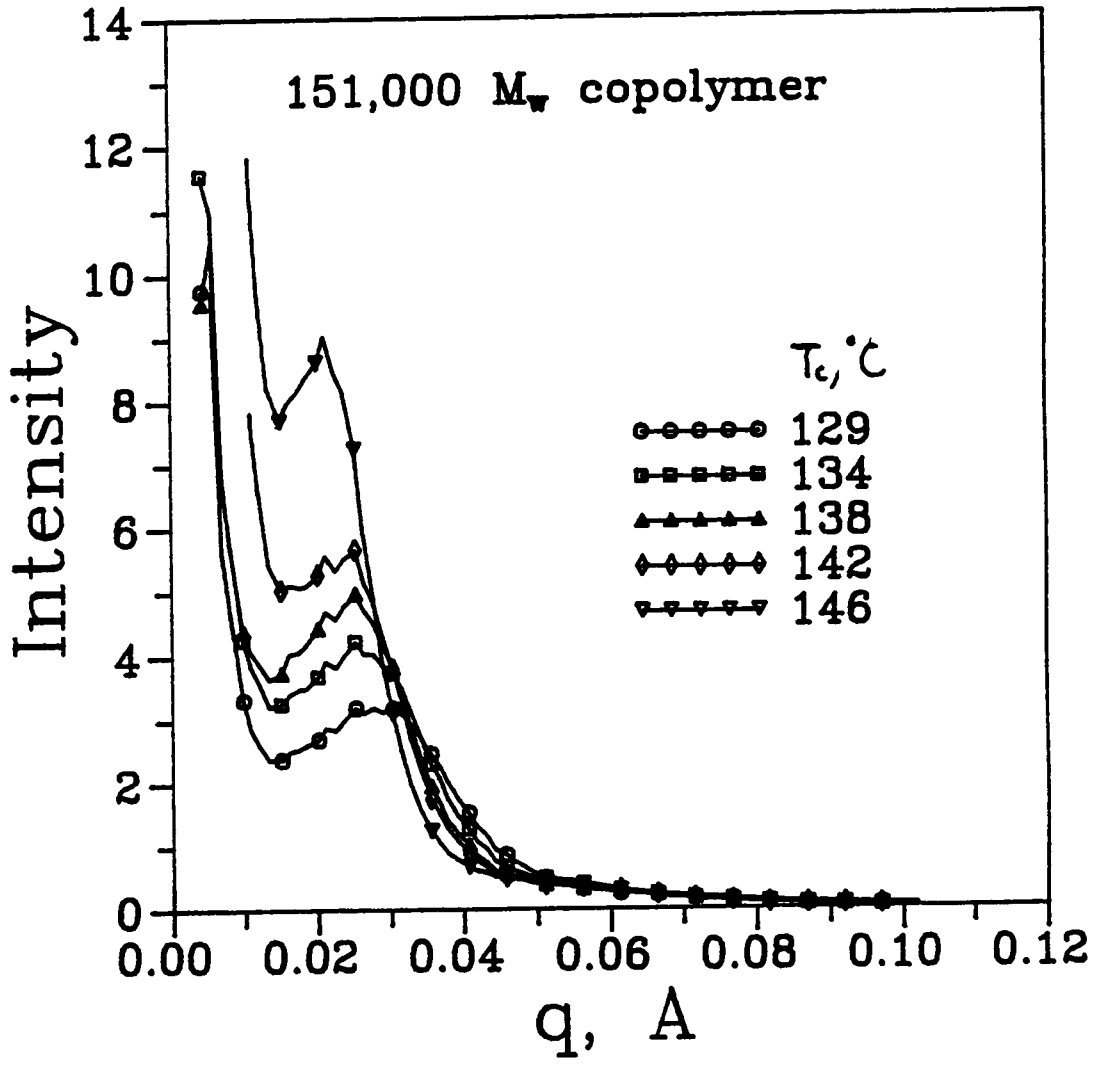


Figure 4.12 SAXS radially averaged intensity I versus scattering vector q for isotactic polypropylene 151,000 M_w copolymer (0.5% ethylene) isothermally crystallized at atmospheric pressure and several crystallization temperatures.

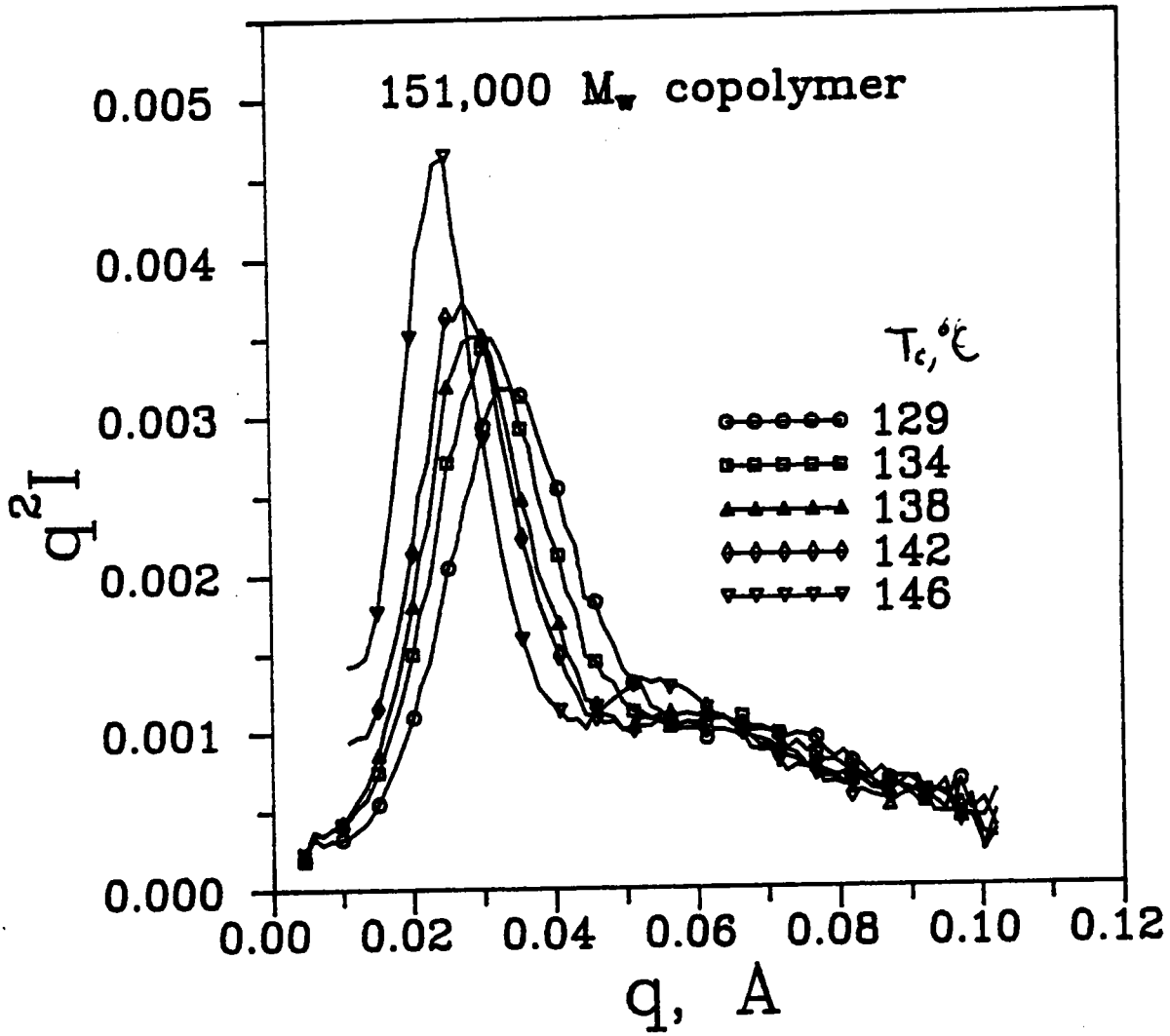


Figure 4.13 SAXS Lorentz corrected data for the data of Figure 4.12.

4.2.2 Atmospheric Pressure Time Series

A series of isothermal crystallizations as a function of crystallization time at a fixed crystallization temperature were performed in order to study the effect of crystallization time on the resulting morphology. The basis for the crystallization time was the time required for the completion of primary crystallization t_∞ which was determined from *a priori* bulk crystallization experiments. Samples were then isothermally crystallized at shorter and longer times at several crystallization temperatures. For times shorter than t_∞, one would expect the material that had not crystallized by the fixed crystallization time would quench on removing the sample from the crystallization bath. This could result in a significant effect on the lamellar morphology. For crystallization times greater than t_∞, one would expect some annealing and crystalline perfecting to occur. This also should affect the resulting lamellar morphology. Since the mechanisms of annealing and crystalline perfecting should behave differently at different temperatures, one might get some additional insight from the SAXS crystallization time experiments.

Two crystallization temperatures, 129°C and 146°C, were chosen for the SAXS crystallization time studies. Isotactic polypropylene has been shown to exhibit Regime III

crystallization behavior at 129°C, while at 146°C Regime II crystallization behavior is seen. Thus this study should also give insight into the effect of crystallization mechanism on the morphology development. Figure 4.14 shows the SAXS one-dimensional radially averaged results for the M_w = 151,000 homopolymer at T_c = 129°C for various times. The shape of the scattering curve changes with crystallization time at a fixed crystallization temperature. The peak becomes sharper and the peak maximum shifts to lower scattering factors with increasing crystallization time up to $4t_\infty$. The scattering curve changes relatively little for $t_c > 4t_\infty$. The most significant change in the scattering curve occurs between the $0.5t_\infty$ and $1t_\infty$. This is most probably a result of the $0.5t_\infty$ curve reflecting the quenching of uncrystallized material. For 129°C and a crystallization time of $0.5t_\infty$, only 50% of the material has crystallized. On removing the sample from the bath, the remaining material undergoes a nonisothermal crystallization as the sample is rapidly cooled to room temperature. This should result in a broader distribution of lamellar thicknesses in the sample crystallized for times shorter than t_∞. For times longer than t_∞, the scattering curve does not change shape as significantly as the change for times shorter that t_∞. The shift in the peak maximum from 0.5 t_∞ to 1 t_∞ (change in long period = 14 Å) is also larger than that from 1 t_∞ to 100 t_∞

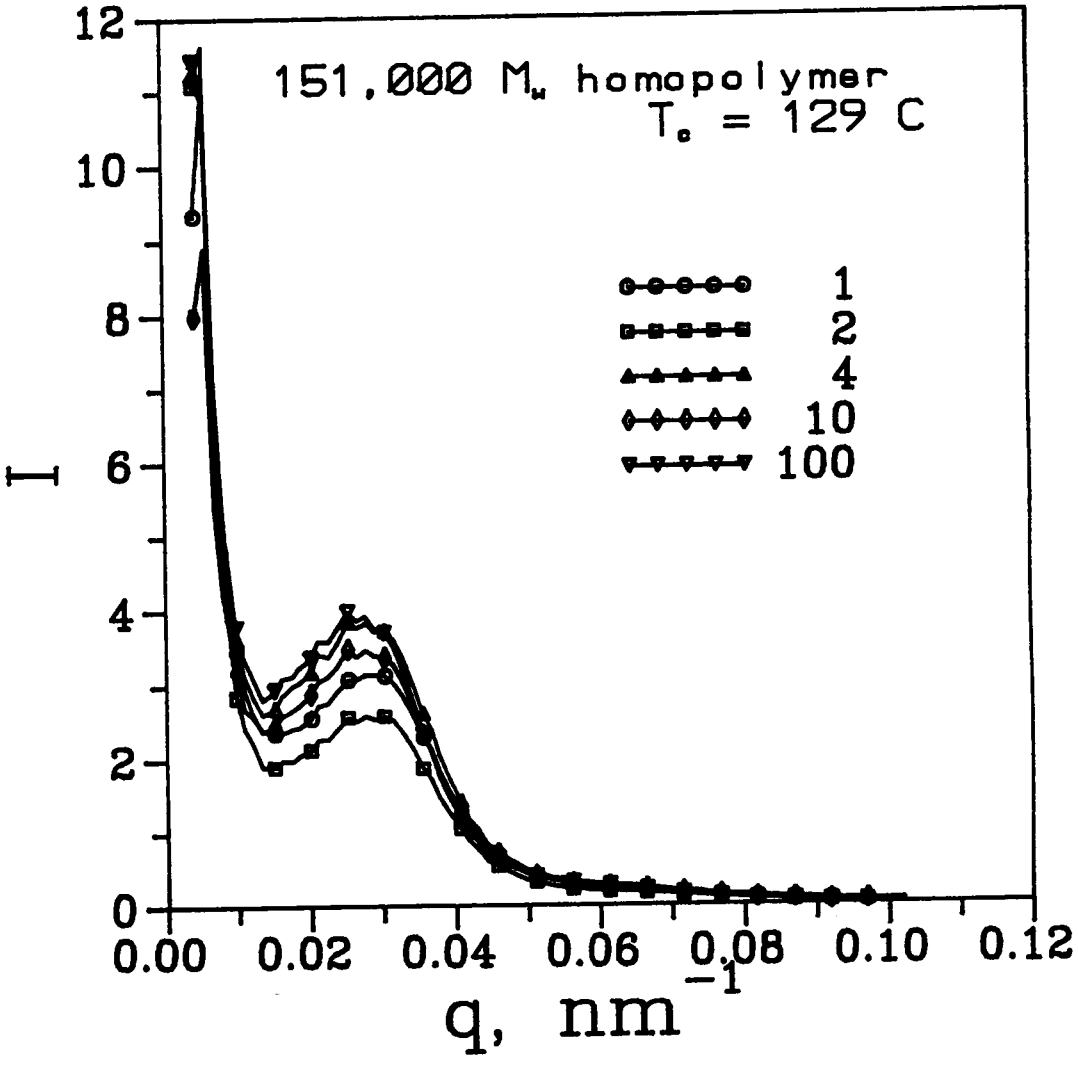


Figure 4.14 SAXS radially averaged intensity versus scattering vector as a function of crystallization time at T_c = 129°C for isotactic polypropylene 151,000 M_w homopolymer.

(change in long period = 9 Å). Figure 4.15 shows the Lorentz corrected SAXS one-dimensional radially averaged data for the homopolymer as a function of t_∞ at T_c = 129°C. The most significant changes occur in peak shape and position between $t = 0.5\ t_\infty$ and $t = t_\infty$. The peak maximum shifts 19 Å. For $t > t_\infty$, the peak maximum only shifts 3 Å. It is interesting that the peak maximum shift for the Lorentz corrected data for $t < t_\infty$ is larger than that for the uncorrected data, while for $t > t_\infty$ the peak maximum shift shows the opposite behavior.

Due to the significantly longer crystallization time at 146°C (t_∞ = 2500 min. versus. 20 min. at 129°C), a somewhat different series of crystallization times was chosen. It was desired to attempt to reproduce the t_∞ series performed for 129°C but also to preserve sample integrity i.e. minimize degradation effects. Figure 4.16 shows the SAXS one dimensional radially averaged data for isotactic polypropylene M_w = 151,000 homopolymer isothermally crystallized at T_c = 146°C as a function of t_∞. The peak shape changes little over the crystallization times considered. At $t = 0.25t_\infty$, the peak is essentially fully developed. The long period does not change within the resolution of the equipment used (1 Å). It is not immediately clear why the curves for $t < t_\infty$ do not more clearly indicate the presence of quenching. The difference in quenched and isothermally crystallized material should be

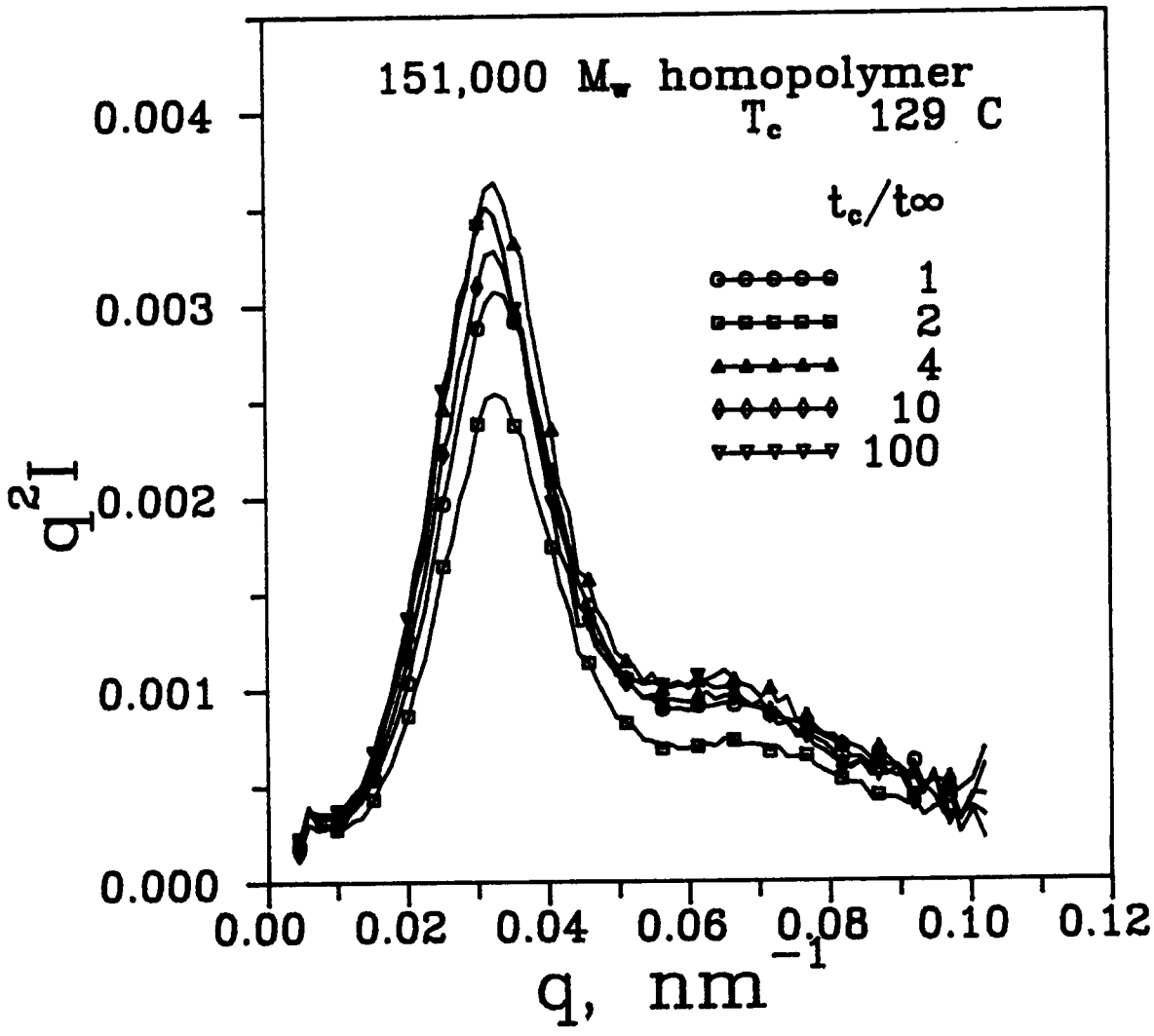


Figure 4.15 SAXS Lorentz corrected data for the data of Figure 4.14.

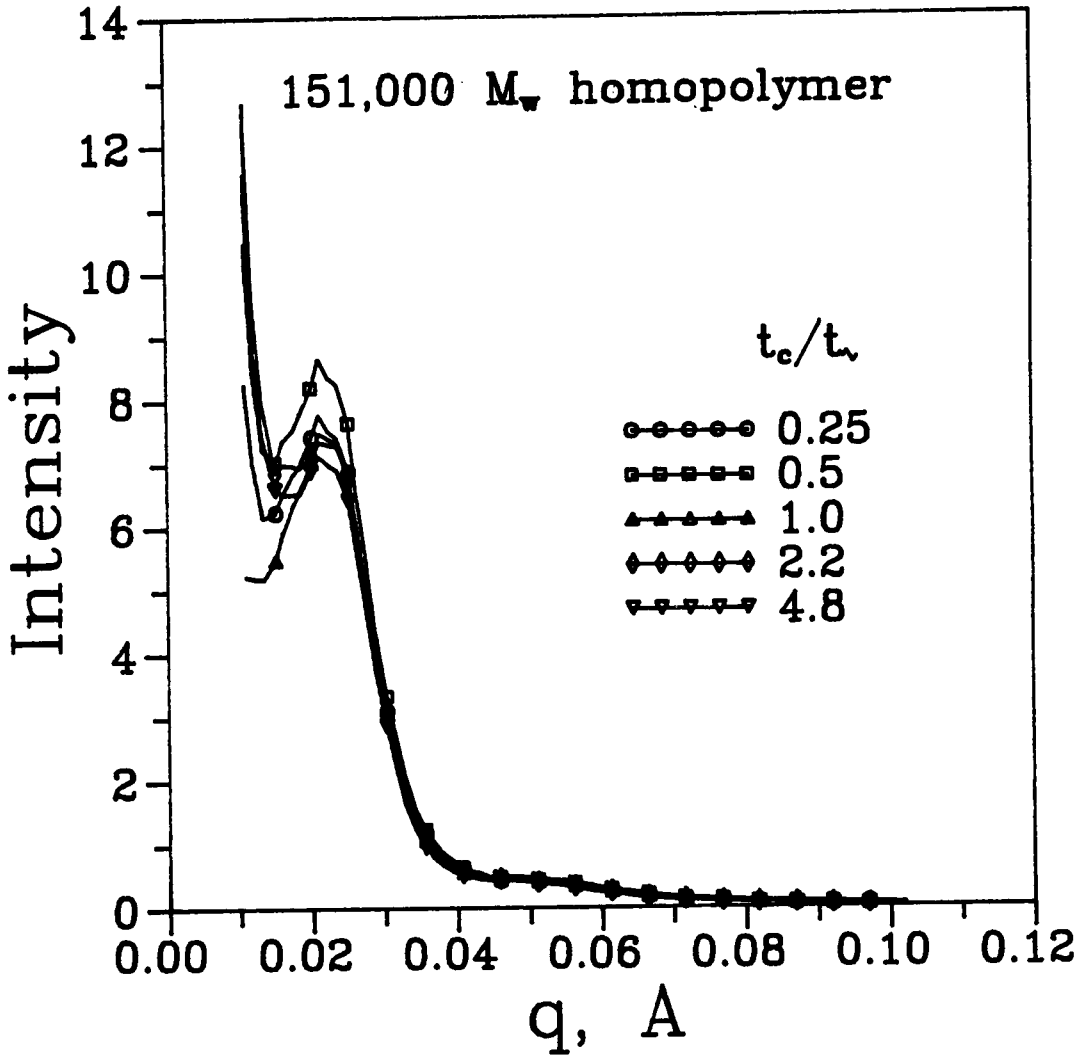


Figure 4.16 SAXS radially averaged intensity versus scattering vector as a function of crystallization time at T_c = 146°C for isotactic polypropylene 151,000 M_w homopolymer.

greater at T_c = 146°C than at T_c = 129°C. Figure 4.17 shows the Lorentz corrected SAXS one-dimensional radially averaged data for the M_w = 151,000 homopolymer as a function of t at T_c = 146 C. As for the uncorrected data, little change is observed in the peak shape as a function of time. While the maximum in the primary peak does not shift with time, the maximum in the secondary peak shifts to higher scattering factors (lower spacing) with increased crystallization time, as a result of crystal perfection.

4.2.3 Elevated Pressure - f(P_c)

Samples that were prepared at a supercooling of 50°C as a function of crystallization pressure were studied using SAXS in order to evaluate the effect of pressure on the morphology of isotactic polypropylene. The lamellar thickness of polyethylene has been shown to increase with increasing crystallization pressure [96]. With pressures above 350 MPa, polyethylene forms extended chains. The available data on the effect of pressure on the lamellar habit is limited for isotactic polypropylene.

The SAXS curve changes significantly from that for atmospheric pressure crystallization to that for crystallization at 25 MPa. Figure 4.18 shows the SAXS one-dimensional radially averaged data for isotactic polypropylene M_w = 151,000 homopolymer as a function of crystallization pressure at a constant supercooling ΔT =

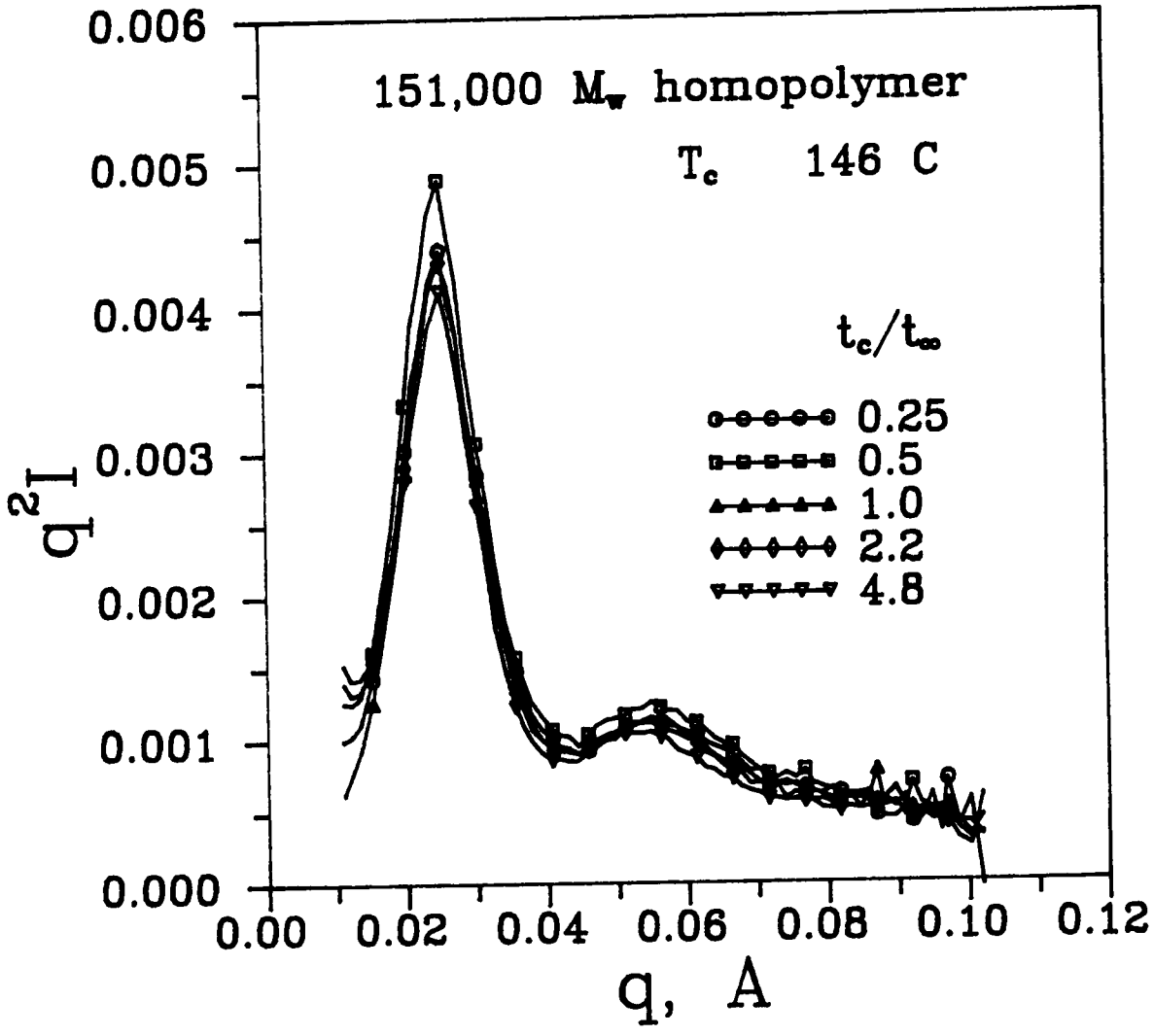


Figure 4.17 SAXS Lorentz corrected data for the data of Figure 4.16

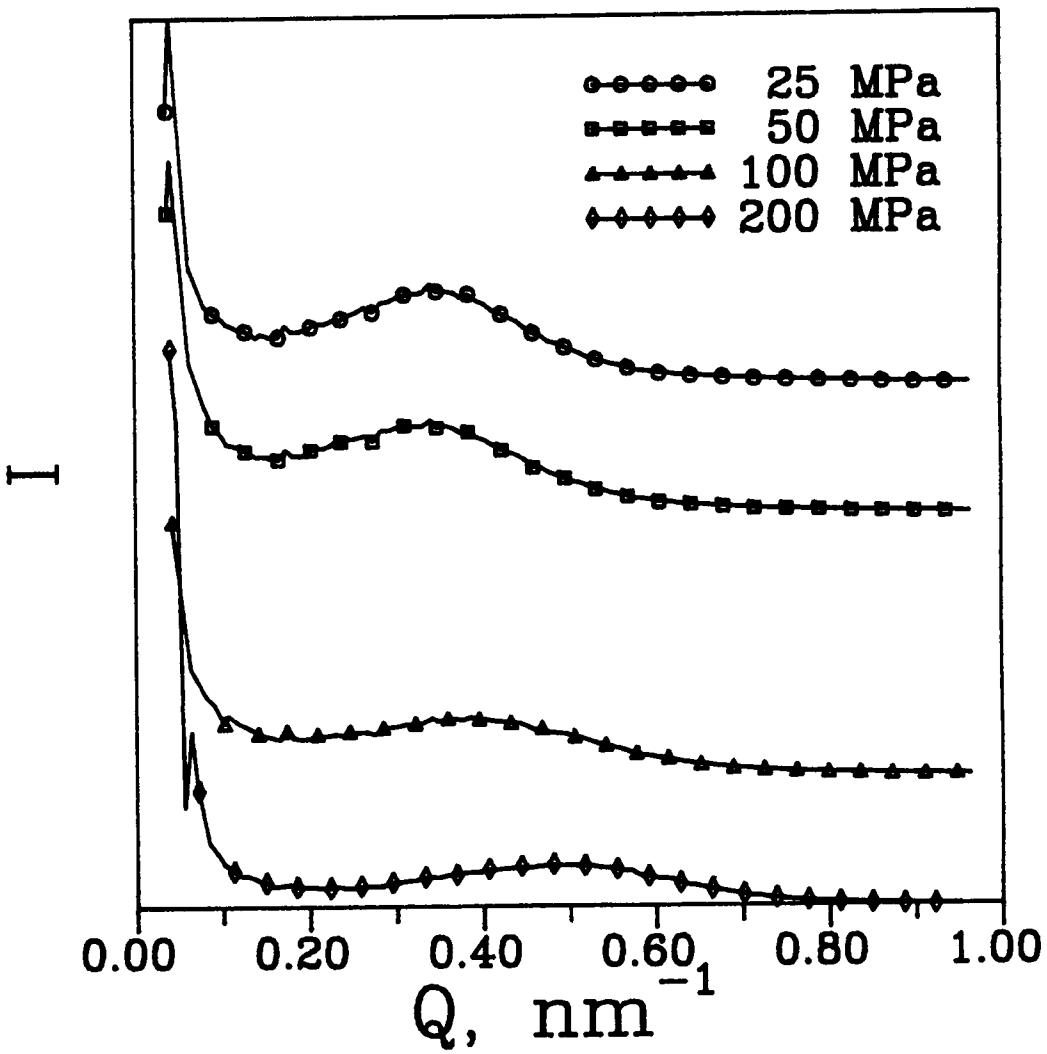


Figure 4.18 SAXS radially averaged intensity versus scattering vector as a function of crystallization pressure.

50°C. The crystallization temperature to be used at each pressure was determined from the T_m^o at that pressure. It is seen that with increasing pressure, the peak maximum shifts to higher scattering factors (smaller long periods). Also the peak becomes broader. The Lorentz corrected SAXS data, shown in Figure 4.19 for the data of Figure 4.18, show similar behavior. The atmospheric pressure crystallized sample exhibits a second-order peak while none of the pressure crystallized samples exhibit this behavior. The peak maximum shifts to higher q values and the initial deviation from baseline intensity also shifts to higher q values, but not as much as the peak maximum shift. This indicates a broadening of the SAXS peak with increasing pressure.

4.2.4 Elevated Pressure - $f(T_c)$

A series of samples were isothermally crystallized at several temperatures at 100 MPa and at 200 MPa to evaluate the change in fold surface free energy with crystallization pressure. Figure 4.20 shows the SAXS one-dimensional radially averaged data for isotactic polypropylene M_w = 151,000 as a function of crystallization temperature at a crystallization pressure of 100 MPa. For the isothermal series, it is seen that on increasing the crystallization temperature, the peak maximum shifts to lower q values (larger long period). The Lorentz corrected one-dimensional

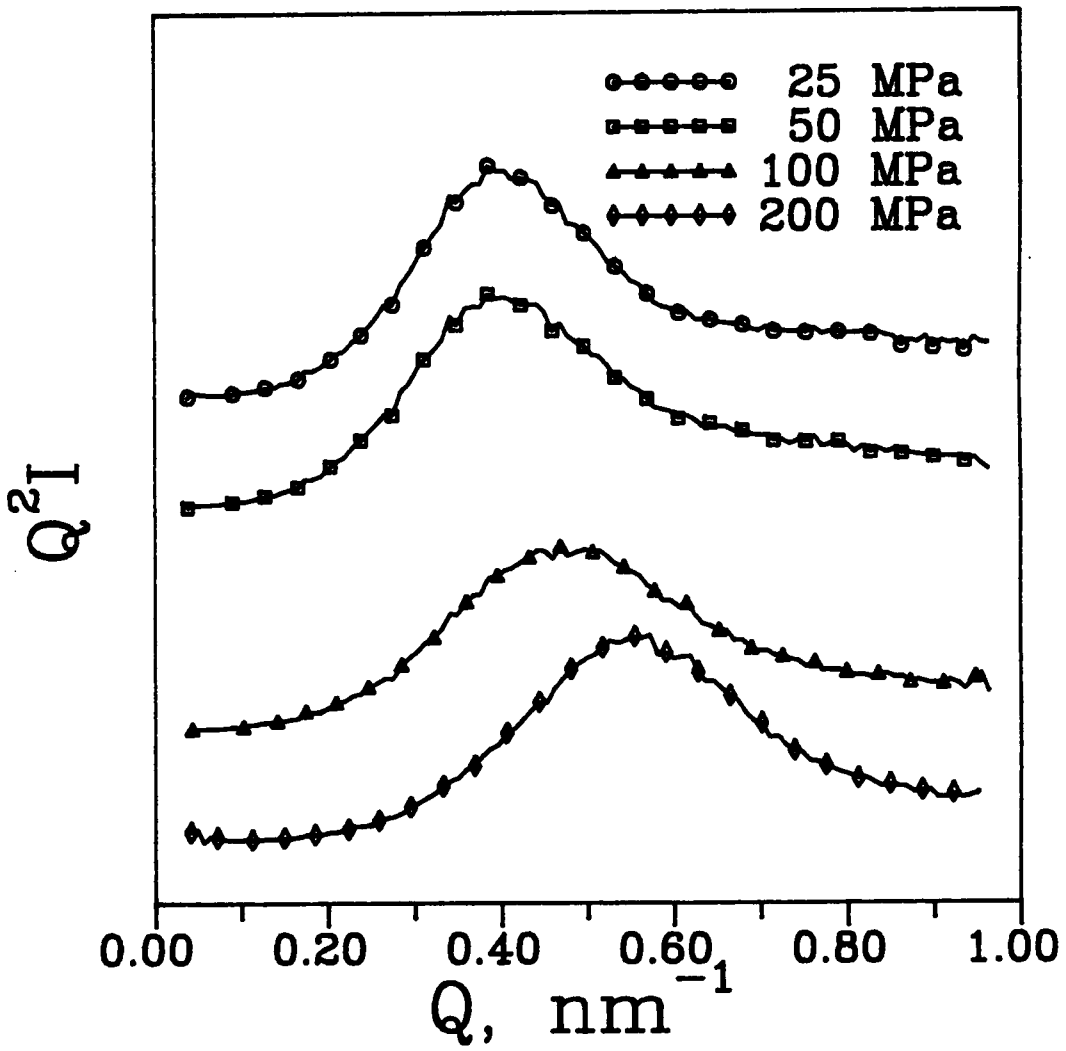


Figure 4.19 SAXS Lorentz corrected data for the data of Figure 4.18.

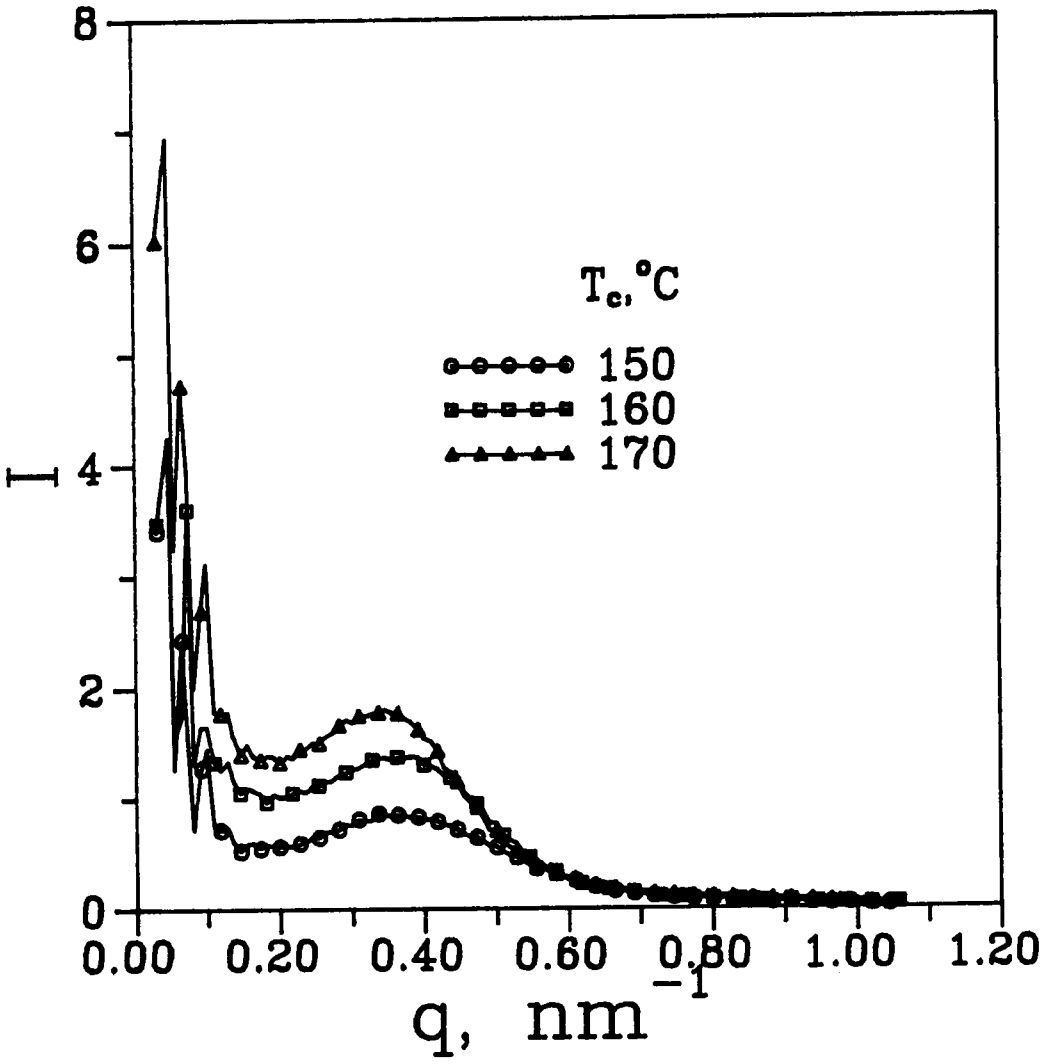


Figure 4.20 SAXS one-dimensional radially averaged intensity as a function of crystallization temperature at a crystallization pressure of 100 MPa.

radially averaged data, shown in Figure 4.21 for the data of Figure 4.20, shows a decrease in peak breadth with increasing crystallization temperature. This trend was also observed for the atmospheric pressure crystallized samples as a function of T_c.

The 200 MPa crystallized samples exhibited lower scattering vectors for the peak maxima with increasing T_c as shown in Figure 4.22 for the one-dimensional radially averaged SAXS data.

4.2.5 Atmospheric Pressure - $f(T_{scan})$

A study of SAXS behavior of atmospheric pressure crystallized samples was performed at several temperatures in order to observe the changes in lamellar structure on approaching the melting temperature ('pre-melting'). The maximum temperature that could be obtained was 145°C. The experiment involved inserting a sample into the temperature controlled sample cell. The sample cell was then placed into the chamber of the SAXS instrument that had been previously set to the desired temperature. Temperature equilibration occurred rapidly. The scattering behavior was then recorded. A new sample was used at each temperature to ensure that the observed behavior was the result of only the current temperature and not a temperature history effect. The isothermal crystallization temperatures chosen for the SAXS temperature study were 129°, 138°, and 146°C. The 129°C

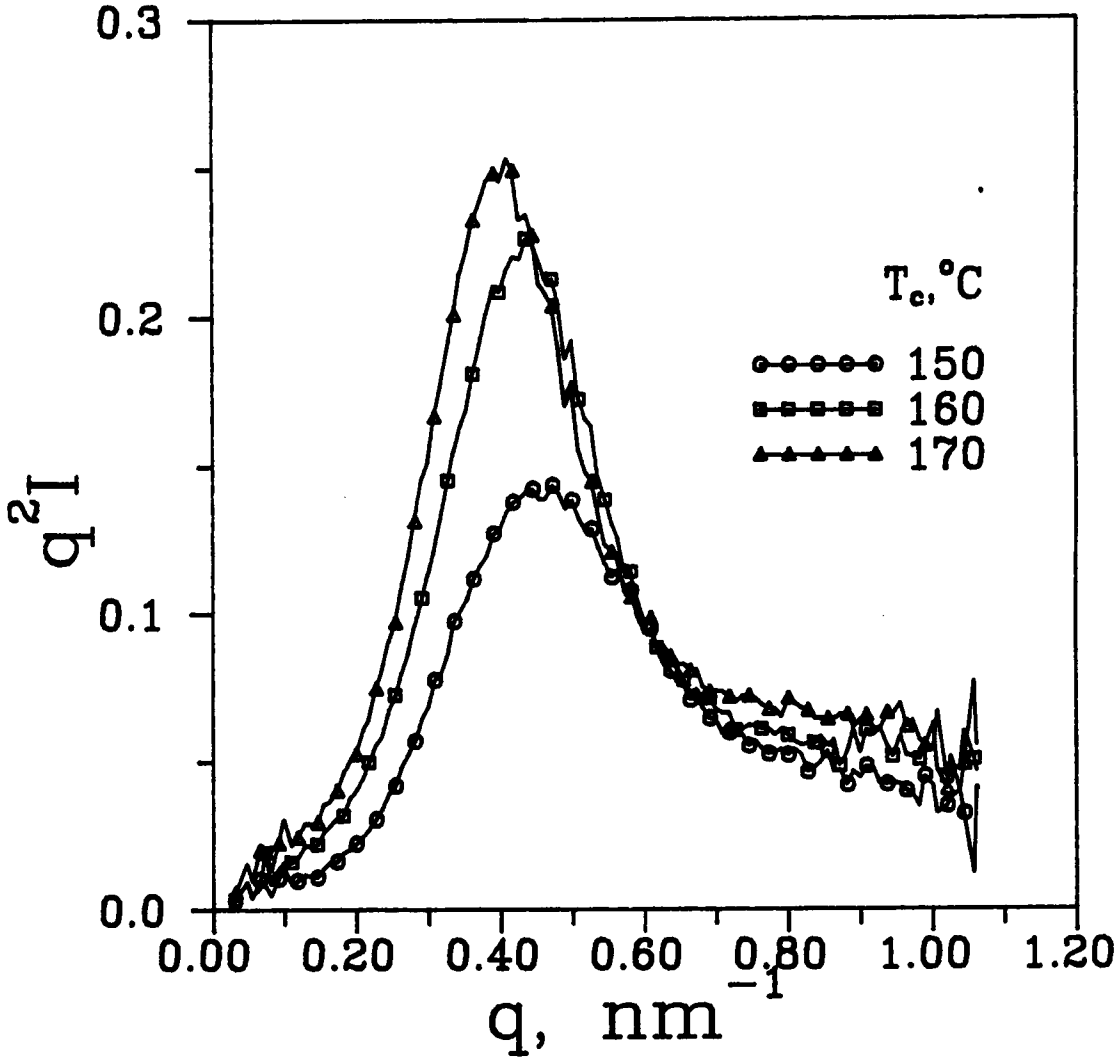


Figure 4.21 SAXS Lorentz corrected data for the data of Figure 4.20

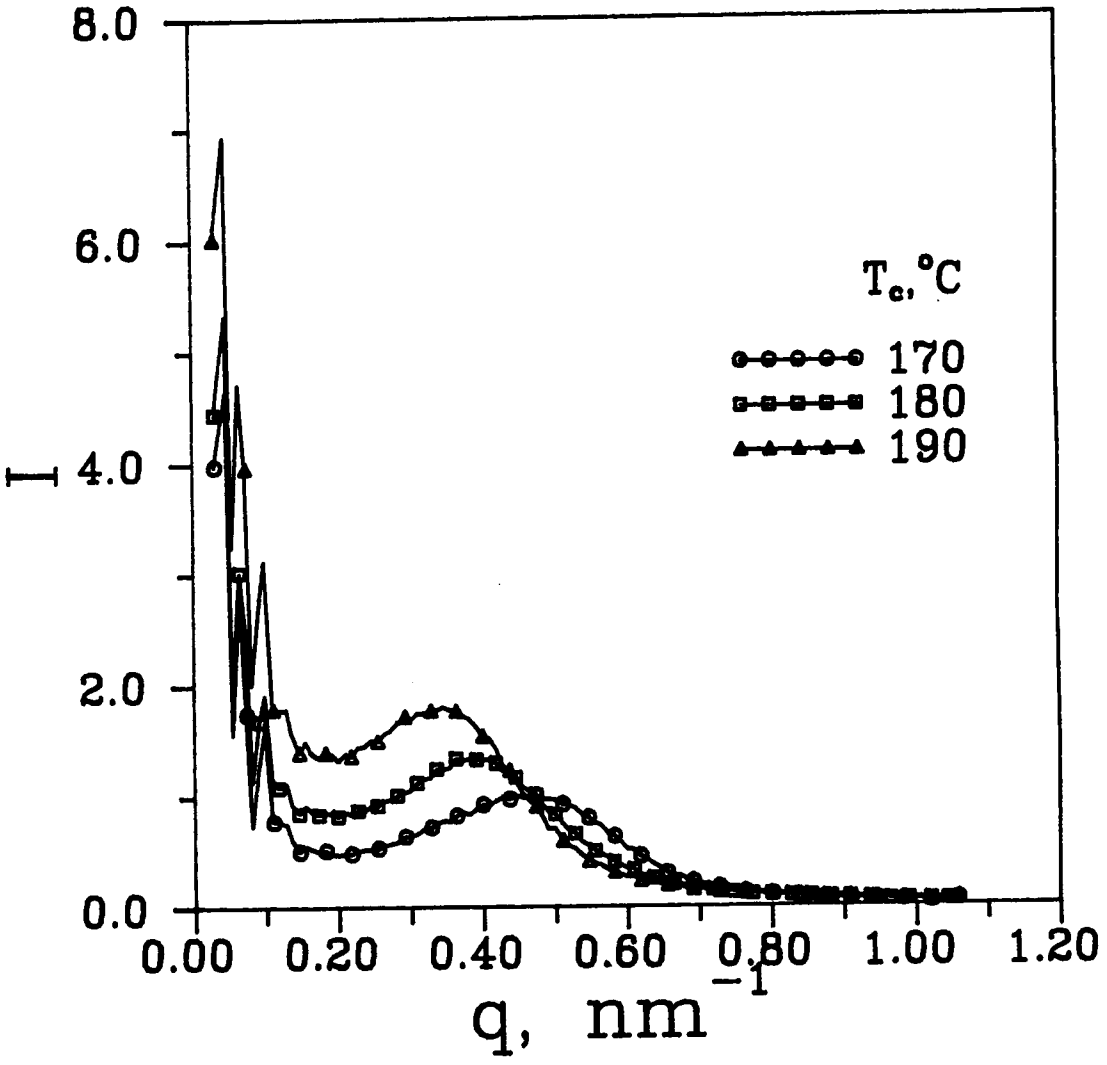


Figure 4.22 SAXS one-dimensional radially averaged intensity as a function of crystallization temperature at a crystallization pressure of 200 MPa.

crystallization temperature is in Regime III, while the 146°C crystallization temperature is in Regime II and the 138°C crystallization temperature is at the Regime II - Regime III transition for this sample. An as-molded sample was also studied at temperatures of 25°, 100°, 130°, and 145°C. These temperatures were chosen with respect to the observed DSC and DLI transition behavior.

Figure 4.23 shows the SAXS q versus I behavior for the T_c = 129°C sample as a function of temperature. Some changes are observed with increasing temperature. In particular the maximum in the q versus I plot shifts to lower q values (increased long periods) with increasing temperature. No change in long period is observed between the 25°C scan and the 100°C scan. Between 100°C and 130°C scans, the long period increases slightly (6 Å) while the largest increase is observed between 130°C and 145°C (19 Å). The long period increases 15% between the 25°C and the 145°C scans. This behavior is expected. The DSC exhibits no melting below 130°C so the only lamellar structural changes observed in the SAXS up to 130°C would be due to thermal expansion effects. The thermal expansion in the C unit cell direction is negligible so that any changes would be an expansion in the amorphous region. Above 130°C in the DSC some melting is observed. The thinner lamellae melt and the lamellar thickness distribution changes, reflecting the melting of the

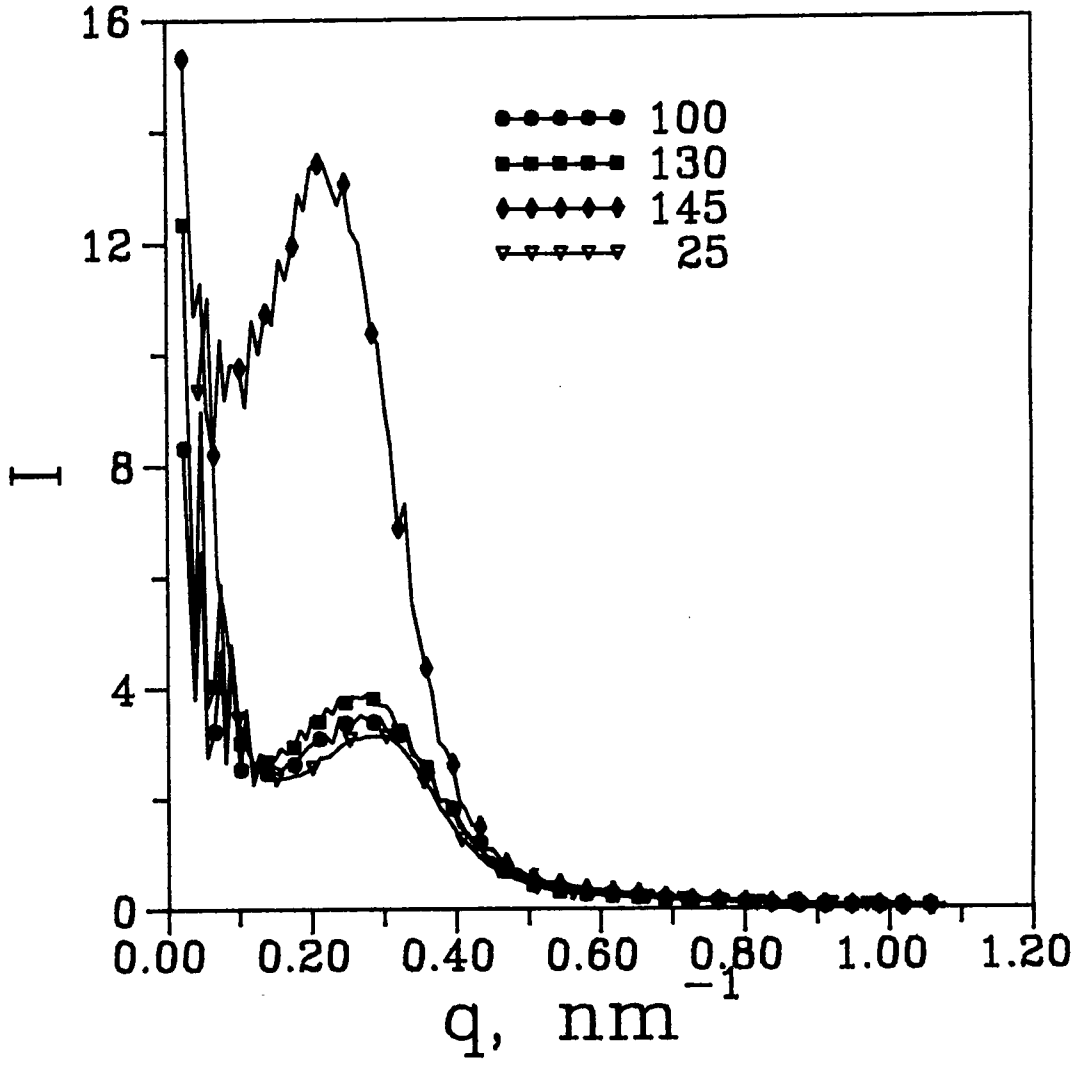


Figure 4.23 SAXS radially averaged intensity I vs scattering vector q for isotactic polypropylene isothermally crystallized at T_c = 129°C, atmospheric pressure; SAXS intensity profiles recorded at temperatures indicated.

thinner lamellae. This should decrease the lamellar thickness distribution (σ_x) while resulting in a larger average lamellar thickness and a corresponding increase in long period.

Figure 4.24 gives the Lorentz corrected long period for the atmospheric pressure crystallized samples as a function of scan temperature. All samples studied showed an increase in long period from 130° to 145°C, as expected. The T_c = 146°C showed the least change, which agreed with the observed DSC behavior. The T_c = 129°C, T_c = 138°C, and the as-molded samples showed about equal increase in long period from 130° to 145°C. A decrease in the observed long period was noted for the T_c = 138°C sample and the as-molded sample from 25° to 100°C.

4.2.6 Elevated Pressure - f(T_{scan})

The SAXS of the elevated pressure samples crystallized at a fixed supercooling of 50°C were studied at several temperatures. Figure 4.25 shows the SAXS q versus I behavior of the 100 MPa sample as a function of temperature. It is seen that the peak maximum shifts to lower q values (increased long period) with increasing pressure while the first minimum in the curve remains relatively unchanged. The

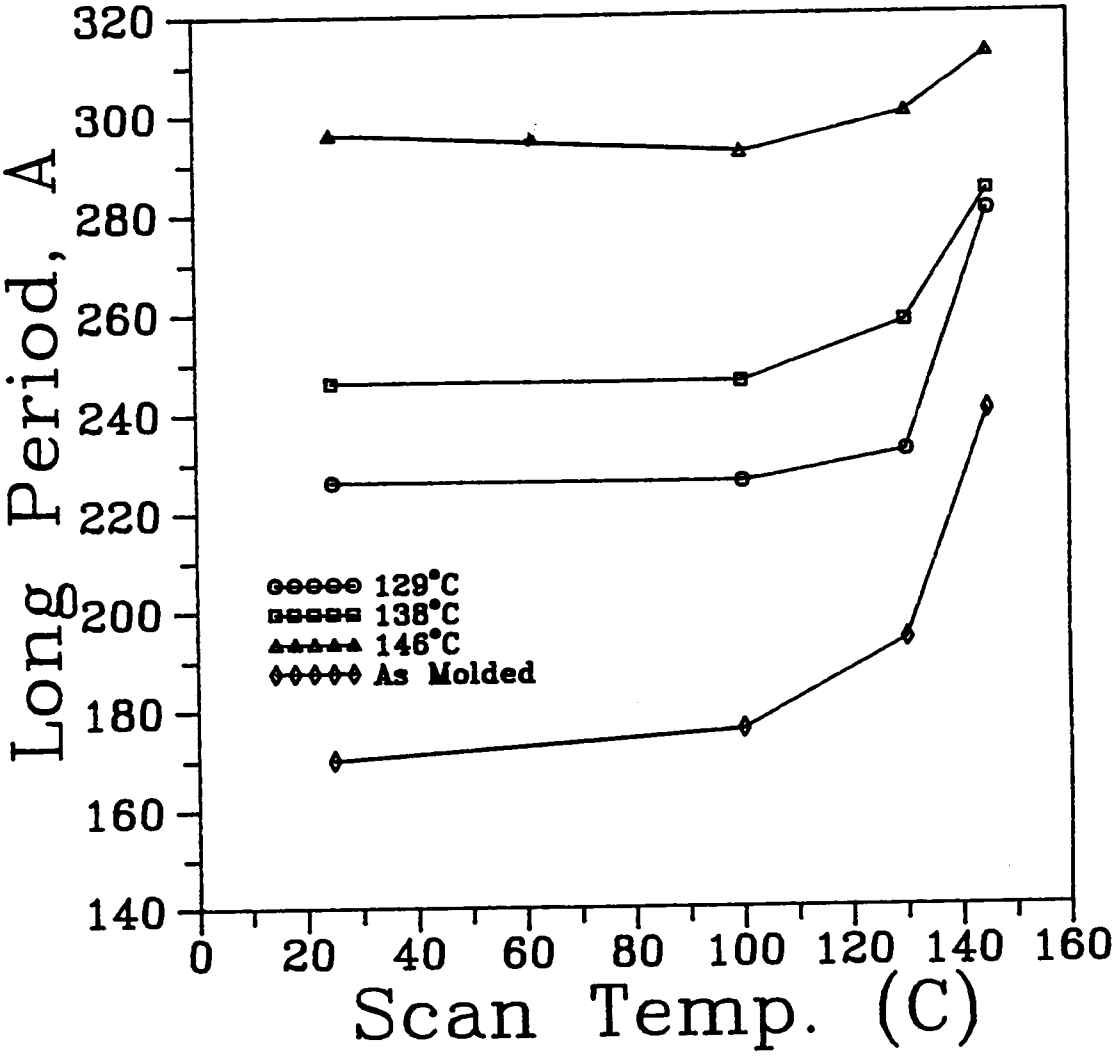


Figure 4.24 SAXS long period from Lorentz corrected data versus in situ scan temperature for isotactic polypropylene isothermally crystallized at T_c = 129°C; atmospheric pressure.

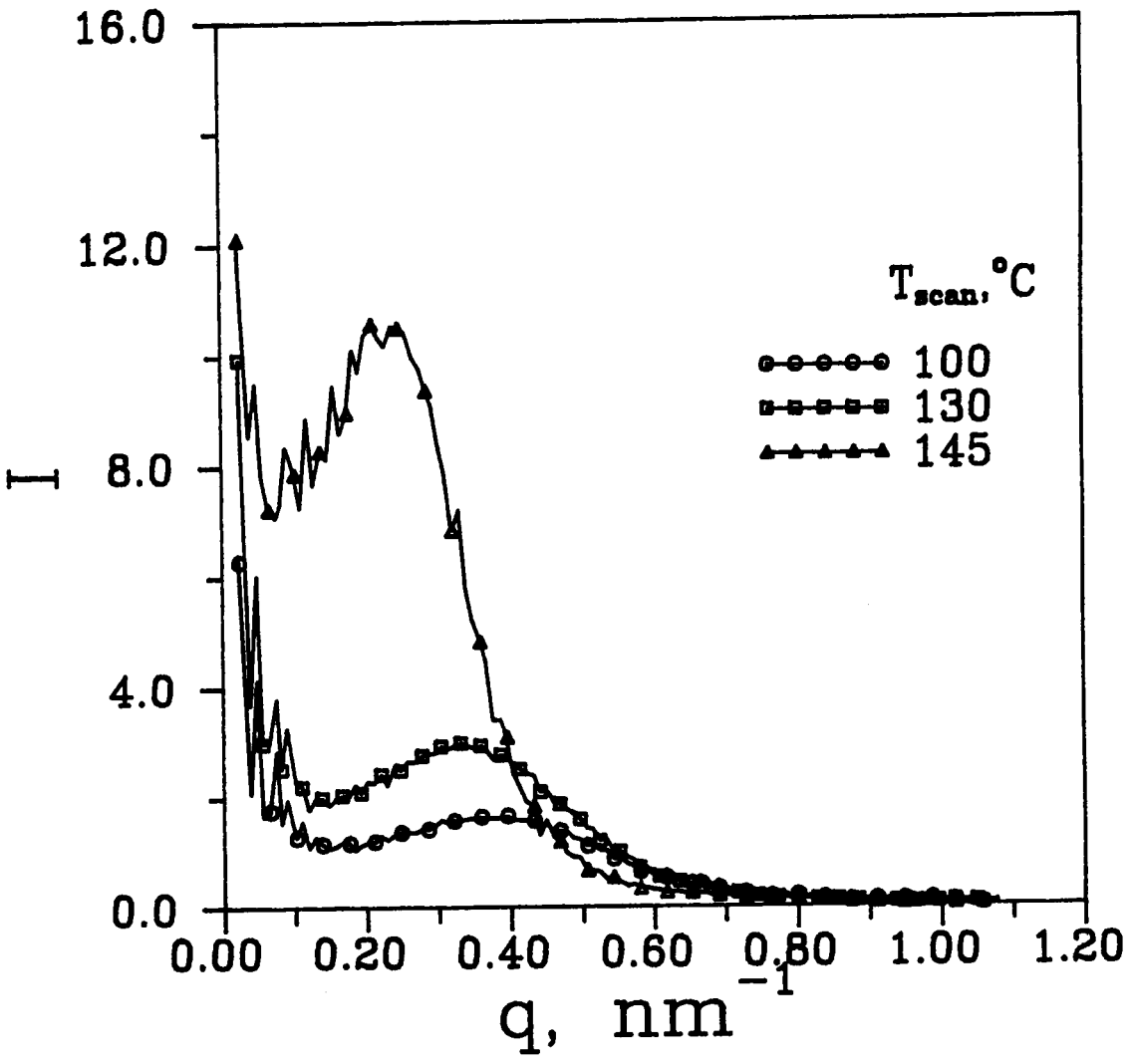


Figure 4.25 SAXS observed intensity profile for the 100 MPa crystallized data as a function of scan temperature.

behavior of the other elevated pressure samples was similar. While the increase in long period with increasing temperature for atmospheric pressure crystallized samples can be accounted for by a melting of thinner lamellae with a corresponding shift in the lamellar thickness distribution, this alone may not account for the observed changes for the elevated pressure crystallized samples. Figure 4.26 shows the observed long period as a function of scan temperature for the elevated pressure crystallized samples. A significant increase in long period is observed with increasing temperature for all pressures. The long period of the pressure samples approached that of the atmospheric pressure crystallized sample. While the DSC exhibits some melting of the pressure crystalized samples at the experimental SAXS temperatures, which would account for at least a portion of the long period increase, there is a possibility of a thickening mechanism for the elevated pressure samples that would not be applicable to the atmospheric pressure crystallized sample.

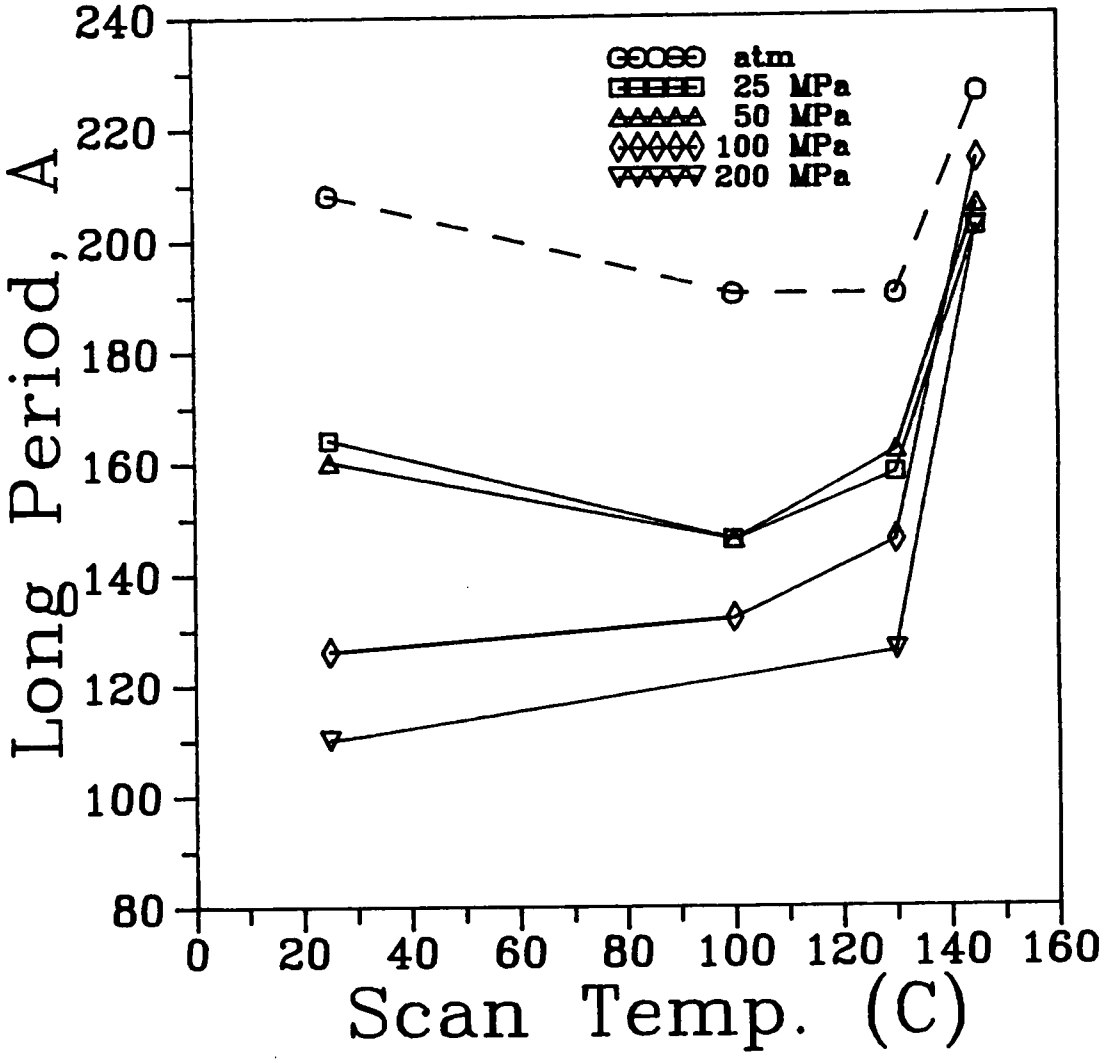


Figure 4.26 SAXS long period from Lorentz corrected data versus in situ scan temperature for isotactic polypropylene isothermally crystallized at ΔT = 50°C; various pressures.

4.3 Thermal Analysis

4.3.1 Differential Scanning Calorimetry

Atmospheric Pressure

Figure 4.27 shows the typical DSC melting behavior of the M_w = 83,000 homopolymer as a function of crystallization temperature. Single peak endotherm behavior is observed up to an isothermal crystallization temperature of 130°C. Convoluted peaks are observed for all other T_c's. An interpretation of the observed melting behavior from the literature proposes that for low T_c (<130°C), the low Tm peak represents melting of crystals formed during isothermal crystallization while the high T_m peak is due to crystals formed due to recrystallization or reorganization. The DSC melting behaviors of the M_w = 83,000 homopolymer and M_w = 151,000 copolymer are similar to that of the M_w = 151,000 homopolymer. Figure 4.28 compares the DSC melting behavior of the M_w = 151,000, M_w = 84,000 homopolymers, and the M_w = 151,000 copolymer (0.5% ethylene). The 151,000 homopolymer and the 151,000 copolymer show similar thermal behavior at this particular crystallization temperature. The 84,000 homopolymer, however, does show a more distinct shoulder at the lower temperatures.

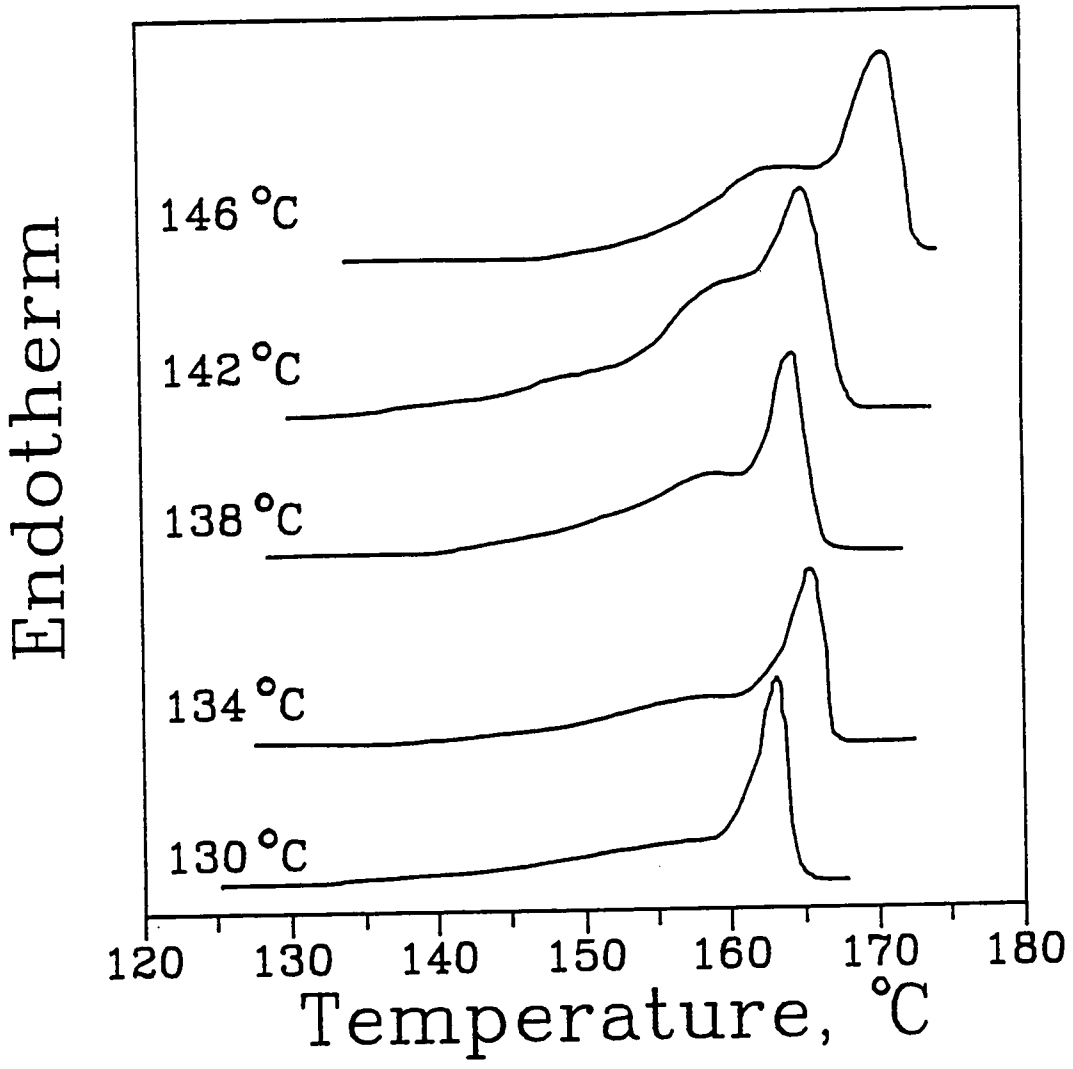


Figure 4.27 DSC melting behavior for isotactic polypropylene 83,000 M_w as a function of isothermal crystallization temperature; heating rate = 10° C/min.

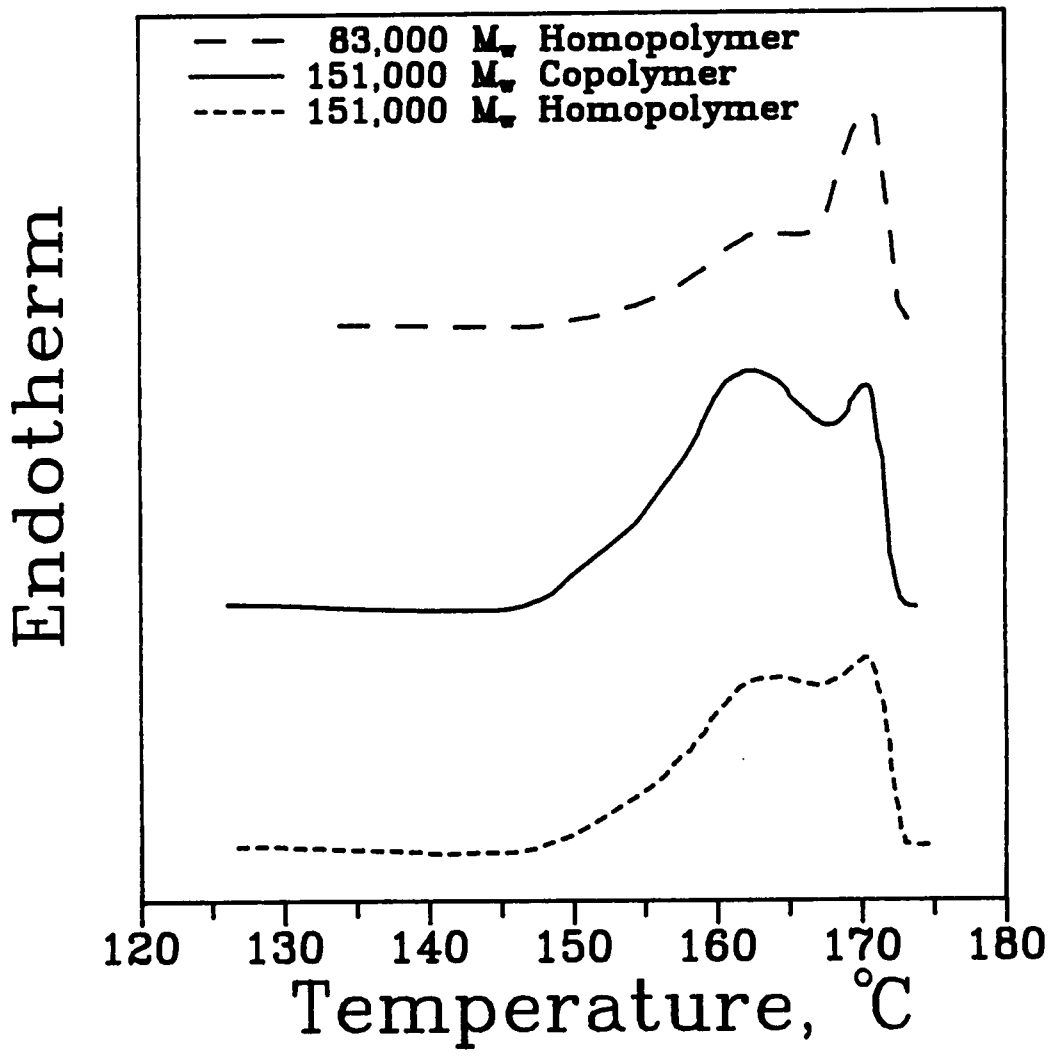


Figure 4.28 Comparison of DSC melting behavior for isotactic polypropylenes isothermally crystallized at atmospheric pressure, T_c = 129°C; heating rate = 10° C/min.

Elevated Pressure

Differential scanning calorimetry at atmospheric pressure was performed on a series of elevated pressure crystallized samples. The samples were prepared at a fixed supercooling of 50° with the crystallization temperature at a given pressure determined by the equilibrium melting temperature at that pressure. Figure 4.29 shows the DSC behavior at a heating rate of 10°C/min. for samples crystallized at several pressures. It is seen that, as the crystallization pressure increases, the endotherm changes shape. The region below the peak melting temperature for atmospheric becomes an increasingly distinct shoulder with increasing pressure. By 150 MPa, this shoulder becomes the dominant peak. The high temperature peak does not completely disappear. This behavior is similar to that reported in the literature for polypropylene [97,98]. Kardos et al. attributed the low temperature peak in DTA experiments to the γ modification of polypropylene. They showed that with increasing heating rate, the peak associated with the γ form increased. At low heating rates (<10°C/min.), two peaks were observed for a sample slow-cooled at 500 MPa. This sample showed only one peak at a heat rate of 40°C/min.

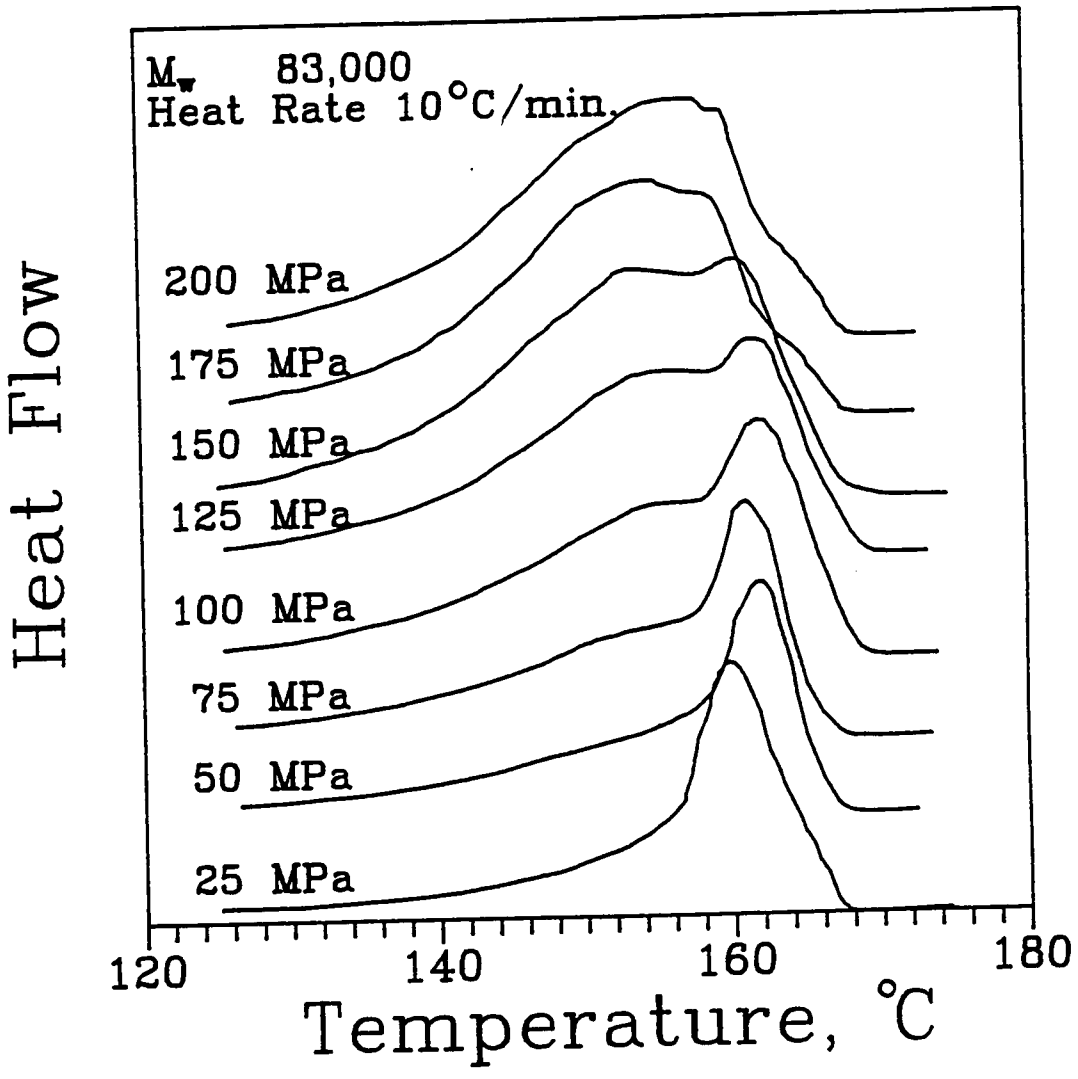


Figure 4.29 Atmospheric pressure DSC melting behavior for isotactic polypropylene isothermally crystallized at ΔT = 50°C, atmospheric and elevated pressure; heating rate = 10°C/min.

4.3.2 Depolarized Light Intensity

Atmospheric Pressure

The depolarized light intensity technique can be used to study the melting behavior of polymers [99]. An advantage of the DLI technique is that is allows simultaneous recording of depolarized light intensity and optical micrographs during crystallization and melting. This allows one to correlate the morphological changes that occur during crystallization or melting with the thermal transitions.

The DLI melting experiments were performed following the DLI bulk crystallization experiments. Thus after following the isothermal crystallization to the end of the primary crystallization, the sample was then heated at a given constant heating rate and the light intensity recorded as a function of temperature through melting of the sample. A series of simultaneous DLI and optical microscopy was also performed in order to directly compare DSC and DLI with the observed morphology and to correlate the DSC and DLI thermal behaviors.

Figure 4.30 displays typically observed DLI melting behavior for isotactic polypropylene isothermally crystallized at various temperatures. On initial heating from the crystallization temperature, there is an increase in

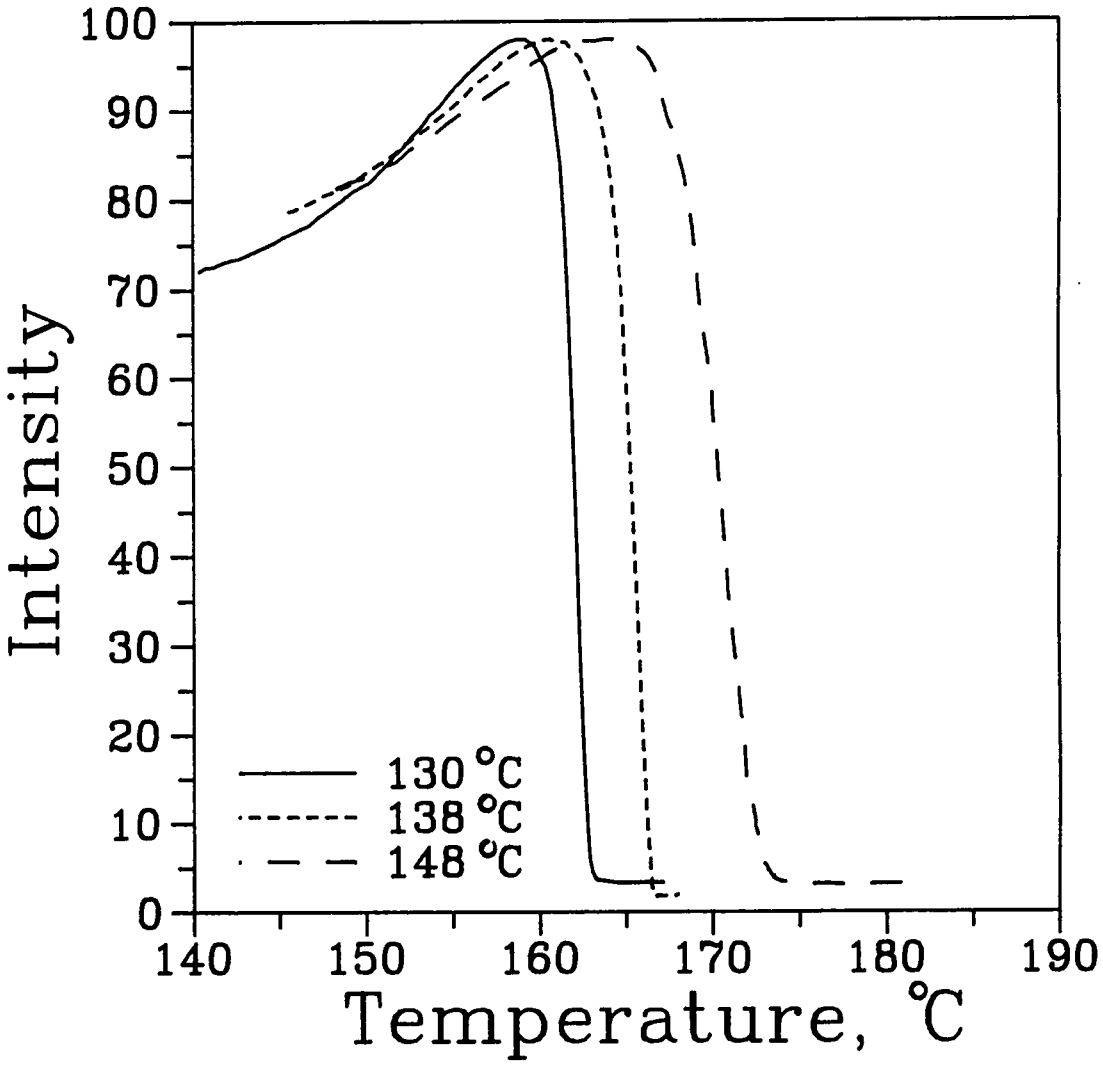


Figure 4.30 Typical depolarized light intensity melting curves as a function of isothermal crystallization temperature for isotactic polypropylene crystallized at atmospheric pressure; heating rate = 10°C/min.

the observed light intensity. This increase can be partially attributed to a change in sample thickness due to thermal expansion. However, this increase is also a result in the change in the internal structure of the spherulites [100]. After reaching the maximum, the light intensity drops sharply. Occasionally, the intensity exhibits a plateau before the final baseline. Visual observations indicate that this initial plateau is not associated with the final melting.

Elevated Pressure

Two sets of DLI experiments were performed on pressure crystallized samples. One set consisted of melting the samples at the crystallization pressure after isothermal crystallization. This allowed quantification of the equilibrium melting temperature as a function of pressure. The second set of DLI experiments consisted of melting the elevated pressure crystallized samples at atmospheric pressure. Depolarized light intensity was recorded on heating at a fixed rate at atmospheric pressure for pressure crystallized samples to correlate with the differential scanning calorimetry. After the initial melt, the sample was recrystallized either by cooling from the melt at a fixed rate or by isothermal crystallization to evaluate the effect of elevated pressure on the sample's behavior. Figure 4.31 shows the DLI behavior of samples isothermally crystallized

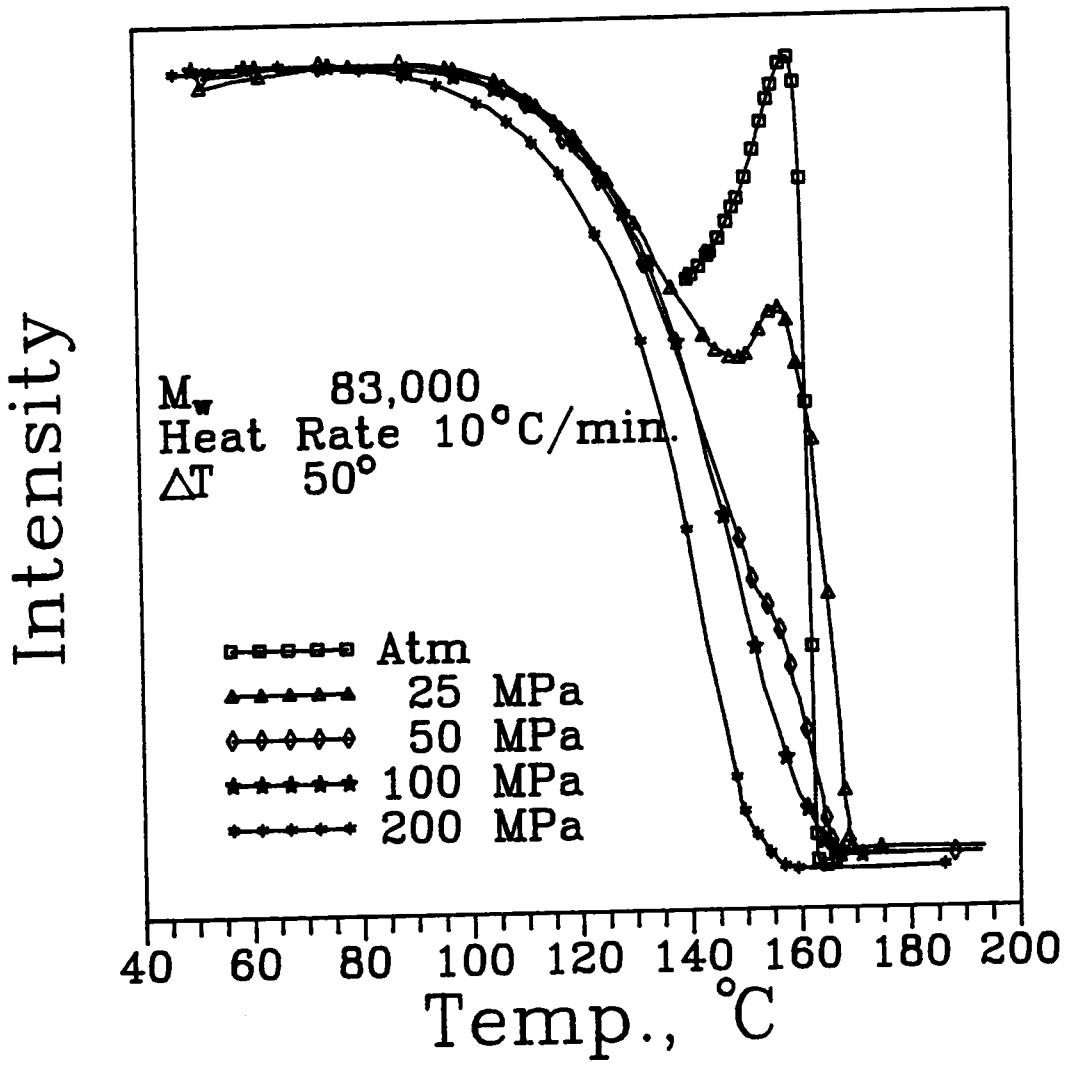


Figure 4.31 Typical depolarized light intensity melting curves as a function of isothermal crystallization temperature for isotactic polypropylene crystallized at various pressures; heating rate = °C/min.

at various pressures at fixed supercooling $\Delta T = 50°$. As seen in Figure 4.31, the 25 MPa crystallized sample behaves qualitatively similar to the atmospheric pressure crystallized sample. Both exhibit an intensity decrease to a plateau, followed by an increase in intensity to a maximum and then a rapid decrease through the return-to-baseline. The 50 MPa crystallized sample shows a slight shoulder on the decreasing intensity portion of the curve in a temperature region similar to the 25 MPa sample. The 100 MPa and 200 MPa crystallized samples show only a continuous decrease to the return-to-baseline after the intensity maximum.

The light intensity versus temperature curves for samples isothermally crystallized and melted at elevated pressures are shown in Figure 4.32 for crystallization pressures of 50 MPa as typical results for the elevated pressure melting behavior observed with depolarized light intensity. All heating rates for the elevated pressure melting experiments were 3°C/min., because of equipment limitations and the massiveness of the elevated pressure crystallization sample cell.

4.4 Infrared Spectroscopy of Polypropylene

4.4.1 Atmospheric Pressure

Infrared spectroscopy has been used to observe crystallinity [101], stereoregularity [102], copolymer

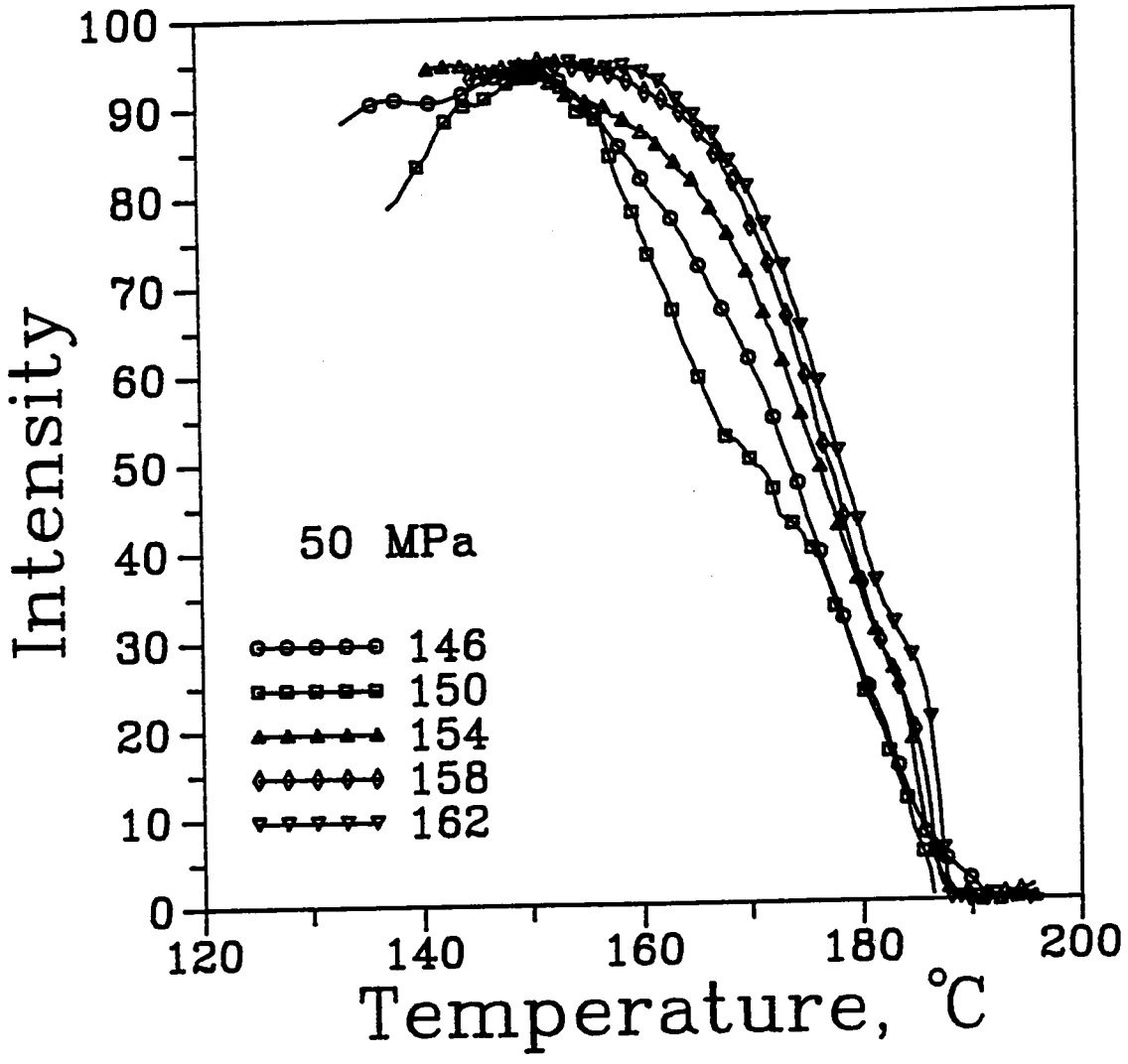


Figure 4.32 Typical depolarized light intensity melting curves as a function of isothermal crystallization temperature for isotactic polypropylene crystallized at 50 MPa; heating rate = 3°C/min.

composition [103], sequence distributions [104], orientation [105], degradation [106], and additive and impurity content [107] in isotactic polypropylene and polypropylene copolymers. In this study FTIR was used to study a series of polypropylene samples (homopolymer and copolymer) isothermally crystallized at atmospheric pressure as well as a series of polypropylene samples crystallized at elevated pressure. For the atmospheric pressure crystallized samples, the FTIR was used to study the differences between homopolymer and copolymer due to composition and constitution. For the elevated pressure crystallized samples, the FTIR was used to study the changes in the arrangement of the chains within lamellae with changing pressure.

Figure 4.33 shows the FTIR spectra for the 151,000 M_w homopolymer at various crystallization temperatures for $4000 < \nu < 400$ cm^{-1}. The spectra show little differences on first observation. Figure 4.34 shows the FTIR spectra of Figure 4.33 for the frequency range $1500 < \nu < 500$ cm^{-1}. However, the relative intensities of certain peaks exhibited a linear dependence on crystallization temperature. Figure 4.35 shows the relative intensities of the indicated peaks with $\nu = 1380$ cm^{-1} the reference frequency. The relative intensities of the 842 cm^{-1} and the 899 cm^{-1} frequencies showed a linear increase with increasing crystallization temperature.

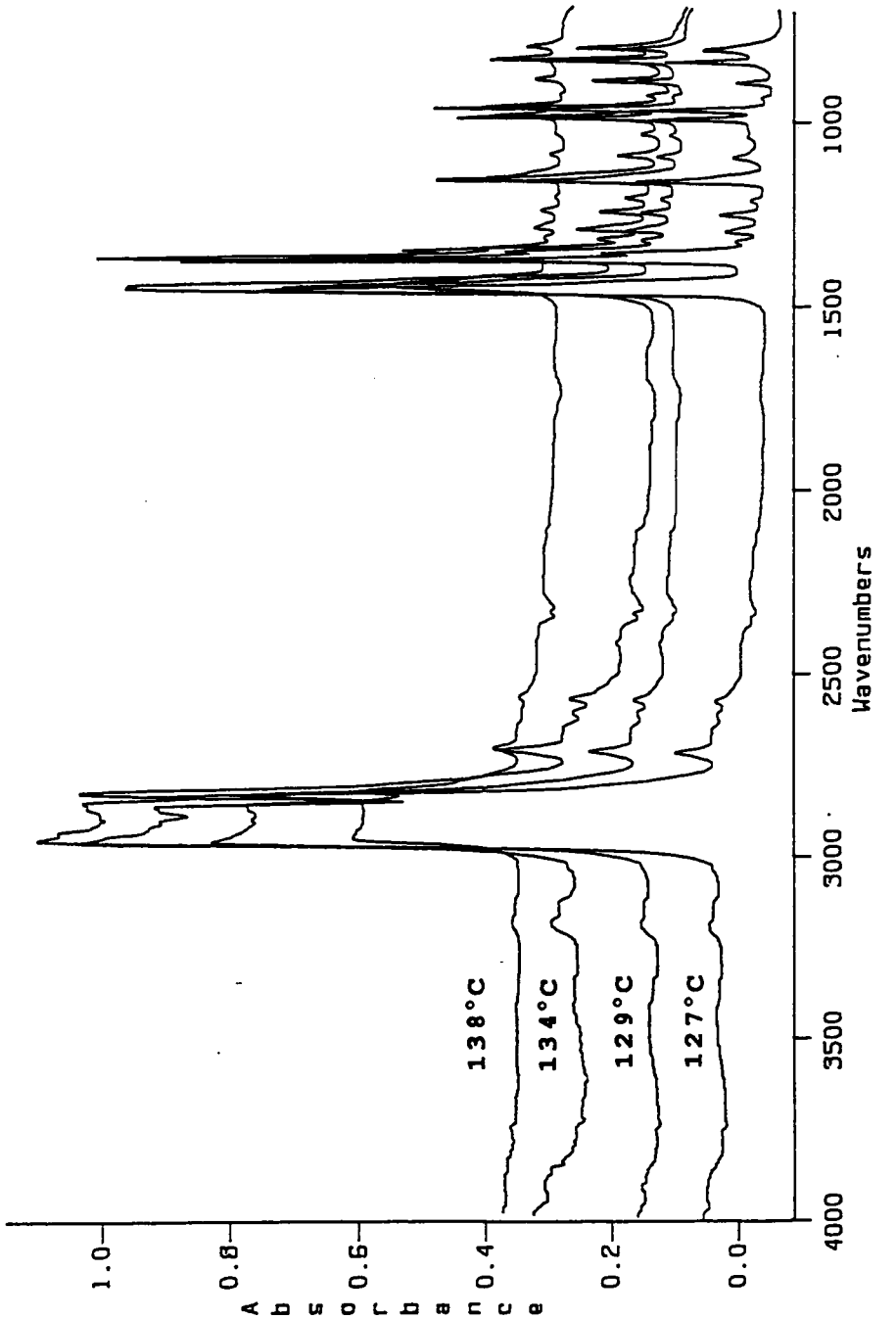


Figure 4.33 Infrared absorbance spectra for isotactic polypropylene 151,000 M_w homopolymer isothermally crystallized at the indicated temperatures.

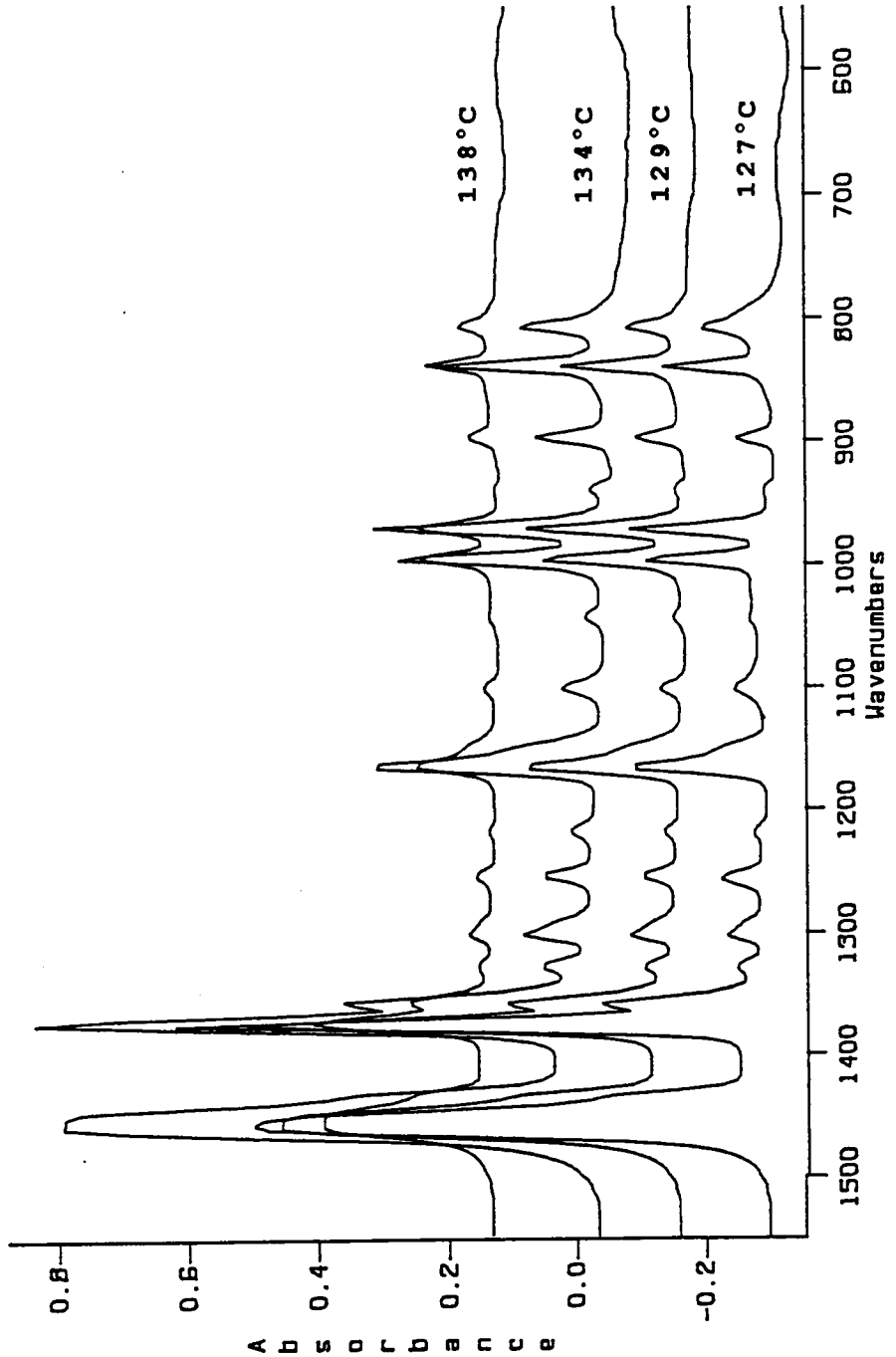


Figure 4.34 Infrared absorbance spectra of Figure 4.33 for the frequency range 1500 $cm^{-1} < \nu < 500\ cm^{-1}$.

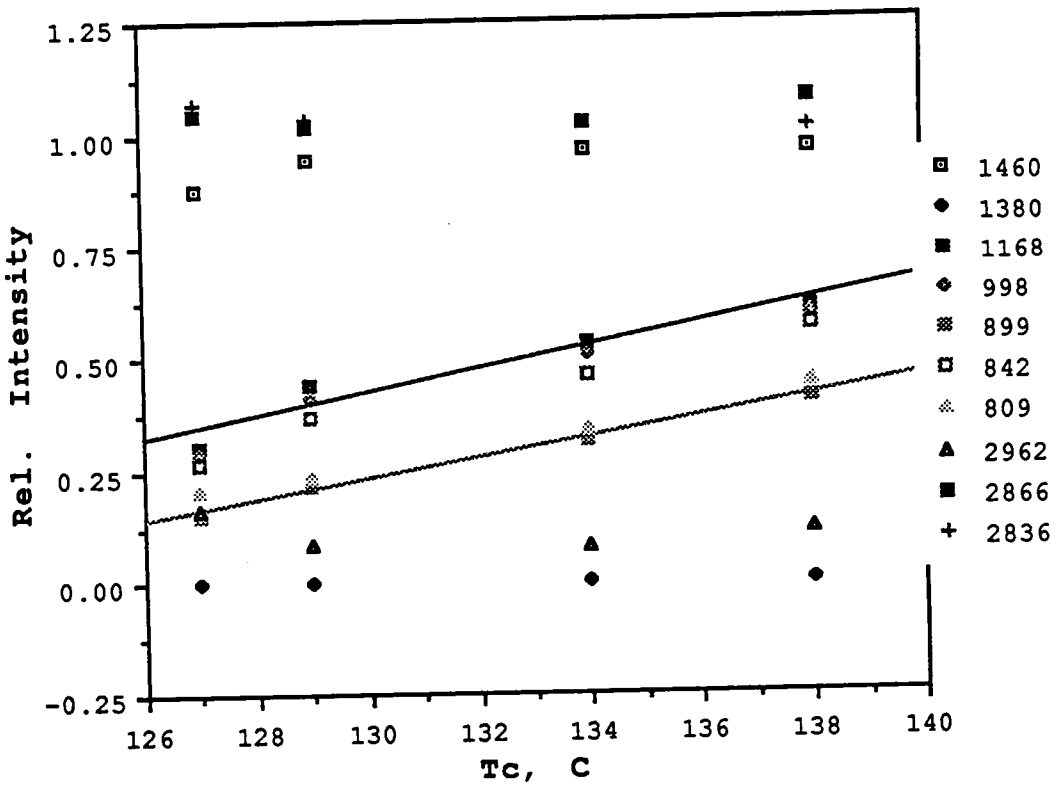


Figure 4.35 Relative intensities of various frequencies (reference frequency = 1380 cm^{-1}) as a function of isothermal crystallization temperature for isotactic polypropylene 151,000 M_w homopolymer.

Figure 4.36 shows the FTIR spectra for the 151,000 M_w copolymer at various crystallization temperatures for 4000 < ν < 400 cm^{-1}. As for the homopolymer the spectra show little differences. Figure 4.37 shows the spectra of Figure 4.35 for the frequency range 1500 < ν < 500 cm^{-1}. Differences in the spectra are made more apparent on a relative intensity basis. Figure 4.38 shows the relative intensities of the indicated frequencies with ν = 1380 cm^{-1} the reference frequency. Several frequencies exhibit a linear behavior with crystallization temperature. The frequencies of the homopolymer that exhibited a linear behavior do not seem to exhibit the same behavior for the copolymer. The relative intensites of the 1460 cm^{-1}, 1168 cm^{-1}, and 2962 cm^{-1} frequencies showed a linear increase with increasing crystallization temperature.

Figure 4.39 shows the FTIR spectra for the 151,000 M_w homopolymer and 151,000 M_w copolymer isothermally crystallized at T_c = 129°C for 4000 < ν < 400 cm^{-1}. Both spectra exhibited absorption frequencies characteristic of isotactic polypropylene. Figure 4.40 shows the spectra of Figure 4.39 for the frequency range 1500 < ν < 500 cm^{-1} Qualitatively, the spectra showed strong similarities, which is to be expected since the homopolymer and copolymer are not that different in chemical composition. The bands at 1460 cm^{-1} (λ = 6.85 μm) and 1379 cm^{-1} (λ = 7.25 μm) have been

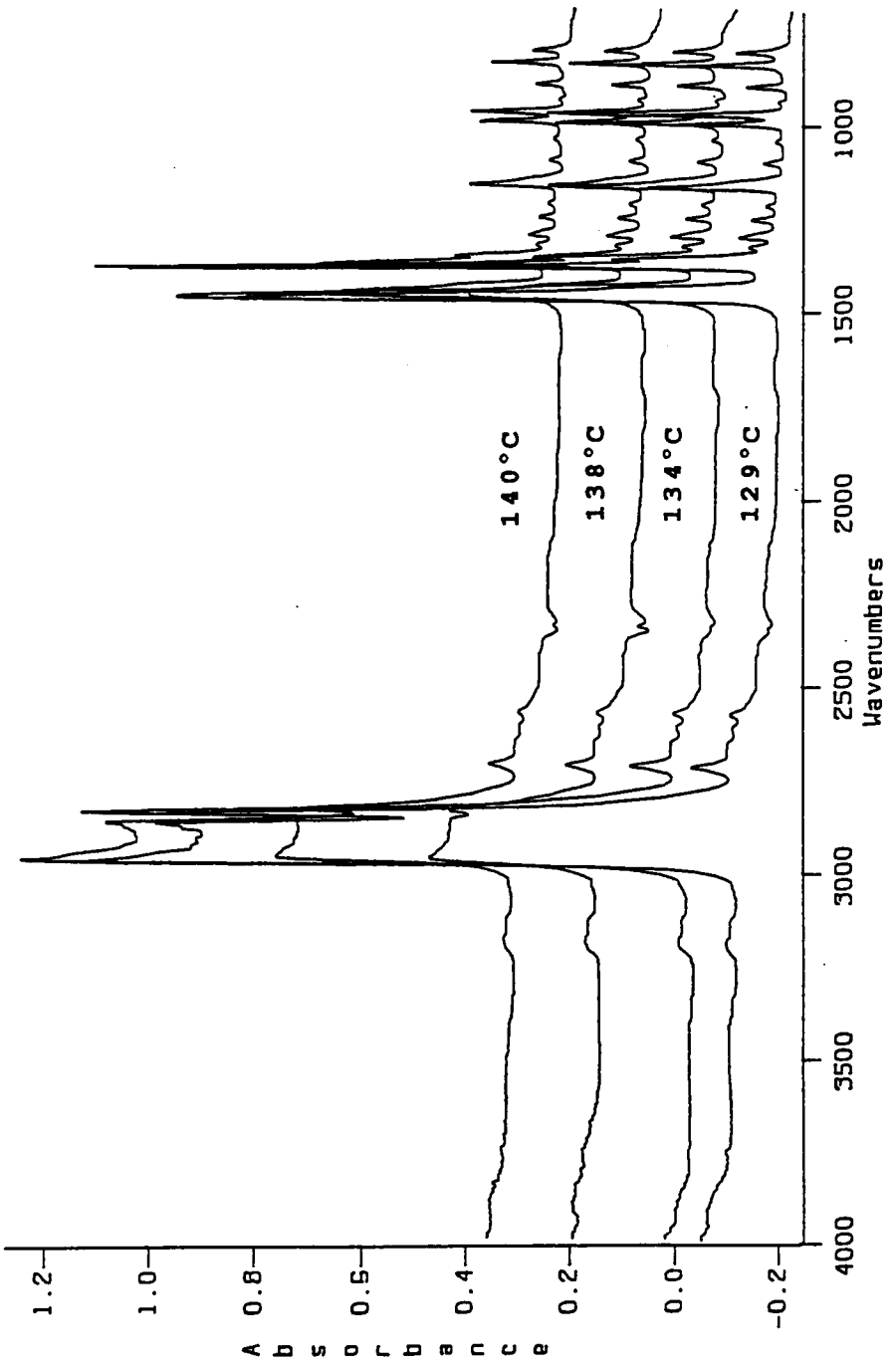


Figure 4.36 Infrared absorbance spectra for isotactic polypropylene 151,000 M_w copolymer isothermally crystallized at the indicated temperatures.

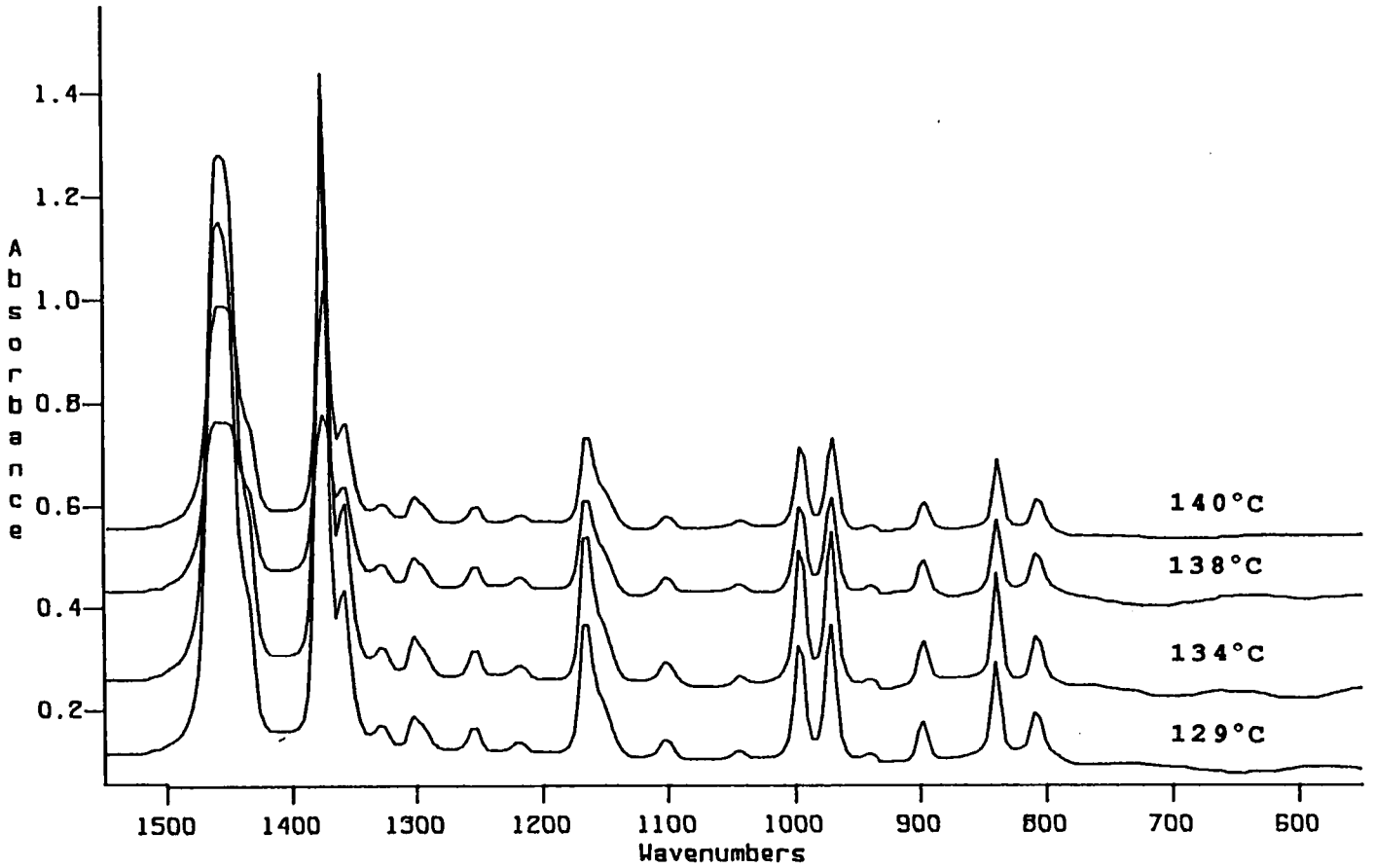


Figure 4.37 Infrared absorbance spectra of Figure 4.36 for the frequency range 1500 $cm^{-1} < \nu < 500\ cm^{-1}$.

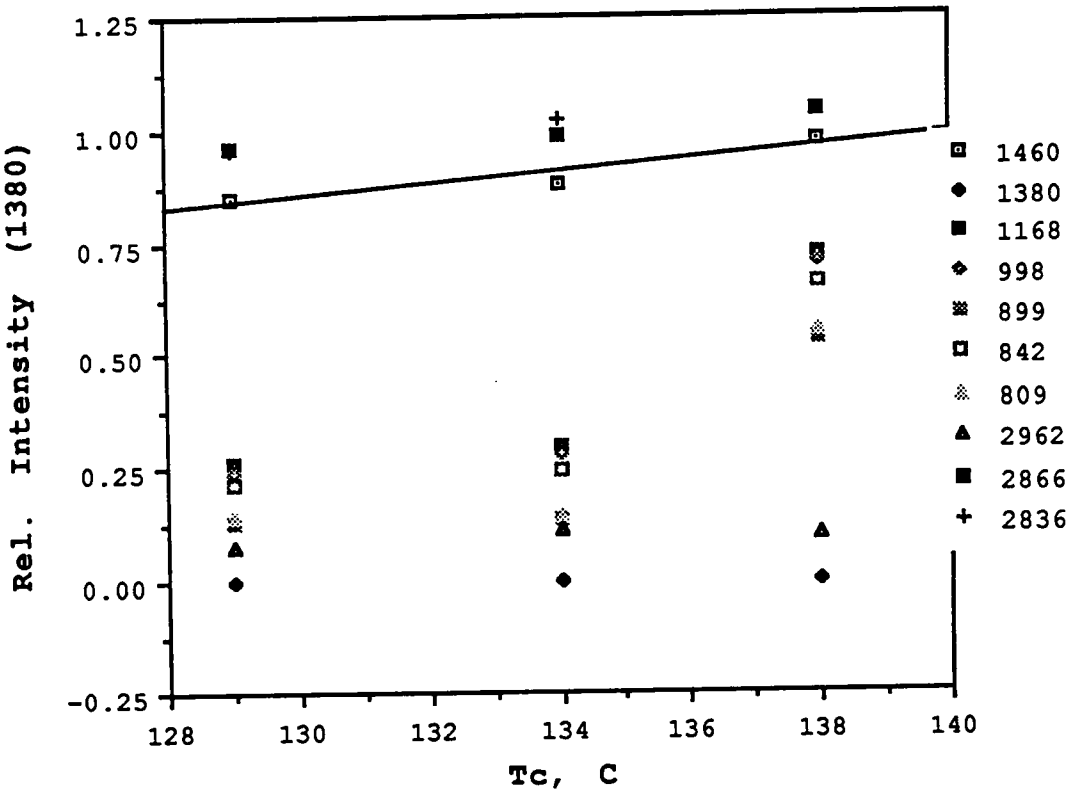


Figure 4.38 Relative intensities of various frequencies (reference frequency = 1380 cm^{-1}) as a function of isothermal crystallization temperature for isotactic polypropylene 151,000 M_w copolymer.

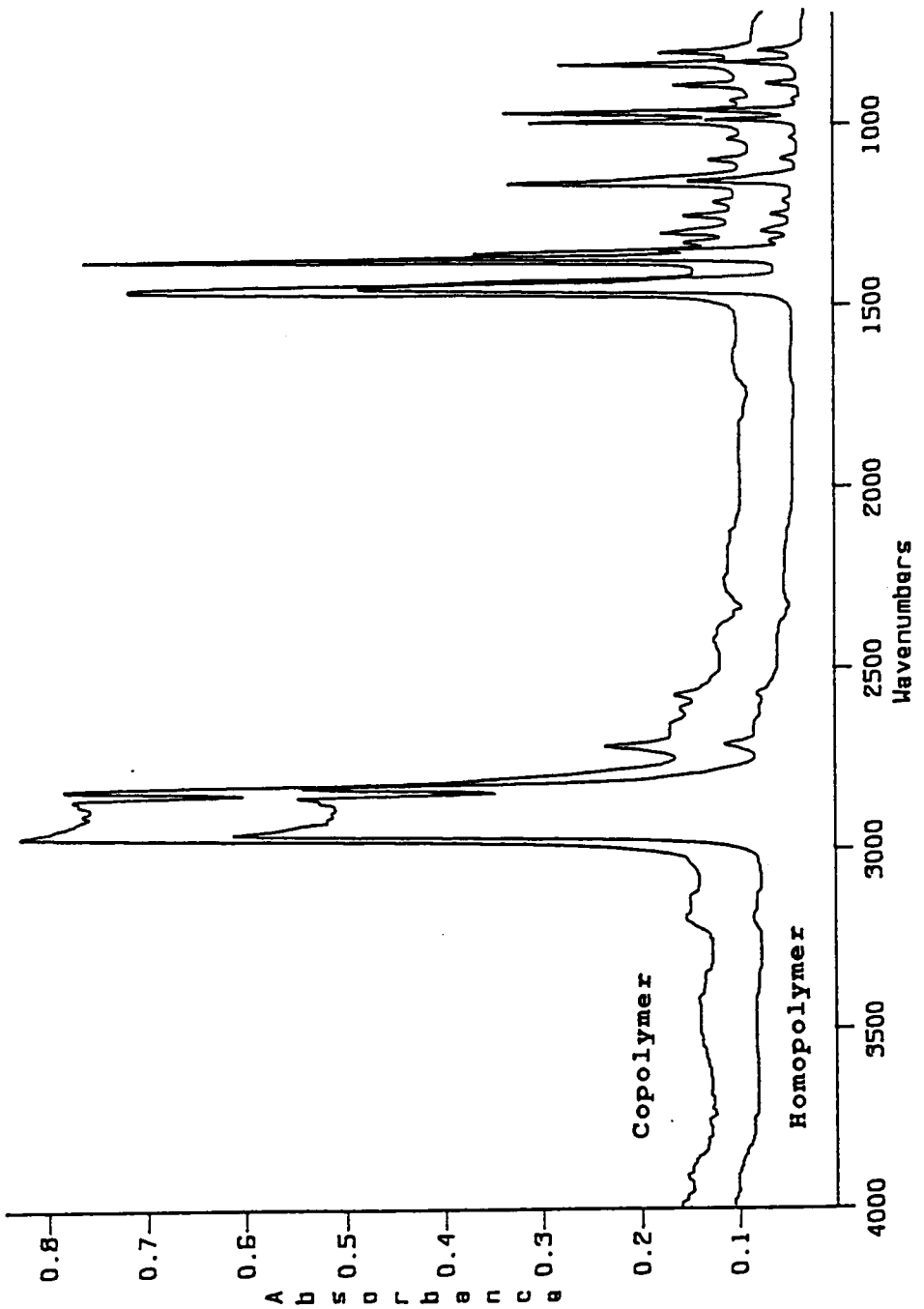


Figure 4.39 Comparison of Infrared absorbance for isotactic polypropylene 151,000 M_w homopolymer and copolymer $4000 < \nu < 400$ cm^{-1}.

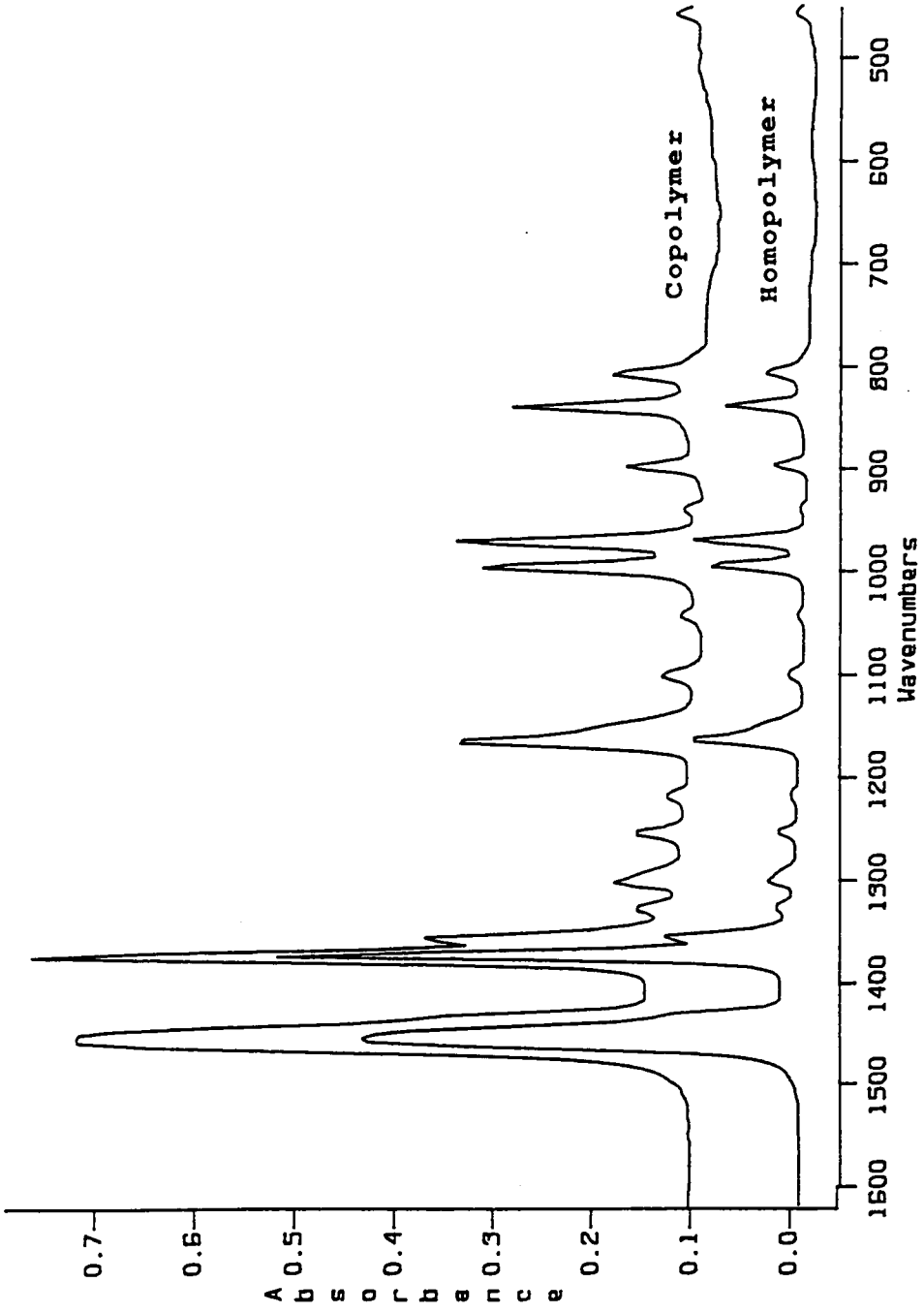


Figure 4.40 Comparison of Infrared absorbance for isotactic polypropylene 151,000 M_w homopolymer and copolymer, 1500 $cm^{-1} < \bar{\nu} < 500\ cm^{-1}$.

considered the bands most reliably assigned to a well-defined vibration. The IR method of most general applicability in determining the composition of ethylene-propylene random copolymers is based on the ratio of the intensity of the two peaks [108]. The two spectra exhibited differences in the ratio of these peaks. While no bands have been associated solely with the amorphous or the crystalline portion, the intensity of the bands at 1168, 998, 899, 842, and 809 cm^{-1} have been shown to decrease with decreasing crystallinity of isotactic polypropylene [109]. These bands exhibited similar intensities for the two samples, indicating similar crystallinities. Table 4.3 gives the intensities of these bands as well as the ratio of the 1460 cm^{-1} and 1379 cm^{-1} bands at several crystallization temperatures for the homopolymer and copolymer. The variation of intesities of these peaks was consistent with WAXD crystallinity variation.

4.4.2 Elevated Pressure

With the proposed crystal structures of the γ form of polypropylene having significantly different arrangements of chain stems within lamellae relative to the α form, it was believed that the IR spectrum would exhibit changes that were dependent on the changes in the crystal structure. Figure 4.41 shows the IR spectra of polypropylene that has been crystallized at several elevated pressures. Figure 4.42 shows the FTIR spectra of the spectra of Figure 4.41 for the

Table 4.3 FTIR Relative Intensities for Isotactic Polypropylene Crystallized at Atmospheric Pressure and Elevated Pressure; Reference Frequency = 1380 cm^{-1}.

T_c, °C	1460	1168	998	899	842	809	2962	2866	2836
Homo.									
129	0.943	.438	.407	.216	.368	.234	.085	1.017	1.032
134	0.961	.532	.505	.316	.458	.337	.080	1.021	1.025
138	0.959	.607	.590	.406	.565	.440	.116	1.074	1.103
127	0.878	.305	.290	.153	.263	.204	.162	1.044	1.068
Copoly									
129	0.851	.265	.240	.130	.215	.144	.077	0.964	0.956
134	0.877	.297	.279	.139	.244	.147	.112	0.985	1.023
138	0.975	.723	.704	.530	.661	.553	.101	1.038	1.039
P_c, MPa									
200	0.700	.199	.141	.049	.117	.060	.000	0.741	0.740
175	0.954	.381	.284	.125	.254	.152	.000	1.054	1.054
125	0.737	.199	.142	.049	.123	.063	.000	0.809	0.808
100	0.860	.418	.312	.134	.273	.155	.000	0.822	0.847
75	0.215	.049	.049	.010	.031	.014	.000	0.227	0.227
50	0.946	.392	.332	.163	.309	.192	.000	0.953	0.977
25	0.237	.061	.061	.022	.046	.024	.000	0.228	0.233

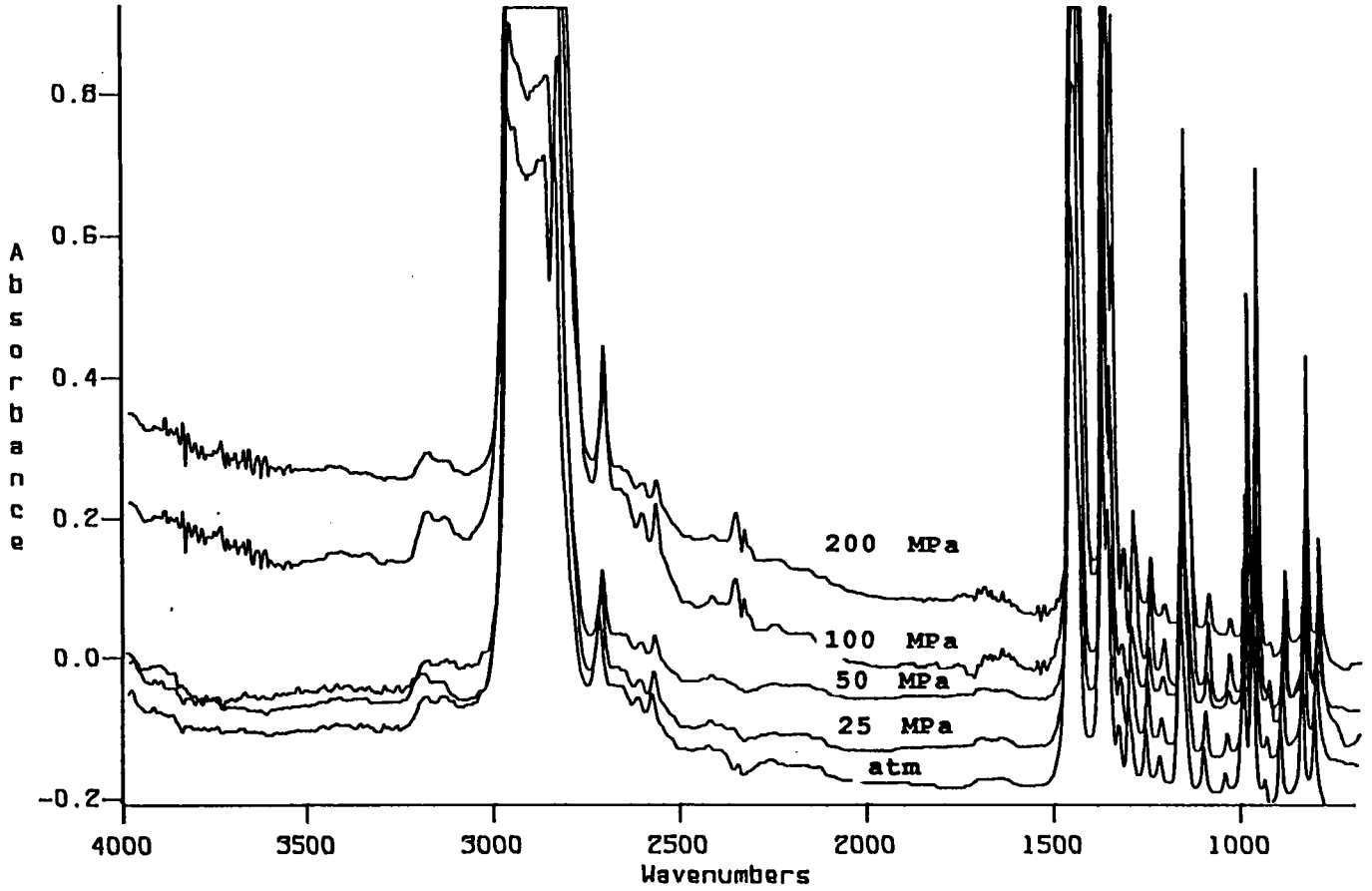


Figure 4.41 Infrared absorbance spectra for isotactic polypropylene 151,000 M_w homopolymer isothermally crystallized at elevated pressure.

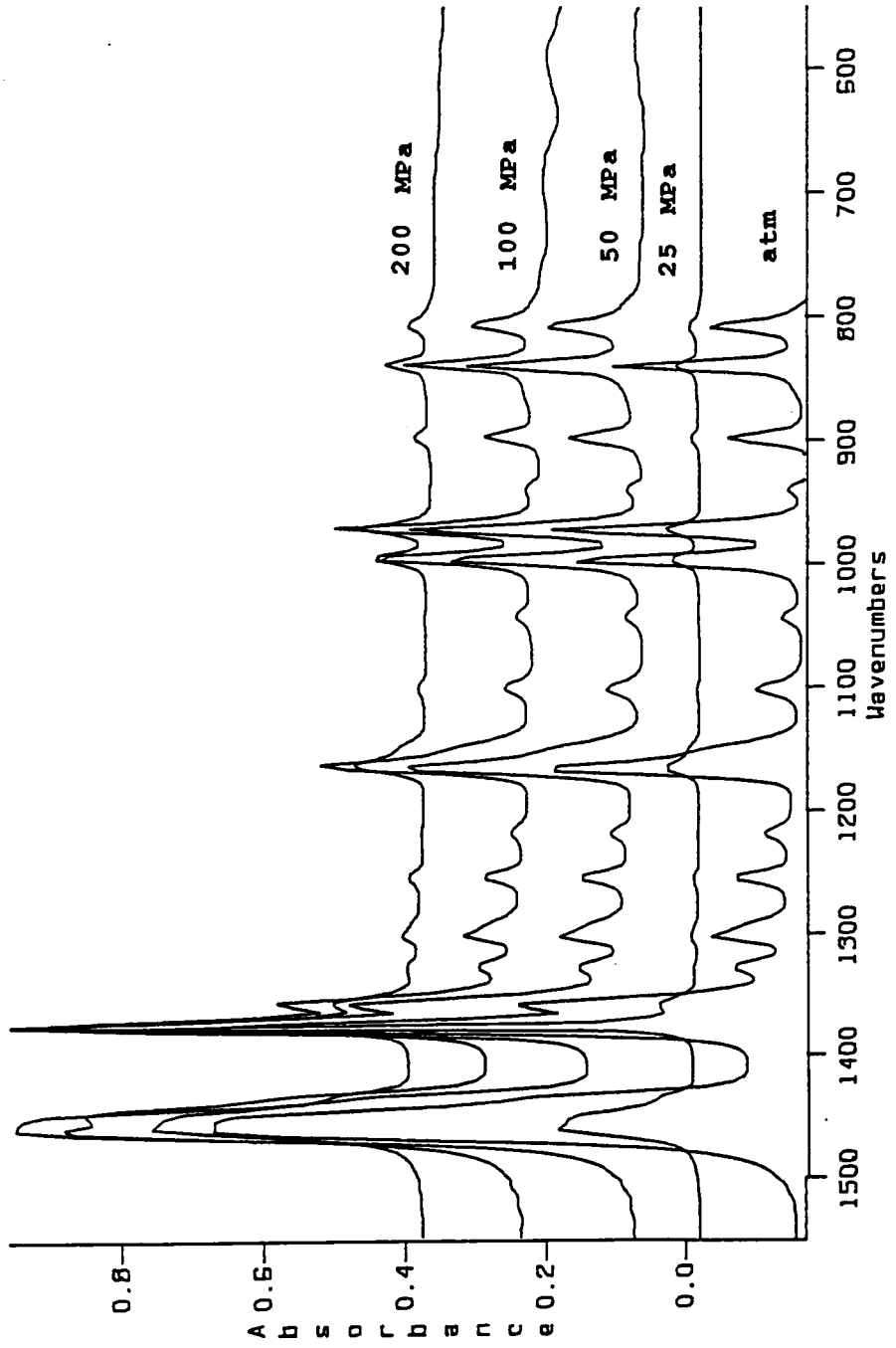


Figure 4.42 Infrared absorbance spectra of Figure 4.41 for the frequency range 1500 $cm^{-1} < \nu < 500\ cm^{-1}$.

frequency range 1500 $cm^{-1} < \nu < 500\ cm^{-1}$. It was observed that the spectra exhibited marked differences in the absorption region of the CH_2 and CH_3 asymmetric and symmetric stretching (2962 cm^{-1} - 2839 cm^{-1}) as well as the region of the CH_2 bending and CH_3 bending (1460 cm^{-1} and 1378 cm^{-1}). The stretching vibrations involve variations in the distance between two directly bonded atoms and have fairly high force constants. Thus the stretching frequencies are largely independent of molecular geometry. Bending vibrations involve angular variations and have weaker force constants. Bending vibrations should then be more influenced by the arrangement of neighboring atoms. However, there is a large overlap of the stretching bands of the methyl and methylene groups, which would limit their practical use in the interpretation of molecular arrangement. Figure 4.43 shows the relative intensities of various frequencies as a function of crystallization pressure P_c with the relative frequency = 1380 cm^{-1}. Table 4.4 gives the absorptions of several frequencies as a function of crystallization pressure.

4.5 Optical and Electron Microscopy

4.5.1 Atmospheric Pressure

Transmission electron microscopy was performed on replicas of permanganic acid etched atmospheric pressure and elevated pressure crystallized samples of the M_w = 151,000

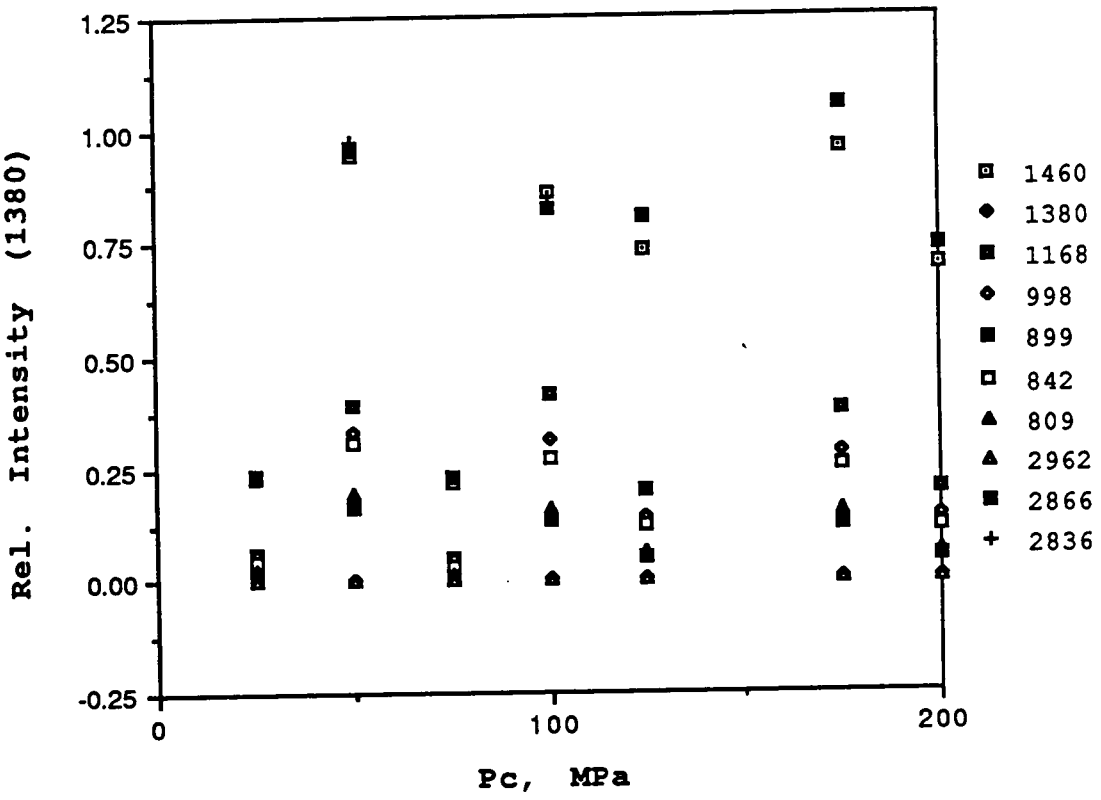


Figure 4.43 Relative intensities of various frequencies (reference frequency = 1380 cm^{-1}) as a function of crystallization pressure for isotactic polypropylene 151,000 M_w homopolymer.

Table 4.4 FTIR Relative Intensities for Isotactic Polypropylene Crystallized at Atmospheric Pressure and Elevated Pressure; Reference Frequency = 2866 cm^{-1}.

Tc,°C	1460	1380	1168	998	899	842	809	2962	2836
Homo									
129	0.927	.983	.430	.401	.212	.362	.230	.067	1.014
134	0.942	.979	.521	.494	.310	.449	.330	.058	1.004
138	0.893	.931	.565	.549	.378	.526	.410	.039	1.027
127	0.841	.958	.292	.277	.146	.252	.196	.114	1.023
Copoly									
129	0.883	.038	.275	.249	.135	.224	.149	.118	0.992
134	0.890	.015	.302	.284	.141	.247	.149	.129	1.038
138	0.940	.964	.697	.678	.511	.637	.533	.062	1.002
Pc,MPa									
200	0.945	.350	.268	.190	.066	.158	.081	.000	0.999
175	0.905	.948	.361	.269	.119	.241	.144	.000	1.000
125	0.911	.237	.246	.176	.060	.152	.078	.000	0.999
100	1.045	.216	.509	.380	.163	.332	.189	.000	1.030
75	0.944	.398	.214	.214	.045	.137	.061	.000	0.997
50	0.993	.049	.411	.349	.171	.325	.201	.000	1.025
25	1.039	.377	.265	.265	.094	.200	.107	.000	1.020

homopolymer and atmospheric pressure crystallized samples of the M_w = 151,000 copolymer. The homopolymer and copolymer exhibited similar features at a fixed crystallization temperature (fixed ΔT). 'Cross-hatching' could be observed in both samples at all crystallization temperatures studied. At low crystallization temperatures, the amount of 'cross-hatching' is significant. With increasing crystallization temperature, the amount of 'cross-hatching' decreased, but did not completely disappear over the crystallization temperature range studied. Figure 4.44a shows the TEM micrograph of the copolymer isothermally crystallized at 135°C (ΔT = 52°). The radial lamellae are observed to be relatively straight over long distances and stacked uniformly. The tangential component was generally shorter but was stacked uniformly. As reported previously [55,11], the thickness of radial and tangential lamellae at low crystallization temperature are similar if not the same. Figure 4.44b shows the TEM micrograph of the copolymer at T_c = 145°C. The lamellar arrangement has changed with the increased temperature. Figure 4.45a shows a view of the homopolymer at a spherulite boundary at T_c = 145°C. Lamellae are observed in the edge-on view as well as views other than edge-on. Figure 4.45b shows a high magnification of the homopolymer at T_c = 135°C at radial-tangential branch junctions. The constancy of the branch angle of ≈80° is

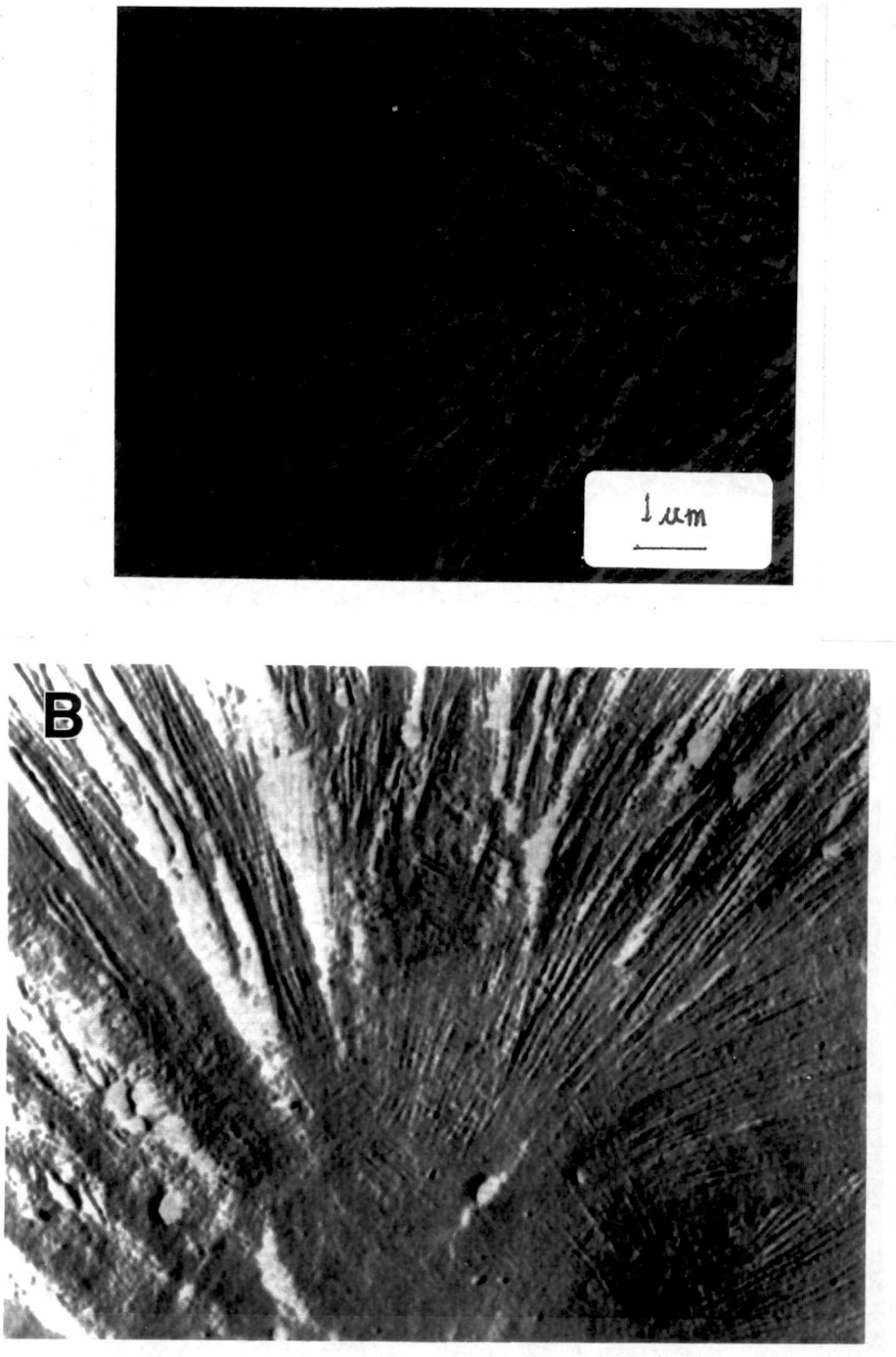


Figure 4.44 TEM micrographs of isotactic polypropylene 151,000 Mw copolymer (0.5% ethylene) isothermally crystallized at atmospheric pressure; A. T_c = 135°C, and B. T_c = 145°C.

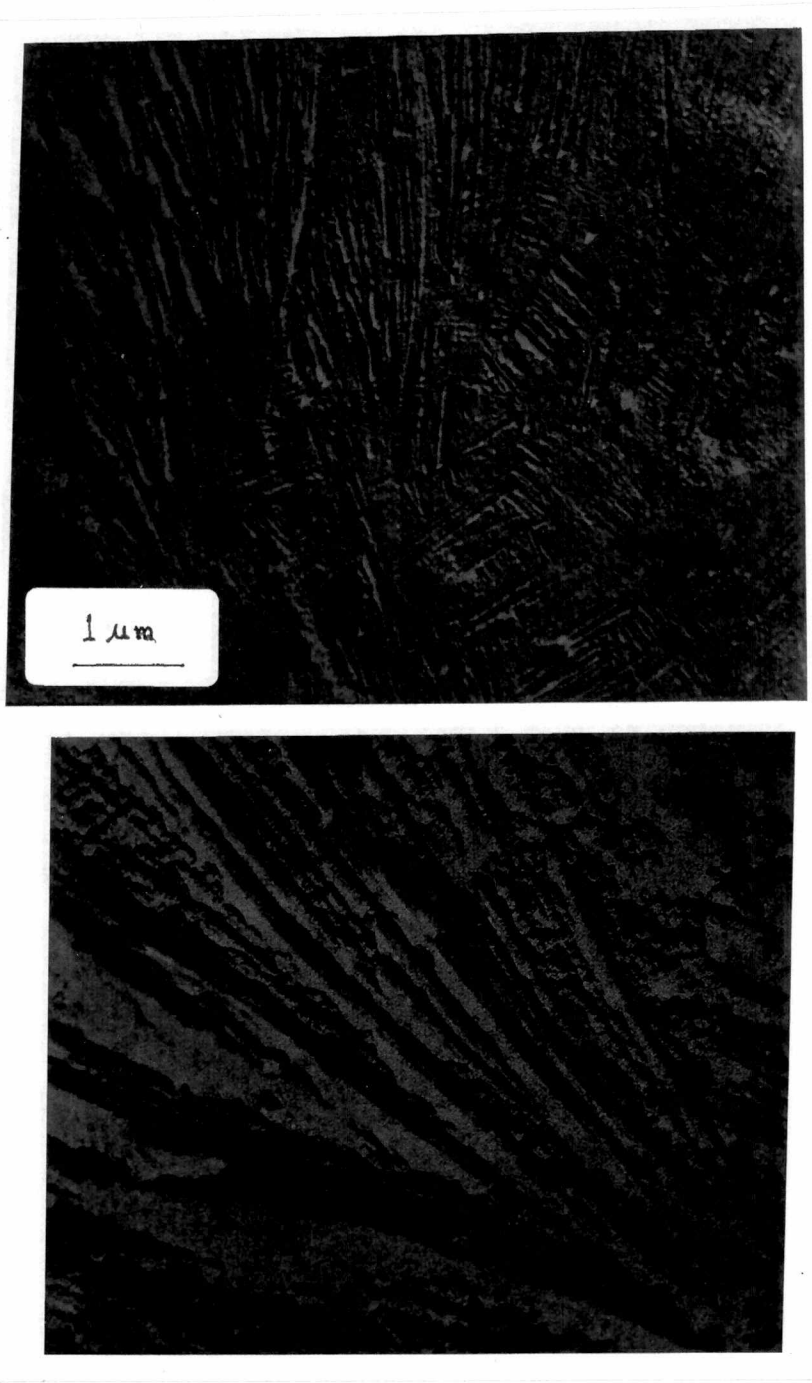


Figure 4.45 TEM micrographs of isotactic polypropylene 151,000 M_w homopolymer isothermally crystallized at atmospheric pressure; A. T_c = 145°C, B. T_c = 145°C.

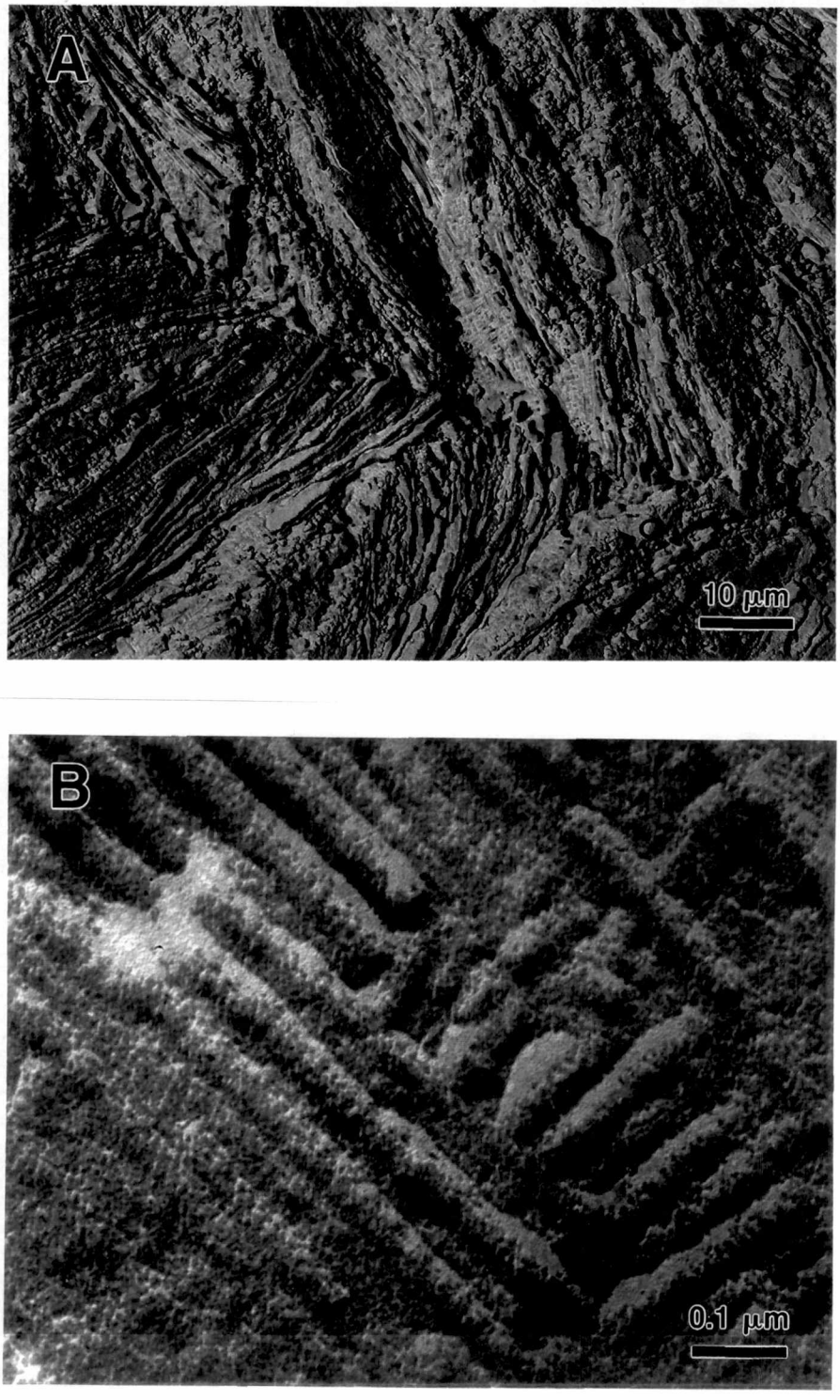


Figure 4.46 TEM micrographs of isotactic polypropylene 151,000 M_w homopolymer isothermally crystallized at atmospheric pressure; A. T_c = 135°C, B. T_c = 145°C, enlargement of tangential branching.

observed. The uniformity of lamellar thickness within the field of observation is also observed.

4.5.2 Elevated Pressure

Optical microscopy and transmission electron microscopy was performed on elevated pressure crystallized samples of the 151,000 M_w homopolymer that were isothermally crystallized at $\Delta T = 50°$. The elevated pressure crystallized samples were prepared as described in section 3.3. Following crystallization, the samples were glass-knife microtomed with a fresh knife at -20°C (knife temperature) and the microtomed surface etched using the permanganic acid technique described previously. The etched surfaces were initially observed on a Nikon Microphot optical microscope in reflection mode to observe the morphology at low magnification. The etched samples were then replicated following standard procedures. It was observed that the etching procedure that was optimized for the atmospheric pressure crystallized samples etched the elevated pressure crystallized samples differently, depending on the crystallization pressure. As the crystallization pressure increased, the etching procedure generated more etch artifacts. It is believed that this reflects a change in the α-γ composition of the sample as a function of pressure. Figures 4.47 - 4.49 show reflection optical micrographs of elevated pressure crystallized samples, and the transmission optical micrographs of microtomed sections of the same

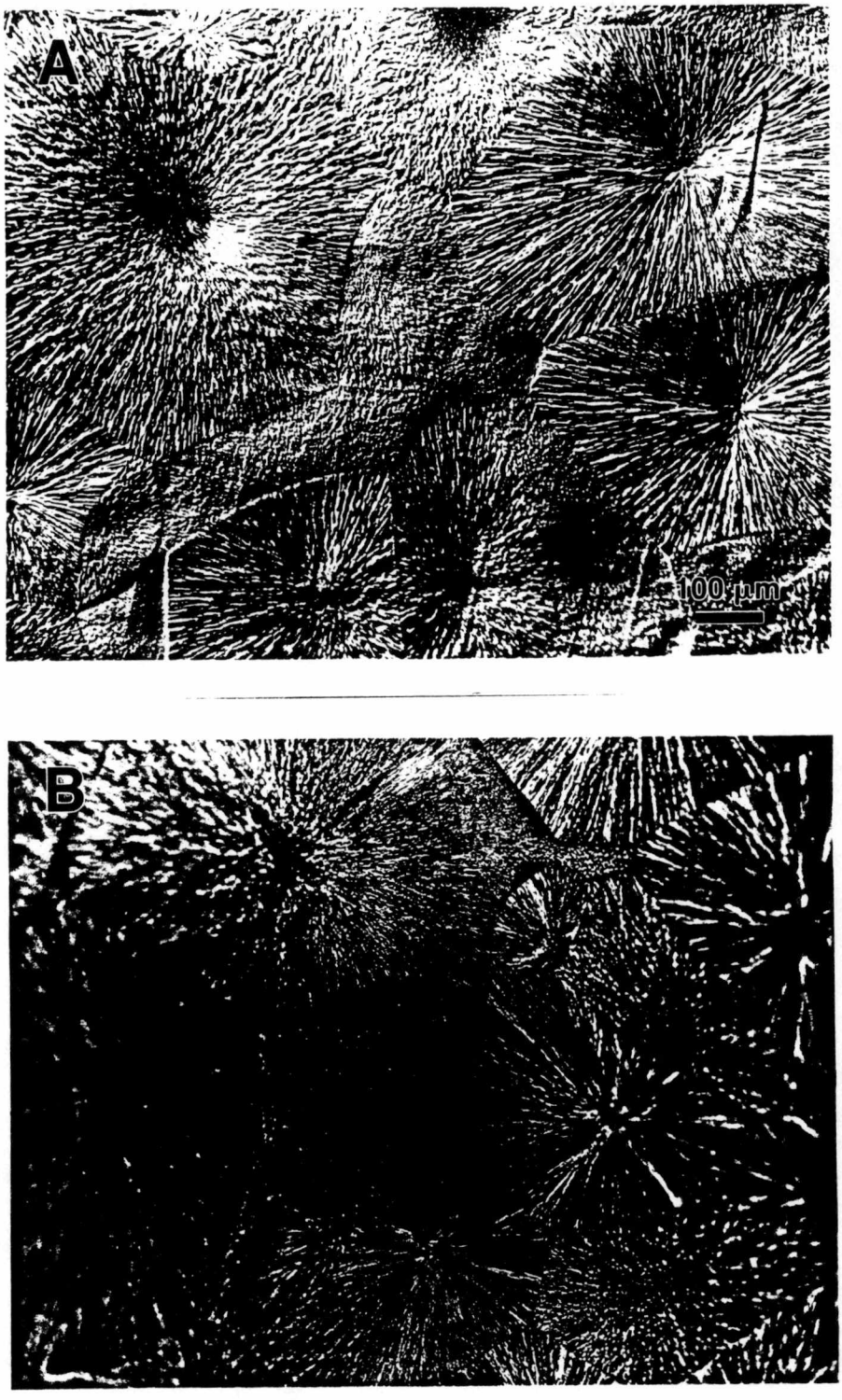


Figure 4.47 Reflection optical micrographs of permanganic etched surfaces of elevated pressure crystallized isotactic polypropylene, 151,000 M_w; A. 25 MPa, B. 50 MPa.

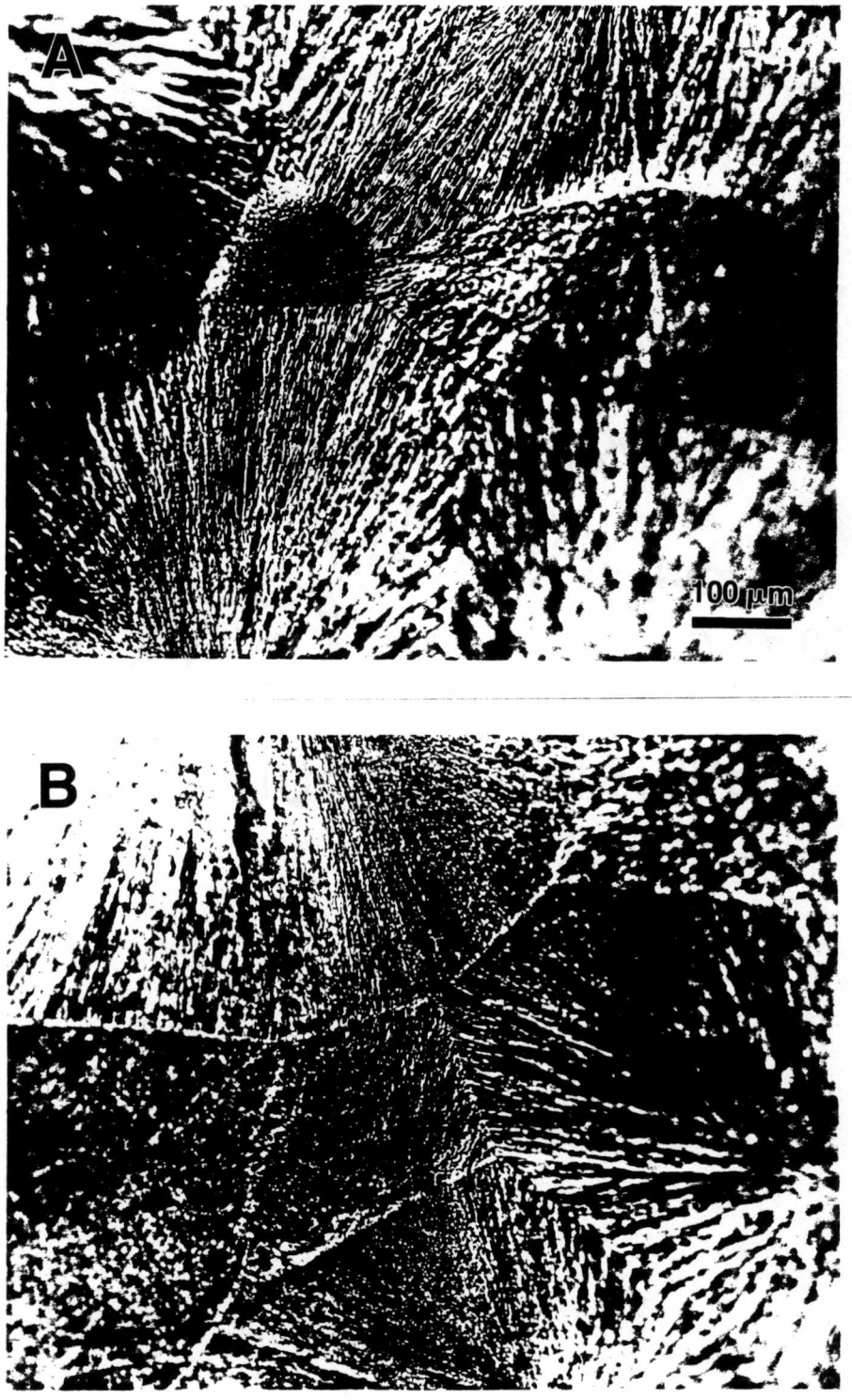


Figure 4.48 Reflection optical micrographs of permanganic etched surfaces of isotactic polypropylene homopolymer, ΔT = 50°C; A. 75 MPa, and B. 100 MPa.

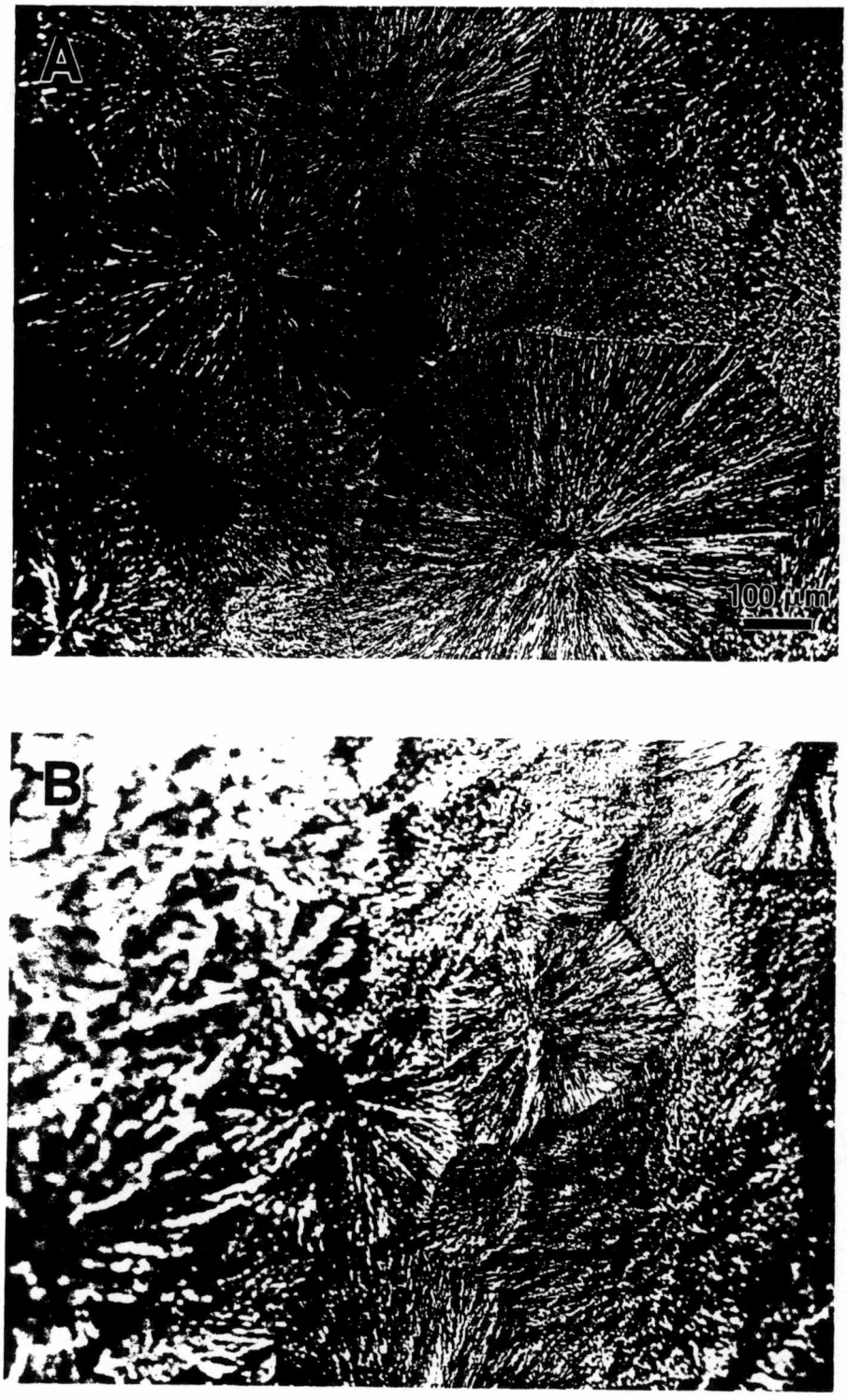


Figure 4.49 Reflection optical micrographs of permanganic etched surfaces of elevated pressure crystallized isotactic polypropylene 151,000 M_w (ΔT = 50°C); A. 125 MPa, and B. 200 MPa.

material. Spherulites were observed at all pressures. However, it is seen that the spherulite texture changed with crystallization pressure.

The transmission electron microscopy revealed a change in lamellar structure with increasing pressure. Figures 4.50 - 4.52 show transmission electron micrographs of elevated pressure crystallized samples. At 25 MPa, the lamellar structure is similar to that observed at atmospheric pressure. This is expected since only a small portion of the material (≈10%) is γ form at this pressure. However, the lamellar packing does not appear as uniform as that observed at atmospheric pressure. Figure 4.50 shows the TEM of 50 MPa crystallized polypropylene. Lamellar structure is still clearly present. The tangential lamella can also still be observed at this pressure, but a significant portion of branching occurs at angles less than the α-α 80° radial-tangential branch angle. The material at this pressure still etches with little obvious damage or artifact formation using the atmospheric pressure etching procedure. Another observation of the change in the nature of the lamellar structure at 50 MPa is the tendency of the lamellae to curve as shown if Figure 4.51. At 75 MPa, the material began exhibiting a more pronounced etch damage, as seen in Figure 4.51. The lamellar packing is significantly less ordered than that at atmospheric pressure. The γ composition is ≈45%,

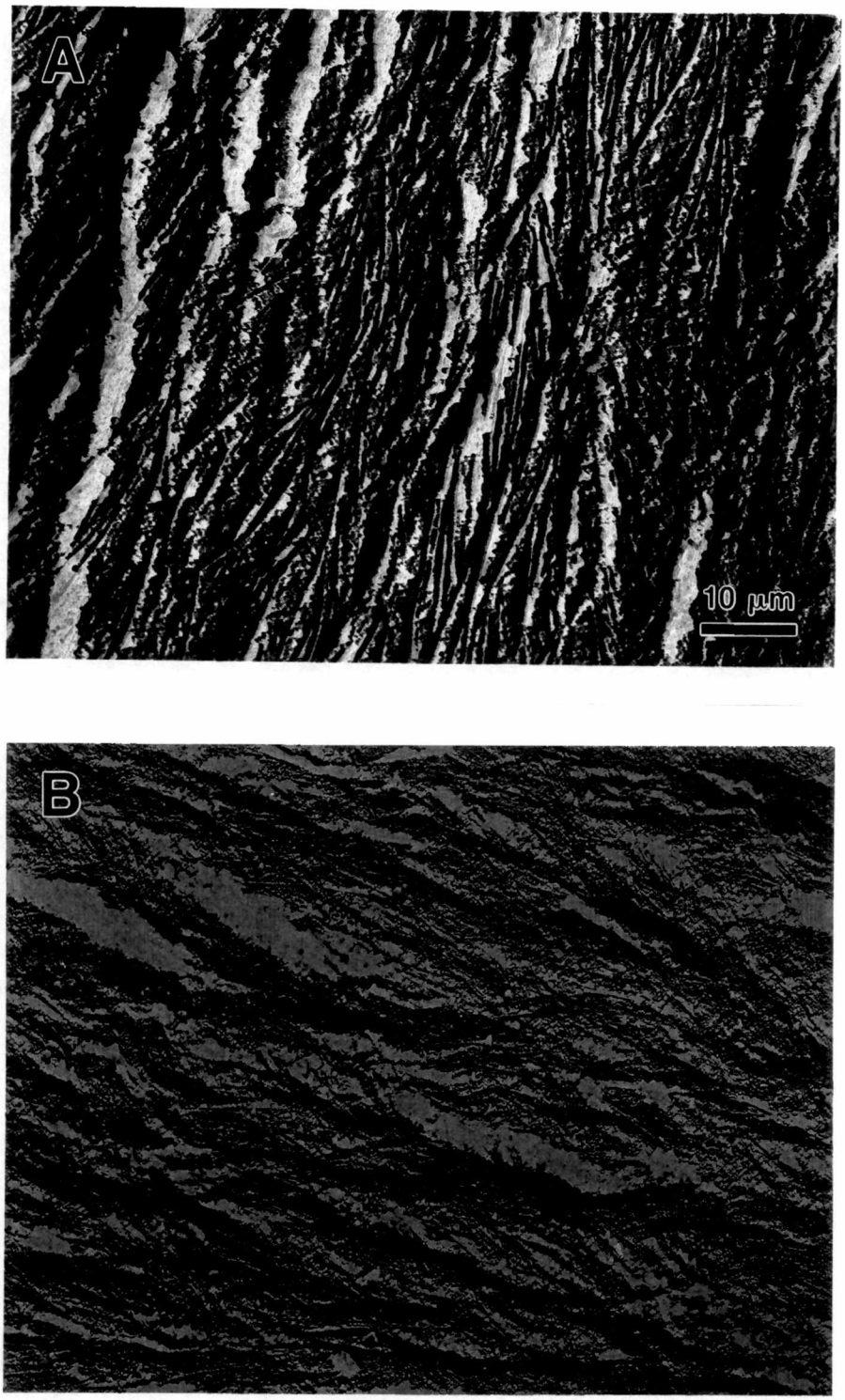


Figure 4.50 TEM micrographs of elevated pressure crystallized isotactic polypropylene 151,000 M_w homopolymer; A. 25 MPa, B. 50 MPa.

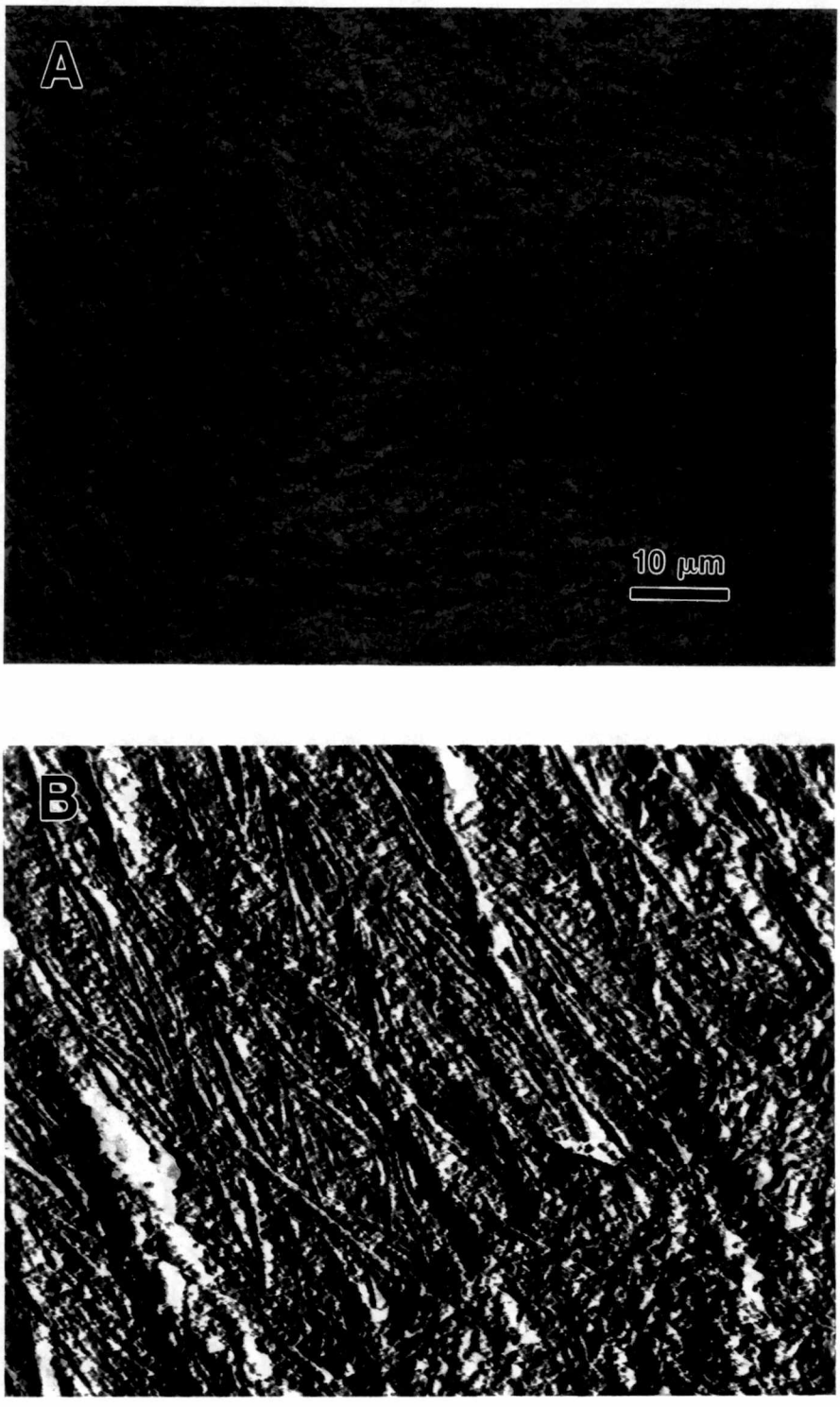


Figure 4.51 TEM micrographs of elevated pressure crystallized isotactic polypropylene 151,000 M_w homopolymer; A. 50 MPa, B. 75 MPa.

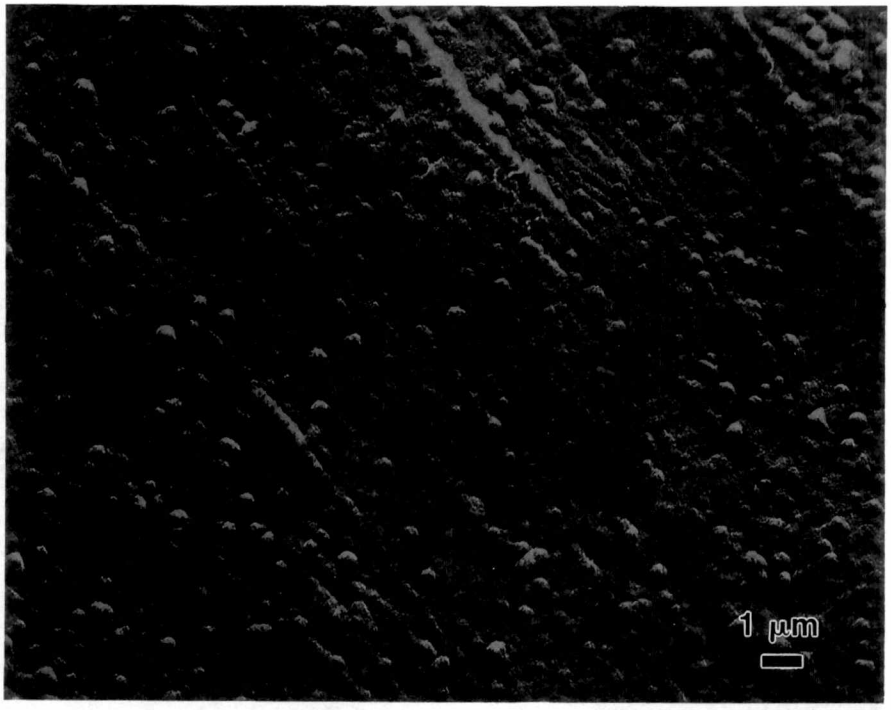


Figure 4.52 TEM micrograph of elevated pressure crystallized isotactic polypropylene 151,000 M_w homopolymer (ΔT = 50°C); Pc = 100 MPa.

but it is difficult to conclude whether one can observe lamellar structures that are a lamellae and γ lamellae. The 100 MPa sample exhibited significant etching damage, as shown in Figure 4.52. While tangential branching could still be observed at 75 MPa in small amounts, none was observed at 100 MPa. The observed loss of the tangential branching can be predicted on the basis of the orthorhombic γ polypropylene crystal structure. Figure 4.53 represents schematically the branching of isotactic polypropylene based on the Lotz-Wittmann epitaxial branching mechanism. Figure 4.53 shows that an α 'daughter' branch on an α 'parent' lamella should give a branch angle of ≈80°, as observed in the TEM (tangential lamellae). Figure 4.53 also shows the γ 'daughter' branch on an α 'parent' lamella, with a corresponding angle of ≈40°. Also, an α 'daughter' branch on a γ 'parent' lamella should give a branching angle of ≈40°. The reduction in branch angle is observed in the TEM's of elevated pressure crystallized samples, where sufficient amounts of the γ form are present.

The possibility of branching on γ lamellae will now be considered. Figure 4.54 shows a schematic of a γ lamellae. In this schematic, with a proposed growth front [008], the lateral edge of the lamella is not as conducive to nucleation of a branch as that of the α lamella. This could lead to a branch occurring at or just behind the growth front and a

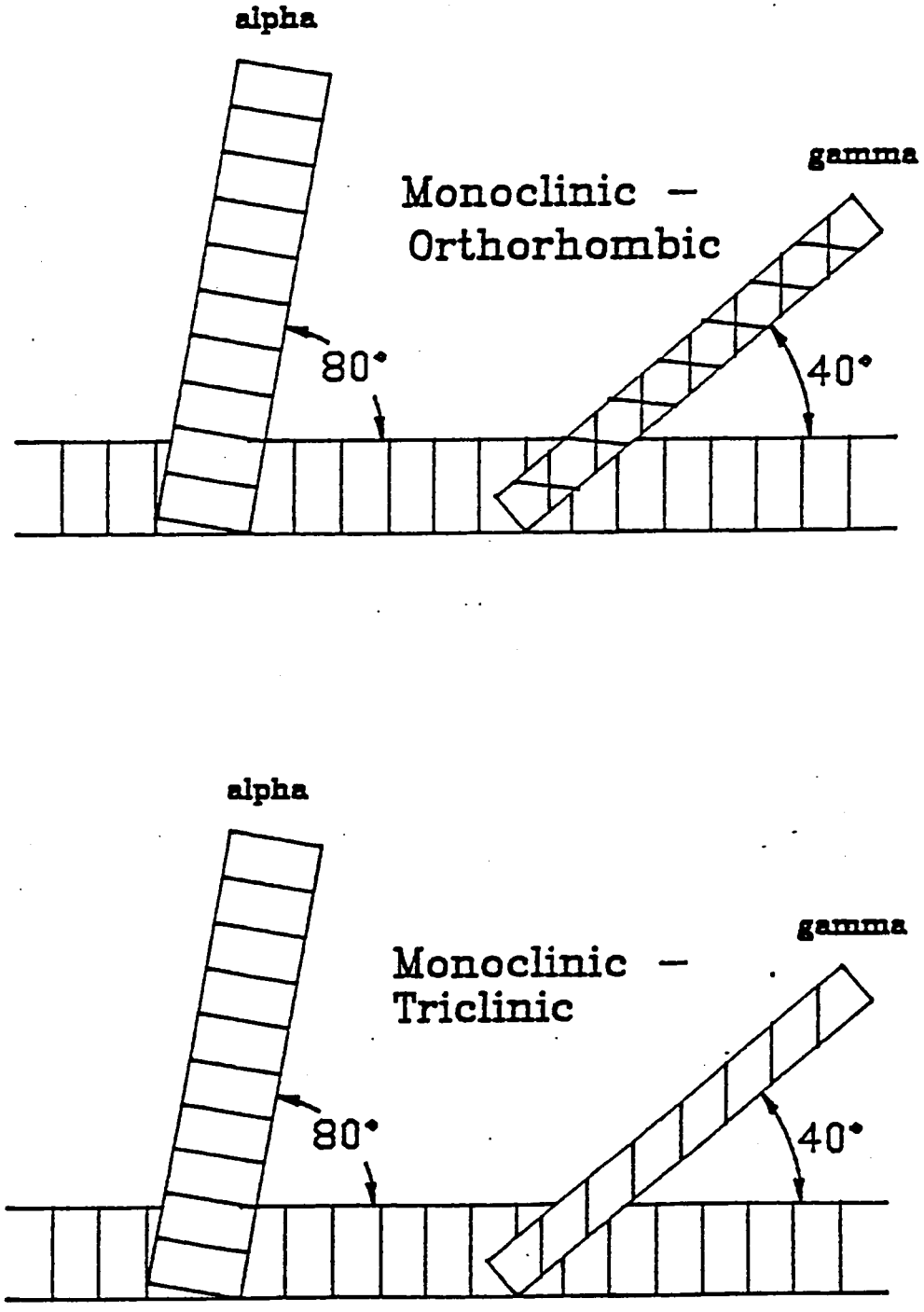


Figure 4.53 Schematic of branching in isotactic polypropylene.

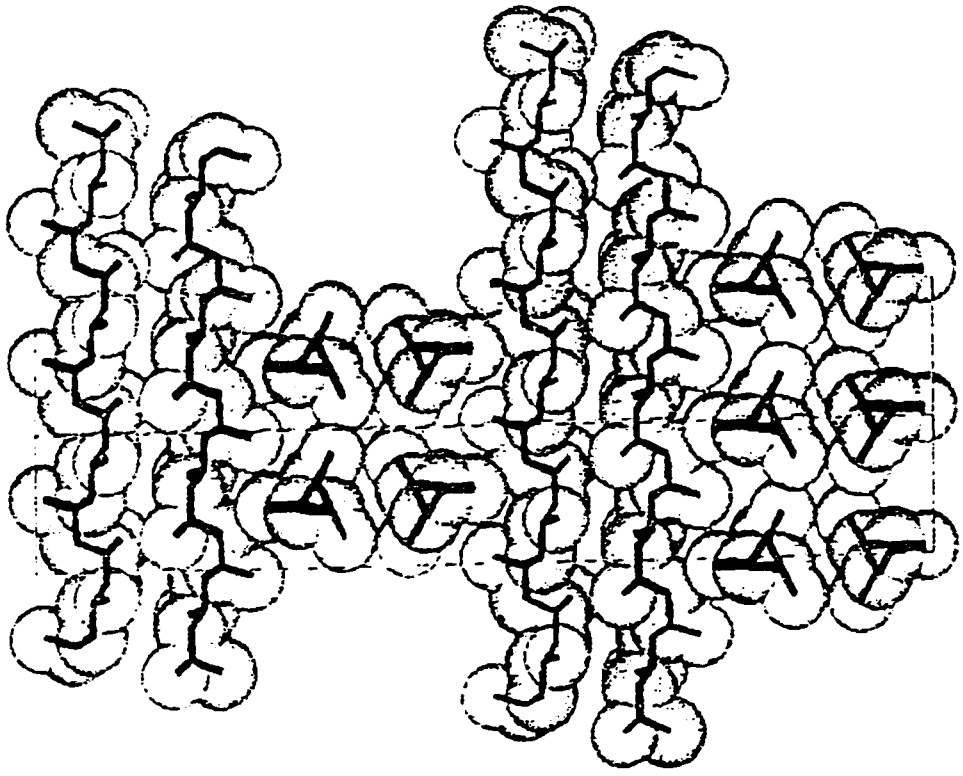


Figure 4.54 Schematic of γ lamellae.

situation of significant branching with little linear growth. Alternatively, the different growth front that results in the [00c] planes being at an angle to the linear growth direction could yield a lateral edge that was similar in nature to that of the α lamella. This should then result in similar branching natures between the two structures.

4.6 Crystallization - Atmospheric Pressure

4.6.1 Linear Growth Rates

The growth rates of isotactic polypropylene at various isothermal crystallization temperatures were obtained by measuring spherulite diameters from photographs as a function of time. The spherulite diameters were linear with time at all temperatures for all samples up to impingement. A plot of average spherulite size versus time of crystallization at crystallization temperatures ranging from approximately 125°C to 155°C for a bulk polypropylene, M_w = 83,000, is shown in Figure 4.55. Most of the diameter-time lines showed positive y-intercepts at time zero,. At higher temperatures (T_c > 145°C) the y-intercept became negative, indicating a significant induction time for the onset of crystallization. Linear growth rates were determined using a least squares method.

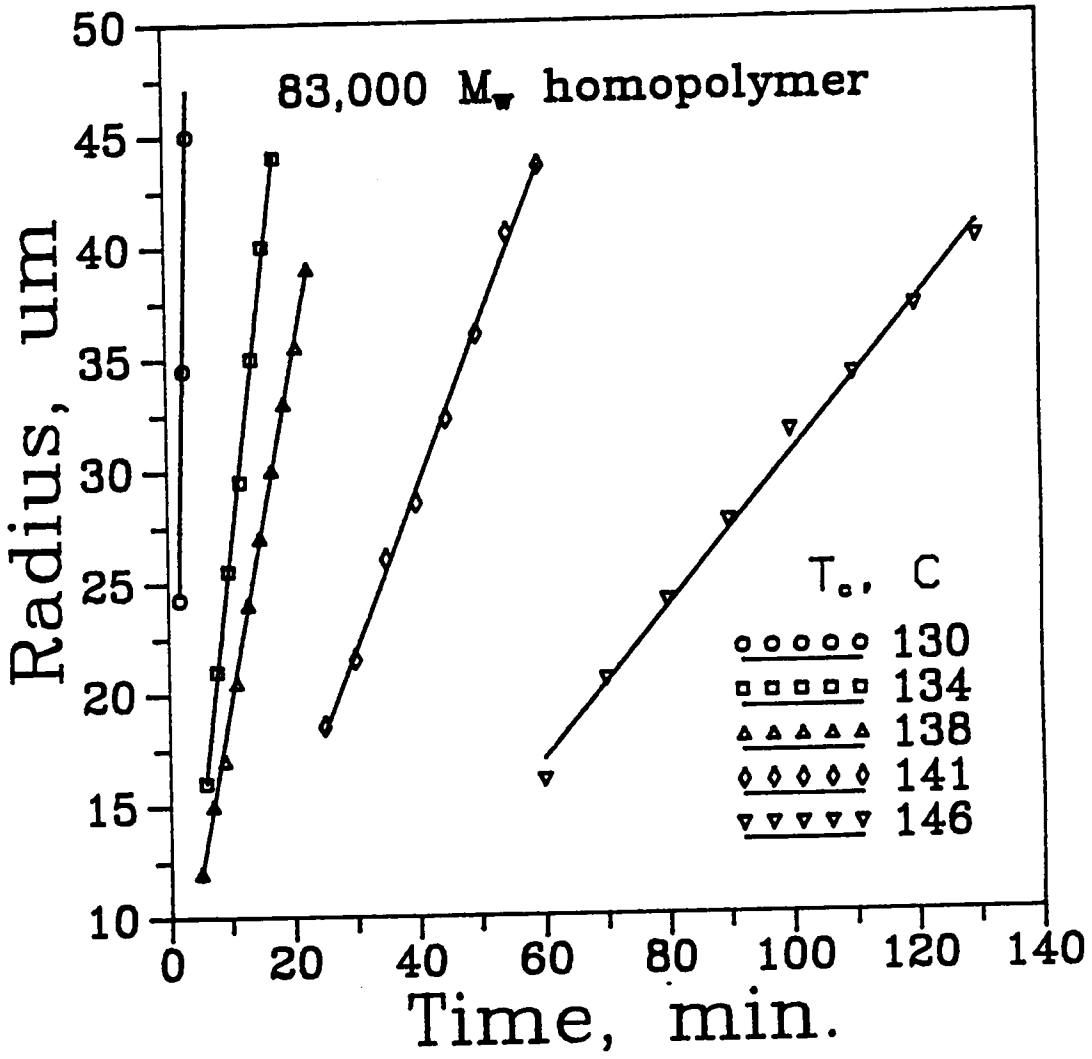


Figure 4.55 Linear growth rate determination from radius versus time at several crystallization temperatures for isotactic polypropylene homopolymer, M_w = 83,000 (atmospheric pressure).

Linear growth rate versus crystallization temperature plots for bulk polypropylene samples are shown in Figure 4.56. With the experimental technique used, growth rates below approximately 125°C were considered to occur nonisothermally and were rejected. While a Regime II - Regime III transition has been shown to occur in polypropylene at approximately 138°C ($\Delta T \approx 50°$), no abrupt change in the growth rate curve is observed. Also, for crystallization temperatures below approximately 150°C, spherulites are observed at all times. For $T_c > 150°C$, a mixture of sheaf-like entities and quadritic entities are observed, although both entities become spherulitic at long times.

In Figure 4.56 is shown the interesting growth rate behavior of the bulk polymer samples. For all samples, the growth rates for $T_c > 145°C$ are essentially the same regardless of specimen at constant temperature. However, below this temperature, the higher molecular weight homopolymer $M_w = 151,000$ has a slightly higher growth rate than the lower molecular weight homopolymer $M_w = 83,000$. Both homopolymers exhibit significantly higher growth rates than the 0.5% ethylene copolymer $M_w = 151,000$. While the homopolymers have similar molecular weight distributions ($M_w/M_n \approx 2.6$) and similar stereoregularities, it is possible that the sequence distributions are sufficiently different

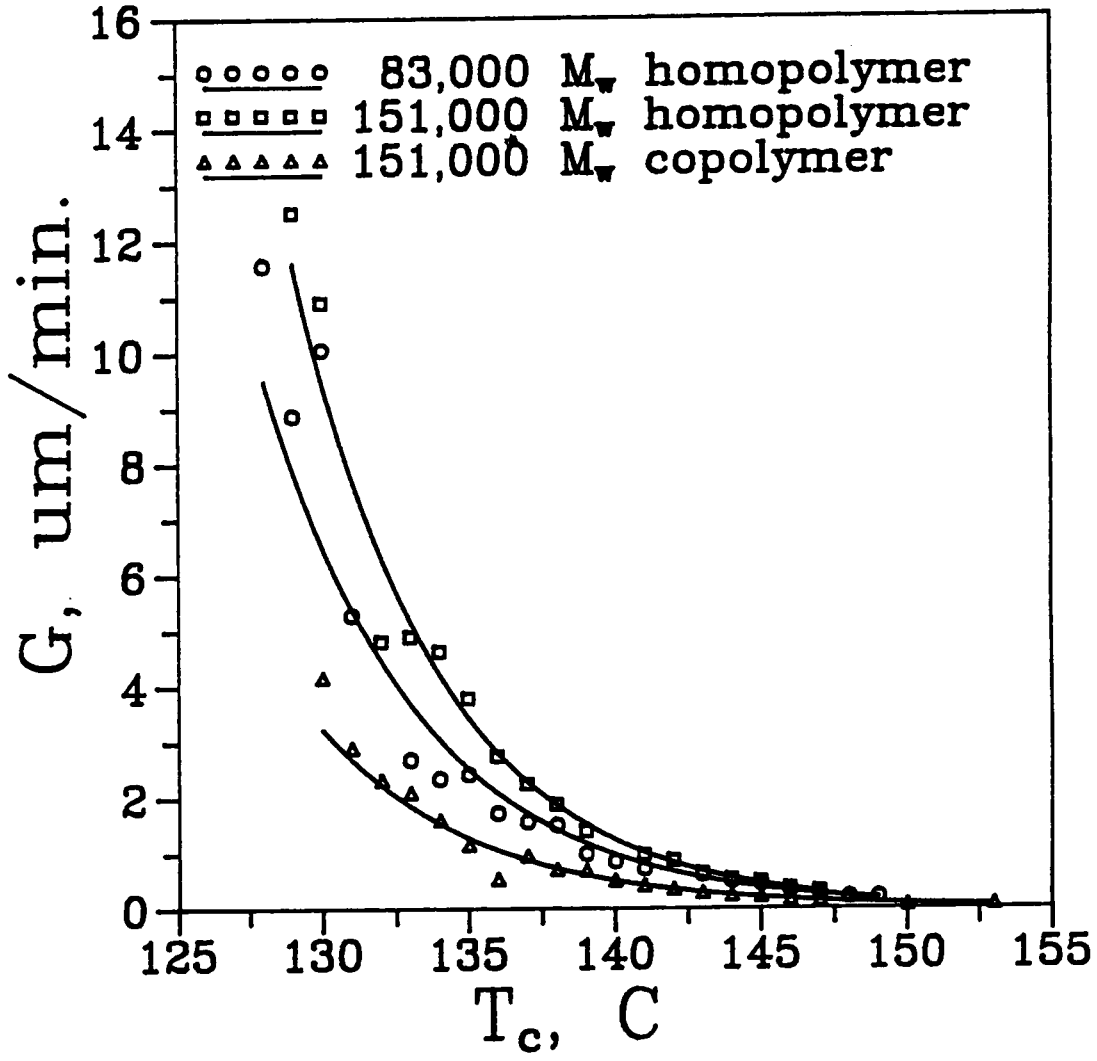


Figure 4.56 Linear growth rates as a function of crystallization temperature for isotactic polypropylene isothermally crystallized at atmospheric pressure.

differences in growth rates. For the observed differences for the copolymer, it is believed that the random incorporation of the ethylene unit sufficiently interrupts the crystallization process. While this disruption would occur at all crystallization temperatures, the crystallization process is slow enough at high crystallization temperatures such that the ethylene unit can be incorporated into the crystal. At low crystallization temperatures, the ethylene unit cannot be incorporated due to time constraints and is rejected, leading to lower growth rates. It is possible that the rejection/incorporation changes with comonomer content.

4.6.2 Induction Times

The induction time was determined from the bulk crystallization depolarized light intensity trace to be the time that the intensity deviated from the baseline intensity. This induction time was found to be a strong function of the isothermal crystallization temperature. Induction time was also somewhat dependent on the sample. Figure 4.57 shows the induction times for the atmospheric pressure crystallized samples as a function of supercooling ΔT. Induction times are relatively long for $\Delta T < 40°C$. It is seen that the high molecular weight homopolymer had the shorter induction times over a significant portion of the supercooling range studied. The induction times of the two homopolymers were comparable

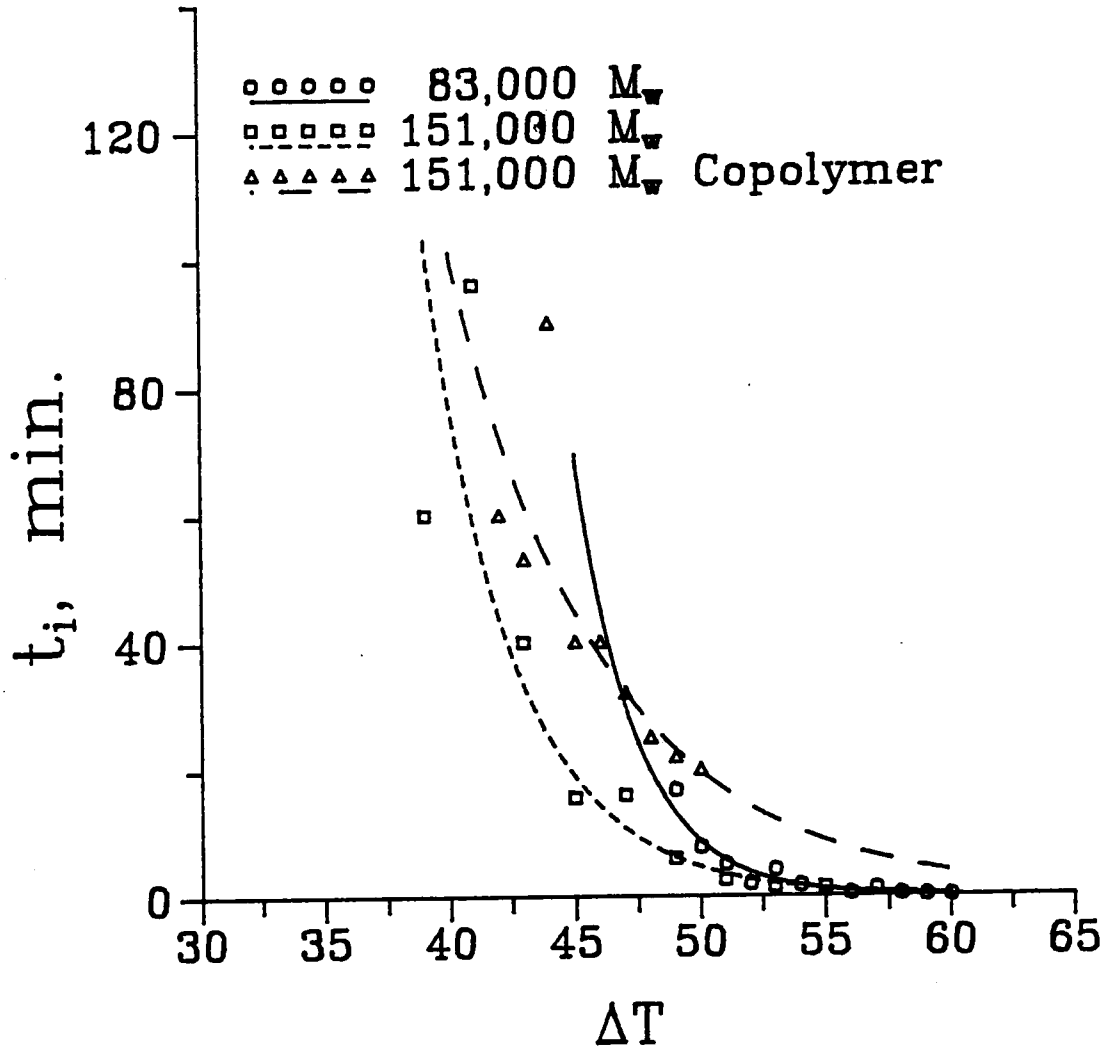


Figure 4.57 Induction times determined from depolarized light intensity (DLI) as a function of supercooling for isotactic polypropylene isothermally crystallized at atmospheric pressure.

for $\Delta T > \approx 50°$ and shorter than that of the copolymer in this range. However, the induction times of the low molecular weight homopolymer became greater than those of the copolymer at $\Delta T < \approx 46°$. It is expected that part of the explanation of the observed induction time behavior is the difference in the catalyst between the homopolymers and the copolymer, since catalyst residues may nucleate polypropylene.

4.6.3 Nucleation Densities

Nucleation densities were determined for atmospheric pressure crystallized samples as a function of isothermal crystallization temperature by counting the number of spherulites within the field of view of the optical micrographs made for linear growth measurements. Figure 4.58 shows the nucleation density versus crystallization temperature for the two homopolymers and the copolymer. The nucleation density decreases exponentially with increasing crystallization temperature. Of the three samples, the 151,000 M_w, homopolymer has the highest nucleation density at all observed crystallizatin temperatures, while the 151,000 M_w ethylene copolymer has the lowest nucleation density. Some differences between the nucleation densities of the samples may be attributed to differences in the catalyst systems used to produce the materials [110]. Also, the reduction in nucleation density for the copolymer relative to

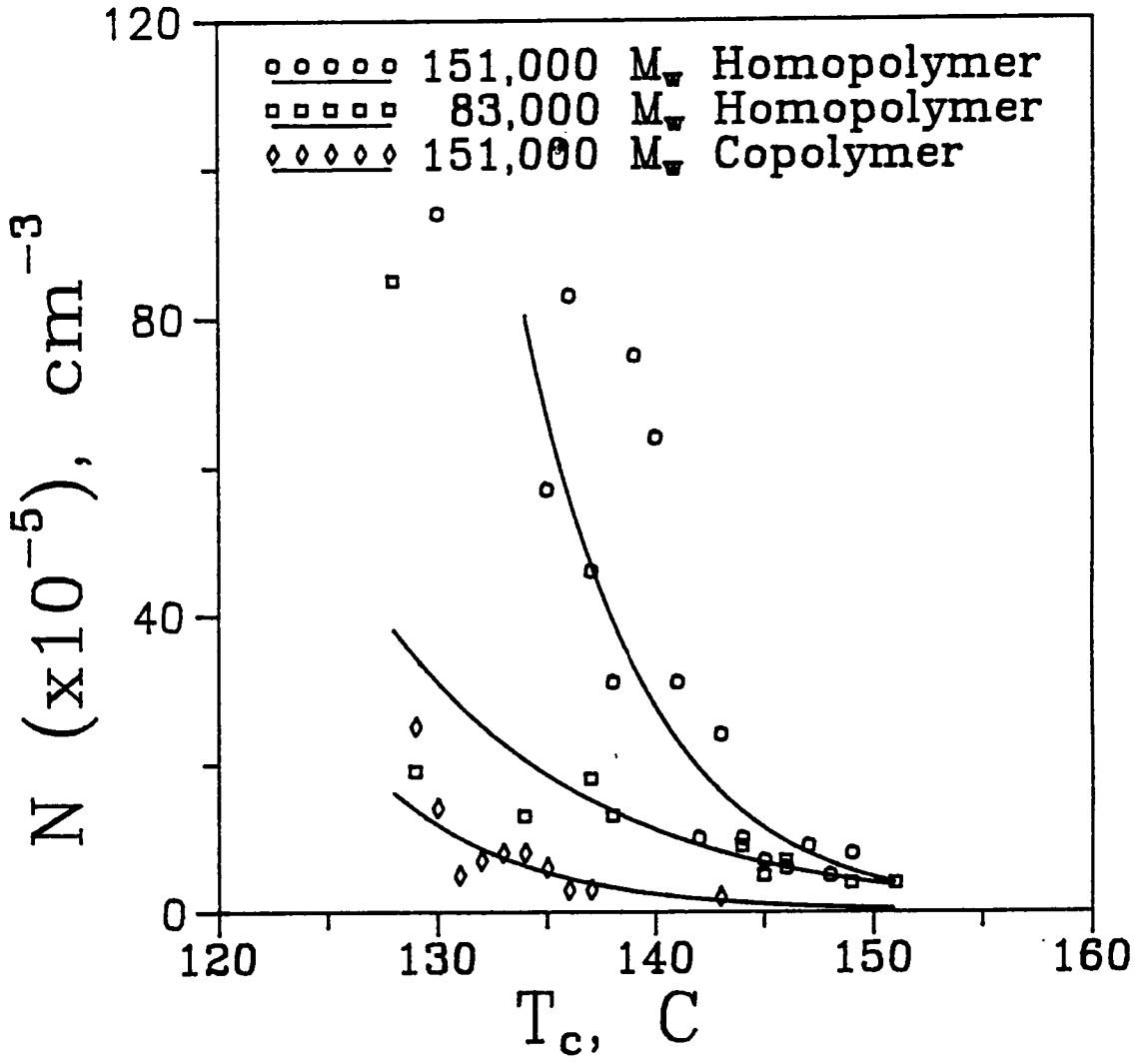


Figure 4.58 Nucleation density N versus crystallization temperature T_c for isotactic polypropylene crystallized at atmospheric pressure.

the homopolymers may be partly due to the presence of the ethylene units which do not act as nucleation points.

4.7 Crystallization - Elevated Pressure

4.7.1 Linear Growth Rates

The linear growth rates of isotactic polypropylene at various isothermal crystallization temperatures at elevated pressure were obtained in a similar manner to atmospheric pressure growth rates, using the equipment previously described. As with the atmospheric data, the spherulitic diameters were linear with time at all temperatures and all pressures considered. A typical plot of average spherulite size versus time of crystallization for several crystallization temperatures at a crystallization pressure of 75 MPa is shown in Figure 4.59. Most of the diameter-time lines showed positive y-intercepts at time zero. Linear growth rates were determined using a least squares method.

Linear growth rates versus crystallization temperature plots for bulk polypropylene isothermally crystallized at various elevated pressures are shown in Figure 4.60 for atm., 25, 50, 75, 100, 150, and 200 MPa. Tseng showed a shift of the growth rate curve to higher temperatures with increasing pressure for linear polyethylene [111]. This shift was fairly constant with pressure. Such behavior is not observed with polypropylene growth rates as a function of pressure.

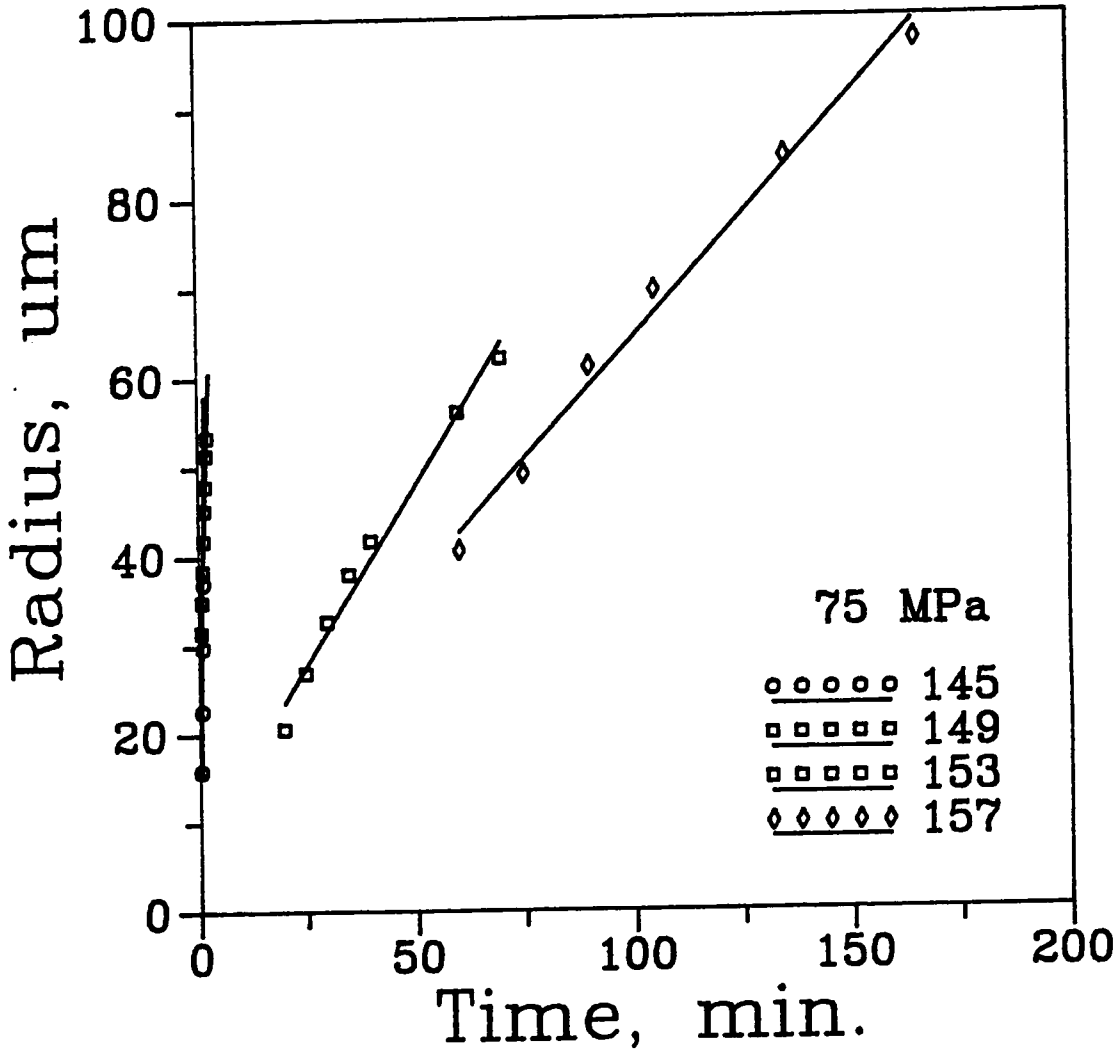


Figure 4.59 Linear growth rate determination from radius versus time at several crystallization temperatures for isotactic polypropylene 151,000 M_w homopolymer (P_c = 75 MPa).

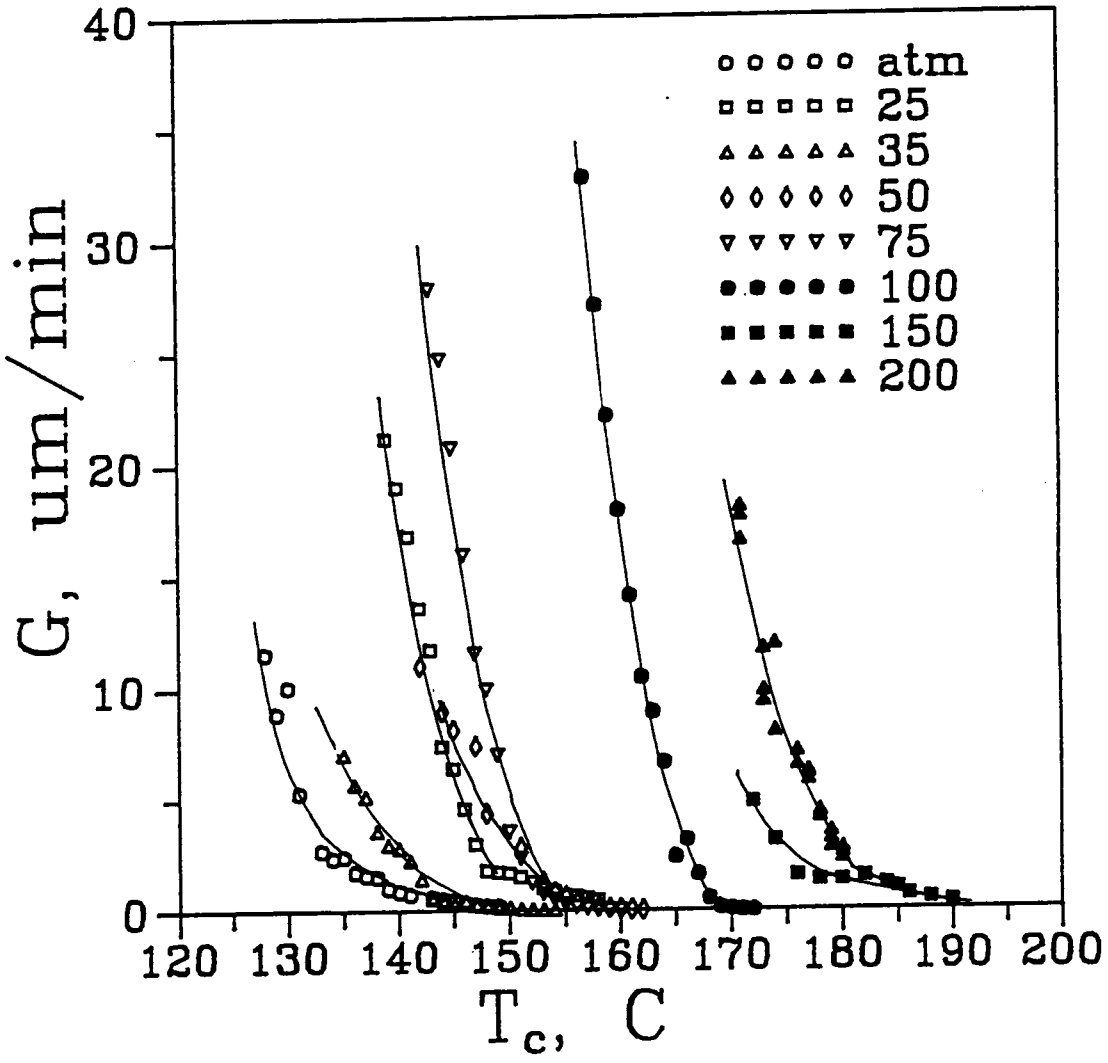


Figure 4.60 Linear growth rates as a function of crystallization temperature for isotactic polypropylene isothermally crystallized at atmospheric and elevated pressure.

On initial application of pressure to 25 MPa, the growth rate curve shifted approximately 12° to higher temperatures. However, with another 25 MPa pressure increase to 50 MPa, the growth rate curve shifted only slightly and the shape of the curve changed, particularly in the higher temperature region. Doubling the pressure from 50 MPa to 100 MPa again caused a significant shift in the growth rate curve (15°) to higher temperatures. The 150 MPa grow rate curve exhibits some unique behavior with respect to those of the other pressures. The data show a levelling off of the growth rate with increasing crystallization temperature, followed by a decrease at higher temperatures. The 200 MPa data and the 150 MPa data coincide at higher crystallization temperatures. The growth rate curves become even steeper. This shifting of the growth rate curve with pressure does not seem to directly correlate with the shifting of the equilibrium melting temperature with pressure. For linear polyethylene, the growth rate curve does shift in correlation to the shift in the equilibrium melting temperatures with pressure.

4.7.2 Induction Times

The induction times for elevated pressure crystallization were determined in the same manner as those for atmospheric pressure crystallization. Figure 4.61 shows the induction times for 25, 50, and 100 MPa as a function of supercooling

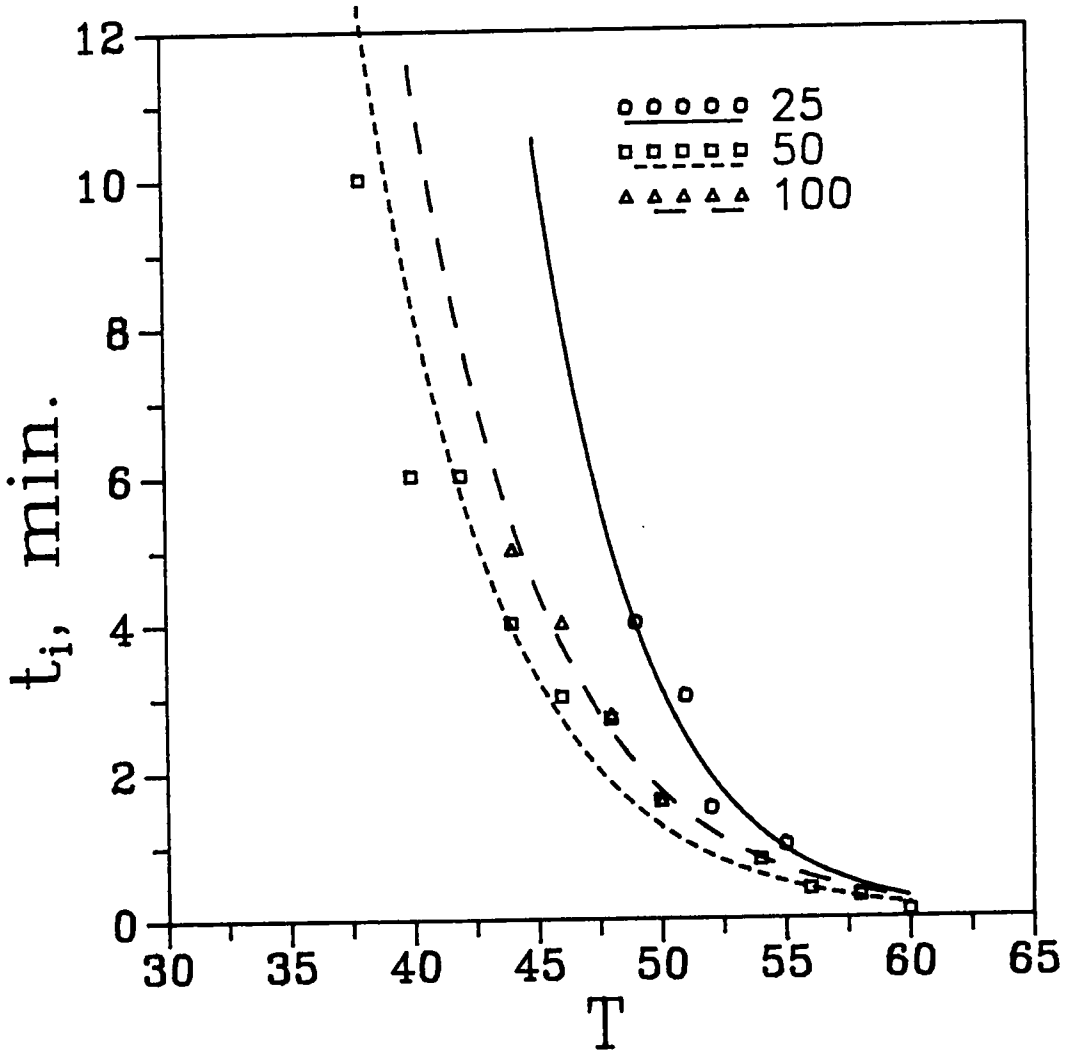


Figure 4.61 Induction times determined from DLI as a function of supercooling for isotactic polypropylene isothermally crystallized at elevated pressure.

ΔT. It is seen that the induction times for 25 MPa are longer than those for 50 or 100 MPa. The induction times for 50 and 100 MPa were similar. Over the same supercooling range, the induction times for the elevated pressure crystallized samples were significantly shorter than those for atmospheric pressure crystallized samples. Figure 4.62 shows the induction time comparison for atmospheric pressure crystallization and elevated pressure crystallization.

4.7.3 Nucleation Densities

Nucleation densities for the elevated pressure crystallized samples were determined in the same manner as those for the atmospheric pressure crystallized samples. Figure 4.63 shows the nucleation density versus crystallization temperature as a function of crystallization pressure from atmospheric pressure to 200 MPa. In all cases, the nucleation density decreases exponentially with increasing crystallization temperature. It was observed that the nucleation densities were similar at all pressures. The shift of the nucleation density curve to higher temperatures with increasing pressure follows the shift in melting temperature with increasing pressure. However, the curves did not overlap at fixed supercooling. At a fixed crystallization temperature, the nucleation density increased with increasing crystallization pressure. This type of behavior has been previously reported for poly(ethylene

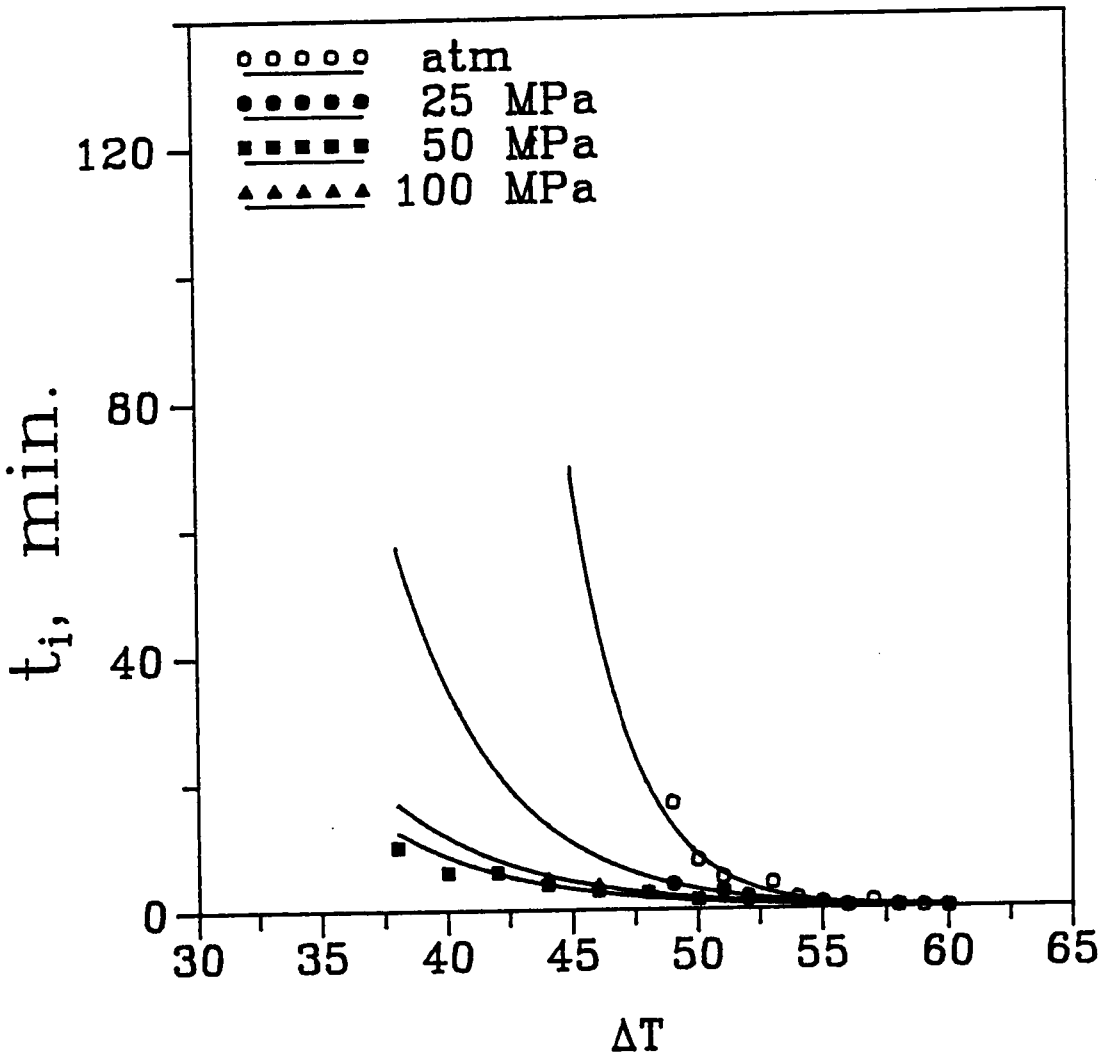


Figure 4.62 Induction times determined from DLI as a function of supercooling for isotactic polypropylene isothermally crystallized at atmospheric and elevated pressure.

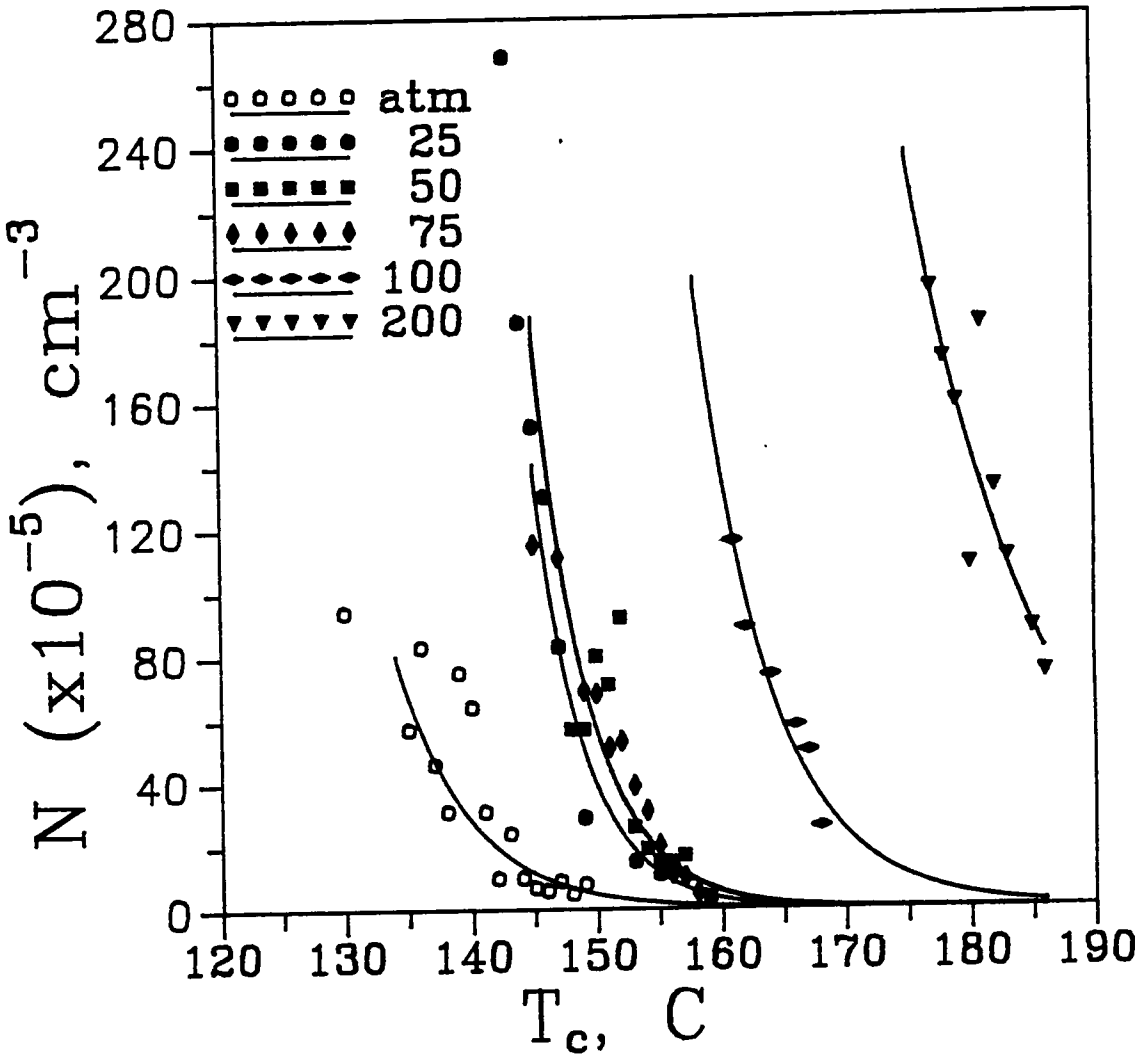


Figure 4.63 Nucleation density N versus crystallization temperature T_c for isotactic polypropylene crystallized at atmospheric and elevated pressure.

terphthalate) [2]. Nucleation densities for isotactic polypropylene crystallized at elevated pressure have been reported [112]. It was observed that the nucleation density at a fixed crystallization pressure was a function of the melt temperature and the time of melting for a sample crystallized at 380 MPa.

Chapter 5

Discussion

5.1 Crystallinity

In order to determine the lamellar thickness of a sample from SAXS based on a simple two-phase model, one must determine the crystallinity of the sample. Crystallinity was determined from WAXD scans using Ruland's method in the 2Θ range 5° to 45° [113]. For the 151,000 M_w homopolymer the crystallinity ranged from 0.53 to 0.72 while for the 151,000 M_w copolymer, the crystallinity ranged from 0.60 to 0.77. The crystallinities increase with increasing crystallization temperature (decreasing supercooling). Figure 5.1 shows the change in crystallinity with crystallization temperature for the 151,000 M_w homopolymer and copolymer. Janimak [48] has recently shown that for a series of polypropylenes of varying tacticities, the X-ray crystallinity exhibits approximately an exponential dependence with isotacticity at constant supercooling. The behavior of the copolymer does not seem to reflect the expected behavior of a homopolymer with comparable tacticity defects, since the crystallinities of the homopolymer and the copolymer are essentially the same. At some crystallization temperatures, the copolymer exhibits higher levels of crystallinity than the homopolymer.

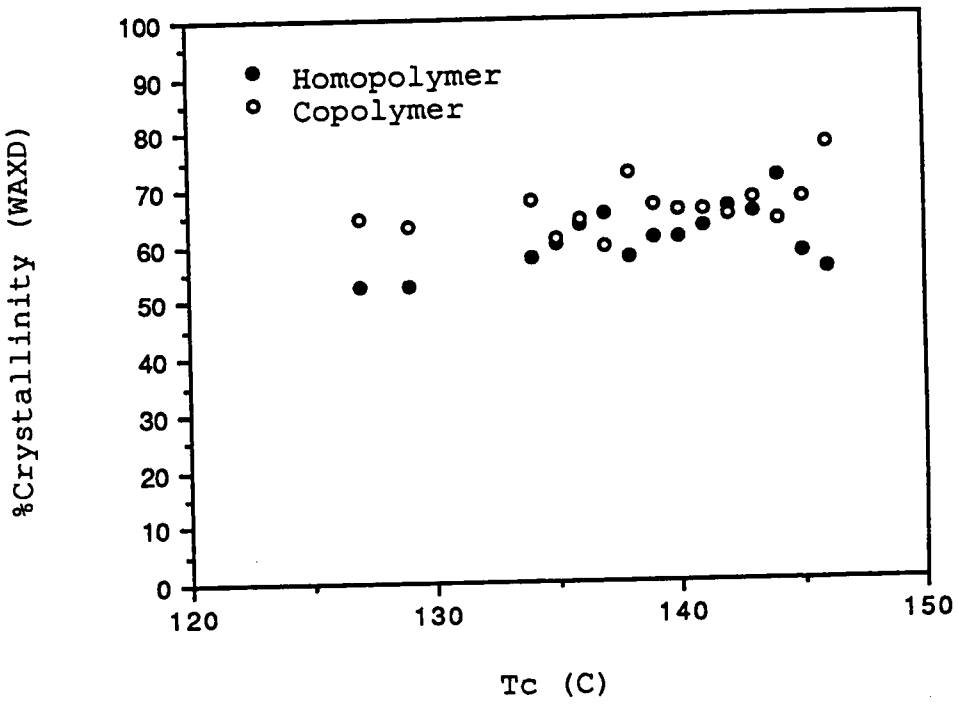


Figure 5.1 Crystallization temperature T_c versus % crystallinity from WAXD for isotactic polypropylene 151,000 M_w isothermally crystallized at atmospheric pressure.

5.2 Small Angle X-ray Scattering

One can use the data obtained from SAXS to evaluate the lamellar thickness, fold surface free energy, and the equilibrium melting temperature. The SAXS data gives an independent measure of T_m^o and σ_e to compare with the values determined from T_m versus T_c (T_m^o) and kinetics (σ_e). The lamellar thickness of polyethylene has been shown to increase with pressure. This increase in lamellar thickness would result in a more stable crystal, since the fold surface (high energy surface) is reduced relative to the volume of the crystal. However, this is not observed with isotactic polypropylene. Instead, the lamellar thickness decreased with pressure. This thinning is explained by observing that the lamellar thickness of the γ form, employing the orthorhombic unit cell, will be nearly 50% thinner than that of the α form at the same stem length since the chain stems in the γ polypropylene form an angle of $\approx 80°$ with respect to alternating layers and an angle of $\approx 40°$ with respect to the lamellar surface. Thus, the observed thinning with pressure supports the proposed orthorhombic unit cell, assuming fixed stem length at a given supercooling .

5.2.1 Atmospheric Pressure - $f(T_c)$

The long period measured from SAXS can be interpreted in simplest terms assuming a two phase model. Then the crystalline (lamellar) thickness, l_c, is given by:

$$l_c = \chi_c(L)$$

where χ_c = crystallinity and L = long period from SAXS. The amorphous thickness, l_a, is then determined by:

$$l_a = L - l_c$$

The experimental data were interpreted using the crystallinity determined from WAXD. Tables 5.1 and 5.2 give the crystalline and amorphous thicknesses for the 151,000 M_w homopolymer and copolymer isothermally crystallized at atmospheric pressure. In general, the lamellar thickness increased with increasing crystallization temperature. Figure 5.2 shows a plot of lamellar thickness from Lorentz corrected data versus crystallization temperature for the homopolymer and copolymer. At constant crystallization temperature, the long period from the q-I data were essentially the same for the homopolymer and copolymer. The long periods from the $q-q^2I$ data were also the same for the homopolymer and copolymer. However, the lamellar thicknesses of the copolymer were slightly larger than those of the homopolymer. Janimak [48] reported a decrease in lamellar thickness with decreasing tacticity for isotactic polypropylene at fixed supercooling. However, at a fixed

Table 5.1 SAXS Data for Isotactic Polypropylene Homopolymer Mw = 151,000 isothermally crystallized at atmospheric pressure.

	Observed I		Lorentz Corr.				
T_c (°C)	Q (nm^{-1})	L (Å)	Q (nm^{-1})	L (Å)	D[a]	H[b]	I_o[c]
127	0.289	217	0.342	184	1.409	0.535	10.1
129	0.277	226	0.328	192	1.335	0.546	11.0
134	0.253	248	0.316	198	1.306	0.598	12.3
136	0.263	238	0.300	210	1.447	0.839	13.5
137	0.263	238	0.300	210	3.236	0.550	6.6
138	0.253	248	0.303	208	1.549	0.532	7.4
139	0.245	256	0.300	210	2.474	0.644	6.2
140	0.253	248	0.277	226	1.183	0.598	25.4
141	0.245	256	0.281	224	1.806	0.744	10.0
142	0.245	256	0.273	230	2.231	0.676	5.1
143	0.227	276	0.273	230	1.250	0.907	62.7
144	0.227	276	0.263	238	1.250	0.912	71.7
146	0.212	296	0.253	248	1.421	0.635	13.4
as mold	0.368	170	0.418	150	2.063	0.411	

Notes:

a $D = D_{max}/D_{min}$ from Observed Intensity where D_{max} is the value of the scattering vector, Q, at maximum intensity and D_{min} is the value of the scattering vector at minimum intensity.

b $H = H_{min}/H_{max}$ from Observed Intensity where H_{min} is the value of the minimum intensity and H_{max} is the value of the maximum intensity.

c I_o = near zero angle scattering intensity

Table 5.2 SAXS Data for Isotactic Polypropylene Copolymer M_w = 151,000 isothermally crystallized at atmospheric pressure.

	Observed I		Lorentz Corr.				
T_c (°C)	Q (nm^{-1})	L (Å)	Q (nm^{-1})	L (Å)	D[a]	H[b]	I_o[c]
127	0.303	104	0.368	170	1.413	0.499	8.1
129	0.277	113	0.356	184	1.350	0.485	9.8
134	0.252	124	0.316	198	1.318	0.532	11.5
135	0.245	128	0.328	192	1.418	0.853	15.3
136	0.245	128	0.300	210	1.283	0.911	26.2
137	0.245	128	0.300	210	3.016	0.756	6.2
138	0.253	124	0.289	218	1.370	0.532	10.5
139	0.227	138	0.300	210	1.314	0.970	47.4
140	0.212	148	0.277	226	1.110	0.714	42.9
141	0.245	128	0.281	224	1.283	0.916	70.2
142	0.191	165	0.290	218			96.4
143	0.227	138	0.263	238	1.314	0.936	69.2
144	0.227	138	0.263	238	1.769	0.754	9.6
145	0.210	150	0.245	256	1.173	0.714	115.3

Notes:

a $D = D_{max}/D_{min}$ from Observed Intensity where D_{max} is the value of the scattering vector, Q, at maximum intensity and D_{min} is the value of the scattering vector at minimum intensity.

b $H = H_{min}/H_{max}$ from Observed Intensity where H_{min} is the value of the minimum intensity and H_{max} is the value of the maximum intensity.

c I_o = near zero angle scattering intensity

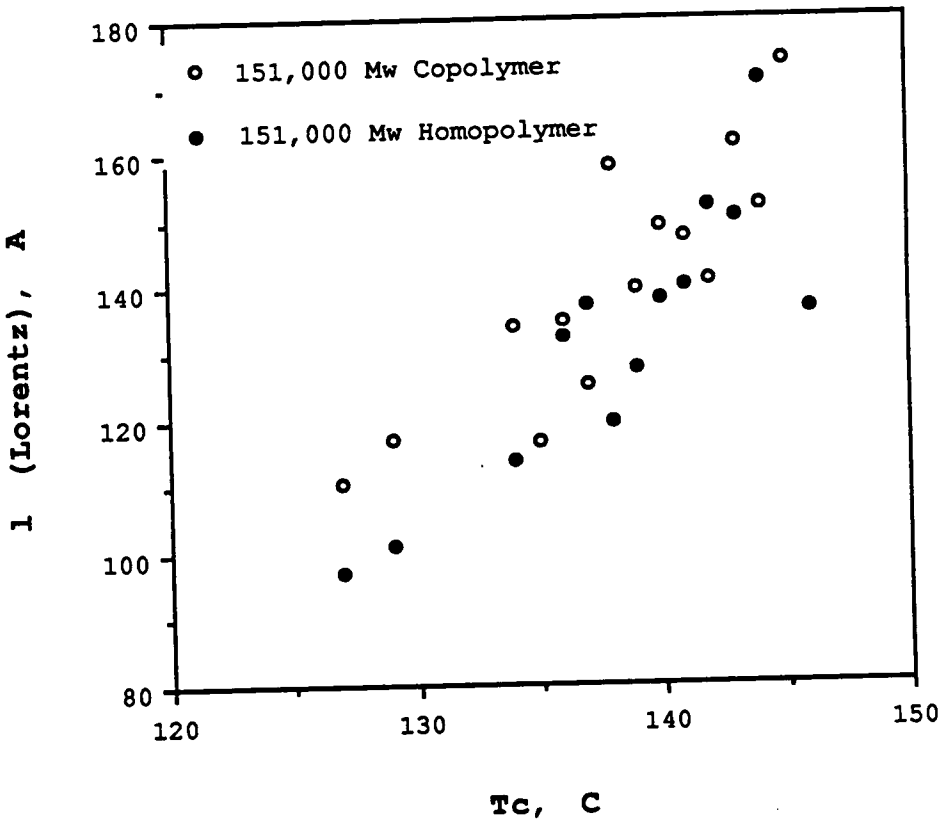


Figure 5.2 Crystallization temperature T_c versus lamellar thickness from SAXS q-I data for isotactic polypropylene 151,000 M_w homopolymer and copolymer isothermally crystallized at atmospheric pressure.

crystallization temperature, the lamellar thickness increased with decreasing isotacticity. Janimak concluded that the inclusion of configurational defects into the crystal must have occurred.

5.2.2 SAXS D, H Values

The observed intensity profile from small angle X-ray scattering is useful in interpreting changes such as the variance in thickness and crystallinity in the lamellar structure of a polymer. The characteristic parameters D, the distance ratio, and H, the height ratio, for the observed intensity profile are defined in Figure 5.3. Tables 5.1 and 5.2 include the D and H parameters for the homopolymer and copolymer, respectively, as a function of crystallization temperature. Figure 5.4 shows the H parameter versus the crystallization temperature T_c for the 151,000 M_w homopolymer and copolymer. There is a general trend to increasing H with increasing T_c, although there is significant scatter in the data. For the homopolymer crystallized below ≈142°C, there is a nearly linear increase in H with increasing crystalization temperature. While the D and H parameters do not change in a simple way with crystallinity distribution or lamellar thickness distribution, some observations from extensive modeling of SAXS behavior can be made. It has been seen that, for H values below ≈0.8, there is a linear relation between H and the apparent long period L_{app}. Above H

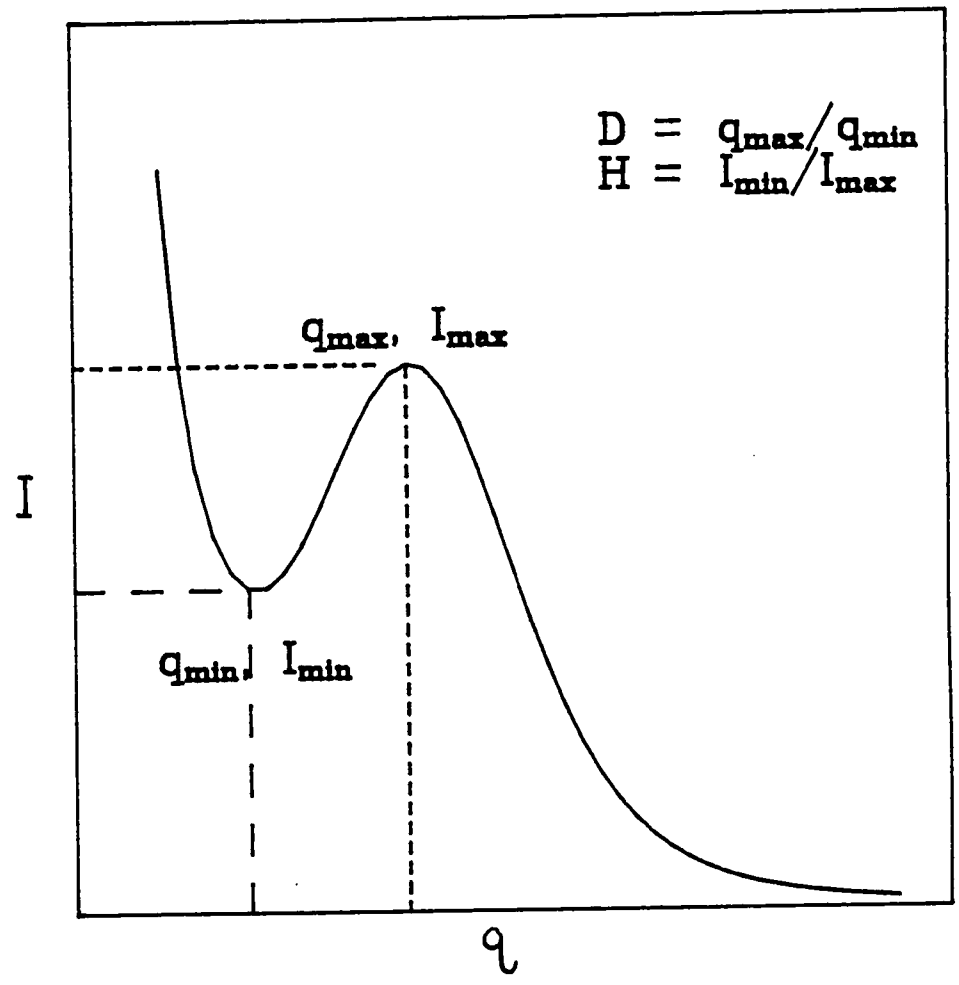


Figure 5.3 Definition of SAXS characteristic parameters D and H.

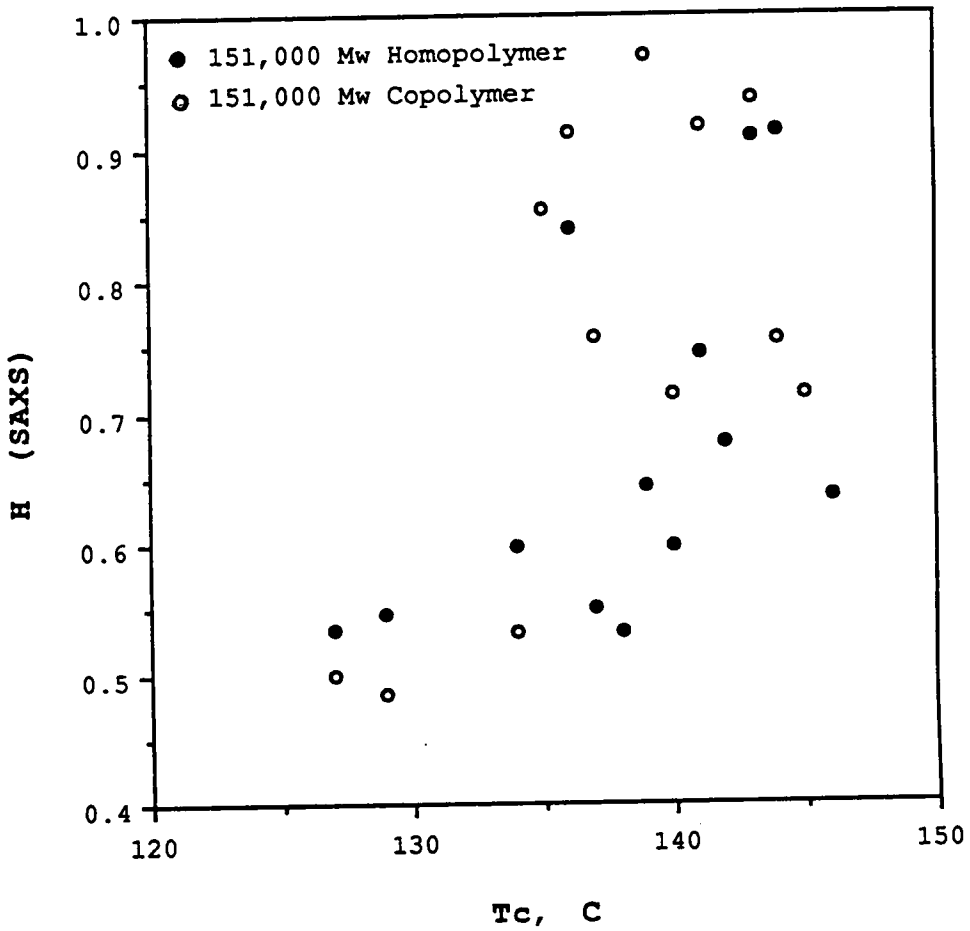


Figure 5.4 Crystallization temperature T_c versus SAXS H for isotactic polypropylene 151,000 M_w homopolymer and copolymer isothermally crystallized at atmospheric pressure.

= 0.8, the correlation between H and L_{app} breaks down. This observation applied to a range of crystallinity distributions and lamellar thickness distributions. This implies that the SAXS observed long period L is increased over the theoretical value due to the effect of the distributions. Figure 5.5 shows the observed SAXS H versus the observed long period for the isothermally crystallized 151,000 M_w homopolymer and copolymer. It is seen that the observed long period for the homopolymer and the H value correlate relatively well up to a long period of ≈130 Å. In applying the results of the SAXS modeling, the observed long period should be reduced by 4 to 8%, depending on the H value, to account for apparent increases from distributions of crystallinity and thickness.

Figure 5.6 shows the D value versus the crystallizatin temperature for the 151,000 M_w homopolymer and copolymer. Both homopolymer and copolymer data exhibit some correlation of D and T_c. The copolymer D is relatively unaffected by changing crystallization temperature, while the homopolymer shows an increase in D with increasing T_c to ≈142°C. From SAXS modeling, the distance ratio D is observed to decrease with increasing thickness vairance σ_x for a given value of crystallinity variance σ_c. The observed trends of the D and H parameters for the SAXS data indicate a change in lamellar structure as a function of crystallization temperature. With increasing crystallization temperature, the lamellar

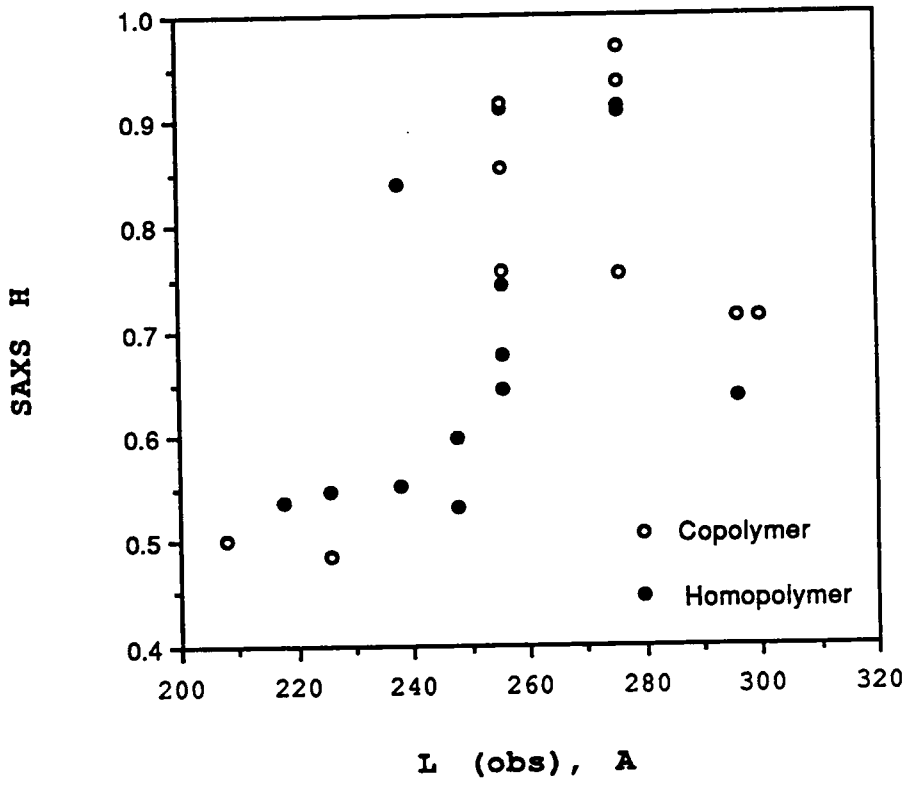


Figure 5.5 SAXS long period from q-I data versus SAXS H for isotactic polypropylene 151,000 M_w homopolymer and copolymer isothermally crystallized at atmospheric pressure.

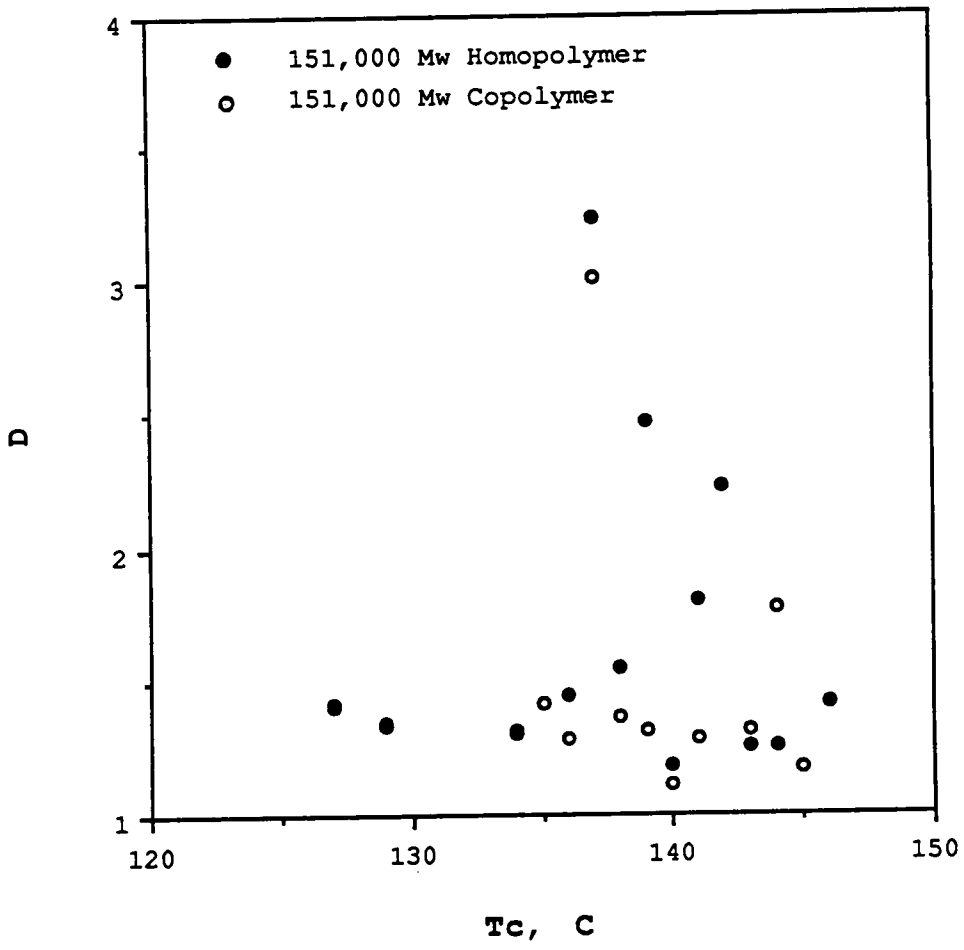


Figure 5.6 Crystallization temperature T_c versus SAXS D for isotactic polypropylene 151,000 M_w homopolymer and copolymer isothermally crystallized at atmospheric pressure.

thickness distribution increases. This is expected, partly due to the branching nature of isotactic polypropylene. It has been shown that on increasing the crystallization temperature for isotactic polypropylene, the relative amount of tangential lamellae decreases and the difference in thickness between radial and tangential lamellae increases. Also, at the higher crystallization temperatures, there is a more significant difference in the material isothermally crystallized and that crystallized on cooling the sample to room temperature.

5.2.3 Elevated Pressure

The long periods observed for the elevated pressure crystallized samples exhibited a decrease with increasing pressure. Table 5.3 gives the SAXS data as a function of crystallization pressure for polypropylene crystallized at a fixed supercooling $\Delta T = 50°C$ and various elevated pressures. As shown in the Results section, the nature of the SAXS for the elevated pressure crystallized samples changes from that of the atmospheric pressure crystallized samples. In particular, the intensity of the scattering decreased with pressure, and the breadth of the scattering curve increased with pressure. The change in intensity with pressure is partly a result in changes in the electron density contrast (the electron density of the amorphous phase versus that of the crystalline phase). The electron density of the

Table 5.3 SAXS Data for Isotactic Polypropylene Homopolymer M_w = 151,000 isothermally crystallized at various elevated pressures, ΔT = 50°C.

	Observed I		Lorentz Corr.				
P_c (MPa)	Q (nm^{-1})	L (Å)	Q (nm^{-1})	L (Å)	D[a]	H[b]	Io[c]
atm	0.263	238	0.300	210	1.447	0.839	13.5
25	0.342	184	0.385	164	2.200	0.500	11.3
50	0.342	184	0.385	160	1.780	0.630	11.0
75	0.360	174	0.425	148	2.290	0.642	17.3
100	0.385	164	0.496	126	2.010	0.640	7.9
125	0.427	148	0.500	124	2.349	0.635	4.5
175	0.473	132	0.555	114	2.370	0.520	4.0
200	0.480	130	0.572	110	2.00	0.48	17.2

Notes:

a $D = D_{max}/D_{min}$ from Observed Intensity where D_{max} is the value of the scattering vector, Q, at maximum intensity and D_{min} is the value of the scattering vector at minimum intensity.

b $H = H_{min}/H_{max}$ from Observed Intensity where H_{min} is the value of the minimum intensity and H_{max} is the value of the maximum intensity.

c I_o = near zero angle scattering intensity

crystalline region of the γ form of polypropylene will be different than that of the α form of polypropylene while the electron density of the amorphous regions of the alpha and gamma forms should be equal. Thus the differences in electron density of the crystalline regions of the two forms will result in a change in the electron density contrast and thus a change in intensity from the α to the γ form. The proposed orthorhombic unit cell of γ polypropylene with the unique arrangement of chain stems would result in such a difference in the electron density of the crystalline phase.

The effect of pressure on the lamellar thickness of elevated pressure crystallized polymers has not been extensively studied. Polyethylene is known to thicken with increasing pressure [114]. The extended chain conformation can be formed with pressures above 350 MPa. If the α and γ forms of polypropylene are crystallized at constant stem length, the γ lamellae would be thinner by approximately 50% since the chain stems in γ polypropylene form an angle of 40° with the lamellar surface and the chain stems in α polypropylene form an angle of 9° with the lamellar surface. This would result in a thinning of the observed lamellar thickness with increasing γ content. It is possible that two distributions of lamellae exist for the samples crystallized at pressures in the range that the α and γ forms coexist. The two distributions may have different thickness

distributions (average lamellar thickness and variance of thickness) and different crystallinities.

The significant reduction in lamellar thickness with increased crystallization pressure was explained on the basis of the α-γ composition and the arrangement of chain stems within the lamellae of the two crystal forms. The face centered orthorhombic unit cell proposed for the γ form will result in lamellae nearly 50% thinner than those of the α form at a fixed stem length. The elevated temperature SAXS supported the proposed orthorhombic unit cell since the lamellar thickness for elevated pressure crystallized material increased rapidly on heating, approaching that of the α lamellae. The elevated temperature SAXS showed that the material does not need to completely melt in order for the thickening to occcur. The elevated temperature WAXD also supported this observation. The DSC of elevated pressure crystallized material indicates some melting of the 100 MPa sample at 145°C, but not a sufficient amount of melting to account for the amount of γ material present in the sample initially. The elevated temperature WAXD also indicate that 145°C was sufficient temperature for the transformation of the γ to α in a relatively short period of time (<30 min.). The literature on γ polypropylene had attributed this transformation of γ to α to a solid-solid transition, based on the γ having a triclinic structure that was only a slight

distortion of the monoclinic structure. This would result in the chain stems of the lamellae only having to tilt slightly to form the monoclinic structure. However, a solid-solid transition of γ polypropylene with the proposed orthorhombic unit cell with chain stems tilted ≈80° to adjacent layers would be an extremely high energy transformation in the solid state. It is currently believed that the material does not undergo a complete melting during the observed transformation. Thus the γ material may convert to a either througn partial melting, an intermediate state, or some 'condis' state. Further investigation of this transformation of γ to α should yield some interesting information on the molecular interactions involved in the transformation

5.2.4 Distance Distribution, Correlation Function

The distance distribution function ρ(r), and the electron density correlation function, γ(r), were analyzed for the SAXS data in order to further interpret the structure of the lamellar system. From the distance distribution function, one can comment on the nature of the scattering system, whether it can be considered as a dilute or a concentrated system. One can also determine the root mean square radius of gyration, <r>, and the invariant, Q, for the system. The <r> can be compared to the long period, L, at least for the trends of <r> and L with changing crystallization conditions. From the electron density

correlation function, one can determine L and compare with $L_{(obs)}$ or $L_{(Lorentz)}$. One can also comment on changes in the nature of the electron density distribution. Figure 5.7 shows the distance distribution functions for the simple geometries of a sphere, rod, and disk. The distance distribution function for the sphere is nearly symmetric, with the peak maximum occurring at a distance equivalent to the sphere's radius. The disk's distance distribution function exhibits a parabolic shape, and the rod's distance distribution function is linear in shape after a distance equal to the diameter of the rod. Table 5.4 gives the results of the distance distribution function and the electron density correlation function analysis for the 151,000 M_w homopolymer crystallized at atmospheric pressure. Table 5.4 also gives the results for the copolymer. The long period determined from the electron density correlation function was about the same as the long period from either the observed q-I data or the Lorentz corrected $q-q^2I$ data. The $L_{(\gamma)}$ does increase with increasing crystallization temperature as do $L_{(obs)}$ and $L_{(LC)}$. Figure 5.8 shows the $\rho(r)$ for the 151,000 M_w homopolymer isothermally crystallized at T_c = 140°C. The function exhibits behavior consistent with a concentrated system in that a minimum occurs with negative values of the distance distribution. In the range of distances comparable to the $L_{(obs)}$ (248 Å), only one maximum

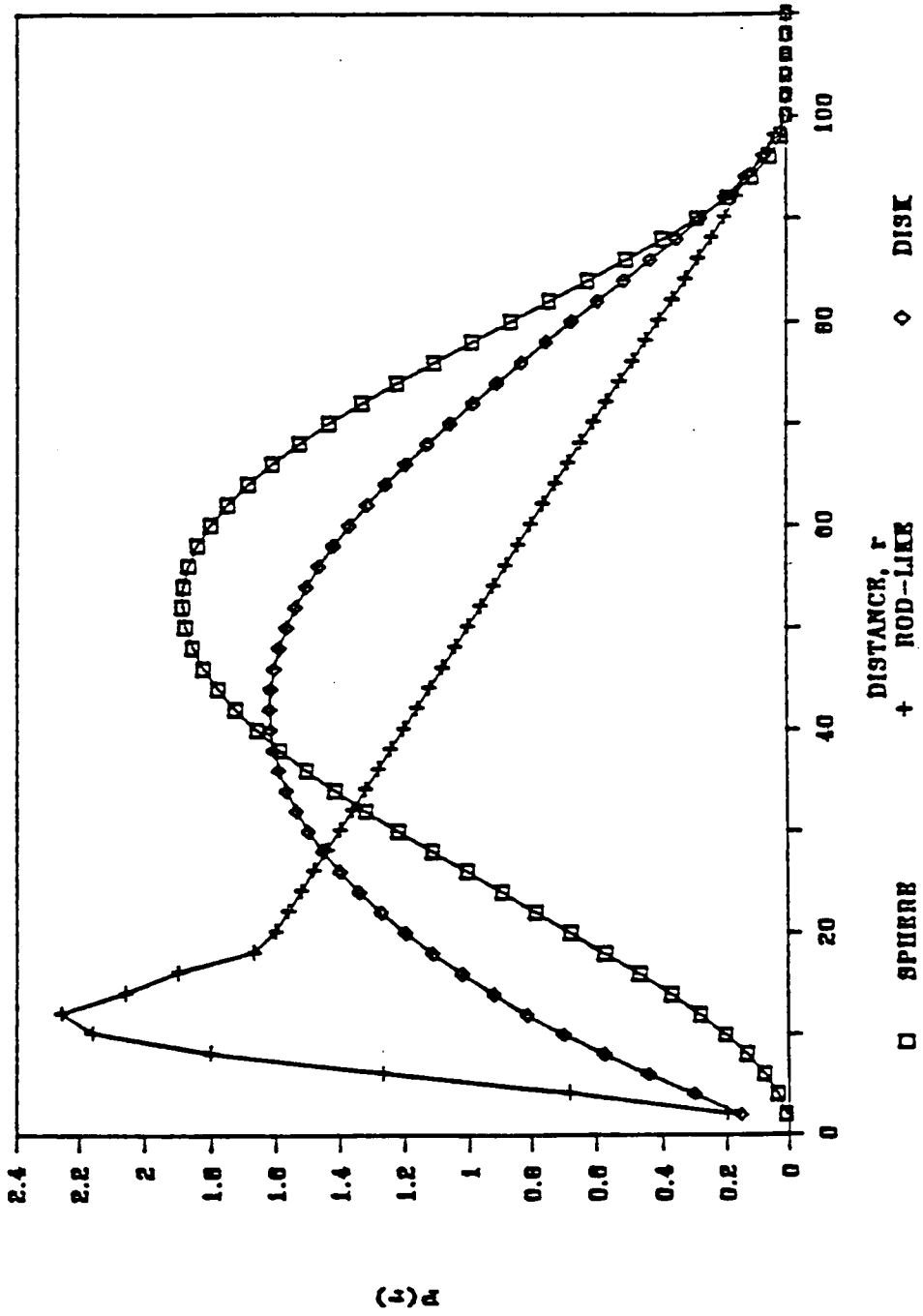


Figure 5.7 Theoretical electron density distribution for spheres, rods, and disks.

Table 5.4 Comparison of Long Periods Determined from SAXS Observed Intensity and Electron Density Correlation Function.

	L, Å (Bragg)				L, Å (γ)		R_g, Å	
	Homopolymer		Copolymer		Homo.	Co.	Homo.	Co.
T_c (°C)	LC	Obs	LC	Obs				
127	184	218	170	208	221	221	106	95
129	192	226	184	226	226	221	108	99
134	198	248	198	248	236	236	112	101
135			192	256		251		129
136	210	238	210	256	252	232	141	144
137	210	238	210	256	266	261	106	115
138	208	248	218	248	262	272	111	104
139	210	256	210	276	266	232	123	153
140	226	248	226	296	267	267	123	121
141	224	256	224	256	271	256	145	156
142	230	256	219	230	281		136	
143	230	276	238	276	256	256	159	158
144	238	276	238	276	261	286	160	139
145			256	300				161
146	248	298			303		112	

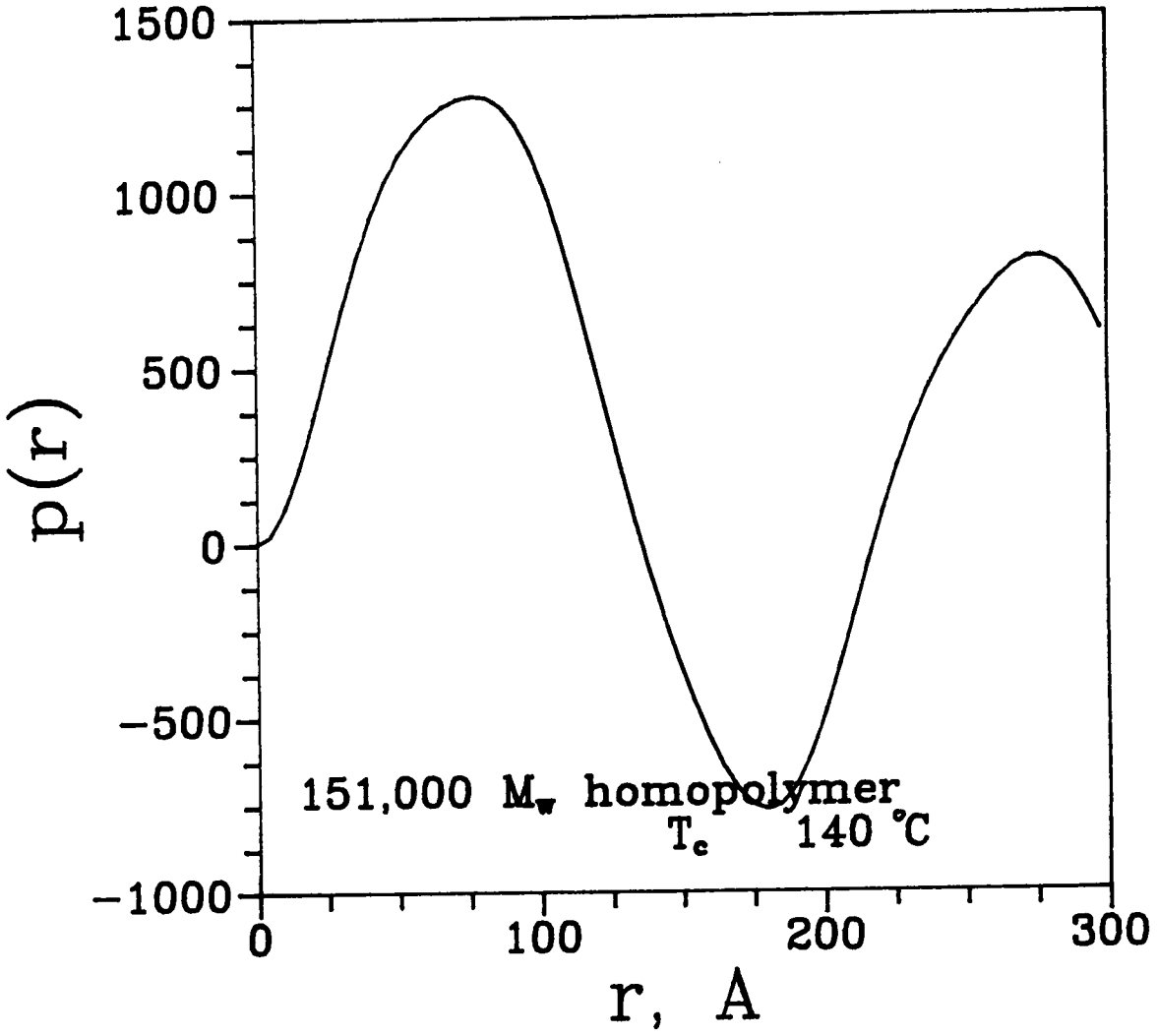


Figure 5.8 Electron density distribution for isotactic polypropylene isothermally crystallized (ΔT = 47°C, atmospheric pressure). SAXS intensity profile recorded at 25°C.

is observed corresponding to a distance of 152 Å. The <r> from the distance distribution function is 122 Å. The $\rho(r)$ of the other crystallization temperatures were similar in shape. The function dampens rapidly to zero in all $\rho(r)$ after the second maximum. The $\rho(r)$ for the copolymer were similar in shape to those of the homopolymer and the <r> showed the same trends. The variation in the values of <r> were larger than the variation in $L_{(obs)}$.

Figure 5.9 shows the electron density correlation function, $\gamma(r)$, for the 151,000 M_w homopolymer crystallized at T_c = 140°C and atmospheric pressure. The long period determined from the $\gamma(r)$ was 263 Å, which is only slightly larger than the long period from q-I data. The shape of the $\gamma(r)$ can give information on the electron density distribution, which then reveals information about the lamellar structure. The experimental curves were most comparable to a two-phase system with long period variation, lamellar thickness variation, and a diffuse phase boundary. The $\gamma(r)$ results were consistent with the literature results for other semicrystalline polymers [115]. Figure 5.10 shows the plot of the long period determined from the correlation function against those from the observed SAXS intensity profile. It is seen that there is a fairly linear relationship between the two measurements, with $\gamma(r)$ giving slightly higher values for the long period.

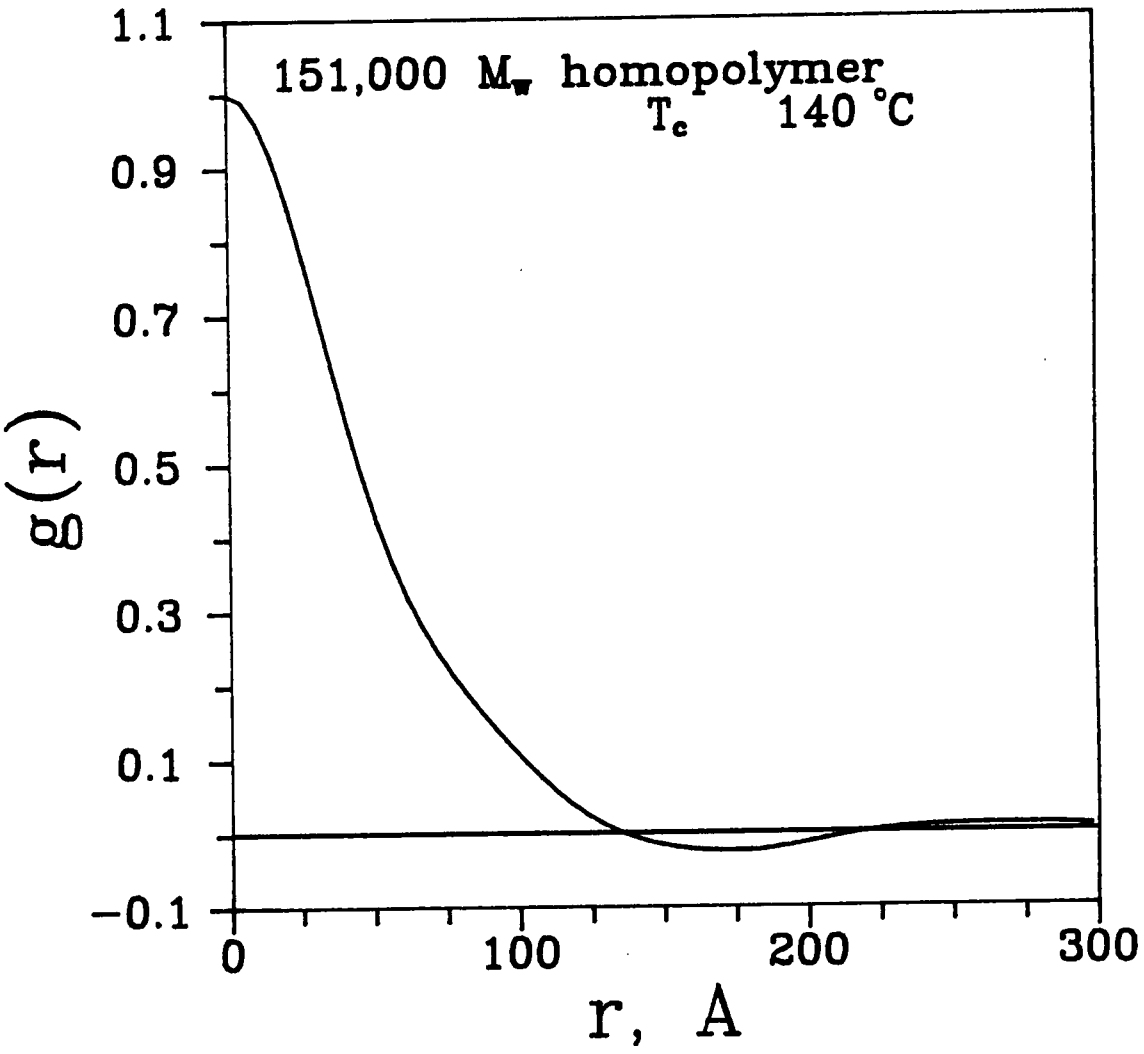


Figure 5.9 Electron density distribution correlation function for isotactic polypropylene isothermally crystallized (ΔT = 47°C, atmospheric pressure). SAXS intensity profile recorded at 25°C.

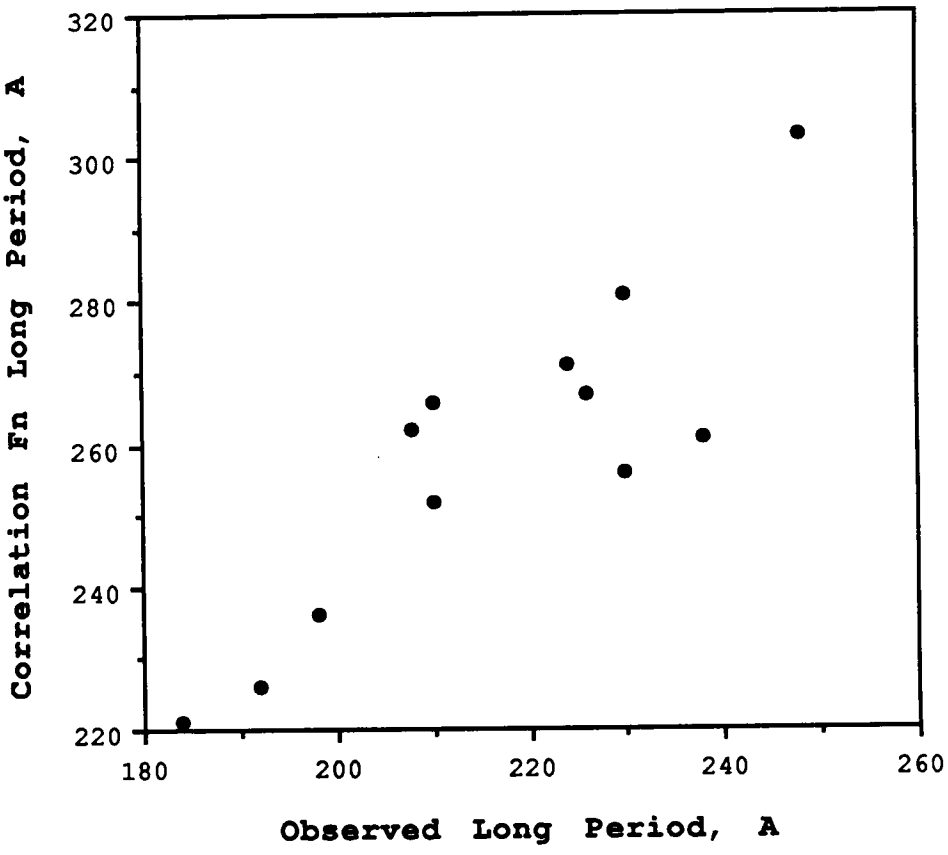


Figure 5.10 SAXS long period from observed intensity profile versus long period from SAXS electron density correlation function.

The distance distribution functions for the 151,000 M_w homopolymer (T_c = 129°C) as a function of in situ SAXS scan temperature are shown in Figure 5.11. The $\rho(r)$ for the 100°C and the 130°C data are only slightly different, as the material indicates only slight melting at 130°C in the DSC. The $\rho(r)$ for the 145°C scan, however, is significantly different than the $\rho(r)$'s for the lower temperatures. The DSC indicates a portion of material has melted on the low temperature shoulder of the peak. The WAXD indicated a decrease in the crystalline peak intensity and an increase in the amorphous scattering, indicating a decrease in the overall crystallinity of the sample. However, the $\rho(r)$ at 145°C exhibits a minimum with a negative frequency, indicating that the distance distribution curve is not based on the dilute system but has interference among the entities within the system. The electron density distribution correlation function, shown in Figure 5.12 for the electron density distributions of Figure 5.11, indicate a shifting of the long period to a higher value for the 145°C scan relative to the 100°C and the 130°C scans. This would correspond to a melting out of thinner, less perfect lamellae, resulting in a shift to higher long periods as well as a decrease in the variance of the lamellar thickness distribution. The in situ distance distributions of all the atmospheric pressure isothermally crystallized samples exhibited behavior

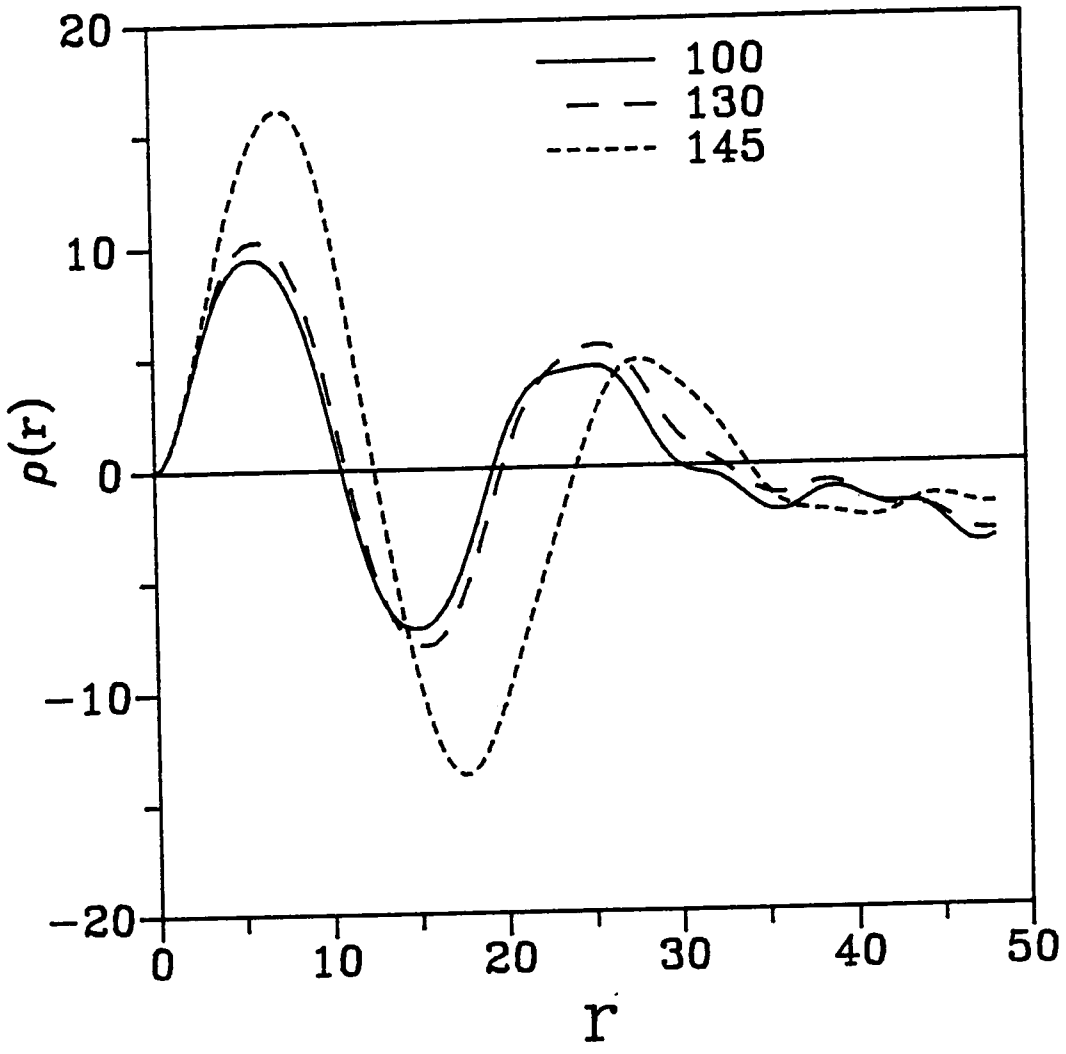


Figure 5.11 Electron density distribution for isotactic polypropylene isothermally crystallized (ΔT = 58°C, atmospheric pressure). SAXS intensity profiles recorded at temperature indicated (°C).

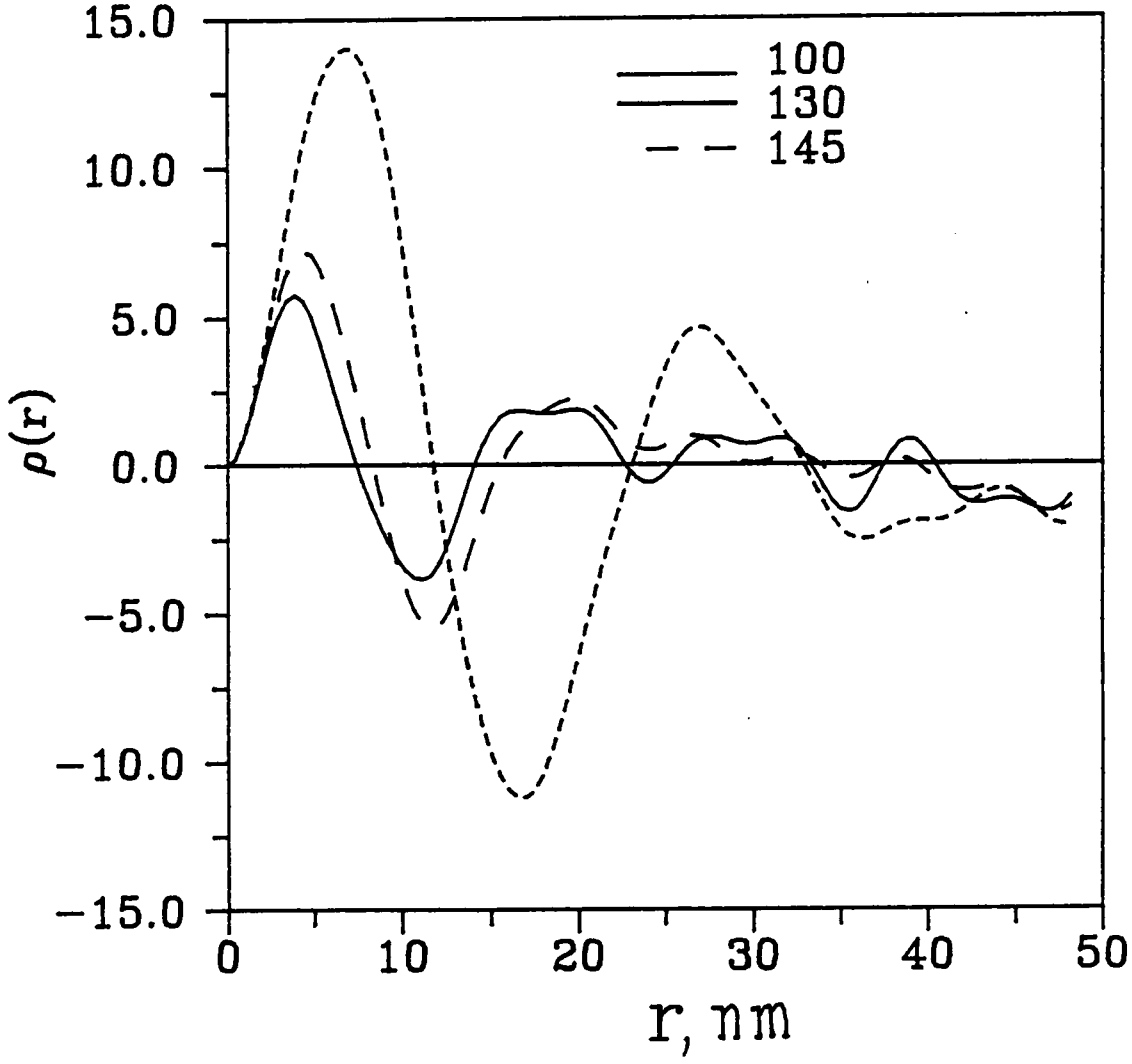


Figure 5.12 Electron density distribution correlation function for isotactic polypropylene isothermally crystallized (ΔT = 58°C, atmospheric pressure). SAXS intensity profiles recorded at temperatures indicated (°C).

characteristic of a dense lamellar scattering system, with no evidence of a dilute scattering system present at any temperature.

Figure 5.13 shows the representative behavior of the electron density distribution of the in situ SAXS for the elevated pressure crystallized data. As with the atmospheric pressure crystallized samples' in situ SAXS, the elevated pressure samples exhibited behavior characteristic of a dense lamellar scattering system. For the 100 MPa data, the density distribution function changes slightly from the 100°C scan to the 130°C scan but changes more significantly for the 145°C, indicating a significant change in the frequency of distance that can be placed within the same type of entities within the particle. The 145°C scan indicates a decrease in the lamellar thickness distribution since the electron density distribution is more periodic. The electron density distribution correlation function shows a significant increase in the long period, as observed in the original SAXS and the Lorentz corrected data.

5.2.5 Interpretation of SAXS behavior

It is desirable to interpret the observed small angle scattering behavior in terms of a model that is capable of explaining the broadening of a melt crystallized polymer's diffraction peak. A simple one-dimensional model is generally sufficient for explaining the observed diffraction

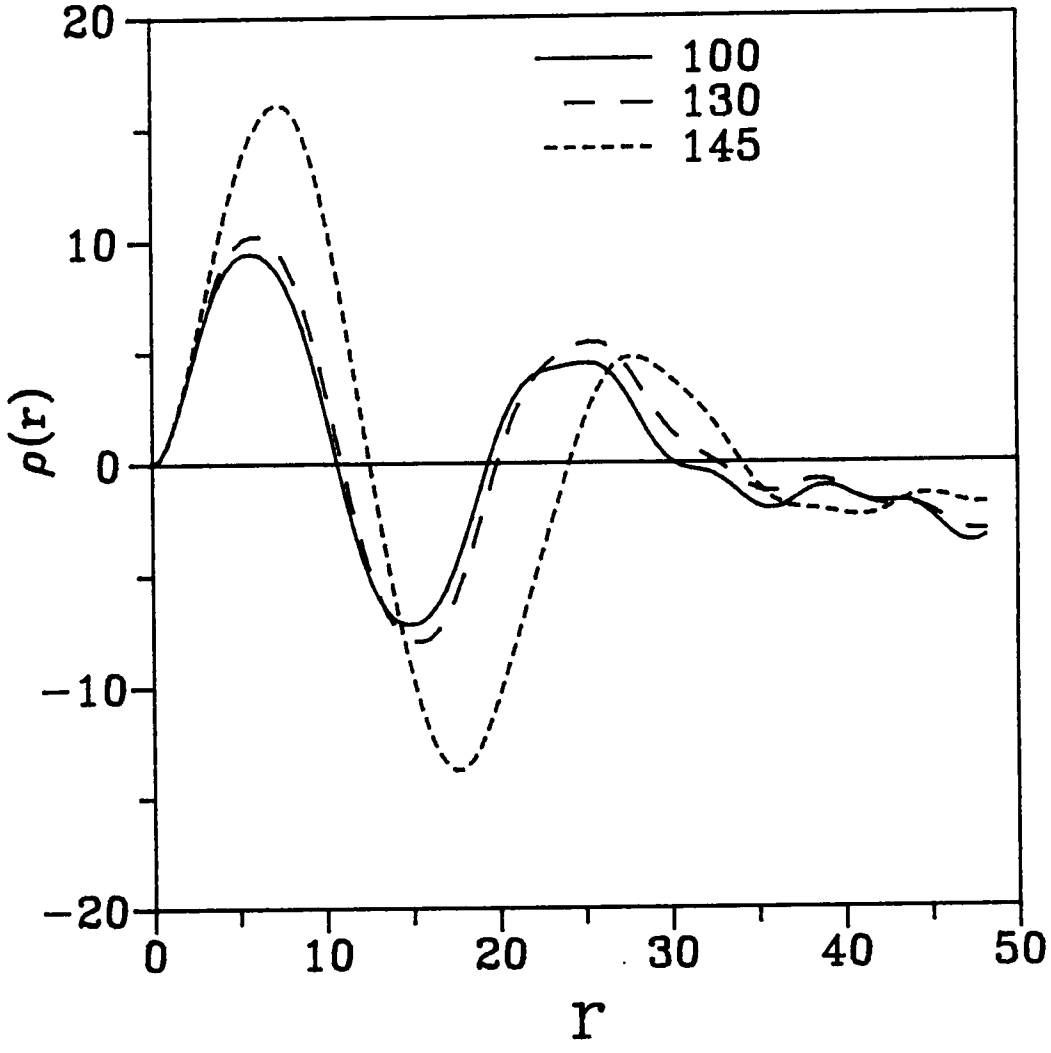


Figure 5.13 Electron density distribution for isotactic polypropylene isothermally crystallized (ΔT = 50°C, P_c = 100 MPa). SAXS intensity profiles recorded at temperatures indicated (°C).

from sedimented stacks of solution grown polymer crystals. This is a result of the low dispersity of thicknesses of the alternating crystalline and amorphous layers making up the stacks. However, the simple one-dimensional models do not predict well the diffraction profile for melt crystallized polymers. This is a consequence of the stack dispersities. Therefore, the simple one-dimensional model must be appropriately modified in order to better predict the diffraction behavior of melt crystallized polymers. The model predictions can be compared to the experimental results by either directly comparing intensity profiles or by comparing the one-dimensional correlation functions. The two approaches tend to emphasize different aspects of the structure. The result is potentially an incomplete viewpoint if only one approach is considered.

Certain assumptions must be made for the one-dimensional model of stacked lamellae, such as stacks of infinite lateral width and a two phase model (crystalline-amorphous) with a relatively sharp electron density transition. These assumptions simplify the model.

Numerous models and variations have been proposed to explain polymer diffraction behavior. Probably the simplest is the single infinite stack model where the number of lamellae is assumed to be sufficiently large so that the stack is effectively of infinite height. In this model, the

distribution statistics describing the crystalline and amorphous thicknesses can be varied. A variation of the single infinite stack model is to assume a finite number of lamellae compose a stack. This results in peak broadening relative to the infinite stack model. Another variation is the variable stack model in which there are fluctuations between stacks as well as fluctuations of lamellae within the stacks.

The details of the various models will not be elaborated in this work. The models' mathematical details can be found in several sources, among which are Ruland [116], Strobl [117], and Blundell [118]. Lee [119] has analyzed the models extensively and summarized the effects of crystallinity distribution and lamellar thickness distribution. The experimental isotactic polypropylene small angle X-ray scattering was interpreted on the basis of the results of Lee's modeling. It was shown that the variable stack model better fit the experimental SAXS intensity profiles from highly dispersed lamellar systems such as low density polyethylene (LDPE), crosslinked polyethylene (XLPE), and linear low density polyethylene (LLDPE). With a given thickness distribution, the calculated intensity profile peak decreased and the near zero angle intensity I_o increased with increased crystallinity distribution.

In applying the modeling results to isotactic polypropylene, it is apparent that the single infinite stack model does not correctly predict the observed intensity profile. The single infinite stack model with either a Gaussian or Asymmetric lamellar thickness distribution predicts a sharp peak for the observed intensity profile or the Lorentz corrected profile over a range of deviations of thickness from 0.05 to 0.20 for a model standard normal distribution. This behavior is shown in Figure 5.14 for the calculated observed intensity profile with a Gaussian thickness distribution and an average crystallinity of 0.5. The variable stack model was able to predict the intensity profile with deviations of crystallinity and deviations of lamellar thicknesses. Figure 5.15 shows the calculated observed intensity profile for the variable stack model with Gaussian thickness distribution with σ_x = 0.10 and Gaussian crystallinity distribution (various σ_c).

The SAXS behavior of the lowest crystallization temperatures for the atmospheric pressure crystallized homopolymer and copolymer exhibited intensity profiles indicative of highly dispersed lamellar systems as predicted by the variable stack model. With increasing crystallization temperature, the SAXS behavior exhibited an increase in the peak maximum, but the low scattering angle minimum, H_{min}, also showed a corresponding increase. The variable stack model

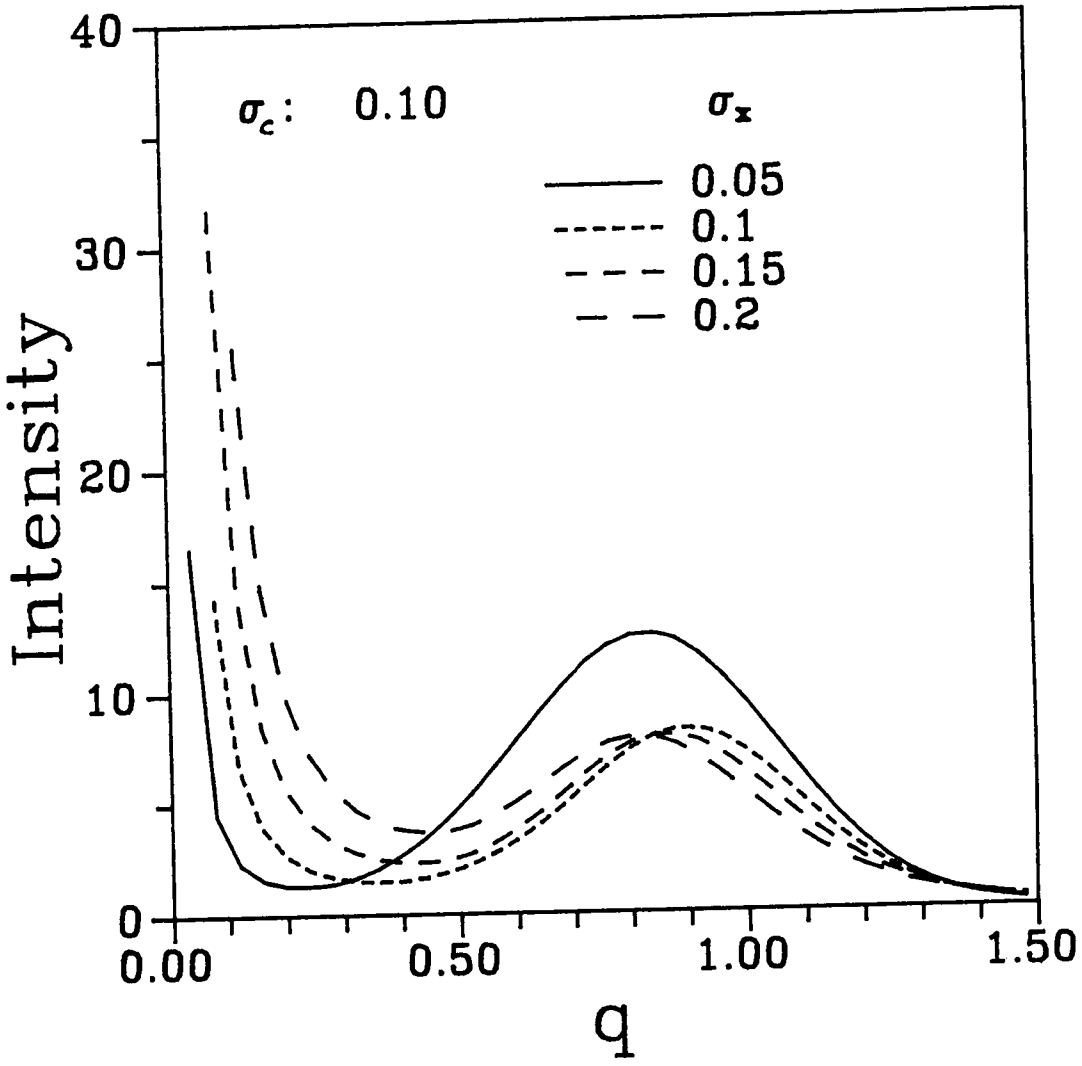


Figure 5.14 Theoretical SAXS intensity profiles from variable stack model with Gaussian thickness distribution (σ_c = 0.1) and Gaussian crystallinity distribution (σ_x as indicated).

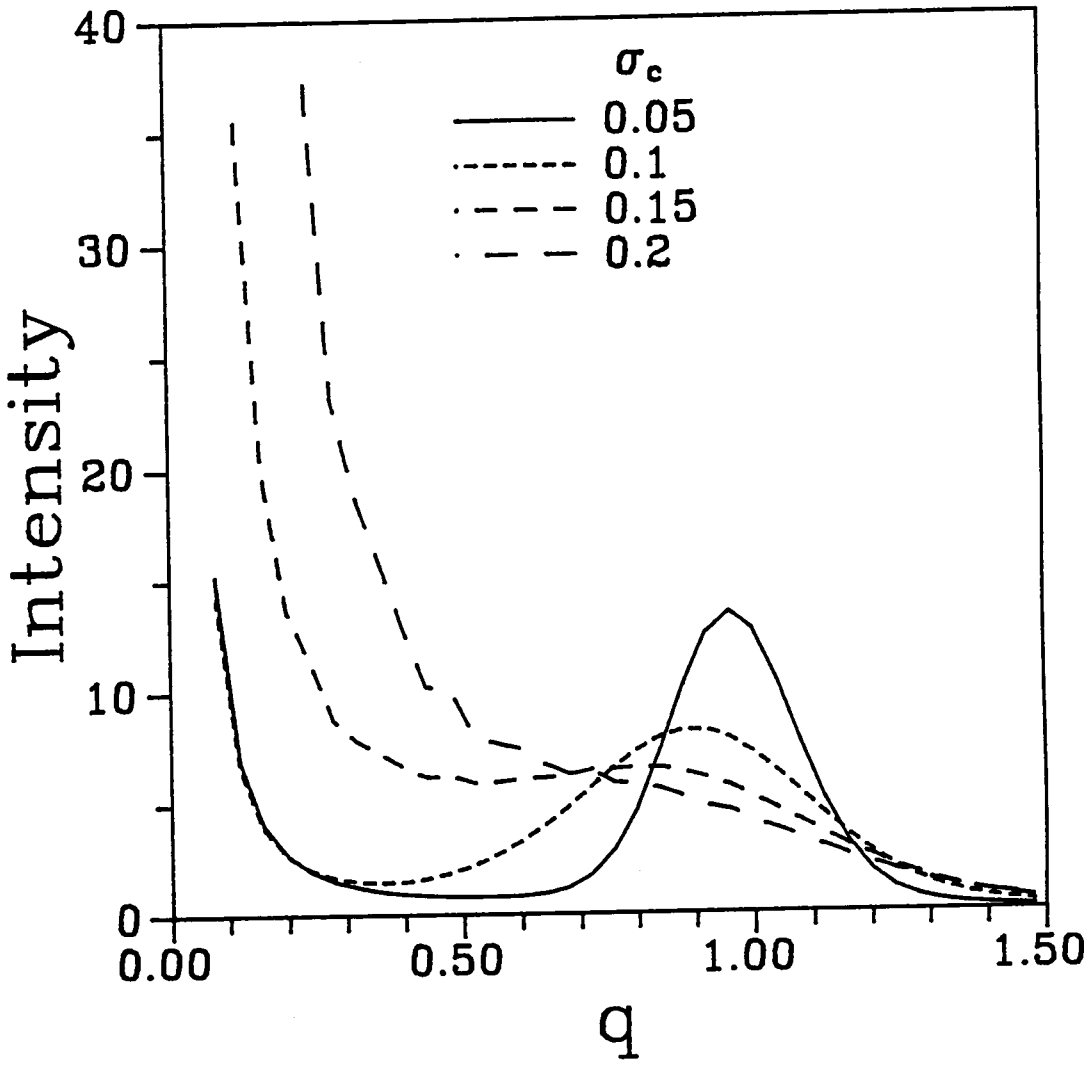


Figure 5.15 Theoretical SAXS intensity profiles from variable stack model with Gaussian thickness distribution (σ_x = 0.1) and Gaussian crystallinity distribution (σ_c as indicated).

predicts an increase in the peak maximum with decreasing crystallinity variation at a fixed thickness variance, but the model predicts a decrease in the low scattering angle minimum.

5.3 Equilibrium Melting Temperature, Fold Surface Energy

5.3.1 Atmospheric Pressure

The equilibrium melting temperature T_m^o is important in describing the relationship of polymer properties to structure and in the analysis of crystallization kinetics and nucleation processes. For the analysis of crystallization growth rate data, T_m^o is needed to determine the degree of supercooling $\Delta T = T_m^o - T_c$. Despite the importance of the equilibrium melting temperature, the experimental determination of T_m^o is often difficult and there is disagreement over the value of T_m^o even for widely studied polymers such as polyethylene and polypropylene.

Several methods, theoretical and experimental, exist for the determination of T_m^o for polymers. The methods are as follows:

1) Extrapolation of T_m for low molecular weight homologs to infinite molecular weight,

2) Extrapolation of T_m versus T_c data to the $T_m = T_c$ line,

3) Extrapolation of T_m versus $1/l$ data to $1/l = 0$.

The first method is a theoretical method developed by Flory and Vrij [120] where from an analysis of the equilibrium melting temperatures of monomeric homologs which form molecular crystals, the equilibrium melting temperature for the infinite chain can be calculated. By utilizing the data for n-paraffins, the T_m^o for infinitely long linear polyethylene was concluded to be 145.5°C .

The idea that T_m^o, T_m, and T_c might be simply related to one another was first mentioned by Lauritzen and Hoffman. The first systematic study showing an increase of T_m with increasing T_c was that of Wood and Bekkedahl on natural rubber. In this method, the observed melting temperature T_m is plotted against the crystallization temperature T_c and the data extrapolated linearly to the line representing the relation $T_m = T_c$. The point of intersection is then taken to represent the T_m^o of the sample. This procedure is based on Flory's statistical thermodynamic considerations of the fusion of polymers

Figure 5.16 shows a plot of T_m versus T_c from DSC for isotactic polypropylene M_w = 151,000 with the extrapolation of the line through the experimental data to the $T_m = T_c$ line to a value of T_m^o = 187°C. the definition of the melting

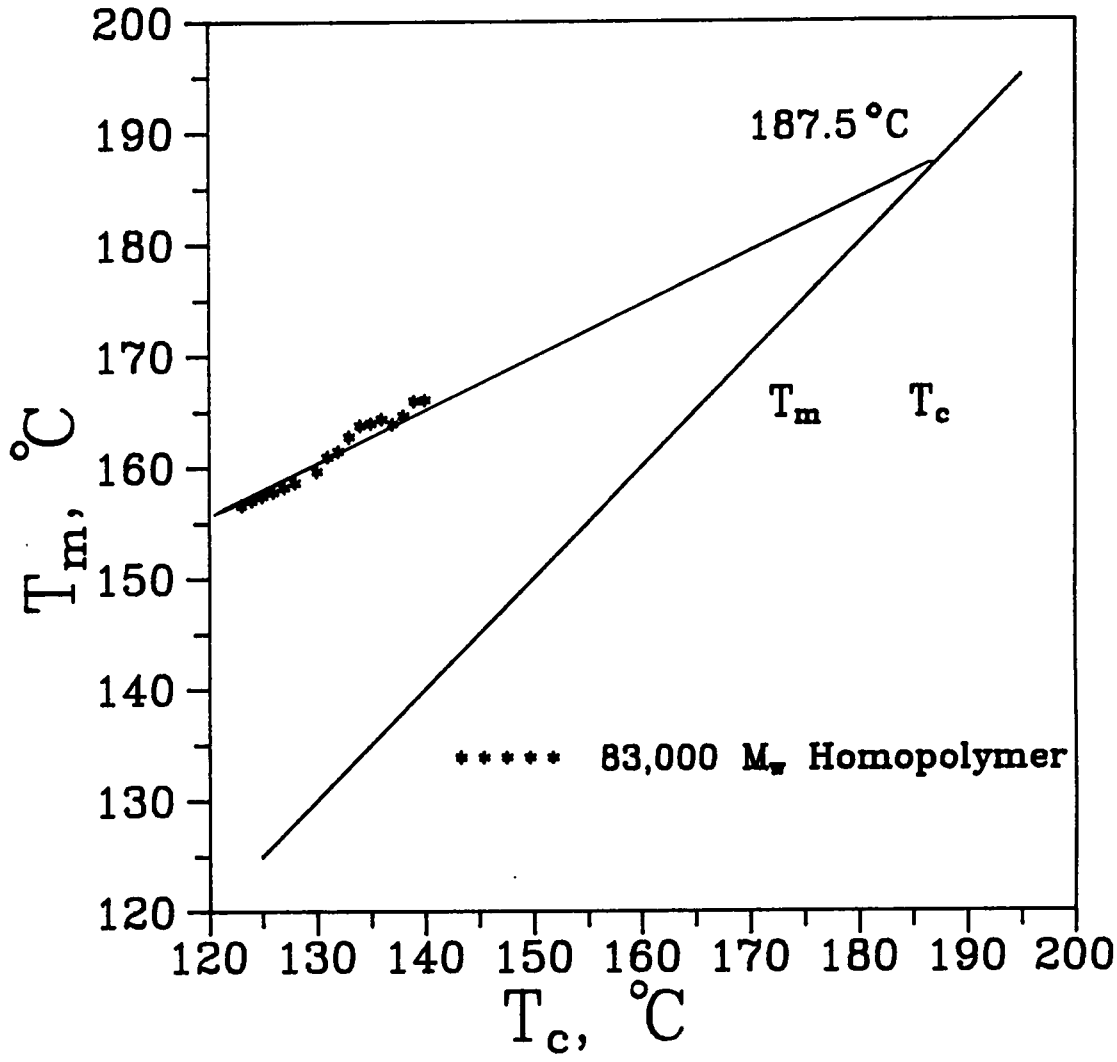


Figure 5.16 Melting temperature (DLI) vs isothermal crystallization temperature for isotactic polypropylene crystallized at atmospheric pressure.

temperature chosen for this figure is the modified return-to-baseline, which is a measure of the melting of the most perfect crystals in the material. The equilibrium melting temperature extrapolation does change depending on the chosen melting temperature. The value determined compares favorably with values in the literature for highly stereoregular isotactic polypropylene [121]. The thickening factor determined from the slope is 2.2 for this material. this is a measure of the increase of the lamellar thickness over that predicted as the critical thickness l_g^*. The T_m^o and γ values obtained for the other isotactic polypropylene samples are similar to those of the 151,000 homopolymer. Table 5.5 reports the values of T_m^o and γ for the samples.

The equilibrium melting temperature T_m^o can be calculated from equation 2.34 which expresses the melting temperature as a function of lamellar thickness. The equation predicts a linear relation for a plot of T_m versus $1/l_c$. This plot evaluates the T_m^o from the intercept and se from the slope. Figure 5.17 shows the plot of T_m versus $1/l_c$ for the 151,000 M_w homopolymer and the 151,000 M_w copolymer. The lamellar thicknesses for the figure are from Lorentz corrected SAXS data, using the crystallinity from WAXD. The melting temperatures are DSC modified return-to-baseline measurements. The equilibrium melting temperature for the homopolymer was determined to be 185.9°C, which was about

Table 5.5 Equilibrium melting temperature and thickening factor for atmospheric pressure crystallization.

Sample	T_m^o (°C)	γ
83,000 M_w	187.8	2.44
151,000 M_w	188.5	1.83
copolymer	188.7	1.60

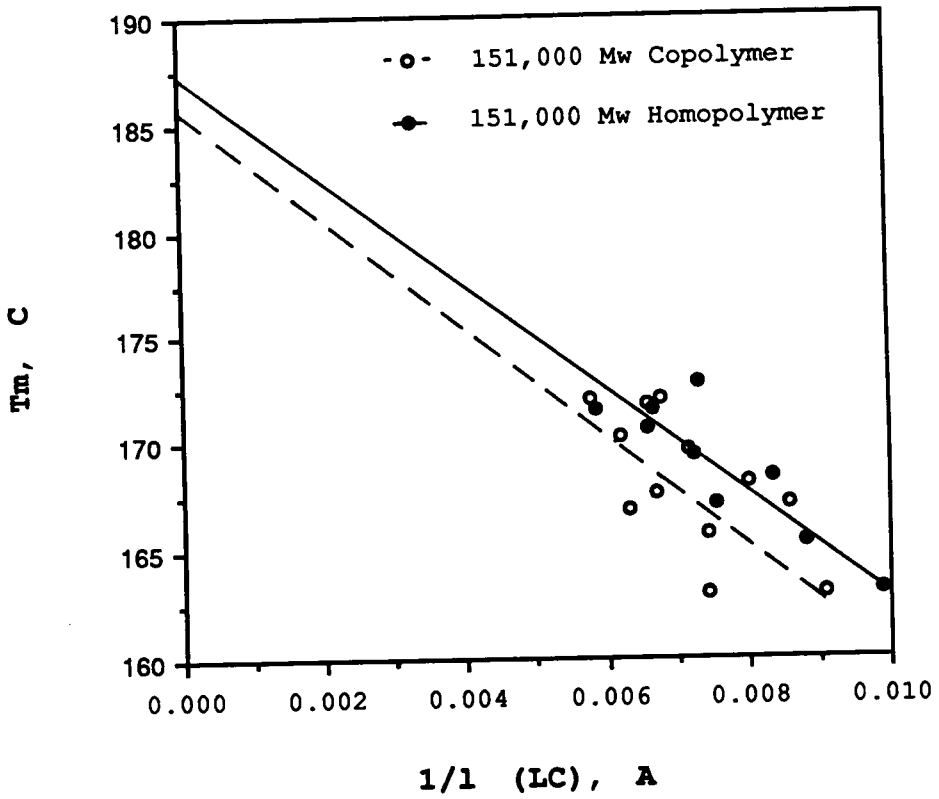


Figure 5.17 Reciprocal lamellar thickness from SAXS Lorentz corrected data vs melting temperature from DSC return-to-baseline for isotactic polypropylene 151,000 M_w homopolymer and copolymer isothermally crystallized at atmospheric pressure.

1.5° below that determined from the plot of T_m versus T_c. The T_m^o for the copolymer was slightly lower, 184.9°C, which was about 2.5° below that determined from the plot of T_m versus T_c.

The fold surface free energies determined from the slope of the T_m versus 1/l data were 47.8 erg/cm^2 and 46.8 erg/cm^2 for the homopolymer and copolymer, respectively. These values are lower than the corresponding σ_e values obtained from the analysis of the kinetics data.

The fold surface free energy can also be determined from the relation between l and ΔT. The lamellar thickness is related to the supercooling through the following relation:

$$l = \frac{2\sigma_e T_m^o \gamma}{\Delta h_f \Delta T} + \gamma\delta l$$

Figure 5.18 shows the plot of l versus $1/\Delta T$ for the homopolymer and the copolymer at atmospheric pressure. The atmospheric pressure equilibrium melting temperature used in this analysis was 185°C. For the homopolymer with input values of Δh_f = 165 J/g and γ = 1.76, the σ_e was determined to be 43.5 erg/cm^2. Using T_m^o = 185°C, Δh_f = 165 J/g and γ = 1.76 for the copolymer, the σ_e was determined to be 52.7 erg/cm^2. This is the σ_e that corresponds to the critical nucleus.

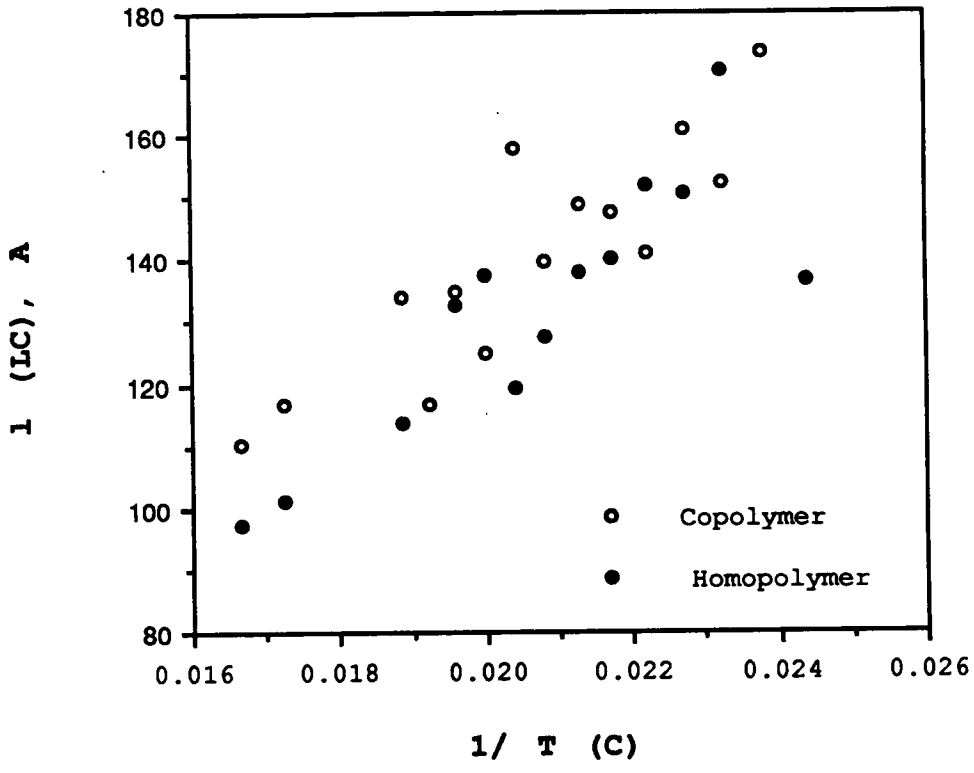


Figure 5.18 Reciprocal supercooling versus lamellar thickness from SAXS Lorentz corrected data for isotactic polypropylene 151,000 M_w homopolymer and copolymer isothermally crystallized at atmospheric pressure.

The σ_e values from the T_m versus 1/l and l_c versus $1/\Delta T$ analyses were lower than those determined by kinetics which are typical of the entire crystal surface. Table 5.6 compares the values of the fold surface free energies evaluated from the kinetics and thermodynamics. The estimates of the surface free energy of a polymer crystal with a diffuse phase boundary can be considerably higher than that of a corresponding tight folded crystal. This is because an extra amount of surface work exceeding that required to form the tightly folded surface is required to create the boundary layer. The quantity $\sigma\sigma_e$, obtained through application of Equation 2.30, is basically a kinetically determined parameter where the σ_e relates to the act of forming one chain fold in the activated state. The quantity σ_e in the Thomson-Gibbs thermodynamic relation refers to a macroscopic average of a larger number of chain folds [122]. For Regime III crystallization, the amount of adjacent re-entry may be considerably less than that for Regime I, although theory predicts that the $\sigma\sigma_e$'s for Regime I and Regime III are equivalent. This is due to the kinetics σ_e relating to the formation of one fold in the activated states. The value from the T_m versus 1/l data, however, is an average of all folds within the sampling volume. Thus, loose folds as well as tight adjacent re-entry folds are averaged together. This should result in significant

Table 5.6 Values of fold surface free energy for isotactic polypropylene

	Values of σ_e (erg/cm^2)		
	kinetics	T_m vs 1/l	l vs $1/\Delta T$
homopolymer	69	47.8	43.5
copolymer	59	46.8	52.7

differences in the measured σ_e's as observed experimentally. A value of σ_e determined in Regime I should give the closest comparison between the kinetics and thermodynamics since the amount of adjacent re-entry is high. The value of σ_e from the l versus $1/\Delta T$ data should be closer to that of kinetics, since the measured l is corrected by the thickening factor γ to l_g^*. Figure 5.19 shows the plot of l_g^* versus T_c for the 151,000 M_w homopolymer. The lines are theoretical curves for l_g^* determined from Equation 2.9 with $\delta l = kT/b_o\sigma$ for σ_e values of 50 and 65 erg/cm^2. The experimental value of l_g^* was determined from $\gamma = l/l_g^*$, where γ is the thickening factor obtained from DSC T_m versus T_c data.

5.3.2 Elevated Pressure

The melting temperatures of samples that were crystallized and melted at pressures ranging from atmospheric pressure to 200 MPa are presented in Figure 5.20. All determinations were made at 3°C/min. and the modified return-to-baseline melting definition described in section 3.4 was used throughout. Extrapolations of the data to the $T_m = T_c$ line yield values of T_m^o according to equation 2.39. The data generally fitted well to a linear relationship. The thickening factor, γ, at each pressure was obtained from the slope of the line. The values of T_m^o and γ at each pressure are presented in Table 5.7. With increasing pressure, the thickening factor increases. This has also been shown to

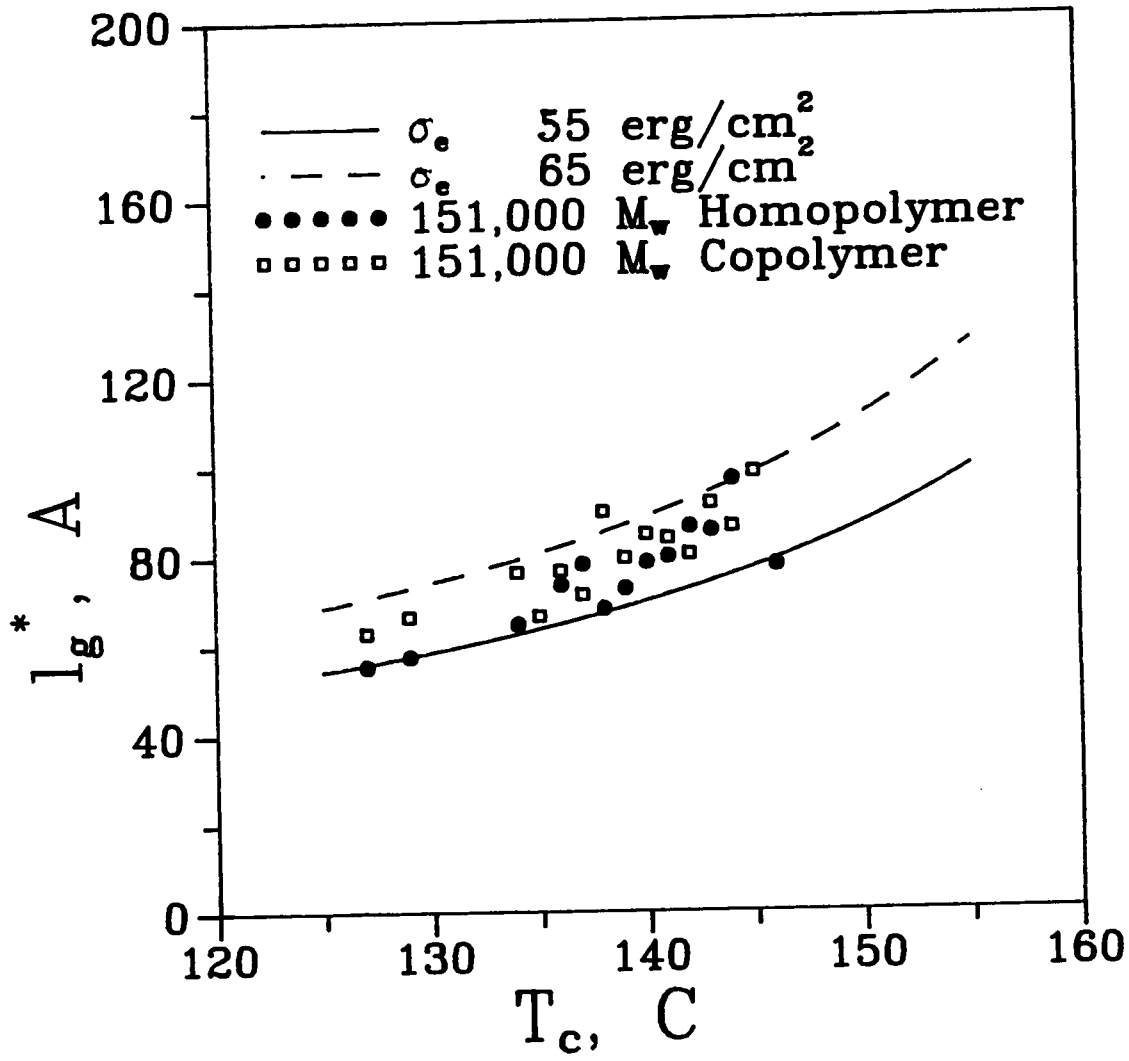


Figure 5.19 Crystallization temperature versus initial lamellar thickness l_g^* calculated from SAXS Lorentz corrected data and DSC thickening factor γ. Curves are theoretical predictions with indicated fold surface free energy σ_e.

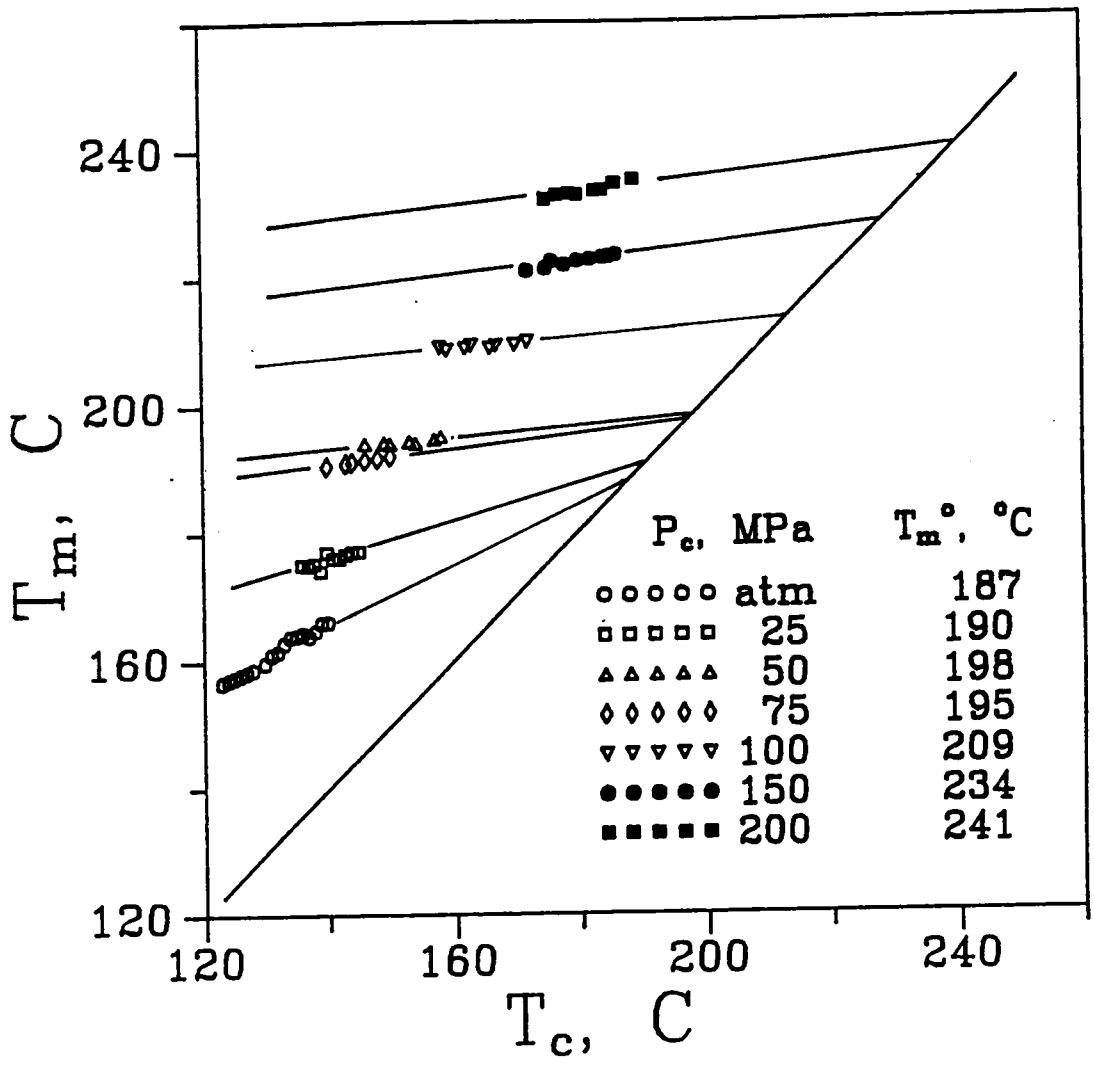


Figure 5.20 Melting temperature (DLI) vs isothermal crystallization temperature for isotactic polypropylene crystallized at atmospheric pressure and elevated pressure.

Table 5.7 Values of the Equilibrium melting temperature, T_m^o, and the Thickening factor, γ, for isotactic polypropylene crystallized at elevated pressure.

Pressure MPa	T_m^o (°C)	γ
atm	187	2.44
25	192	3.61
50	197	19.2
75	195	6.67
100	209	15.9
150	234	4.55
200	241	6.67

occur with linear polyethylene [123]. This indicates that the thickening process is more effective with increasing pressure. Figure 5.21 gives the equilibrium melting temperature as a function of pressure for isotactic polypropylene.

The equilibrium melting temperature T_m^o and the fold surface free energy σ_e for the elevated pressure crystallized samples can be determined in a similar manner to those at atmospheric pressure. Samples appropriate for SAXS analysis were prepared for two pressures, 100 and 200 MPa, as a function of isothermal crystallization temperature. The melting temperatures were recorded at elevated pressure using the technique previously described. The lamellar thicknesses were determined from the SAXS Lorentz corrected data and the crystallinity from WAXD. The T_m^o and σ_e were then calculated from Equation 2.34 which expresses the melting temperature as a function of lamellar thickness. Figure 5.22 shows the plot of T_m versus 1/l for the 151,000 M_w homopolymer isothermally crystallized at 100 and 200 MPa. For 100 MPa, the T_m^o was determined to be 214.6°C while the T_m versus T_c data gave T_m^o = 209.2°C. The σ_e was 4.3 erg/cm^2, using the Δh_f of the α form of isotactic polypropylene. This was significantly lower than the value of σ_e = 109 erg/cm^2 (II) obtained from the kinetics analysis. The σ_e value would yield an unrealistic value for the work of chain folding. The value

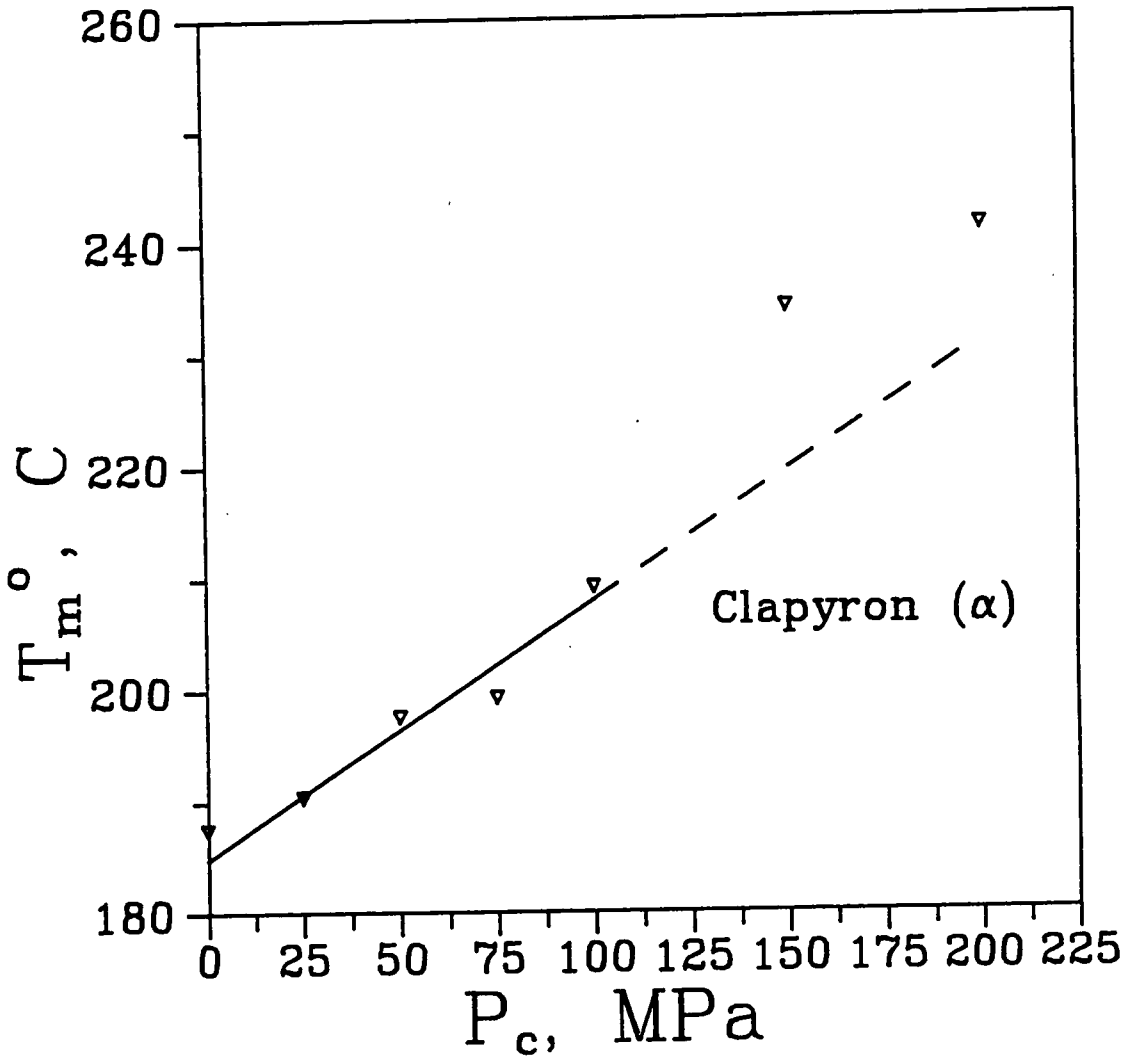


Figure 5.21 Equilibrium melting temperature T_m^o vs crystallization pressure for isotactic polypropylene. Line represents theoretical calculation from Clapeyron equation for α polypropylene.

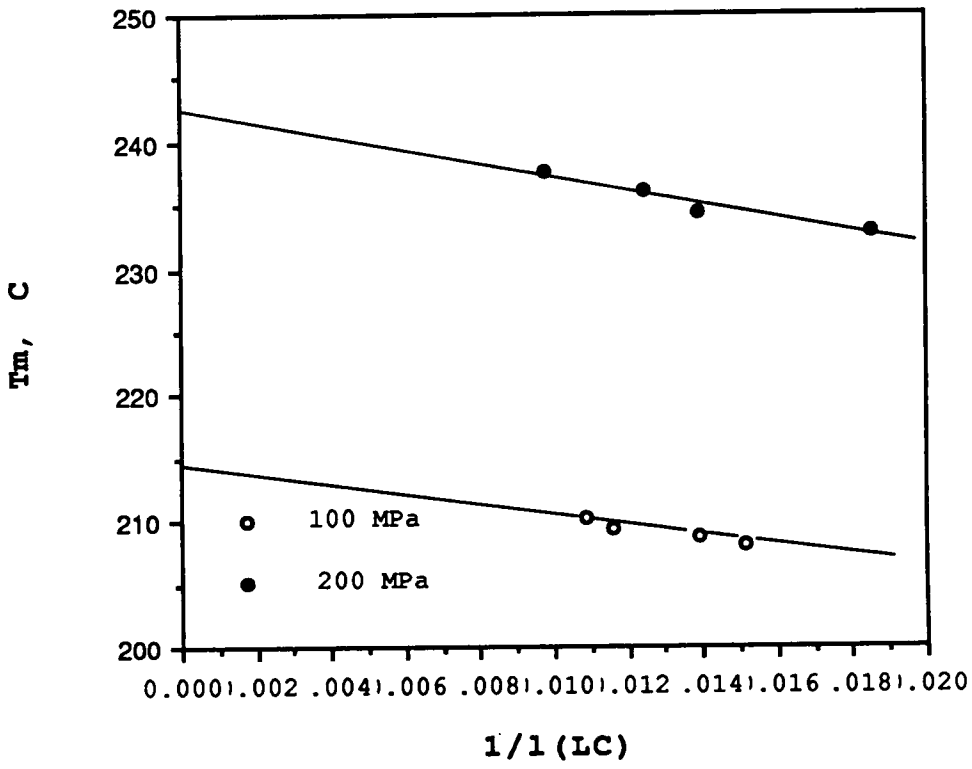


Figure 5.22 Reciprocal lamellar thickness from SAXS Lorentz corrected data versus melting temperature from DLI for isotactic polypropylene isothermally crystallized at 100 MPa and 200 MPa.

of T_m^o from the T_m versus 1/l data for 200 MPa was 242.6°C, which was within 1°C of the value obtained from the T_m versus T_c data (241.3°C). The σ_e value for the 200 MPa data was 5.0 erg/cm^2, again considerably lower than that from the kinetics analysis (51.1 erg/cm^2 Regime II). It is unclear why the values of σ_e from thermodynamics are lower than those from kinetics, although similar behavior was also observed for the atmospheric pressure data. While some error may be incurred in the use of the Δh_f of the α form, this factor alone cannot account for the differences in the σ_e values. To obtain a value of σ_e approaching that of the atmospheric data (≈65 erg/cm^2) would require a Δh_f on the order of ten times that used in the analysis. There is no data to support a significant change in Δh_f for the γ form although a small change would be expected.

5.4 Kinetics Analysis

The isotactic polypropylene elevated pressure kinetics exhibited behavior that has not been previously observed in other polymers. The product of the lateral and fold surface free energies $\sigma\sigma_e$ increased to a value nearly three times the atmospheric pressure value. However, as the pressure reached a value where a significant amount of the γ form was present the kinetics yielded results that were comparable to those of atmospheric pressure. Thus the unusual behavior existed at pressures where the two crystal structures coexisted. A

mechanism based on the arrangement of the chain stems in the unit cells of the two structures is proposed to account for the unusual behavior. This 'poisoning' mechanism is important, since no similar mechanism has been previously proposed to describe the competition between two crystal structures during crystallization that results in deactivation of the growth front of one crystal form by the other form. The kinetics analysis of linear growth rate data yield important information concerning the crystallization mechanism. One can determine the crystallization regimes, the nucleation constants, the surface free energies, and the work of chain folding. Clark and Hoffman [124] recently analyzed much of the available literature of polypropylene growth rates using secondary nucleation theory. In this analysis, polypropylene was found to exhibit a Regime II - Regime III transition, but no evidence of a Regime I - Regime II transition was seen. The data, however was from polypropylene with molecular weights greater than about 150,000 (viscosity average). Recently Cheng et al. [125] observed a Regime I - Regime II transition and a Regime II - Regime III transition within a low molecular weight fraction of polypropylene (M_n = 15,000). The experimental linear growth rates were analyzed using secondary nucleation theory, and the results are reported for atmospheric pressure and elevated pressure in this section.

5.4.1 Atmospheric Pressure Kinetics

Spherulitic growth rates in the temperature range of the literature Regime I through Regime III have been analyzed using secondary nucleation theory. According to equation (1) the growth rate data should conform to a linear plot with the abscissa X and the ordinate Y given by

$$X = \frac{1}{fT\Delta T}$$

$$Y = \log G + \frac{U^*}{2.3R(T_c - T_\infty)}$$

The factor 2.303 in equation (3) is ln(10) and the factor f is given by $f = 2T_c/(T_m^o+T_c)$. The factor f, which has a low value of 0.93 at T_c = 125°C in this analysis at atmospheric pressure, compensates for the temperature dependence of Δh_f. The data were analyzed in this manner in order to more easily compare the results with the literature. The nucleation constant K_g and the preexponential G_o were then evaluated from the slope and the intercept, respectively.

Values of parameters used in the kinetics analysis are presented in Table 5.8. The value of U^* = 1500 cal/mole, used in this kinetics analysis, is generally somewhat different than the values obtained from various activation energy experiments in the literature [126]. However, this value of U^* has been applied in the literature and will be used in the present analysis. Alternately, the data were

Table 5.8 Isotactic Polypropylene Input Parameters for Atmospheric Pressure Kinetics Analysis.

Parameter	Value	Source
T_m^o, °C	187	This Work
T_g, °C	-12	M Jarrigeon [127]
Δh_f, J/g	209	W.R. Krigbaum [128]
ρ_c, g/cm^3	0.936	
<u>α PP unit cell</u>		
a, Å	6.65	
b, Å	20.96	
c, Å	6.50	
β	99.3°	
<u>[110] growth plane</u>		
a_o, Å	5.49	
b_o, Å	6.26	
<u>[040] growth plane</u>		
a_o, Å	6.56	
b_o, Å	5.24	

analyzed with various values of U^* in order to observe the effect of the value of U^* on the kinetics analysis. The value of T_g = -13°C, taken from the literature [129], can possibly be argued as inappropriate (see [130] for other T_g values). The kinetics analysis for polypropylene is relatively insensitive to changes in T_g.

The equilibrium melting temperature T_m^o = 187°C was determined in the previous section. This value is in good agreement with values reported in the literature using the T_m versus T_c analysis [131]. Also, values from T_m versus 1/l analysis [132] are similar. A change of ±2°C can have an effect on the kinetics analysis results.

A plot of log G + $U^*/[2.3R(T_c - T_\infty)]$ versus $1/T\Delta Tf$ is shown in Figure 5.23 for the isotactic polypropylenes. It is seen that the data do not fit a single line but fit well to two lines. The transition is interpreted as a Regime II - Regime III transition because a Regime I - Regime II transition would have exhibited a downward change in slope. 83,000 M_w homopolymer, 151,000 M_w homopolymer, and the 151,000 M_w copolymer, respectively. Again, a Regime II - Regime III transition is observed. No clear evidence is observed for a Regime I - Regime II transition. The Regime I - Regime II transition should occur at approximately T_c = 148°C, employing the supercooling of 37°C for the Regime I - Regime II transition observed by Cheng et al. for the low molecular

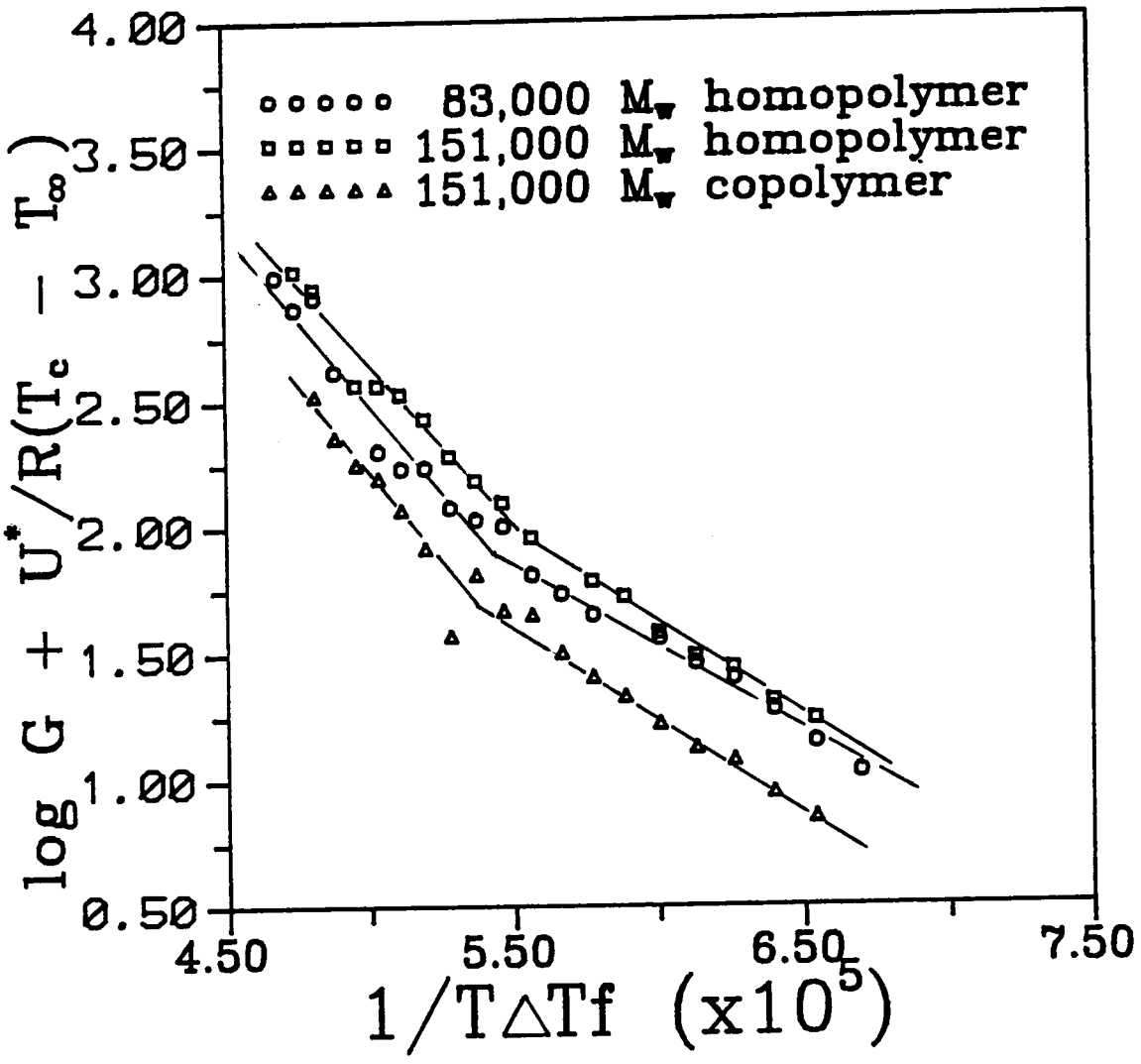


Figure 5.23 Kinetics analysis for isotactic polypropylene crystallized at atmospheric pressure. (U^* = 1500 cal/mole, T_m^o = 187°C, T_g = -12°C).

weight polypropylene. While only a few experimental growth rates were obtained at T_c's greater than the predicted I-II transition, no change is observed in the kinetics. It is clear that more data points would be beneficial in the high T_c data analysis, but the crystallization of polypropylene at these temperatures is exceedingly slow and there is relatively little variation in growth rate at these temperatures. The results of the kinetics analysis for Regimes II and III are presented in Table 5.9 and compared with literature data. Once K_g was determined from the plots, other parameters characteristic of crystal growth were determined. The product $\sigma\sigma_e$ was evaluated using the K_g and appropriated relation from secondary nucleation theory. For Regime II, $\sigma\sigma_e$ is determined using the following:

$$\sigma\sigma_e = \frac{K_{g(III)}}{2b_o T_m^o \Delta h_f k}$$

while for Regime III (and Regime I) the relation is:

$$\sigma\sigma_e = \frac{K_{g(II)}}{4b_o T_m^o \Delta h_f k}$$

The corresponding values of σ_e were then obtained by dividing the product $\sigma\sigma_e$ by σ obtained from the relation:

$$\sigma = \alpha \Delta h_f (a_o b_o)$$

Table 5.9 Kinetics Analysis of Isotactic Polypropylene Crystallized at Atmospheric Pressure.

Sample	K_g ($\times 10^{-5}$)	log G_o	$\sigma\sigma_e$ erg^2/cm^4	σ_e erg/cm^2	q kcal/mole	III/II	ΔT
			Regime II				
83,000	1.786	4.55	841	73	7.2	1.63	138.6
151,000	1.550	5.66	730	64	6.3	2.17	136.4
151,000 copoly.	1.821	6.01	860	75	7.4	1.57	137.1
			Regime III				
83,000	2.915	7.34	686	60	5.9		
151,000	3.358	9.93	790	69	6.8		
151,000 copoly.	2.859	8.44	674	59	5.8		

where α = 0.1 [21]. This σ is applicable in all regimes. The work of chain folding is then determined from the relation

$$q = 2\sigma_e a_o b_o$$

The K_g values for Regime II and Regime III were slightly lower than the average of the literature values of the K_g's for Regime II (1.58×10^5 K^2) and Regime III (3.34×10^5 K^2). Also the ratio $K_{g(III)}/K_{g(II)}$, theoretically predicted as 2.0, was less than the literature average (2.09) although the experimental K_g's and the ratio were within the range of the literature results. The corresponding fold surface free energy σ_e and work of chain folding q from the experimental data were comparable to those values reported in the literature for isotactic polypropylene and are reasonable and consistent with values of other polymers. In the case of the experimental temperature range for the present study of isotactic polypropylene, the temperature dependence of G is dominated by the nucleation term $\exp[-K_g/T\Delta Tf]$ while the diffusion term $\exp[-U^*/R(T_c-T_\infty)]$ acts as a relatively unimportant correction term. Hammami has shown that for a series of polypropylenes, a maximum in the growth rate - crystallization temperature relation is predicted to occur near 80°C. The term $\exp[-U^*/R(T_c-T_\infty)]$ would certainly become more dominant in $G(T_c)$ below this maximum.

The values of σ, σ_e, and q for the experimental data are compared with those of other polymers, which are presented in Table 2.3. For the -C-C- backbone polymers, as the backbone stiffens, the equilibrium melting temperature increases. The stiffening of the backbone also results in a lower σ because of the smaller entropy decrease. Consequently, the work of chain folding increases because the more stiff chain is harder to bend to make the fold.

The value of U^* was varied from 750 to 5250 cal/mole in order to check the effect of U^* on the crystallization kinetics. Figure 5.24 shows a plot of crystallization kinetics for polypropylene M_w = 83,000 with different values of U^*. It is seen that, over a wide range of U^* values, the data can be fit reasonably well to two lines. For values of U^* up to 3000 cal/mole, there was only a small effect on the resulting K_g's for Regimes II or III. Also, the regime transition temperature showed little change. For values of U^*>3000 cal/mole, the effects became more significant. The K_g of Regime III showed the largest change, with over a 40% increase in $K_{g(III)}$ over the value with U^* = 1500 cal/mole. While the constants T_m^o and T_g do not vary as widely as the U^* values considered, the effect of changing T_m^o and T_g values on the kinetics was considered. As shown previously [133], a 1°C change in T_m^o causes approximately a 5% change in K_g, σ_e, and q. Changing T_g has relatively little effect on K_g

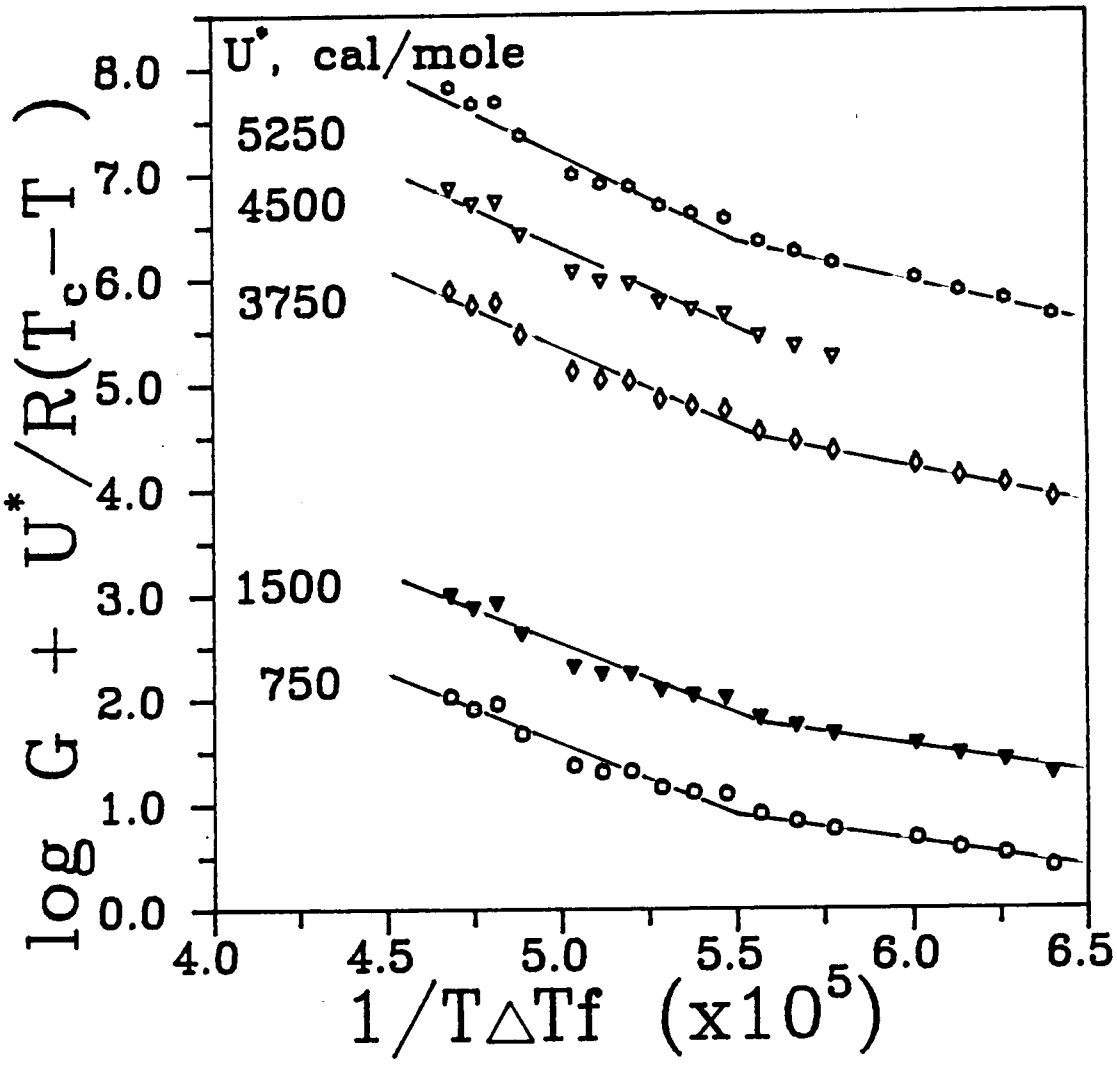


Figure 5.24 Kinetics analysis of atmospheric pressure crystallized isotactic polypropylene with variation of U*.

however. Variation in T_m^o does not affect σ, but changes in Δh_f affect σ and not σ_e. Chosing different growth planes affects σ_e.

It is observed that the kinetics curve shifts upward with increasing U^*. The K_g of Regime III increases slightly more rapidly than that of Regime II with increasing U^* while the rate of increase in the G_o's of both regimes is essentially the same. The increase in K_g's and G_o's is linear with increasing U^*. Table 5.10 summarizes the kinetics analysis as a function of U^*. Dalal observed that changing U^* from 1500 cal/mole to 3000 cal/mole had a significant effect of the kinetics analysis for cis-poly(isoprene) [134]. At U^* = 3000 cal/mole, the data exhibited a clear Regime II-Regime III transition with a slope ratio of ≈2. When U^* was changed to 1500 cal/mole, the data fit well to a single line which was assigned to Regime II and had a similar K_g to the Regime II data with U^* = 3000 cal/mole. A significant difference between the kinetics of poly(isoprene) and polypropylene is the region of the growth rate curve in which regimes are observed. For polypropylene, the Regime II-Regime III transition occurs well into the high temperature side of the growth rate curve. From a calculated growth rate curve (from results of kinetics analysis), the growth rate maximum occurs at approximately 80°C (ΔT = 107°) while the II-III transition occurs at ≈138°C (ΔT = 49°). This implies that the

Table 5.10 Kinetics Analysis with Variation of U* for Isotactic Polypropylene, Mw = 83,000 Crystallized at Atmospheric Pressure.

U^*(J/mole)	K_g($x10^{-5}$)		log G_o	
	III	II	III	II
3138	2.99	1.39	8.06	4.25
6276	3.15	1.47	9.34	5.36
9414	3.30	1.56	10.62	6.47
12552	3.46	1.64	11.90	7.58
15690	3.62	1.73	13.18	8.69
18828	3.78	1.81	14.47	9.79
21966	3.93	1.90	15.75	10.90
25104	4.09	1.98	17.03	12.01

transition occurs in the nucleation controlled region of the growth rate curve. However, for poly(isoprene), where the growth rate can be measured over sufficient crystallization temperature range to obtain a bell shaped growth rate curve, the Regime II-Regime III transition occurs near the maximum in the growth rate curve. Thus, the Regime II data are in the nucleation controlled region of the curve while much of the Regime III data are in the diffusion controlled region of the curve. This explains why the Regime III data of cis-poly(isoprene) are more significantly affected by the change in the activation energy U* for the diffusion component of the secondary nucleation theory. Thus with polypropylene exhibiting a Regime II-Regime III transition relatively far from the diffusion controlled region of the growth rate curve, the kinetics analysis was not significantly affected by a change in U^*.

The effect of changing T_g and T_m^o was also evaluated for the isotactic polypropylene 83,000 M_w homopolymer kinetics. The most significant change occurred with change in T_m^o. The effect of changing T_g was much less significant. This follows with the reasoning for the effect of changing U^* on the kinetics, since T_g has more effect on data in the diffusion controlled region. The effect of a small change (1°C) in T_m^o has previously been reported to be about a 5% change in both K_g and G_o [135]. Table 5.11 compares the

Table 5.11 Kinetics Analysis for Isotactic Polypropylene 83,000 M_w Homopolymer - $f(T_m^o, T_g)$

	K_g ($\times 10^{-5}$), K^2		log G_o	
	III	II	III	II
		T_m^o = 187°C		
T_g, °C				
-20	3.12	1.46	9.20	5.25
-10	3.15	1.47	9.38	5.39
0	3.19	1.50	9.58	5.55
		T_m^o = 215°C		
-20	8.84	4.90	15.05	9.15
-10	8.94	4.95	15.29	9.33
0	9.05	5.03	15.57	9.55

kinetics results with changing T_m^o and T_g. It is seen that a higher value of Tmo that has been reported in the literature gives significantly different results for the kinetics. However, Wunderlich [124] has stated that the results of the kinetics analysis with T_m^o = 212°C for isotactic polypropylene are unrealistic and that the value of 187.5°C is probably correct.

5.4.2 Elevated Pressure Kinetics

The unusual elevated pressure kinetics cannot be explained without the orthorhombic unit cell of the γ form of isotactic polypropylene. The resulting values of the $\sigma\sigma_e$ product at intermediate pressures are nearly three times larger than those at atmospheric pressure or 200 MPa pressure. In the cases of atmospheric pressure crystallization and 200 MPa crystallization, only a single crystal structure is present. This suggests that the unusual crystallization behavior at the intermediate pressures is related to the presence of the two crystal structures which interfere with each other.

While only limited attempts have been made in the past to study the effects of pressure on crystallization behavior, even fewer studies have applied secondary nucleation theory to the crystallization behavior at elevated pressure. No study in the past has performed this evaluation for isotactic polypropylene. Secondary nucleation theory has been applied

to the elevated pressure crystallization kinetics of cis-polyisoprene [136], linear polyethylene [137], and poly(ethylene terephthalate [138], with acceptable results. Secondary nucleation theory should be applicable to the kinetics of elevated pressure, provided that the crystallization mechanisms at atmospheric pressure and elevated pressure are similar. Also, the parameters used in secondary nucleation theory must be corrected for the effect of pressure. While the effect of pressure on U^* and T_g is unknown at this time for isotactic polypropylene, it is clear from the preceding section that variations in these parameters do not significantly affect the results of the kinetics analysis within reasonable variations of these parameters. Using dielectric relaxation at elevated pressure, Dalal [139] has determined the effect of pressure on the parameters U^* and T_g for cis-poly(isoprene). It was observed that for the pressure range 0 to 200 MPa, the change in T_g with pressure, dT_g/dP, was approximately 17.8°K/100 MPa. The value of U^* increased approximately 13%, from 17.6 KJ/mole to 19.9 KJ/mole. While the U^* values are higher than those typically used for isotactic polypropylene at atmospheric pressure, the change in U^* of 13% has been shown to have little effect on the K_g for polypropylene.

Spherulitic growth from the melt was observed at all crystallization temperatures studied at each pressure. This

indicates some similarities in the crystallization mechanisms at atmospheric pressure and elevated pressure. Table 5.12 lists the parameters used in the kinetics analysis of the elevated pressure data. Since the effect of pressure on U^* is presently unknown, the value of U^* was held constant, which is a reasonable assumption [72]. The change in T_g with pressure (dT_g/dP) for several polymers is approximately 20°C/100 MPa as predicted by free volume theories from the ratio of compressibility to expansivity. Saur and Pae [140] esimated the change in T_g with pressure, dT_g/dP, for isotactic polypropylene from E versus P data to be 20°C/kbar using the data of Boyer [141]. The available literature values of dT_g/dP agree with these predictions. The equilibrium melting temperature is incorporated into the dominant term $\exp[-K_g/(T\Delta Tf)]$ and is important in kinetics analysis. The T_m^o's reported in section 5.3 using the plot of T_m versus T_c were used in the kinetics analysis. As shown previously, the dT_m^o/dP of 23°C/100 MPa agrees well with that for other polymers. However, other values of dT_m/dP for isotactic polypropylene have been published [142]. Accordingly, a value of dT_m^o/dP = 38°C/100 MPa was also used as an alternate in analyzing the crystallization kinetics, with some interesting results.

The plots of log G + $U^*/R(T_c - T_\infty)$ versus $1/T\Delta Tf$ at atm., 25, 50, 75, 100, 150 and 200 MPa are shown in Figures

Table 5.12 Isotactic Polypropylene Input Parameters for Kinetics Analysis at Various Elevated Pressures.

Press(MPa) Parameter	atm	25	50	75	100	150	200
Tg(°C)	-12	-7	-2	5	1-	18	28
Tmo(°C)	187	190	198	195	209	234	241
U*(cal/mole)	1500	1500	1500	1500	1500	1500	1500
Δhf	209	209	209	209	209	209	209

5.25 to 5.27 respectively. The data are fitted to lines with correlation coefficients of 99% or greater. It is seen that from the linear growth rate kinetics analysis, the crystallization behavior changes with pressure. At atmospheric pressure and at 25 MPa, the kinetics exhibit a Regime II-Regime III transition clearly. The kinetics data for atmospheric pressure and 25 MPa essentially coincide. On increasing the pressure to 50 MPa, the data exhibit behavior indicative of a Regime I-Regime II transition. Interestingly, this I-II transition temperature at 50 MPa occurs lower than the II-III transition temperature for the atmospheric data and the 25 MPa data. Over the experimental temperature range, no evidence of a Regime II-Regime III transition is observed at this pressure. At a crystallization pressure of 75 MPa, the data appear to exhibit no regime transition over the experimental temperature range. The 100 MPa kinetics data exhibit a Regime I-Regime II transition. The 150 MPa data exhibited both a Regime I-Regime II transition and a Regime II-Regime III transition. The 200 MPa data exhibited only a Regime II-Regime III transition over the experimental crystallization temperature range. Figure 5.28 shows the behavior of the regime transition supercoolings with crystallization pressure. There does not appear to be a trend in the data. However, the plot of the regime transition temperature as a

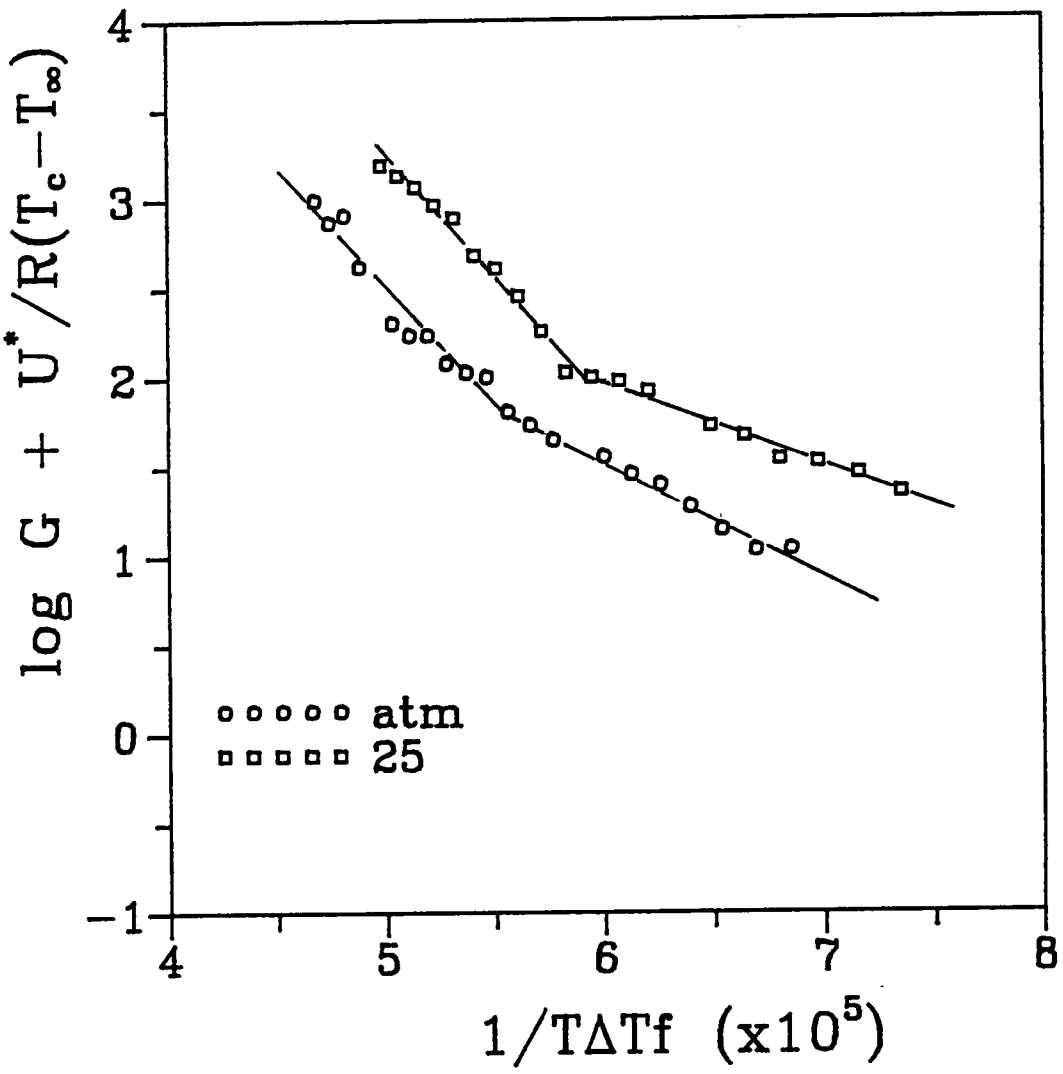


Figure 5.25 Kinetics analysis for isotactic polypropylene crystallized at atmospheric pressure and 25 MPa.

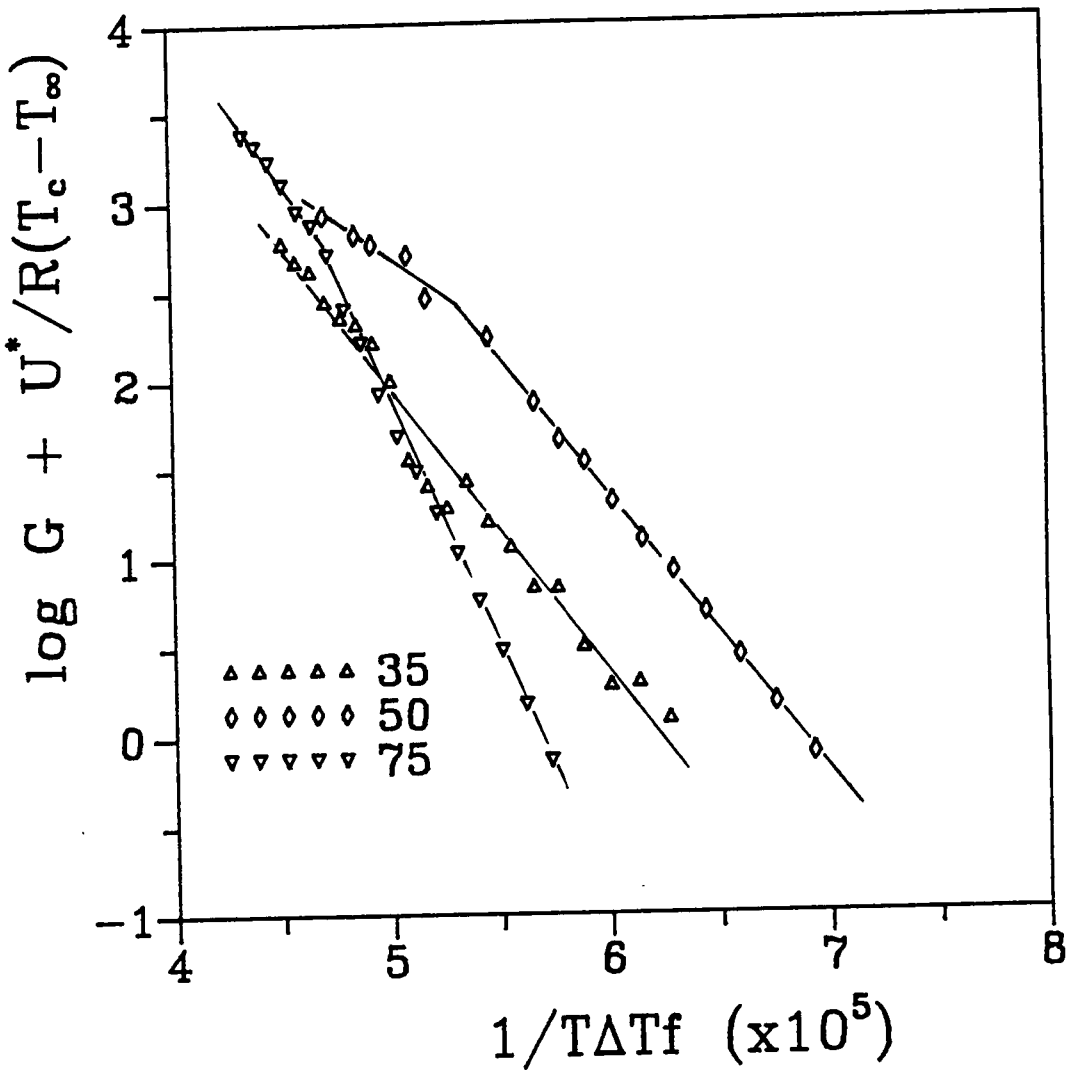


Figure 5.26 Kinetics analysis for isotactic polypropylene crystallized at 35, 50, and 75 MPa.

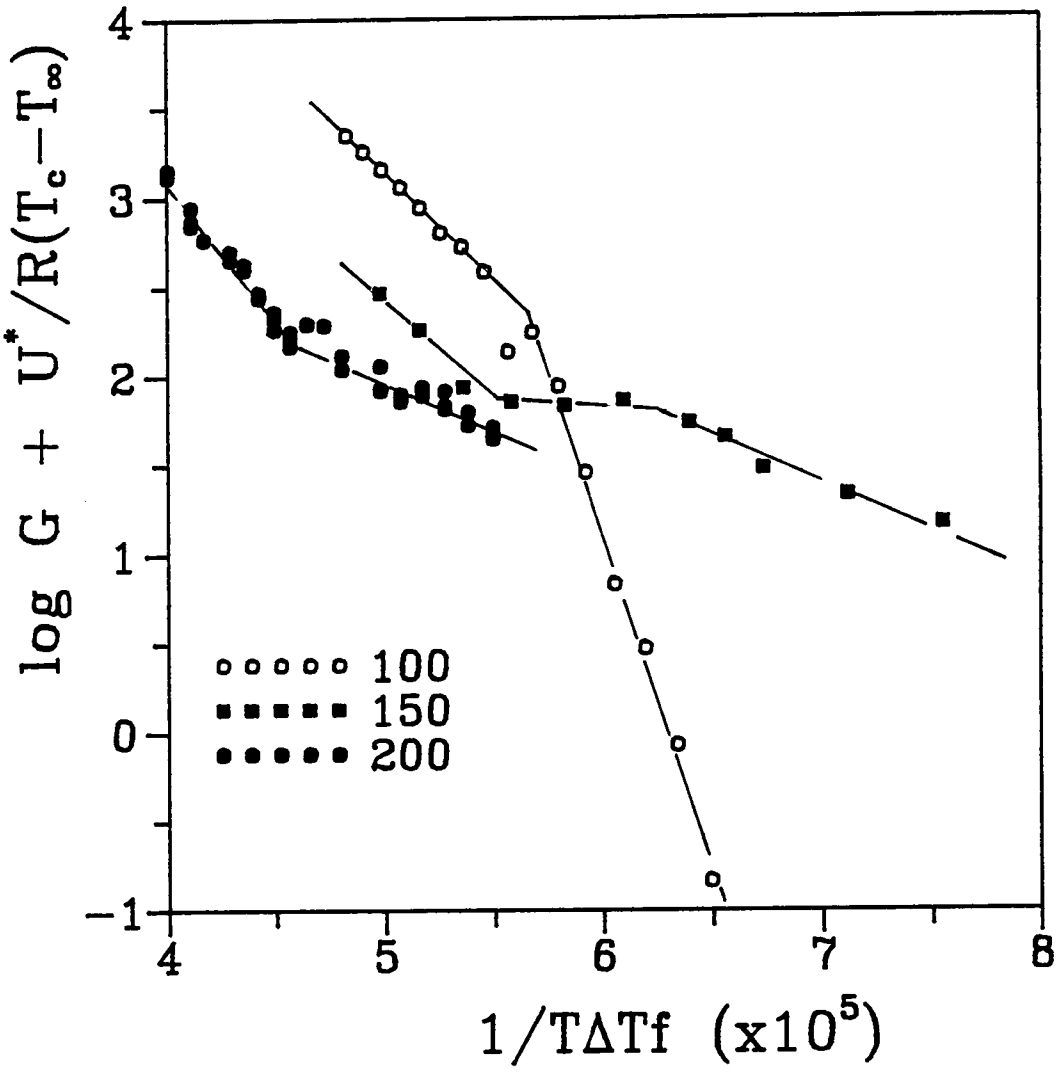


Figure 5.27 Kinetics analysis for isotactic polypropylene crystallized at 100, 150, and 200 MPa.

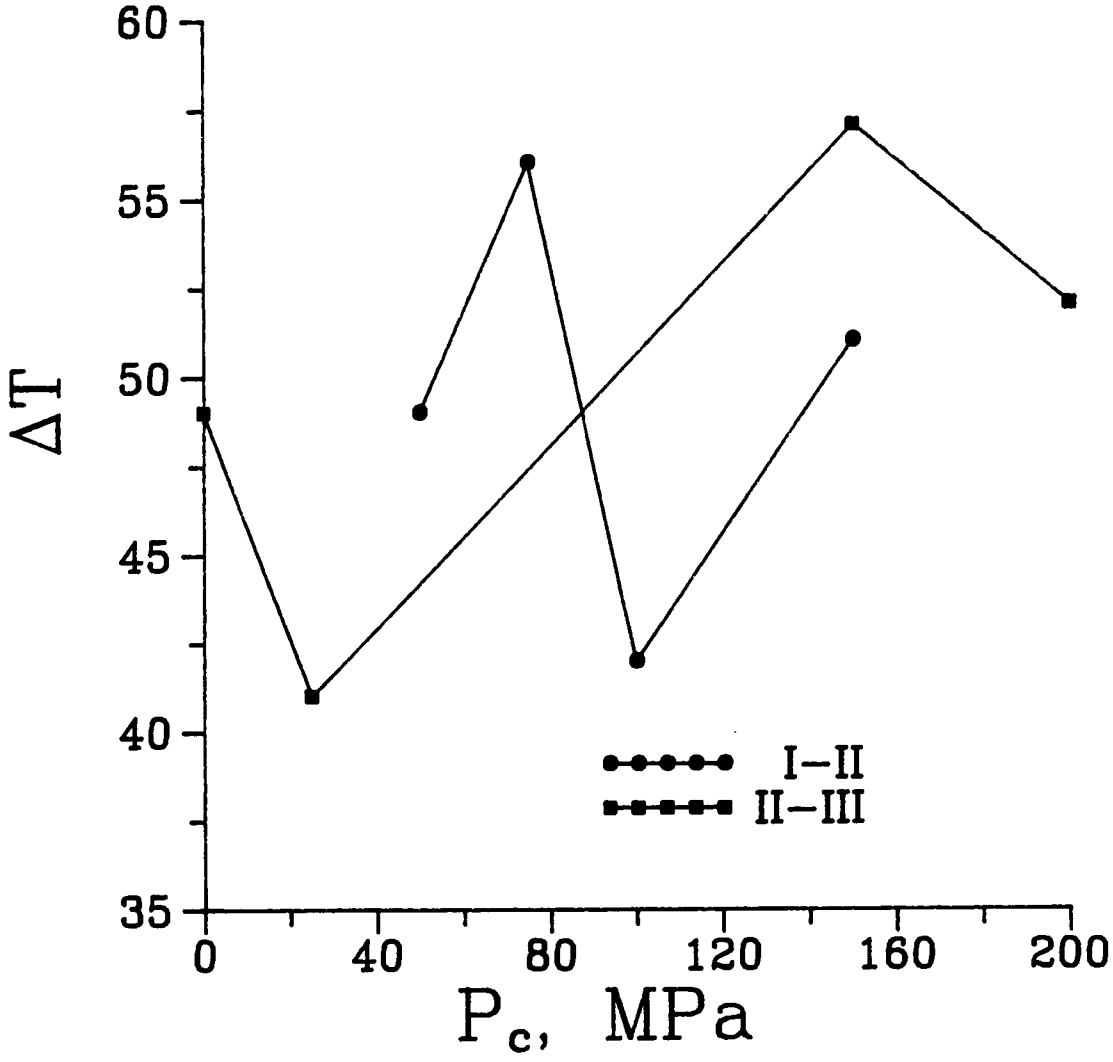


Figure 5.28 Supercooling of regime transitions versus crystallization pressure.

function of crystallization pressure, shown in Figure 5.29, exhibits a linear relation between the Regime II-Regime III transition temperature and the crystallization pressure.

Table 5.13 gives the result of the kinetics analysis of the crystallization of isotactic polypropylene at elevated pressure with experimentally determined T_m^o's. The data are analyzed using a_o and b_o for the α-form monoclinic unit cell. While it is known that the crystal structure of polypropylene changes with pressure, in the pressure range of the experimental kinetic data, the composition is a mixture of crystal forms α and γ. At the highest crystallization pressure studied of 200 MPa, there is approximately 100% of the γ form present. It is known that α and γ crystal forms can coexist on the lamellar level at atmospheric pressure (for low molecular weight polypropylene) and the electron microscopy of elevated pressure crystallized materials up to 100 MPa show evidence of the coexistence of the two crystal forms for elevated pressure and high molecular weight material [144]. Table 5.14 gives the results of the kinetics analysis with equlibrium melting temperatures calculated using dT_m^o/dP of 23°C/100 MPa and 38°C/100 MPa.

The nucleation constant K_g changes with increasing pressure for isotactic polypropylene. This is shown in Figure 5.30 where K_g is plotted versus P_c. K_g increases nonlinearly with increasing crystallization pressure.

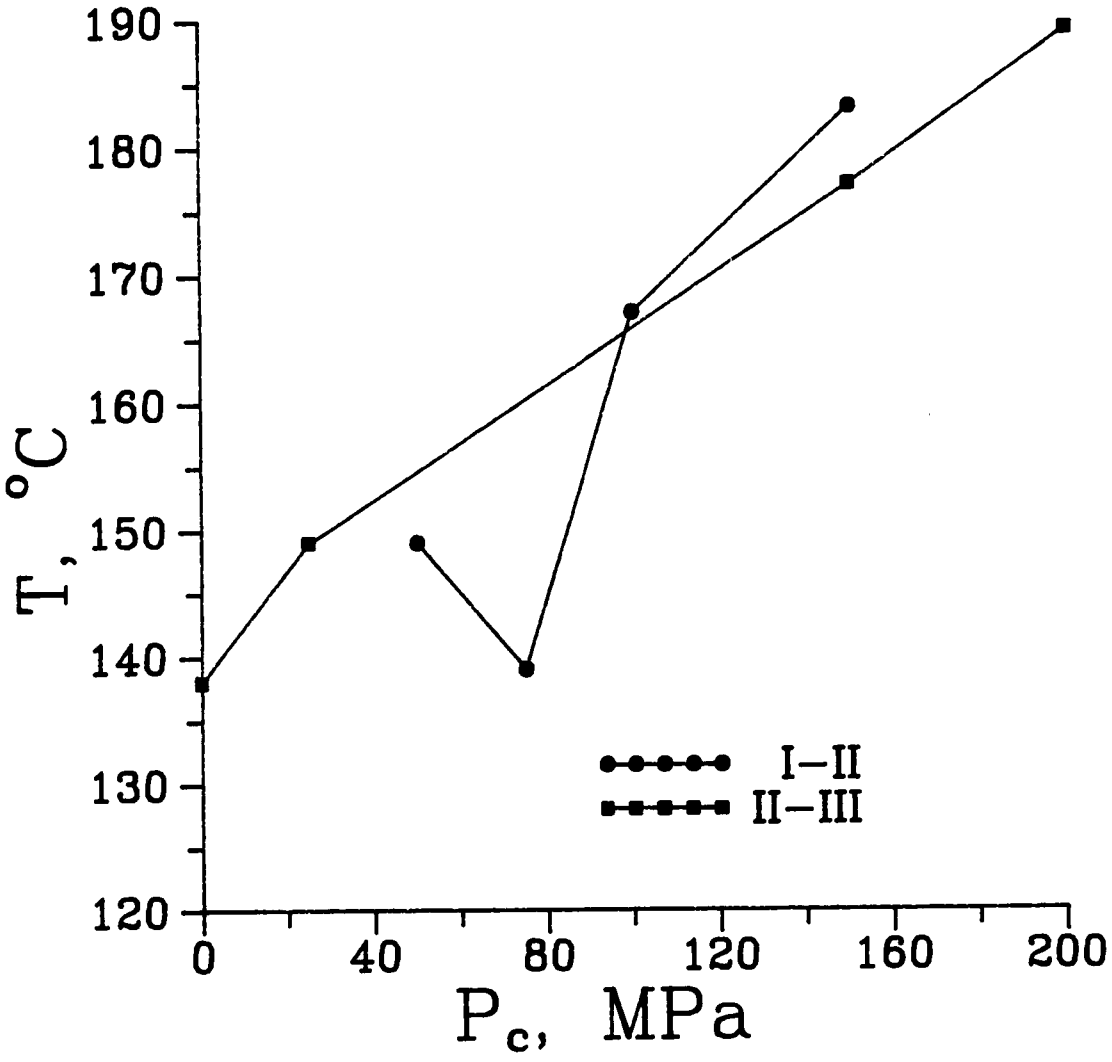


Figure 5.29 Crystallization Pressure P_c (MPa) versus regime transition temperature $T_{II/III}$ for isotactic polypropylene.

Table 5.13 Kinetics Analysis of Isotactic Polypropylene Crystallized at Elevated Pressure.

Data		log G_o	K_g ($\times 10^{-5}$) K^2	$\sigma\sigma_e$ erg^2/cm^4	σ_e erg/cm^2	q kcal /mol	Slope Ratio	ΔT
atm	III	9.34	3.15	743	64.6	6.4	2.14	47
	II	5.36	1.47	694	60.3	6.0		
25	III	10.01	3.11	725	63.0	6.2	2.88	41
	II	4.79	1.08	503	43.7	4.3		
35	I or III	9.92	3.67	851	74.0	7.3		
50	II	4.74	0.92	424	36.9	3.6	3.93	49
	I	10.80	3.62	833	72.4	7.2		
75	II	11.06	4.06	1847	160.6	15.9	1.53	56
	I	15.32	6.21	1412	122.8	12.2		
100	II	9.20	2.79	1254	109.0	10.8	3.11	42
	I	23.74	8.68	1951	169.7	16.8		
150	III	7.76	2.46	523	45.5	4.5	7.0	57
	II	2.74	0.35	149	13.0	1.3		
	I	4.85	1.13	240	20.9	2.1	3.2	51
200	III	9.44	3.63	778	67.7	6.7	2.65	52
	II	4.96	1.37	588	51.1	5.1		

Table 5.14 Kinetics Analysis with Variation of T_m^o for Isotactic Polypropylene Crystallized at Elevated Pressure.

Pressure	Regime	dT_m/dP = 23 K/kbar		dT_m/dP = 38 K/kbar	
		log G_o	K_g x10^{-5}	log G_o	K_g x10^{-5}
atm	III	9.34	3.15		
	II	5.36	1.46		
25	III	10.01	3.11	10.71	3.67
	II	4.79	1.08	5.15	1.32
35	I or III	9.92	3.67	11.10	4.62
50	II	4.74	0.92	5.07	1.22
	I	10.80	3.62	13.04	5.27
75	II	11.06	4.06	13.18	6.09
	I	15.32	6.21	19.63	9.92
100	II	9.20	2.79	11.74	5.09
	I	23.74	8.68	34.63	17.47
200	III	9.44	3.63	14.66	9.64
	II	4.96	1.37	9.09	5.22

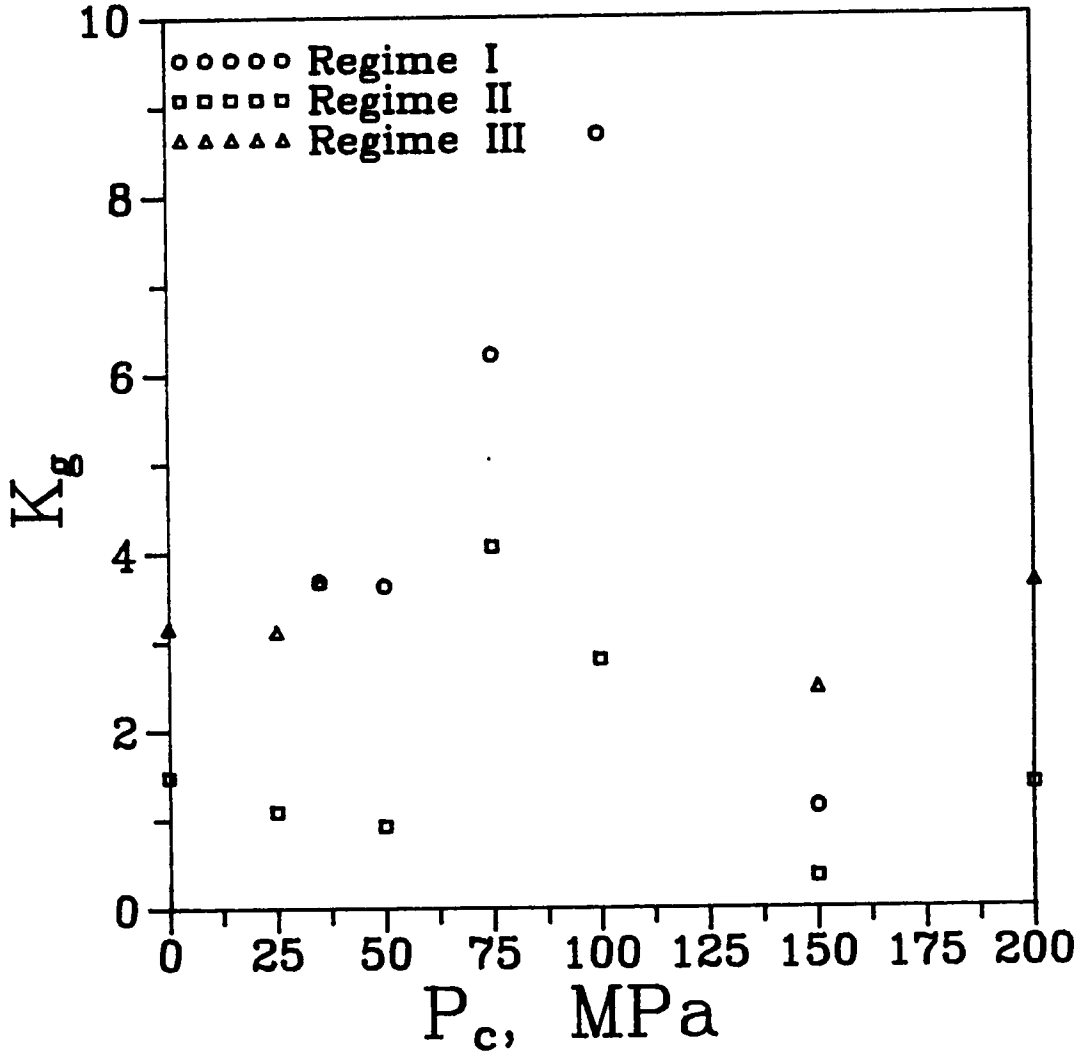


Figure 5.30 Nucleation constant K_g versus crystallization pressure P_c.

Assuming no change in lateral surface free energy σ, the fold surface free energy σ_e also increases with increasing pressure. The work of chain folding q also shows an increase with increasing pressure. For linear polyethylene, this large increase in K_g and σ_e is not observed. Tseng showed that the σ_e values up to 200 MPa are relatively constant. However, in studies of cis-polyisoprene at elevated pressure, a doubling of σ_e was observed over a narrow pressure range. With cis-polyisoprene, the σ_e was fairly constant up to 100 MPa, then increased to nearly double the value. The value of σ_e then remained relatively constant with pressure up to the maximum experimental pressure of 300 MPa. This variation in the effect of pressure on fold surface free energy must indicate a difference in the conformational structure of the folds present in these polymers. For cis-polyisoprene, the change in σ_e with pressure was explained in terms of fold conformation. With the change in stem tilt in the γ lamellae, the fold conformation may also change.

5.4.3 Analysis of Kinetics Results

The linear growth rate curve can be extended to beyond the limits of the experimental data by using the linear growth kinetics analysis results. Figure 5.31 shows such the linear growth rate G as a function of crystallization temperature calculated using the kinetics results for the

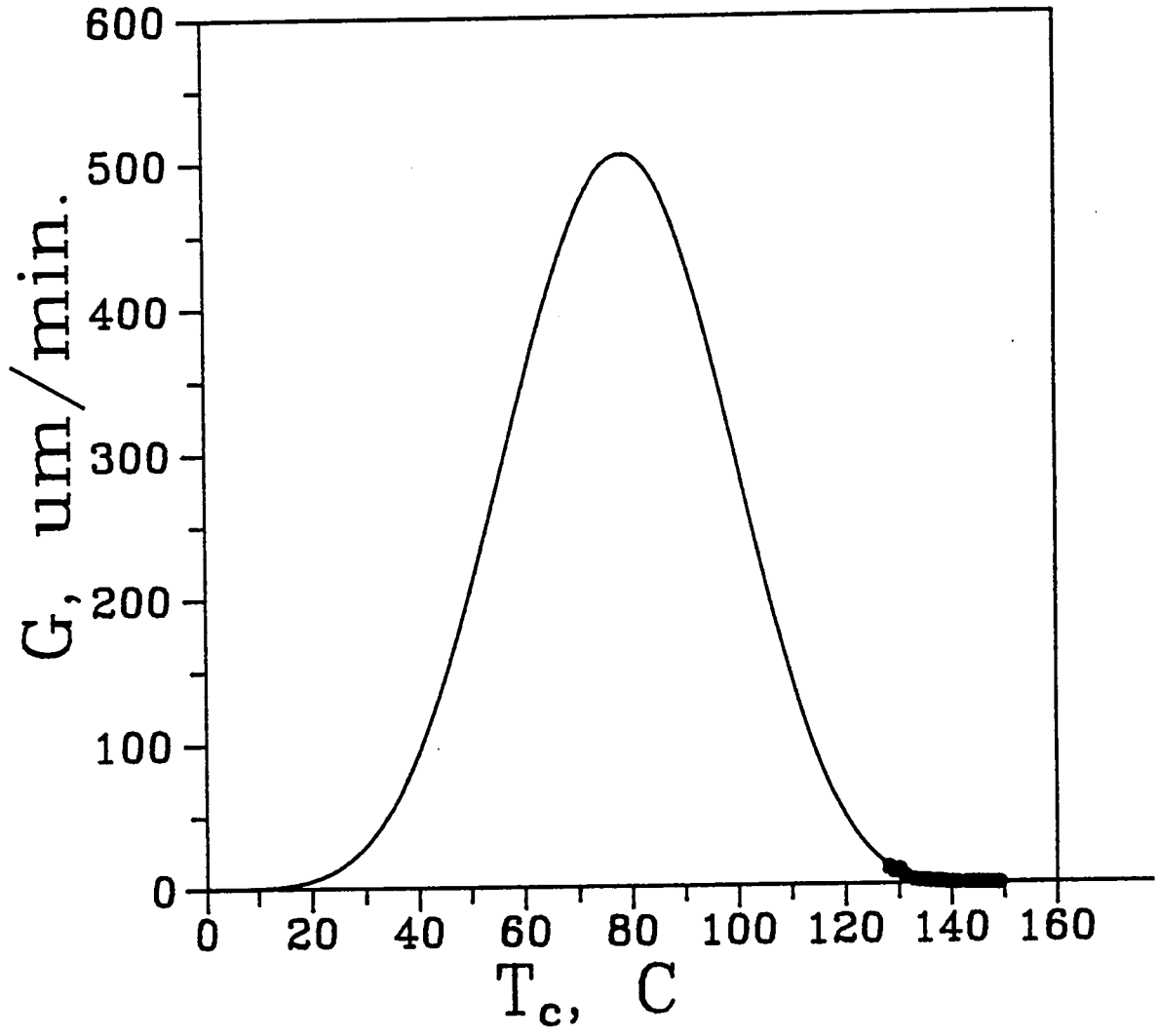


Figure 5.31 Calculated linear growth rates with experimental data superposed on the curve (isotactic polypropylene 151,000 M_w homopolymer, atmospheric pressure).

151,000 M_w homopolymer in equation 2.30. The experimental data are plotted on the curve also. It is seen that the experimental data cover a rather limited portion of the entire curve, well into the nucleation controlled region of the curve. The theoretical curve exhibits a maximum near 80°C. The shape of the growth rate curve is determined by the relative rates of the nucleation and diffusion components of the growth rate equation 2.30. Figure 5.32 shows the theoretical diffusion and nucleation components separately for the 151,000 homopolymer. The two curves cross at approximately 120°C. The shape of the growth rate curve in the region in which regime transitions occur is determined by the supercoolings of the transitions and the shape of the growth rate curves for the regimes. The transitions occur where the growth rate curve of a given regime crosses the growth rate curve of an adjacent regime. In isotactic polypropylene the Regime II-III transition ($\Delta T \approx 50°$) occurs in the nucleation controlled portion of the curve. Figure 5.33 shows schematically the behavior of the growth rates as a function of crystallization temperature if the separate curves for Regimes I, II, and III are represented completely. It is then clearly seen that the experimental growth rate curve is determined by the relative growth rates and the supercoolings.

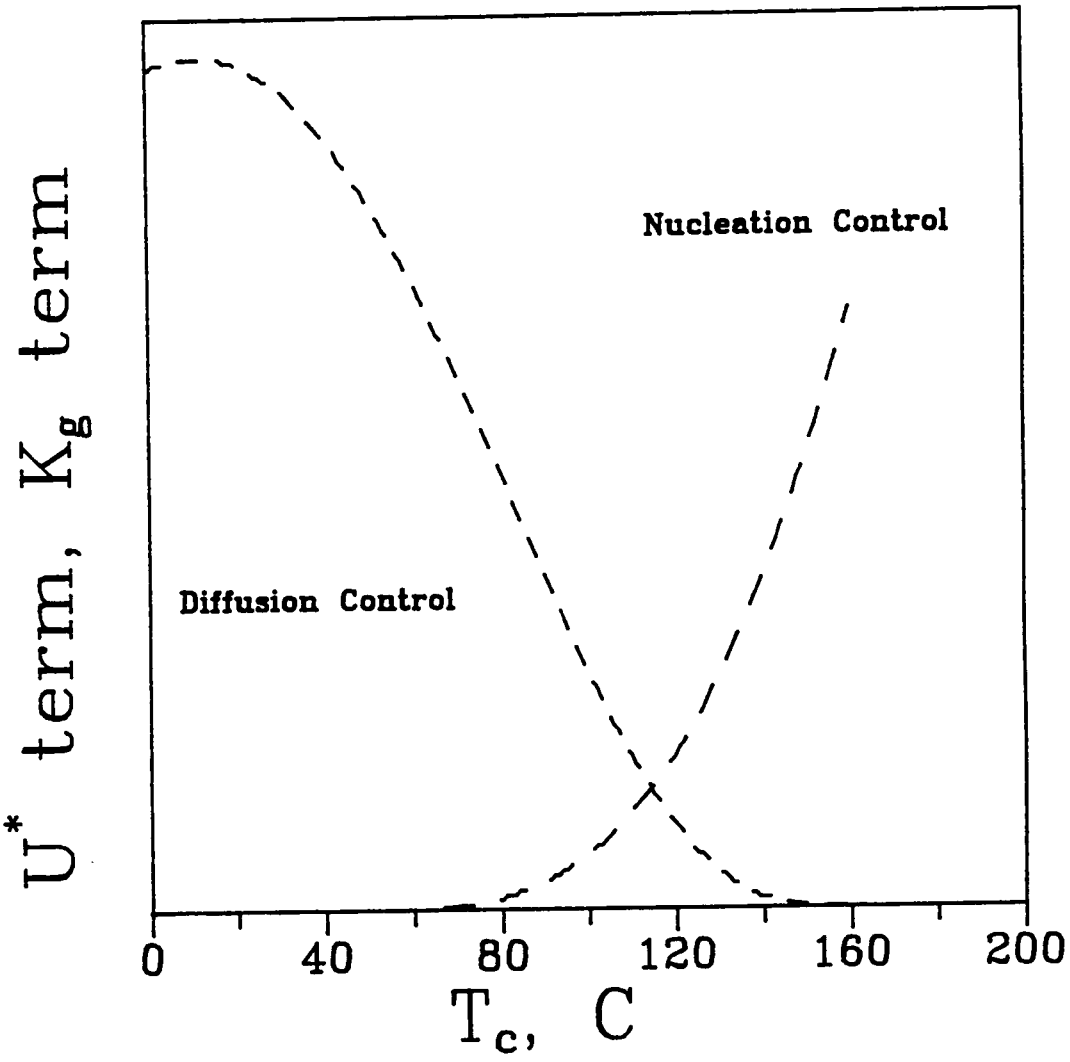


Figure 5.32 Nucleation and diffusion components of linear growth rate for isotactic polypropylene 151,000 M_w homopolymer.

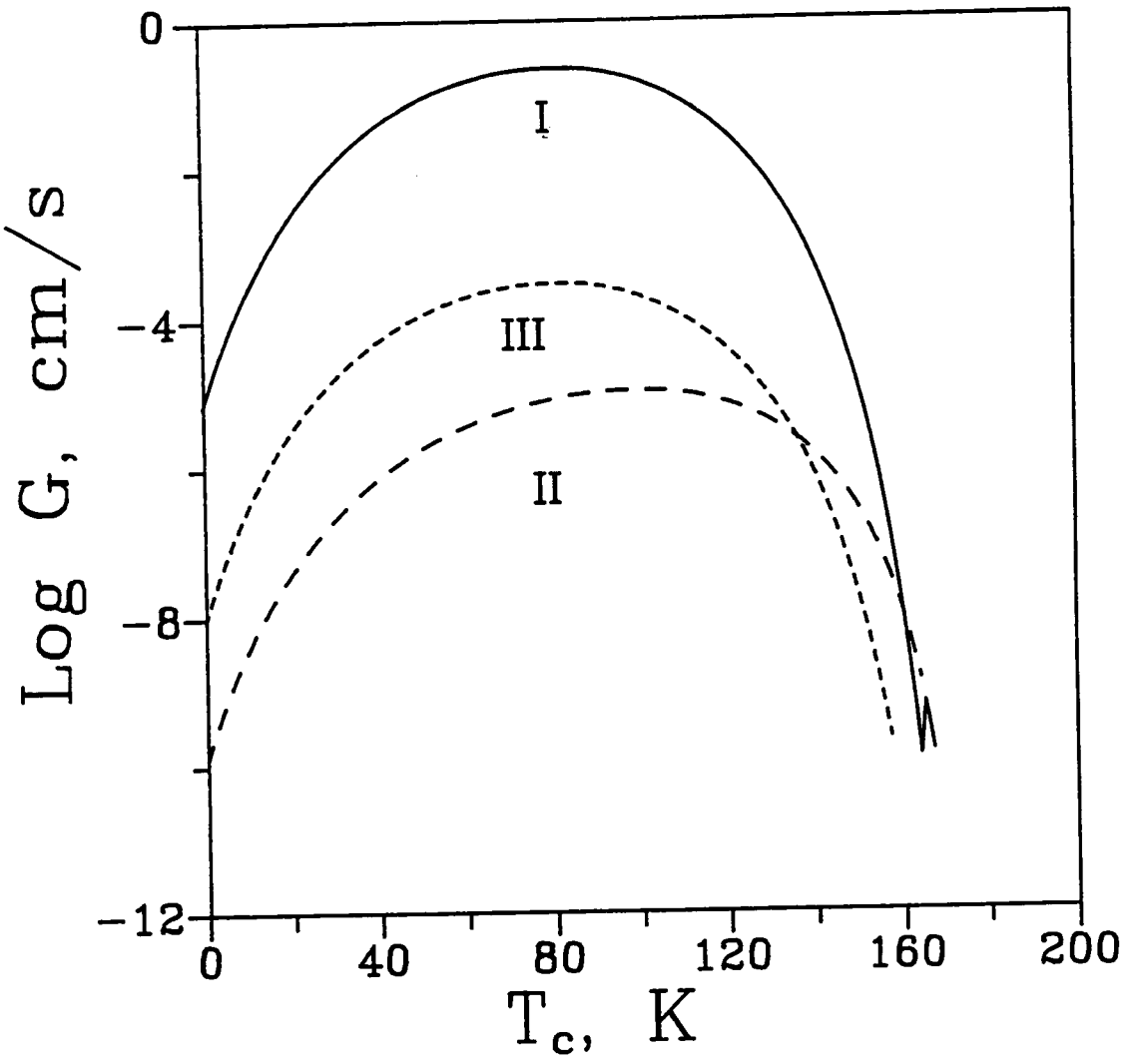


Figure 5.33 Crystallization temperature vs log of the linear growth rate for Regimes I, II, and III calculated from kinetics analysis for isotactic polypropylene 151,000 M_w homopolymer crystallized at atmospheric pressure.

Estimation of isotactic polypropylene Regime I-II Transition

The Regime I-II transition for high molecular weight polypropylene, which has not been observed experimentally, can be estimated from kinetics theory. A Regime I-II transition that has been reported for a low molecular weight isotactic polypropylene can be used as a check of the theoretical calculation. The Regime I-II transition can be estimated using the relationship [144]:

$$\frac{G_I}{G_{III}} = \frac{L_I}{L_{III}} \qquad [5.10]$$

where L, the substrate length, is given by the product of the width a_o and the number of stems on a substrate n. At the Regime I-II transition, the growth rate in Regime I, G_I, must equal that in Regime II, G_{II}. Theory estimates that $L_{III} \approx 2\text{-}4\ a_o$. By assuming that $0.1\ \mu m < L_I < 1\ \mu m$, the Regime I-II transition is then predicted to occur between 153°C and 160°C. This would then give the supercooling ΔT for the Regime I-II transition to occur between 34° and 27°. Janimak reported a Regime I-II transition of $\Delta T = 37°$ for a relatively low molecular weight isotactic polypropylene (M_w = 25,000). Figure 5.33 shows the calculated growth rates for

Regimes I, II, and III for the 151,000 M_w homopolymer as a function of crystallization temperature. In this figure, the Regime I curve is estimated with $L_{III} = 2a_o$, $L_I = 1\mu m$. The agreement between the observed supercooling of the Regime I-II transition and the theoretical estimate is good, considering the difference in molecular weights and the assumptions involved in the theoretical estimation. The ΔT of the Regime I-II transition for polyethylene has been shown to decrease by 1-2° with increasing molecular weight for a similar molecular weight range [145].

Comparison of Linear Growth and Half-Time Kinetics

While it has been shown that the reciprocal bulk crystallization half-time, $1/t_{1/2}$, can be used in place of the linear growth rate in the analysis of secondary nucleation kinetics [146, 147], the application of the half-time data in secondary nucleation kinetics analysis has shortcomings. While the regime behavior can be observed and the supercoolings of regime transitions can be determined, the technique does not yield a true K_g.

It was desired to compare the results from kinetics using linear growth data and half-time data for isotactic polypropylene crystallized at atmospheric pressure and elevated pressure. Also, Hammami has recently shown that the half-time data could be corrected for nucleation effects to yield a K_g equal to that from linear growth kinetics [50].

For heterogeneous, spherulitic crystallization, the Avrami equation rate constant k can be expressed as:

$$k = \frac{4\pi}{3} G^3 N$$

where G is the linear growth rate and N is the nucleation density. Alternately, the rate constant can be related to the half time as:

$$k = \frac{\ln(2)}{(t_{1/2})^3}$$

Now relating the two expressions for the rate constant gives the following expression:

$$\frac{1}{t_{1/2}} = \left[\frac{4\pi}{3} \frac{1}{\ln(2)}\right]^{1/3} N^{1/3} G$$

The equation can then be solved for G and the resulting expression substituted for G into the secondary nucleation theory. Then an expression relating the half-time and nucleation density to the crystallization temperature takes on the form:

$$\left(\frac{1}{t_{1/2}}\right) = \left[\frac{4\pi}{3} \frac{1}{\ln(2)}\right]^{1/3} N^{1/3} \left\{G_o \exp\left[\frac{-U^*}{R(T_c - T_\infty)}\right] \exp\left(\frac{-K_g}{T\Delta Tf}\right)\right\}$$

Rearranging and taking the log of both sides of the equation gives the following:

$$\ln\left(\frac{1}{t_{1/2}}\right)-\left[\frac{1}{3}\ln\left(\frac{4\pi}{3\ln(2)}\right)+\frac{1}{3}\ln(N)\right]+\frac{U^*}{R(T_c-T_\infty)} = \ln(G_o) - \frac{K_g}{T\Delta Tf}$$

Thus one can correct half-time data wih the term $\left[\frac{1}{3}\ln\left(\frac{4\pi}{3\ln(2)}\right)+\frac{1}{3}\ln(N)\right]$ and then obtain K_g from the half-time data directly. Figure 5.34 shows the kinetics analysis for linear growth data, reciprocal half-time data, and nucleation corrected reciprocal half-time data for the 83,000 M_w homopolymer crystallized at atmospheric pressure. In all cases, the data exhibited two regimes. However, the nucleation correction did not produce a K_g value comparable with that from linear growth kinetics. Table 5.15 gives the results of the kinetics analysis for atmospheric pressure data. Table 5.16 gives the results of the kinetics analysis for the elevated pressure data. In the case of the atmospheric pressure 83,000 M_w data, the K_g for nucleation corrected half-time for Regime II is further from the linear growth K_g than before correction. The half-time data for elevated pressure also were not corrected to the linear growth value by the nucleation correction. Also, the half-time data for elevated pressure, which showed a Regime II-Regime III transition at all pressures, did not exhibit a Regime I-Regime II transition after correction as the linear

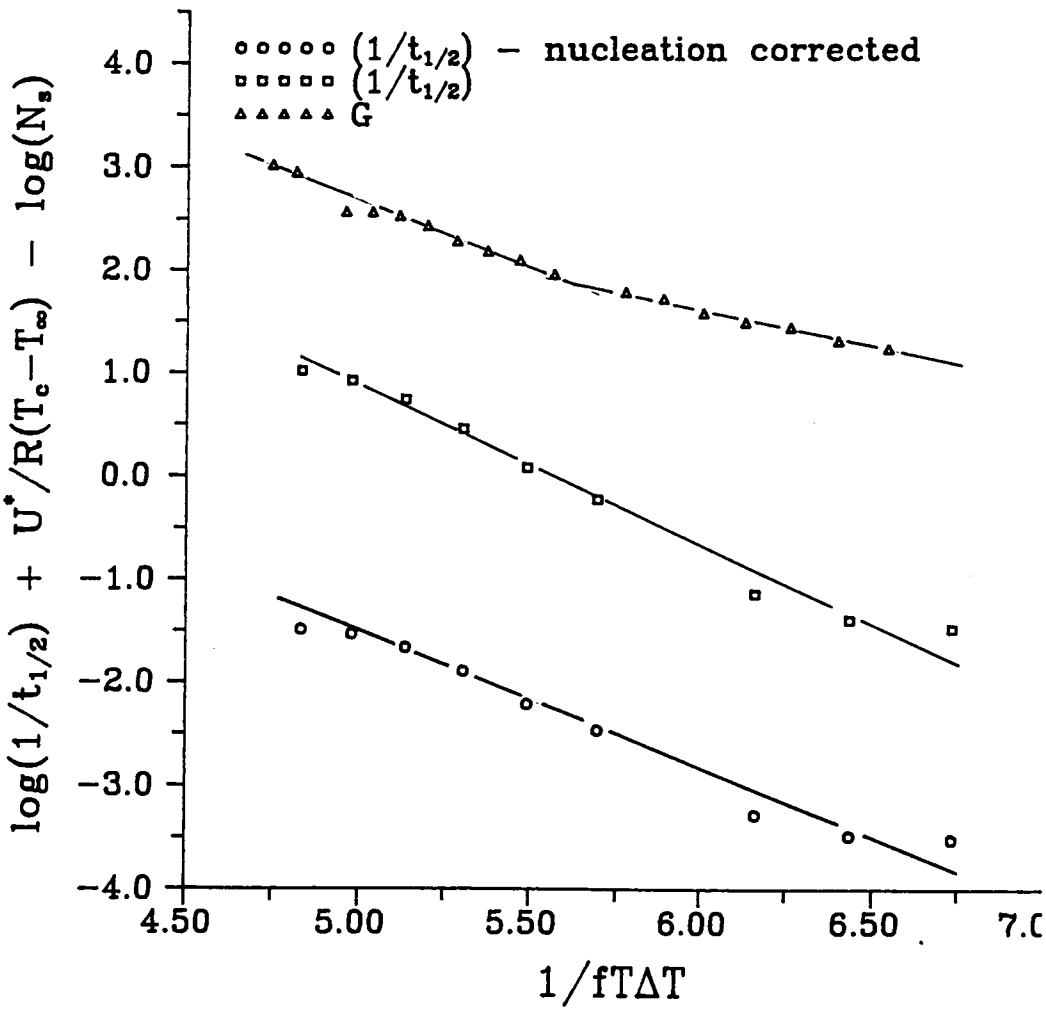


Figure 5.34 Kinetics analysis comparison for linear growth data, half-time data, and nucleation corrected half-time data.

Table 5.15 Comparison of Kinetics Analysis from Linear Growth Data, Half-Time Data, and Nucleation Corrected Half-Time Data for Atmospheric Pressure Crystallization.

		Linear Growth		Half-Time		Nucleation	
Sample	Regime	$K_g x 10^{-5}$	log G_o	$K_g x 10^{-5}$	log G_o	$K_g x 10^{-5}$	log G_o
83,000	II	1.550	5.66	2.12	4.83	3.09	4.99
homo.	III	3.358	9.93	5.20	11.94	5.195	9.70
151,000	II	1.786	4.55	3.41	8.24	3.136	5.25
homo.	III	2.915	9.34				
151,000	II	1.821	6.01	2.30	5.21	2.164	2.93
(copoly)	III	2.859	8.44				

Table 5.16 Comparison of Kinetics Analysis from Linear Growth Data, Half-Time Data, and Nucleation Corrected Half-Time Data for Elevated Pressure Crystallization.

		Linear Growth		Half-Time		Nucleation	
Pressure	Regime	$K_g x 10^{-5}$	log G_o	$K_g x 10^{-5}$	log G_o	$K_g x 10^{-5}$	log G_o
atm	II	1.786	5.36	2.12	4.83	3.136	5.25
	III	2.915	9.34	5.2	11.94		
25	II	1.08	4.79	0.41	1.55	0.216	
	III	3.11	10.01	1.70	4.85	0.616	
50	I	3.62	10.80				
	II	0.92	4.74	1.06	3.59	0.647	0.71
	III			2.14	6.46	1.353	2.54
75	I	6.21	15.32				
	II	4.06	11.06	1.36	4.04	0.818	0.72
	III			2.60	6.97	1.596	2.48
100	I	8.68	23.74				
	II	2.79	9.20	0.99	3.18	0.556	0.15
	III			2.28	6.47	1.348	3.71

growth data did for 50, 75, and 100 MPa. Hammami concluded that the nucleation correction treatment for half-time data was valid. The observed slope differences between linear growth kinetics and half-time kinetics were attributed in large part to the fact that bulk crystallization incorporates nucleation and growth while the linear growth kinetics do not. It is not clear why the nucleation correction technique appeared to be valid for Hammami's data but does not correct the data in the present investigation. It is possible that the narrow spread of Hammami's K_g and C_3 values (all of which were Regime III) and the relatively similar nucleation densities led to a fortuitous coinciding of the linear growth kinetics slopes and the nucleation corrected half-time slopes.

With the apparent failure of the nucleation corrected half-time kinetics analysis to predict the K_g of the linear growth rate kinetics analysis, it was desired to attempt to explain the differences between the two kinetics analyses on components other than nucleation. With polypropylene at atmospheric and elevated pressure, a significant amount of the material can crystallize as a branching component. This component, which could be considered as an in-filling, would not be accounted for in the Avrami theory without modification but would contribute to the observed bulk crystallization. It has been shown that the Avrami analysis

for polymers frequently gives nonintegral n values. Therefore, an attempt was made to calculate the bulk crystallization behavior from the linear growth data and compare with the observed bulk crystallization behavior in order to estimate the branching. The difference should be due to 'secondary' crystallization processes such as branching and in-filling. The Avrami equation for the depolarized light intensity experiment can be expressed as:

$$\exp\left[-\left(\frac{4\pi}{3}NG^3\right)t^3\right] = \frac{I_\infty - I_t}{I_\infty - I_o}$$

for spherulitic growth. The bulk crystallization behavior can then be calculated from the linear growth and nucleation density. Figure 5.35 shows the plot of the comparison of experimental bulk crystallization and linear growth calculated bulk crystallization. It is observed that the two curves are different, with the experimental bulk crystallization showing a faster crystallization rate. The values of the Avrami exponent were similar (3 for the calculated data and 3.1 for the experimental data), but the values of the Avrami k were different by an order of magnitude. However, this order of magnitude difference does not cause an order of magnitude change in the time required for the completion of primary crystallization as determined from the bulk crystallization curve. It is possible that the

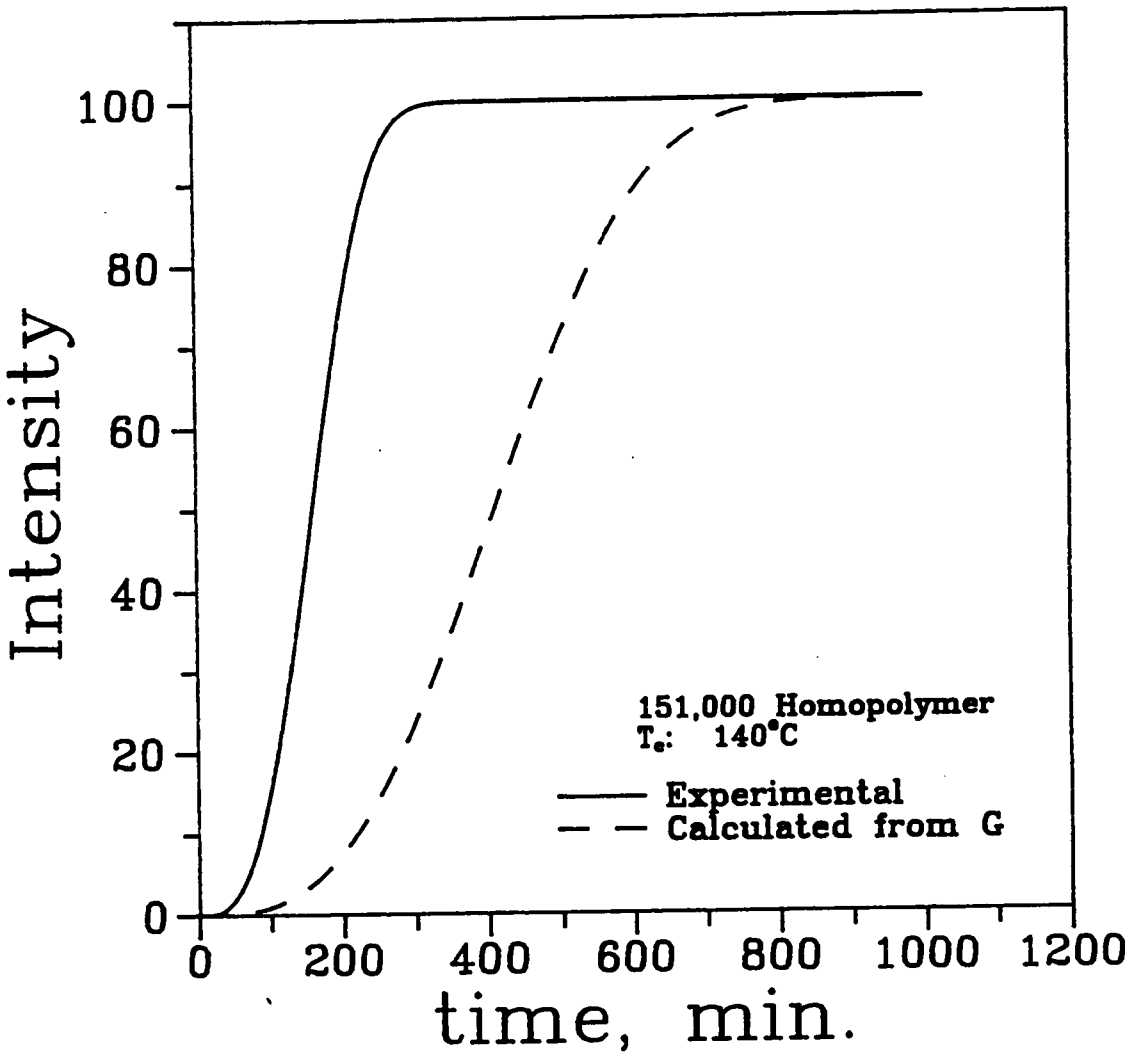


Figure 5.35 Comparison of experimentally observed bulk crystallization behavior and that theoretically calculated from linear growth rate for isotactic polypropylene homopolymer T_c = 140°C.

differences between the two bulk crystallization curves are due to secondary crystallization and branching. The expression of Hammami for nucleation correction could possibly be adjusted with a factor to account for the secondary crystallization and the radial-tangential branching.

5.4.4 Pressure Dependence of σ_e

The observed change in the nucleation constant K_g with pressure can be explained on the basis of several possibilities. These include a change in crystal structure, heat of fusion, crystallization regime, growth face, or fold conformation. Each change and its affect on σ_e will now be discussed.

Change in Crystal Structure

Pressure-induced changes in crystal structure have been observed for several polymers. This change in crystal structure could result in a change in σ_e if the fold conformation changes . A fold conformational change almost certainly would be required to connect adjacent stems in different crystal structures. The change in crystal structure can also involve changes in heat of fusion and melting temperatures. It is known that the melting temperature at atmospheric pressure of the γ form is lower than that of the α form by $\approx$10-15°C. However, this

comparison of melting temperatures is for a low molecular weight γ (< 15,000 M_w) and a relatively high molecular weight α. When the molecular weight difference is accounted for, the melting temperatures of the α and γ forms are similar. This seems to indicate that the observed atmospheric melting behavior of elevated pressure crystallized polypropylene is partly due to the melting of the thinner γ lamellae followed by the melting of recrystallized material.

Change in Heat of Fusion

A change in the heat of fusion with pressure could result in an apparent change in σ_e. This change in σ_e would be observed in values determined from both the lamellar thickness and the growth rate. For this analysis, the Δh_f was assumed constant at the atmospheric pressure value since no information was available on the pressure dependence of Δh_f of isotactic polypropylene. While some dependence on pressure may be expected, this should not be large. A step change could be expected with a change in crystal structure.

Change in Crystallization Regime

The value of σ_e determined from the experimental kinetics data is dependent on the crystallization regime assumed as well as the value of σ, b_o, Δh_f, and T_m^o. The change in Δh_f with pressure has been discussed. A change in b_o should not be large, based on the monoclinic and

orthorhombic crystal structures. The lateral surface energy σ may change, particularly in light of Hoffman's recent definition of σ being due to the change in entropy from the melt state to the crystal state. The entropy of the monoclinic and orthorhombic crystal structures should be different, based on the difference between chain stem arrangements within the two crystal structures. However, this change should not be large.

Change in fold conformation

The conformation of a tight fold connecting two adjacent stems can change if the crystal structure changes or if the growth face changes. With a change in either, the separation and orientation of chain stems can change. No change in growth face has been reported for atmospheric pressure crystallization of isotactic polypropylene, but a change in growth face has been suggested for cis-poly(isoprene) β crystals [149].

5.4.5 Poisoning

From the optical microscopy and the electron microscopy results, it is clear that α polypropylene and γ polypropylene do not form distinct spherulites in the pressure range where both forms exist. Thus, the two forms must be present in the same spherulite, most likely as different lamellae.

As the γ content increases, the kinetics undergo significant changes. However, the changes observed cannot be assigned to α polypropylene or γ polypropylene. At lower pressures (< 50 MPa), it would seem that the α form generates the dominant lamellae. The observed Regime II-III transition reflects this. The observed Regime I-II transition at P_c > 35 MPa would indicate a change from α dominant to γ dominant lamellae. The kinetics behavior at 200 MPa, where the Regime II-Regime III transition is observed, should be attributed to γ-only growth. On the basis of the Brückner-Meille γ polypropylene crystal structure, the α form and the γ form differ only in terms of sheets of non-parallel chains. If, during α-dominated growth, a chain attampted to deposit on the growth face in a non-parallel fashion, the growth face would be 'poisoned' with the chain stem out of crystallographic register. This condition can be illustrated by Figure 5.36a which shows a schematic representation of an α growth face and the poisoning by a non-parallel chain deposited on the growth face. This poisoning would reduce the rate of secondary nucleation. Under conditions of γ-dominated growth, the γ growth front could be poisoned in like manner by the deposition of a chain in a parallel fashion. This condition is depicted schematically in Figure 5.36b. The change in secondary nucleation could be responsible for the observed shift in regimes.

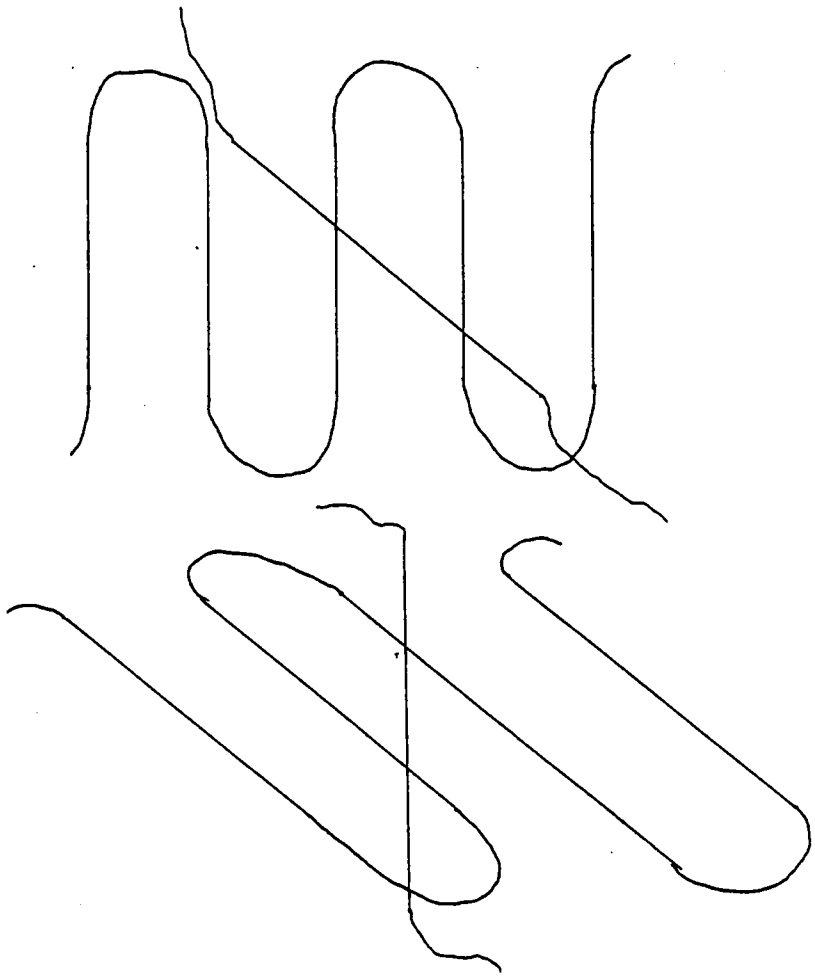


Figure 5.36 Schematic of growth front poisoning for isotactic polypropylene; A. α growth front, B. γ growth front.

The $\sigma\sigma_e$ was observed to increase with increasing pressure in the crystallization pressure range where both α and γ polypropylene are present. If the growth is determined by the dominant lamellae, one would not necessarily expect the change in $\sigma\sigma_e$ to be gradual, but rather a step change with change in the crystal structure would be expected. If one considers the relative rates of surface nucleation and lateral spreading, one can see that under conditions of poisoning, that the kinetics change. This is due to the effect of the rate of surface nucleation being reduced relative to the rate of lateral spreading. Thus the observed increase in the $\sigma\sigma_e$ value is a reflection of the change in the relative rates. .

Chapter 6

Conclusions

The elevated pressure crystallization of isotactic polypropylene showed unusual behavior. Linear growth rates shifted to higher temperature with increasing pressure but the shift was not linear or even consistent. On analyzing the kinetics data with secondary nucleation theory, unusual behavior occurred that has not previously been reported for polymers. At intermediate pressures, where a mixture of the two crystal structures is present, the crystallization mechanism changed as seen by the change from a Regime II-III transition at atmospheric pressure to a Regime I-II transition. This is an indication of an overall reduction in the rate of surface nucleation relative to the rate of lateral spreading. This reduction in surface nucleation was explained on the basis of a 'poisoning' or deactivation of the growth front of a given lamella by deposition of a chain stem in a manner inconsistent with that lamella's crystal structure. Indirect evidence that supported this hypothesis was the 150 and 200 MPa kinetics results which again showed a Regime II-Regime III transition. This pressure region is sufficiently high to ensure that a significant portion of the material is in the γ form. A mechanism to explain this 'poisoning' behavior was developed on the basis of the orthorhombic crystal structure for the γ form.

6.1 Morphology

While the morphology of the elevated pressure crystallized samples retained a spherulitic texture, the nature of the spherulites had changed. Optical microscopy revealed a change in the nature of the birefringence of the spherulites, which can be related to a change in the lamellar structure as exhibited at atmospheric pressure. The nature of the lamellar structure at atmospheric pressure has been shown to consist of a complex network of near orthogonal branching lamellae ('cross-hatching'), which changes with crystallization pressure. Indeed, the transmission electron microscopy revealed a change in the lamellar habit of the elevated pressure samples. It is observed that essentially all of the 'cross-hatch' branch lamellae are extinguished with only moderate application of pressure (<50 MPa). With increasing pressure, the lamellae appear more curved, and additional branching angles were observed. It is known that isotactic polypropylene changes crystal structure with increasing crystallization pressure. This change in structure is not abrupt, but rather the composition of the polypropylene changes from all α form (monoclinic) at atmospheric pressure to all γ form by approximately 200 MPa. At pressures between atmospheric and 200 MPa, the two forms apparently coexist, possibly on the lamellar level. The SAXS data showed a decrease in lamellar thickness with increasing

pressure to a value at 200 MPa that was considerably less than that at atmospheric pressure. The orthorhombic unit cell predicts this change on the basis of the angle between chains within the lamellae.

6.2 Thermal Behavior

The equilibrium melting temperatures of the elevated pressure crystallized samples were determined from T_m versus Tc plots for all pressures and from T_m versus 1/l plots for 100 and 200 MPa. The results showed that the T_m^o does not shift simply with pressure. At low pressures, the dT_m^o/dP is approximately 23°C/100 MPa, but the 150 MPa and 200 MPa melting data did not fall on this line but rather above the extrapolated line. UP to 100 MPa, the Clapeyron equation fit the data well, except for the 75 MPa melting temperature. The increase at 150 and 200 MPa would result in a near doubling of the dT_m^o/dP value.

6.3 Crystallization behavior

While the nature of the tangential lamellar branching in isotactic polypropylene is unique among polymers, the nature of the changes in isotactic polypropylene crystallization with pressure was also unusual. At low pressures (<35 MPa), the kinetics exhibited behavior consistent with that at atmospheric pressure. However, with further increase in pressure to 100 MPa, the kinetics showed a change from Regime

II - Regime III behavior to Regime I - Regime II behavior with comparable growth rates. As the pressure was further increased, the kinetics again showed a change from the Regime I - Regime II behavior, back to a Regime II - Regime III behavior at 150 and 200 MPa. This was explained on the basis of the change in crystal structure and a poisoning mechanism was proposed to account for the crystallization behavior.

6.4 Growth Front 'Poisoning'

The idea of competition between two crystal structures resulting in a deactivation of the lamellar growth front is novel for polymers. The experimental evidence, however, supports such a hypothesis. The SAXS data supports the Brückner structure in that at 145°C, the long period of all elevated pressure samples approached that of the atmospheric pressure sample. This indicates that if the stem length is fixed by the supercooling, then on transformation of the γ to the α, the lamellar thickness should increase by $\approx$1.55 times the initial value. This increase is indeed observed with the change with temperature of long period at atmospheric pressure taken into account. The literature had proposed that the transformation of γ to α was a solid-solid transformation without melting occurring. This was based on the triclinic structure that was only a slight distortion of the a monoclinic and not the non-parallel arrangement of chain stems proposed in Brückner's model. It is hard to

visualize a solid-solid transformation below a melting temperature for chain folded materials, such that the chain stems could go from non-parallel in the γ to parallel in the α. However, in comparing the DSC at atmospheric pressure of pressure crystallized samples to the observed SAXS behavior, one must conclude that at 145°C, the material is not significantly melted, and not melted to the extent to account for complete melting of all γ present ($\approx$50% - 100%). This would imply that the material do not enter a true melt state, but some intermediate disordered state (condis) that has sufficient mobility so that the nonparallel chain stems can realign to a parallel arrangement. The two structures, one with parallel chain stem arrangement and the other with non-parallel chain stem arrangement, cannot crystallize together. The necessary chain stem arrangement of one structure would not allow the crystallization of the other structure.

Chapter 7

Further Work

7.1 T_m^o of γ Polypropylene

The equilibrium melting temperature of γ polypropylene has not been evaluated at atmospheric pressure. This can be accomplished by two independent methods. First, a low molecular weight isotactic polypropylene that crystallized in the γ form can be studied. The melting temperature and the lamellar thickness as a function of isothermal crystallization temperature can be used to evaluate T_m^o. The second method can employ a high molecular weight isotactic polypropylene. The sample can be crystallized at pressures above 200 MPa to ensure complete crystallization in the γ form as a function of crystallization temperature. The T_m^o at each pressure can then be evaluated in a manner similar to the atmospheric pressure data. The atmospheric pressure T_m^o can then be evaluated from the T_m^o versus P_c data extrapolated to atmospheric pressure. Independently evaluating the T_m^o will allow for the effect of molecular weight on T_m^o. The fold surface free energies can be evaluated from the T_m versus 1/l data for the low molecular weight atmospheric pressure data and for the high molecular weight elevated pressure data and compared.

7.2 Stem Length Determination in α and γ PP

To further confirm the results of the SAXS analysis that indicate a decrease of lamellar thickness with increasing pressure in accord with the orthorhombic structure, a study of the Raman longitudinal accoustic mode (LAM) can be undertaken. The Raman LAM can give the stem length in the lamellae which can then be compared to the estimated stem length fom the SAXS analysis.

7.3 Copolymer Studies

Additional studies of polypropylene copolymers can be performed at atmospheric pressure and elevated pressure. A series of increasing ethylene content copolymers with random distribution of the comonomer can be studied at atmospheric pressure to better understand the effect of the comonomer on the crystallization behavior. This information could include an analysis of comonomer incorporation into the crystal as a function of content. Additional comonomers can be studied as well.

7.4 Additional Elevated Pressure Studies

The effect of pressure on the melt state can be studied in further detail by changing the melt conditions and following the effect on the crystallization behavior. Melting at atmospheric pressure followed by crystallization at elevated pressure can be compared to melting at elevated

pressure followed by crystallization at elevated pressure. The state of the melt could be significantly affected by the application of pressure which could result in changes in the crystallization behavior. Additional electron microscopy studies can resolve the lamellar thickness changes directly for the γ form of isotactic polypropylene.

References

1. A. Keller, Phil. Mag., 2, 1171 (1957).

2. E.W. Fischer and G.F. Schmidt, Angew. Chem. 74, 551 (1962) .

3. P.H. Till, Jr., J. Polym. Sci., 24, 301 (1957) .

4. G. Natta and P. Corradini, Nuovo Cimento Suppl 15, 1 (1960).

5. H.D. Keith et al., J. Appl. Phys 30, 1485 (1959).

6. A. Turner-Jones et al., Makrom. Chem. 75, 134 (1964).

7. S. Brückner and S.V. Meille, Nature 340, 455 (1989).

8. D.R. Morrow and B.A. Newman, J. Appl. Phys. 39, 4944 (1968).

9. F.J. Padden and H.D. Keith, J. Appl. Phys. 30, 1479 (1959) .

10. D.R. Norton, Ph.D. dissertation, Univ. of Bristol, 1984.

11. D.R. Norton and A. Keller, Polymer 26, 704 (1985) .

12. A.J. Lovinger, J.O. Chua, and C.C. Gryte, J. Polym. Sci. Polym. Phys. Ed. 15, 641 (1977) .

13. J. Henson, M.S. thesis, Univ. of Tenn. Knoxville, 1979.

14. J.W.S. Hearle, "Polymers and Their Properties.", vol. 1, John wiley and Sons, New York, 1982.

15. B. Lotz and Wittmann, J. Polym. Sci., Phys. 24, 2017 (1986).

16. F.J.Padden, Jr. and H.D. Keith, J. Appl. Phys. 44, 1217 (1973).

17. P.J. Flory, J. Am. Chem. Soc., 84, 2857 (1962).

18. K. Hermann, O. Gerngross, and W. Abitz, Z. Phys. Chem., 10, 371 (1930).

19. E.W. Fischer, Z. Naturforsch, 12A, 1171 (1957).

20. M.I. Bank and S. Krimm, J. Polym. Sci., Polym. Symp. 53, 347 (1975)

21. J.D.Hoffman, Faraday Discuss. Chem. Soc., 68, 378 (1979)

22. C.M.Guttman and E.A. Dimarzio, Macro. 15, 525(1982).

23. J.D.Hoffman, Polymer 24, 3 (1983).

24. E.W.Fischer, H. Godddar, and G.F. Schmidt, Proc. Conf. on Polymer Struct. and Mech. Prop., April 19-21 (1967).

25. L Mandelkern. Proc. Sagamore Army Material Res. Conf., 20th, Syracuse Univ. Press, Syracuse, New York (1975).

26. P.J. Flory and D.Y. Yoon, Nature 272, 226 (1978).

27. J.D.Hoffman, and R.L. Miller, Macro. 21, 3038 (1988).

28. ,E.A. DiMarzio, C.M. Guttman, and J.D. Hoffman, Faraday Discuss. Chem. Soc. 68, 210 (1979).

29. J.I. Lauritzen,Jr., and J.D. Hoffman, J. Res. Nat. Bur. Stand. 64A, 73 (1960).

30. F.P. Price, J. Polym. Sci. 42, 49 (1960).

31. Frank, F.C. and M. Tosi, Proc. Roy. Soc. A265, 323 (1961).

32. D.M. Sadler, Polymer 24, 1401 (1983).

33. J.I. Lauritzen, J.I., and J.D. Hoffman, J. Appl. Phys. 44, 4430 (1973).

34. P.J. Phillips, Polymer Preprints 20, 483 (1979).

35. J.D. Hoffman and J.J. Weeks, J. Res. Nat. Bur. Stand. A66, 13 (1962).

36. T. Suzuki and A.J. Kovacs, Polymer J. 1, 82 (1970).

37. J.D. Hoffman and J.J. Weeks, J. Chem. Phys. 37, 1723 (1962).

38. J.I. Lauritzen, Jr., J. Appl. Phys., 44, 4353 (1973).

39. I.C. Sanchez, and E.A. Dimarzio, J. Res. Nat. Bur. Stand. A76, 213 (1972).

40. J.D. Hoffman, Polymer 26, 1763 (1985).

41. C.M. Guttman, E.A. DiMarzio, and J.D. Hoffman, Polymer 22, 1466 (1981).

42. J.J. Point and A.J. Kovacs Macro. 13, 399 (1979).

43. J.I. Lauritzen, Jr., and Passaglia, J. Res. Nat. Bur. Stand. A71, 261 (1967).

44. J.D. Hoffman et al., J. Res. Natl. Bur. Stand. 79A, 671 (1975).

45. P.J. Phillips and N. Vatansever, Macro. 20, 2138 (1987).

46. S.Z.D. Cheng, J. Chen, and J.J. Janimak, Polymer 31, 1018 (1990).

47. S. Lazcano et al. Polymer 29, 2076 (1988).

48. J.J. Janimak, PhD dissertation, Univ. of Akron (1991).

49. H.T. Tseng, PhD dissertation, Univ. of Utah (1984).

50. E.N. Dalal, PhD dissertation, Univ. of Utah (1983).

51. J.D.Hoffman, G.T. Davis, and J.I. Lauritzen, Jr., "Treatise on Solid State Chemistry," N.B. Hannay, Ed., Plenum Press, New York (1976) Vol. 3.

52. P.H. Geil, F.R. Anderson, B. Wunderlich, and T. Arakawa, J. Polym. Sci. A2, 3707 (1962).

53. B. Wunderlich and T. Arakawa, J. Polym. Sci. A2, 3697 (1964).

54. D.C. Bassett and B. Turner, Nature 240, 146 (1972).

55. D.C. Bassett and B. Turner, Phil. Mag. 29, 925 (1974).

56. H.T. Tseng and P.J. Phillips, Macro. 18, 1565 (1984).

57. B.C. Edwards and P.J. Phillips, J. Polym. Sci., Polym. Phys. Ed. 13, 2117 (1975).

58. Kardos, J.L., A.W. Christiansen, and E. Baer, J. Poly. Sci. A2, 4, 777 (1966).

59. P.J. Phillips and B.C. Edwards, J. Polym. Sci., Polym. Physics Ed. 14, 377 (1976).

60. C.K.L. Davies and M.C.M. Cucarella, J. Mat. Sci. 15, 1557 (1980).

61. E. Baer and J.L. Kardos, J. Polym. Sci. A3, 2827 (1965).

62. S. Gogolewski and A.J. Pennings, Polymer 18, 654 (1977).

63. C.K.L. Davies and M.C.M. Cucarella, J. Mat. Sci. 15, 1557 (1980).

64. T.G. Fox and P.J. Flory, J. Appl. Phys. 28, 581 (1950).

65. J.H. Gibbs and E.A. Dimarzio, J. Chem. Phys. 28, 373 (1958).

66. J.M. O'Reilly, J. Polym. Sci., 57, 429 (1962).

67. Mizoguchi and Ishikawa (1975).

68. J.H. Magill, J. Appl. Phys. 35, 3249 (1(64).

69. M. Gopolan and L. Mandelkern, J. Phys. Chem. 71, 3833 (1967).

70 J.G. Fatou and L. Mandelkern, J. Phys. Chem. 69, 417 (1965).

71. E. Ergoz, J.G. Fatou, and L. Mandelkeer, Macro. 5, 142 (1972).

72. J.D. Hoffman, L.J. Frolen, G..S. Ross, and J.I. Lauritzen, Jr., J. Res. Nat. Bur. Stand. A79, 671 (1975).

73. R.C. Allen, Ph.D. dissertation, Virginia Polytechnic Institute 1984.

74. P.G. de Gennes,, J. Chem. Phys., 55, 572 (1971).

75. G. Natta,, J. Polym. Sci. 16, 143 (1955).

76. J.C. Randall, Polymer Sequence Determination: Carbon 13 NMR Method (1977).

77. P.H.Geil, "Polymer Single Crystals," Interscience, New York (1963).

78. Grubb and Keller (1980).

79. P. Debye, Ann. Physik 46, 809 (1915).

80. G. Porod, Acta. Phys. Austr. 3, 255 (1948)

81. A. Guinier and G. Fournet, "Small Angle Scattering of X-rays," New York, John Wiley (1955).

82. D. Glotter, J. Appl. Cryst. 12, 166 (1979).

83. M. Mucha, J. Poly. Sci.: Symp. 69, 79 (1981).

84. D. Cwankin, Vysokomol. Soedin 6, 2083 (1964).

85. Y. Tanabe, G.R. Strobl, and E.W. Fischer, Polymer 27, 1147 (1986).

86. Y.D. Lee, PhD dissertation, Univ. of Tenn (1989).

87. J. Dlugosz et al., Polymer 17, 471 (1976).

88. J.M. Schultz, J.S. Lin, and R.W. endricks, J. Poly. Sci.: Phys. 14, 2291 (1976).

89. H.H. Song et al. Macro. 21, 1180 (1988).

90. P. Scherrer, Nachr. Ges. Wiss., Gottingen 98 (1918) in "Kolloid-Chemie," R. Zsigmandy, Ed. Spanner, Leipzig (1920).

91. J.L. Kardos, A.W. Christiansen, and E. Baer, J. Polym. Sci. A2, 4, 777 (1966).

92. S.V. Meille, S. Brückner, and W. Porzio, Macro., 23 4114 (1990).

93. R. Napolitano, B. Pirozzi, and V. Varriale, J.Polym Sci., Phys. 28, 139 (1990).

94. K.D. Pae, J. Polym. Sci. A2, 6, 657 (1968).

95. D.R. Morrow, Trans. NY Acad. Sci. 30, 1130 (1968).

96. B. Wunderlich and T. Arakawa, J. Polym. Sci. Pt. A, 2, 3697 (1964).

97. J.L. Kardos, A.W. Christiansen, and E. Baer, J. Polym. Sci.: A2, 4, 777 (1966).

98. J.A. Sauer and K.D. Pae, J. Appl. Phys. 39, 4959 (1968).

99. E. Dalal and P.J. Phillips, Macro. 16, 1754 (1983).

100. E.M. Barrall, J.F. Johnson, and R. S. Porter, Applied Polymer Symposia 8, 191 (1969).

101. A. Wlochowicz and M. Eder, Polymer 22, 1285 (1981).

102. J.L. Koenig and A. van Roggen, J. Appl. Polym. Sci. 9, 359 (1965).

103. M.E. Tunnicliffe, J. Polym. Sci. Pt C 7, 187 (1964).

104. G. Bucci and T. Simonazzi, J. Polym. Sci Pt C 7, 203 (1964).

105. J.P. Hobbs et al., Macro. 16, 193 (1983).

106. S. Krimm, Adv. Polym. Sci. 2, 51 (1960).

107. J.P. Luongo, J. Appl. Polym. Sci. 3, 302 (1960).

108. J. Dechant, "Ultrarotspektroskopische Untersuchungen An Polymeren," Akademie-Verlag, Berlin (1972).

109. A. Wlochowicz and M. Eder, Polymer 22, 1285 (1981).

110. E. Maruscelli, M. Pracell, and L. Crispino, POlymer 24, 693 (1983).

111. H.T. Tseng, Phd dissertation, Univ. of Utah (1984).

112. J.H. Reinshagen and R.W. Dunlap, J. Appl. Polym. Sci. 19, 1037 (1975).

113. W. Ruland, Acta. Cryst. 14, 1180 (1961).

114. B. Wunderlich and T. Arakawa, J. Polym Sci. A2, 3697 (1964).

115. G.R. Strobl, M.J. Schneider, and I.G. Voigt-Martin, J. Polym. Sci., Phys. 18, 1361 (1980).

116. W. Ruland, Colloid Polym Sci. 255, 417 (1977).

117. G.R. Strobl and N. Muller, J. Polymer Sci. 11, 1219 (1973).

118. D.J. Blundell, Polymer 19, 1258 (1978).

119. Y.D. Lee, PhD dissertation, Univ. of Tenn (1989).

120. P.J. Flory and A. Vrij, J. Am. Chem. Soc. 84, 3548 (1963).

121. S.Z.D. Cheng et al, Macro. 23, 298 (1990).

122. F. Gornick and J.D. Hoffman, Ind. and Eng. Chem. 58, 41 (1966).

123. H.T. Tseng and P.J. Phillips, Macro. 18, 1565 (1985).

124. E.J. Clark and J.D. Hoffman, Macrom. 17, 878 (1984).

125. S.Z.D. Cheng et al., Macro. 23, 298 (1990).

126. J. Klein and B.J. Briscoe, Porc. Roy. Soc. London A365, 53 (1979).

127. M. Jarrigeon et al., J. Macrom. Sci., Phys. 13, 1417 (1975).

128. W.R. Krigbaum and J. Uematsu, J. Polym. Sci. Pt A 3, 767 (1965).

129. M. Jarrigeon et al., J. Macorm. Sci., Phys. B17, 1 (1980).

130. B. Wunderlich et al., J. Polym. Sci., Phys. 71, 19 (1984).

131. R.J. Samuels, J. Polym Sci., Phys. 13, 1417 (1975).

132. J.J. Janimak, PhD dissertation, Univ. of Akron (1991).

133. E.J. Clark and J.D. Hoffman, Macrom. 17, 878 (1984).

134. E.N. Dalal, PhD dissertation, Univ. of Utah (1983).

135. E.J. Clark and J.D. Hoffman, Macrom. 17, 878 (1984).

136. N. Vatansever, PhD dissertation, Univ. of Tenn. (1986).

137. H.T. Tseng, PhD dissertation, Univ. of Utah (1984).

138. H.T. Tseng, PhD dissertation, Univ. of Utah (1984).

139. E.N. Dalal, PhD dissertation, Univ. of Utah (1983).

140. Sauer and Pae, "Effects of Pressure on Properties and Processability of Polymers", from Proceedings of the 4th International Conference on High Pressure, Kyoto (1974).

141. R.F. Boyer, J. Macrom. Sci. Phys. B7, 487 (1973).

142. C. Nakafuku, Polymer 22, 1673 (1981).

143. D.R. Morrow and B.A. Newman, J. Appl. Phys. 39, 4944 (1968).

144. J.D. Hoffman, Polymer 24, 3 (1983).

145. J.D. Hoffman and R.L. Miller, Macro.21, 3038 (1988).

146. A. Hammami, MS thesis, Univ. of Tenn., (1990).

147. W.S. Lambert, MS thesis, Univ. of Tenn., (1988).

148. Edwards (1975).

Vita

Richard A. Cambpell was born in Clarksdale, Mississippi on May 29, 1960. He entered Mississippi State University in August of 1978, adn received a Bachelor of Science degree in Chemical Engineering in May of 1982. He then attended the University of Southern Mississippi, studying polymer science. In August of 1986, he entered the University of Tennessee, Knoxville to study polymer engineering in the Department of Materials Science and Engineering. He earned his Master of Science degreee in Polymer Engineering in May 1991. He will earn his Doctor of Philosophy degree in Polymer Engineering in August of 1991.

He is married to the former Sandra Watson of Jackson, Mississippi, and they are currently expecting their first child in October.

After completion of his degree requirements, he will accept employment with Shell Development Company in the plastics department of the Westhollow Research Center in Houston, Texas.